THE AUXILIARY ENVELOPE TRACKING RF POWER AMPLIFIER SYSTEM

A thesis submitted to Cardiff University

In candidature for the degree of

Doctor of Philosophy

By

Zubaida Yusoff, M.Sc.

Centre for High Frequency Engineering

School of Engineering

Cardiff University

United Kingdom

March 2012

DECLARATION

This work has not previously been accepted in substance for any degree and is not concurrently submitted in candidature for any degree.

Signed ……. (candidate)

Date ……

STATEMENT 1

This thesis is being submitted in partial fulfilment of the requirements for the degree of PhD.

Signed ……. (candidate)

Date ……

STATEMENT 2

This thesis is the result of my own independent work/investigation, except where otherwise stated.

Other sources are acknowledged by explicit references.

Signed ……. (candidate)

Date ……

STATEMENT 3

I hereby give consent for my thesis, if accepted, to be available for photocopying and for inter-library loan, and for the title and summary to be made available to outside organisations.

Signed ……. (candidate)

Date ……

ABSTRACT

The advancement of the mobile communication industry increases the need for RF power amplifier (RFPA) to be more efficient and linear. The communication network that is shifting towards smaller micro-cell or nano-cell network has also motivated the design of the RF power amplifier to be simple, compact and cost efficient. In this research work, a novel technique for efficiency and linearity improvement of the RFPA is presented. A simplistic approach in the technique called 'Auxiliary Envelope Tracking' (AET) system has promoted the design for small and straightforward AET tracking generator, a key component in the system. The use of low cost components in the AET tracking generator has made the technique commercially attractive.

The AET technique proposes a separation in generating DC and AC components of the AET signal that biases the drain of the RFPA. The separation eases the generation of the signals resulting in low power consumption that leads to efficiency improvement. The investigation of the gain characteristic of gallium nitride (GaN) RFPA has shown an important RFPA attribute where the gain varied substantially as the drain voltage increases. By using the AET technique, the gain characteristic is harnessed to get linearity improvement.

In order to validate the technique, AET measurement systems for two-carrier and WCDMA signals were developed and experimented. A special Class AB RFPA is designed and implemented to use dedicatedly for this investigation. In two-carrier signal measurement, a tracking generator is developed that consists of an envelope amplifier (EA) and a diplexer. The RFPA and the tracking generator are then combined to be an integrated AET block. In order to accommodate the high peak-to-average ratio (PAR) and high bandwidth WCDMA signal, a broadband RF transformer was designed as part of the AET tracking generator to replace the diplexer.

The two-carrier and WCDMA signals measurement results have proven that the AET technique is a valid technique for efficiency and linearity improvement. The improvements were achieved with simple, compact and cost-effective implementation.

KEY CONTRIBUTION

Contribution 1: Novel technique for efficiency and linearity enhancement in the RF power amplifier system called the Auxiliary Envelope Tracking (AET) system.

Contribution 2: Investigation of gallium-nitride (GaN) RF power amplifier gain variation characteristic that is beneficial for linearity improvement in the AET system.

Contribution 3: Development and experimentation of simple and small AET tracking generators using low cost components.

Contribution 4: Realisation of an efficient and linear Class AB power amplifier prototype to be used in conjunction with the AET system from direct import of transistor non-linear model in a computer-aided design environment.

Contribution 5: Practical experimentation and demonstration using two-carrier and WCDMA signal by providing investigation and results to validate the AET as an efficiency and linearity improvement technique.

ACKNOWLEDGMENTS

I would like to express a deepest gratitude to my supervisor, Prof. Steve Cripps for his dedicated supervision on my research project. His enthusiasm, guidance and motivation gave me a continuing drive throughout this project. I would also like to express my profound thanks to my second supervisor Dr. Jonathan Lees for his support and mentoring over the last few years. I would also like to thank Prof. Paul Tasker and Prof. Johannes Benedikt for giving me the opportunity to carry out this research work at the Centre for High Frequency Engineering, Cardiff University.

I would like to thank Yayasan Telekom Malaysia for the financial support. This work would not have been possible without this support.

It is a pleasure to work with an excellent team at Centre of High Frequency Engineering that has provided me an intellectually stimulating environment and enjoyable atmosphere. Here I would like to thank the whole team and especially to Muhammad Akmal, Vincenzo Carrubba, Nur Sharizan Mohamed Dan, Simon Woodington and Shaiful Hashim. In particular, I would like to thank Robert Smith for his help in proof reading the thesis.

My time in Cardiff School of Engineering is more enjoyable with great friendship that made the tougher times much more bearable, and the easier times thoroughly enjoyable. I would like to express my special thanks to Haziah Abdul Hamid, Izan Jaafar and Nadhrah Yatim.

Finally, I would like to express the biggest ‘thank you’ to my family. I would like to thank my husband Nor Azhan Nordin for his endless love and support throughout this research endeavour. I am grateful to my parents Hj. Yusoff and Hjh. Zaharah for their infinite love and encouragement since I was a child. Also, I would like to thank my lovely children; Irdina, Humaira and Ziyad, for their smiles and laughter that always make my day.

LIST OF PUBLICATIONS

1. **Yusoff**, **Z.,** Woodington, S., Lees, J., Benedikt, J., Tasker, P.J., Cripps, S.C., "High Linearity Auxilliary Envelope Tracking(AET) System using GaN Class-J Power Amplifier" IEEE Power Amplifier Symposium, Arizona, USA, 13th -14th September 2010.

   Abstract - A technique which we term Auxiliary Envelope Tracking (AET) is proposed, where a small amplitude tracking voltage is superimposed on the fixed DC bias to an RF power amplifier (RFPA). This represents a potentially useful alternative to a conventional ET system, and in particular significant linearity improvement can be obtained. Using a 2GHz two-carrier signal with 1MHz separation, an AET system has been developed using a 10W GaN Class J power amplifier which demonstrates large reduction in third order intermodulation products (10-25dB), and has less than -30dBc IM3 level at average drain efficiency of 40%. This linearity improvement is remarkable inasmuch as the AC power consumption of the injected AET signal can be lower than 10% of the DC supply.

2. **Yusoff, Z.,** Akmal, M., Carrubba, V., Lees, J., Benedikt, J., Tasker, P.J., Cripps, S.C., "The benefit of GaN characteristics over LDMOS for linearity improvement using drain modulation in power amplifier system," 2011 Workshop on Integrated Nonlinear Microwave and Millimetre-Wave Circuits (INMMIC), vol., no., pp.1-4, 18-19 April 2011.

   Abstract - This paper reports that significant linearity improvement can be obtained in gallium nitride (GaN) RF power amplifiers (RFPAs) in comparison to laterally diffused metal oxide semiconductor (LDMOS) RFPAs through the use of a modulated drain supply. It is shown that the gain characteristic of a GaN RFPA has significant variation with the drain bias voltage and this results in a 10-20dB reduction in intermodulation (IM) levels. The LDMOS RFPA was measured and the result showed that the gain of LDMOS did not change substantially with drain bias voltage. As a consequence, when the LDMOS RFPA is measured using modulated drain bias, the IM levels showed only a much smaller improvement. These results

appear to indicate that GaN devices have an important advantage over LDMOS in linear RFPA applications.

3. **Yusoff, Z.,** Lees, J., Benedikt, J., Tasker, P.J., Cripps, S.C., "Linearity improvement in RF power amplifier system using integrated Auxiliary Envelope Tracking system," IEEE MTT-S International Microwave Symposium (IMS) Digest, 2011, vol., no., pp.1-4, 5-10 June 2011.

   Abstract - A new technique called Auxiliary Envelope Tracking (AET) is proposed, which demonstrates substantial improvement in linearity of RF power amplifiers. A small amplitude envelope-tracking voltage is superimposed on the fixed DC bias of a specially designed 25W GaN HEMT Class AB RF power amplifier (RFPA). A large improvement in third-order intermodulation (IM3) distortion has been observed while maintaining low fifth-order intermodulation (IM5). The overall drain efficiency of the RFPA is also observed to improve, even when the power consumption of the envelope tracking generator is included. The AET concept uses a simple and easily integrated system that consists of an RFPA, a diplexer and an envelope amplifier.

JOINT PUBLICATIONS

1. Akmal, M., Lees, J., Jiangtao, S., Carrubba, V., Yusoff, Z., Woodington, S., Benedikt, J., Tasker, P. J., Bensmida, S., Morris, K., Beach, M., McGeehan, J., "An enhanced modulated waveform measurement system for the robust characterization of microwave devices under modulated excitation," 2011 European Microwave Integrated Circuits Conference (EuMIC), pp.180-183, 10-11 Oct. 2011.
2. Carrubba, V., Clarke, A. L., Akmal, M., Yusoff, Z., Lees, J., Benedikt, J., Cripps, S. C., Tasker, P. J., "Exploring the design space for broadband pas using the novel “continuous inverse class-F mode”," 2011 41st European Microwave Conference (EuMC), pp.333-336, 10-13 Oct. 2011.

ACHIEVEMENT DURING PHD COURSE

- Honourable Mention, of the IEEE MTT-S Student Paper Competition at the International Microwave Symposium 2011, Baltimore, MA, USA, for paper entitled: "Linearity improvement in RF power amplifier system using integrated Auxiliary Envelope Tracking system.", Finalist Student Paper Competition.

MICROWAVE THEORY AND TECHNIQUES SOCIETY

THE INSTITUTE OF ELECTRICAL AND ELECTRONICS ENGINEERS, INC.

2011 IEEE MTT-S International Microwave Symposium

Student Paper Competition

Honorable Mention

is hereby awarded to:

Zubaida Yusoff

For the paper

"Linearity Improvement in RF Power Amplifier System using Integrated Auxiliary Envelope Tracking System"

Baltimore, Maryland

June 9, 2011

MICROWAVE THEORY AND TECHNIQUES SOCIETY FOUNDED 1952

Jeff Pond
IMS2011 General Chairman

Robert Weikle
IMS2011 Student Paper Competition Chair

LIST OF ACRONYMS

4G - Fourth generation mobile communications system
AC - Alternate Current
ACPR - Adjacent Channel Power Ratio
ADS - Advanced Design System
AET - Auxiliary Envelope Tracking
AM - Amplitude Modulation
CAD - Computer-Aided-Design
CCDF - Complementary Cumulative Distribution Function
CW - Continuous Wave
DC - Direct Current
DPD - Digital Predistortion
DSP - Digital Signal Processing
EA - Envelope Amplifier
EDGE - Enhanced Data for Global Evolution
EER - Envelope Elimination and Restoration
EM - Electromagnetic
ET - Envelope Tracking
FDD - Frequency Division Duplexing
Fe_2O_3 - Iron Oxide
FET - Field Effect Transistor
GaAs - Gallium Arsenide
GaN - Gallium Nitride
HBT - Heterojunction Bipolar Transistor
HEMT - High Electron Mobility Transistor
HF - High Frequency
I - In-phase
IF - Intermediate Frequency
IL - Insertion Loss
IM3 - Third-Order Intermodulation
IM5 - Fifth-Order Intermodulation
IMN - Input Matching Network

LDMOS - Laterally Diffused Metal Oxide Semiconductor

LF - Low Frequency

LINC - Linear Amplification using Nonlinear Components

LTE - Long Term Evolution

MESFET - Metal Semiconductor FET

MnO - Manganese Oxide

MnZn - Manganese Zinc

NiO - Nickel Oxide

NiZn - Nickel Zinc

OFDM - Orthogonal frequency-division multiplexing

OMN - Output Matching Network

PA - Power Amplifier

PAR - Peak-to-Average Ratio

PBO - Power Back Off

PLL - Phase-Locked Loop

PM - Phase Modulation

PSG - Power Signal Generator

Q - Quadrature

RF - Radio Frequency

RFPA - Radio Frequency Power Amplifier

SiGe - Silicon Germanium

TETRA - Terrestrial Trunked Radio

TV - Television

VCO - Voltage-Controlled Oscillator

VHF - Very High Frequency

VNA - Vector Signal Analyser

WCDMA - Wideband Code Division Multiple Access

TABLE OF CONTENTS

CHAPTER 1

INTRODUCTION

1.1 Research Motivation

The mobile communication industry has experienced a lot of changes over the past two decades. Mobile handsets have transformed from a device that conveys voice only to a multi-functional device that we call a *smartphone*. The growing demand for broadband internet and video streaming (e.g. YouTube and internet TV) increases the need for high RF signal spectral efficiency [1]. High spectral efficiency means that the RF transmission network needs to be equipped with high linearity RF power amplifiers (RFPAs). The RFPAs not only need to be linear but also power-efficient. *Smartphone* features consist of various data and voice applications that can shorten the *smartphone* battery life compared to previous versions of mobile handsets. From the network operator point of view, the power-efficiency requirement does not only come from the mobile handset RFPAs but also comes from the base station transmission network. There is both commercial and environmental motivation to make the base station RFPA more efficient. The running costs of the base station RF transmitter are a major contributor to the overall communication network cost, and the power consumed by the entire network is placing substantial demands on the future power generation and supply infrastructure [2], [3]. Hence, the RFPAs for both mobile handsets and base stations need to be power efficient to minimize running costs.

Other than the linearity and efficiency requirement for the RFPA, the research motivation for this project also comes from the problem of data transmission bottlenecks in the 4G networks that is identified from its early deployment [4]. This problem is caused by massive data being transmitted in

the insufficient capacity network [4], [5]. The continuous advancement on the *smartphone* applications including the picture, video and social networking that caused this problem has increased the mobile data traffic. The network operator is trying to solve the problem by providing more capacity, however, there are penetration issues using macro-cell network due to the propagation characteristic of 4G. As the frequency increases, the signal attenuation in the propagation channel also increases [6]. Therefore, the solution being implemented by the communications industry is the micro-cell network that can deliver high capacity over short distances [5]. In this micro-cell network architecture, all of the equipment especially the RF transmitter needs to be compact in terms of size and weight, and have a simplistic design. The cost of micro-cell equipments must also be low due to its massive deployment.

1.2 Research Objectives

In this research project, the focus was centred around base station RFPA design. The first research objective was to explore a new technique called 'Auxiliary Envelope Tracking' (AET) to improve the linearity and efficiency of RFPAs. In this system, the RFPA's drain port is biased with modulated signal and by correctly tracking the input signal envelope, the RFPA's drain efficiency can be improved. The gain variation behaviour of a gallium nitride (GaN) high electron mobility transistor (HEMT), which was observed at early stage, was then exploited to improve the RFPA's linearity.

The second objective of this research project was to investigate the effectiveness of the AET system using the classical two-carrier signal measurement. This two-carrier signal measurement was the first step in exploring the linearity performance before testing the AET system with more complex modulated signals. To measure the efficiency of the RFPA, either continuous-wave (CW) or two-carrier signal measurements can be used.

The third objective of this research project was to design the necessary building blocks for the 2-carrier signal measurements of the AET system. An RFPA, a diplexer and an envelope amplifier (EA) are required for these

measurements. The RFPA design should represent a compromise between efficiency and linearity in order to investigate the performance when it is included in the AET system. The diplexer and the EA design approach must also be simple and cost effective in order for the system to be implemented in micro-cell network and for the system to be commercially attractive.

Finally, the fourth objective for this research project was to test the AET system with a complex modulated signal, in this case; WCDMA. The WCDMA signal measurement is required to show that the AET system is applicable for the current wireless technology where a stringent requirement is imposed on linearity and efficiency. Since the WCDMA signal bandwidth is larger and has higher peak-to-average ratio (PAR) than the two-carrier signal measurement, necessary changes to the AET system building block design were taken to accommodate these requirements.

1.3 Thesis Organisation

The documentation of this thesis is organised into nine chapters. The summary of each chapter is presented as follows:

Chapter 2 reviews the linearity and efficiency enhancement techniques in the literature to give the reader an introduction of the methods and procedures that have been used to improve the linearity and efficiency of RFPAs. Both the conventional envelope tracking system (ET) and the AET system are described and the comparison between ET and AET is then highlighted to give a clear understanding of the benefit of the AET system.

Chapter 3 presents the initial measurements of the GaN RFPA, where the RFPA gain was observed to change substantially as the drain bias voltage was varied. Previously designed GaN RFPAs (i.e. 10W GaN Class J RFPA [7] and 10W GaN Inverse Class F RFPA [8]) and the special designed 25W GaN Class AB RFPA were measured and the gains for all these GaN RFPAs have shown the gain variation behaviour. A 20W LDMOS RFPA was measured and no significant variation in gain was observed as the drain bias

voltage was varied. The 25W GaN HEMT transconductance model is also analyzed and the transconductance is shown to vary with drain bias voltage in simulation.

Chapter 4 presents the mathematical concept of AET in terms of efficiency and linearity. The characteristics in the GaN gain variation behaviour are modelled from measured 25W GaN Class AB RFPA data. The gain variation is then analysed mathematically to show its effect on linearity improvement. The analysis of separating of the AC and DC components of the AET signal has directed the concept to the efficiency improvement. The efficiency analysis is then extended to the WCDMA signal simulation to compare of the efficiency of the AET system, ET system and the RFPA biased at a fixed drain supply.

Chapter 5 describes the process of designing the 25W GaN Class AB RFPA. This RFPA is specially designed for this project to investigate the performance of the AET system. The RFPA design considerations are explained at the beginning of the chapter. Various schematics were simulated using a computer-aided-design (CAD) tool. The layout of the RFPA is drawn based on the properties of the high frequency laminate chosen. Finally, the complete fabricated RFPA with the passive components connected is measured and the performance of the RFPA is displayed.

Chapter 6 presents the two-carrier signal measurements of the AET system. In this chapter, the operation of this 2-carrier signal measurement is described. The design of the two building blocks of the AET system namely the diplexer and the EA is explained. The AET signal that biased the RFPA is defined and measured during the operation. Finally, the RFPA performance in the AET system is shown, and this performance is compared to the RFPA performance at a fixed drain supply.

Chapter 7 describes the design of the RF broadband transformer as an AET tracking generator for the WCDMA signal measurement. The chapter

explains why this RF broadband transformer is required for WCDMA application. The transformer equivalent circuit models are then investigated to see the criteria that affect the transformer performance. The process of RF broadband transformer design for WCDMA applications is then described by considering the ferrite core material, the size of the toroidal core and the number of windings. The most applicable transformer design for the WCDMA application, which has high bandwidth and PAR, is chosen for the integrated AET block.

Chapter 8 presents the complete AET system setup for the WCDMA measurements. The chapter starts with information on WCDMA signal generation. Each building block in the AET system is described. In this AET system, there are two signal paths; the RF path and the envelope path. On the RF path of the AET system, the building blocks are the delay line and the driver power amplifier. On the envelope path, the building blocks are an envelope detector, a buffer amplifier, the EA and the RF broadband transformer. The AET system measurement procedure is then described in detail. The chapter concludes with a discussion on the results of the RFPA with the AET system compared to at a fixed drain voltage.

Chapter 9 concludes the thesis by outlining research contributions to the advancement of the RFPA system. This chapter also discusses potential area of improvement to the AET system that can be investigated in the future.

1.4 References

[1] Raab, F.H. et al., "RF and Microwave Power Amplifier and Transmitter Technologies - Part 1", High Frequency Electronics, May 2003.

[2] "The Green CDMA Base Station", [Online]. Available: http://www.huawei.com/uk/about-huawei/publications/communicate/hw-082748-28228-30196-hw_082689-hw_082746.htm

[3] "Alternatives for Powering Telecommunications Base Stations", [Online]. Available: http://www.motorola.com/web/Business/Solutions/Industry%20Solutions/Ser

vice%20Providers/Wireless%20Operators/GSM/Network%20Overview/_Documents/Static%20files/6872_MotDoc.pdf

[4] Principi, B., "4G World: the deployment of microcellular networks", Telecom Engine Article, October 31, 2011. [Online]. Available: http://www.telecomengine.com/article/4g-world-deployment-microcellular-networks

[5] Boch, E., "Delivering on the 4G user experience promise with micro-cellular networks" Telecom Engine Article, October 6, 2011. [Online]. Available: http://www.telecomengine.com/article/delivering-4g-user-experience-promise-micro-cellular-networks

[6] Chae, C, Suh, C., Katz, M., Park, D.S. and Fitzek F. H. P., "Comparative Study of Radio Channel Propagation Characteristics for 3G/4G Communication Systems". WWRF 11, June, 2004.

[7] Wright, P., Lees, J., Tasker, P.J., Benedikt, J., Cripps, S.C., "An Efficient, Linear, Broadband Class-J-Mode PA Realised Using RF Waveform Engineering", IEEE/MTT-S International Microwave Symposium Digest, 7-12 June 2009, pp. 653-656.

[8] Wright, P., Sheikh, A., Roff, C., Tasker, P.J., Benedikt, J., "Highly efficient operation modes in GaN power transistors delivering upwards of 81% efficiency and 12W output power," 2008 IEEE MTT-S International Microwave Symposium Digest, 15-20 June 2008, pp.1147-1150.

CHAPTER 2

LITERATURE REVIEW AND THE INTRODUCTION OF THE AET SYSTEM

2.1 Introduction

Envelope tracking (ET) is an efficient enhancement technique that is used for base station power amplifier system. The ET system uses a linear RF power amplifier (RFPA), but allows the supply voltage to track the signal envelope, thus significantly improving the efficiency of the RFPA. In this research project, a variation of ET system that we call 'Auxiliary Envelope Tracking' (AET) is introduced and this new proposed technique is motivated by the stringent requirement of linearity and efficiency in recent wireless standards. Unlike the ET system, the AET system does not require the RFPA to be linear inasmuch as this technique improves both linearity and efficiency of the RFPA. Moreover, the AET system focuses on a simple and cost-efficient design.

2.2 Linearity Enhancement Technique

In this subsection, the linearity enhancement techniques are summarized to give an introduction of the available techniques in the literature. RFPA linearity is essential to ensure the accuracy of the amplitude and phase amplification of an input RF signal. There are three main linearity enhancement technique groups in the literature including feedback, feedforward and predistortion. These three groups are summarized as follows.

2.2.1 Feedback Linearization Technique

There are four categories in the feedback linearization technique namely, RF feedback, envelope feedback, polar feedback and Cartesian feedback. The basic configuration of a feedback system is shown in Figure 2.1.

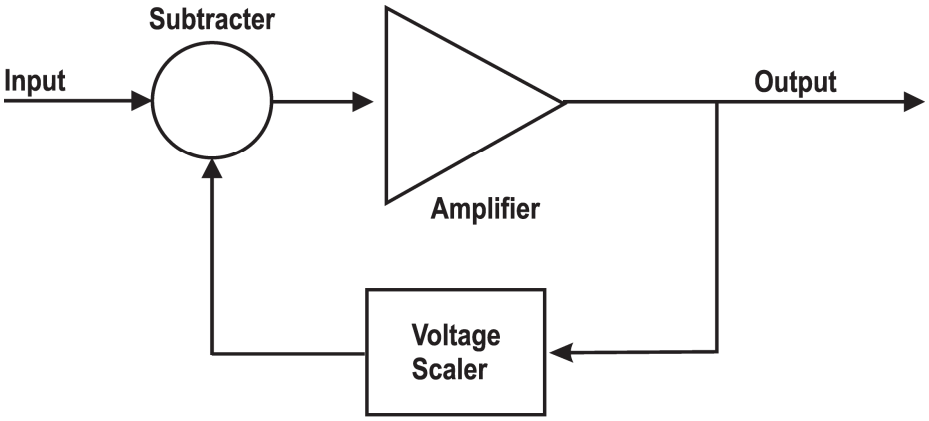

Figure 2.1: The basic feedback system (Figure is adapted from [1]).

In an RF feedback system, a part of the RF output signal is processed as an error signal through a voltage scaler and later the error signal will be combined and subtracted from the RF input signal [1], [2]. The resulting output signal will be more linear; however, will be affected by some gain loss due to the input voltage reduction. The gain loss has a much higher impact at RF frequencies as compared to audio frequencies; therefore the RF feedback technique is used more at HF and LF band [1-3]. The signal path delay is however an even bigger problem at higher frequencies [1], [2], [4]. There are many variations of this RF technique that improve the performance. Among these are replacing the voltage divider with an active stage using an amplifier [5], and employing a Cartesian loop in the forward path [6].

Envelope feedback is also known as modulation feedback [1]. In this type of feedback, shown in Figure 2.2, the envelope of the RF output signal is detected and is used as the feedback element in terms of amplitude or phase [1], [4].

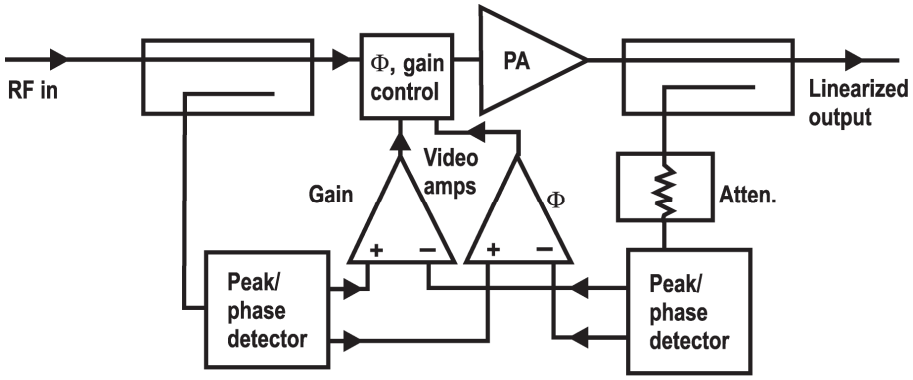

Figure 2.2: The envelope feedback system. (Figure is adapted from [4])

When amplitude is the only element used in the feedback path, is termed amplitude envelope feedback, the amplitude modulation-amplitude modulation (AM-AM) distortion can be corrected. Amplitude envelope feedback however does not correct the amplitude modulation-phase modulation (AM-PM) distortion when the RFPA enters the compression region. It also introduces 'parasitic' AM-PM distortion that is caused by the amplitude feedback device. This problem is alleviated by using both amplitude and phase as the feedback elements, is termed as vector envelope feedback. This feedback system, however, still encounters the delay problem [4]. A detailed analysis of this technique can be found in [1] and [4]. An early application of this technique at the RFPA stage is described in [7] and this technique was applied in a transmitter that is presented in [8].

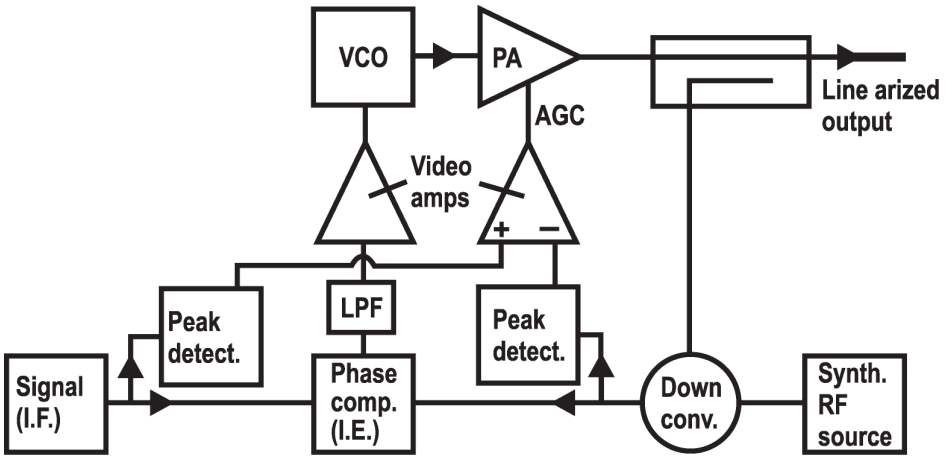

Figure 2.3: The polar feedback system (Figure is adapted from [4]).

The polar feedback technique is a form of vector envelope feedback that uses both amplitude and phase as the feedback elements. This technique was first developed by Petrovic [9] to improve the AM-PM nonlinearities in a transmitter. The key building block to the system design, as shown in Figure 2.3, is the voltage-controlled oscillator (VCO) that is part of the phase-locked loop (PLL) where this loop is included in the feedback path. In this polar feedback system, the amplitude and phase correction are carefully controlled in two separate loops. Excellent AM-AM and AM-PM performance in the transmitter output, however, is limited by the high bandwidth requirement of the PLL [1]. A recent application of this technique in an RFIC can be found in [10] while its use in a multimode handset can be found in [11].

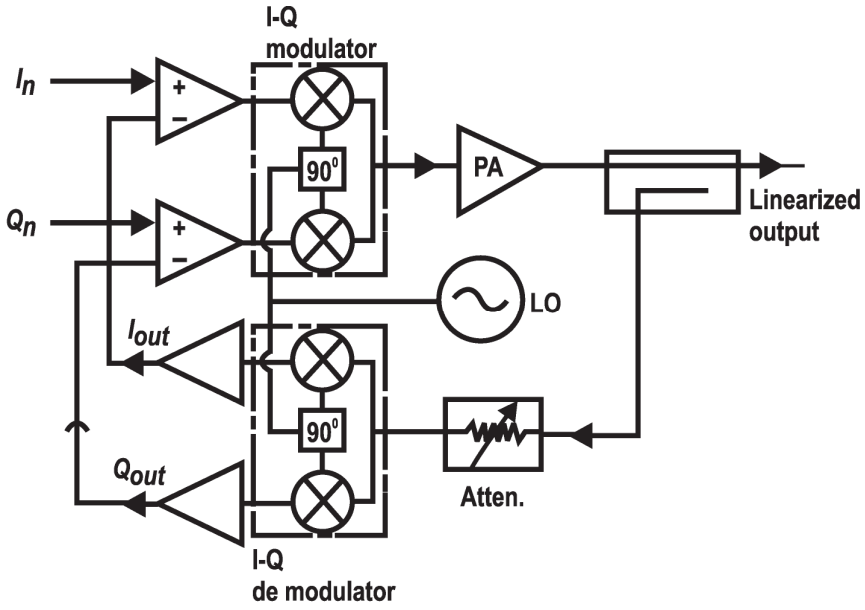

Figure 2.4: The Cartesian feedback system (Figure is adapted from [4]).

The high bandwidth requirement for the polar feedback PLL is overcome with a fourth feedback technique that called the Cartesian feedback technique. In this technique, the attenuated intermediate-frequency (IF) signal is processed in the Cartesian form; in-phase (I) and quadrature (Q) signal. As shown in Figure 2.4, the dynamic PLL or VCO in the polar feedback system is no longer needed in the Cartesian feedback system. The downconverted 'I' and 'Q' output signals are fed back to the differential amplifier which is then

compared with the 'I' and 'Q' input signals for envelope correction in terms of amplitude and phase. The orthogonal nature of I and Q feedback path ensures the amplitude and phase nonlinearities are corrected independently. The Cartesian feedback technique was first designed for VHF transmitters [12] and recently has been applied to the terrestrial trunked radio (TETRA) standard that operates between 300 to 500 MHz [13].

2.2.2 Feedforward Linearization Technique

The second group of linearity enhancement techniques is feedforward technique. The feedforward technique was first introduced by Black in his 1928 patent [14]. It is relevant to note that the feedforward technique was patented before the feedback approach; this highlights the gain loss problem in feedback systems which was particularly troublesome in the early electronic era, and persists today at GHz frequencies. The basic configuration of the feedforward technique is shown in Figure 1.5. Unlike the feedback system, this feedforward technique has the corrective process at the output of the RFPA. As shown in Figure 2.5, there are two amplifiers; the main amplifier (the RFPA) and the 'error' amplifier. The 'error' amplifier linearises the compressive RFPA at higher output power by injecting additional power into the system [1]. More analysis on the feedforward system can be found in [1] and [4]. Nowadays, this technique has developed into an improved design that is called adaptive feedforward that is based on power minimization and gradient signals [15]. A recent application of this feedforward technique for a wideband communication system can be found in [16].

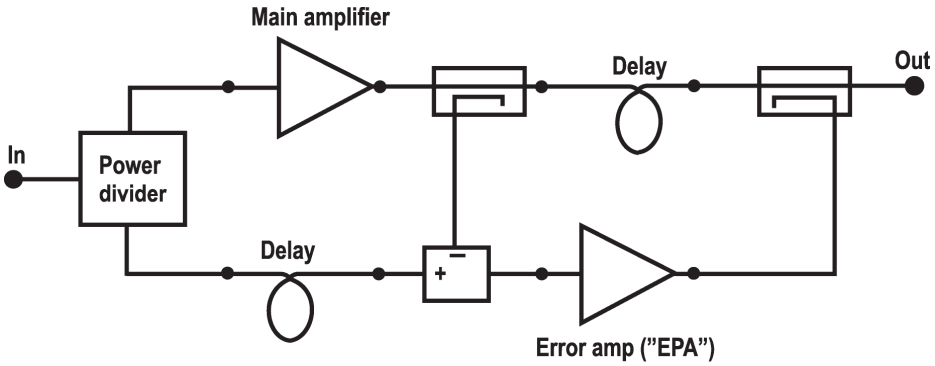

Figure 2.5: The basic feedforward system (Figure is adapted from [4])

2.2.3 Predistortion Linearization Technique

The final linearity enhancement technique is predistortion. The basic concept of predistortion is illustrated in Figure 2.6. The output signal from a predistorter is a 'distorted' signal with the intention to linearise the output of the RFPA signal. For example, the insertion of expansive behaviour of the 'distorted' signal can linearise the compressive behaviour of the RFPA at higher power. In short, the linearity of the RFPA is achieved by the combination of the nonlinearities from the RFPA and the predistorter. This operation is quite similar, from a mathematical perspective, to the feedforward technique explained earlier however the difference is that the predistortion corrective action is done at the input of the RFPA.

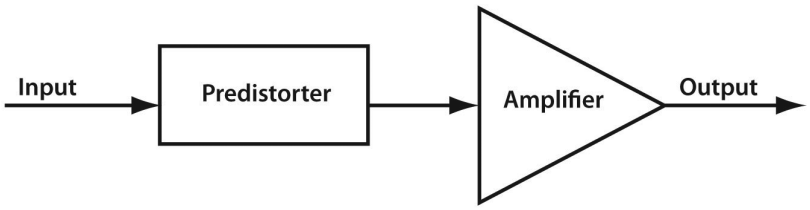

Figure 2.6: The basic configuration of predistortion technique

This predistortion technique can be divided into analog and digital predistortion. Digital predistortion (DPD) has become a popular technique in the literature recently and this is mainly due to the available digital signal processing (DSP) capabilities to process different types of signal i.e. analog baseband, digital baseband, analog IF, digital IF or analog RF input signals. The digital predistorters can be divided into two categories; predistorter for memoryless RFPA and predistorter for RFPA with memory. For narrowband applications, a simple digital predistorter is sufficient where the predistorter modeling is characterized by the AM-AM and AM-PM of the RFPA [17] [18]. However, for wideband applications, the RFPA exhibits electrical and thermal memory effects. Therefore, the digital predistorter needs to model these nonlinear effects and the popular nonlinear models used are Volterra series model [19], Hammerstein model [20] and Wiener model [21].

Although the DSP in digital predistortion technique can offer higher bandwidth signal processing, the analog predistortion on the other hand presents a simplistic approach that uses simple analog circuitry [4, 22].

2.3 Efficiency Enhancement Technique

In this section, the efficiency enhancement techniques for RFPA are summarized. There are three main techniques, and most researchers today are adapting these techniques into their designs. The techniques are the Doherty amplifier, the Chireix outphasing power amplifier (PA) and the envelope elimination and restoration (EER) RFPA system.

2.3.1 Doherty Amplifier

The Doherty amplifier was first introduced in 1936 as a technique to improve the efficiency of amplifiers [23].

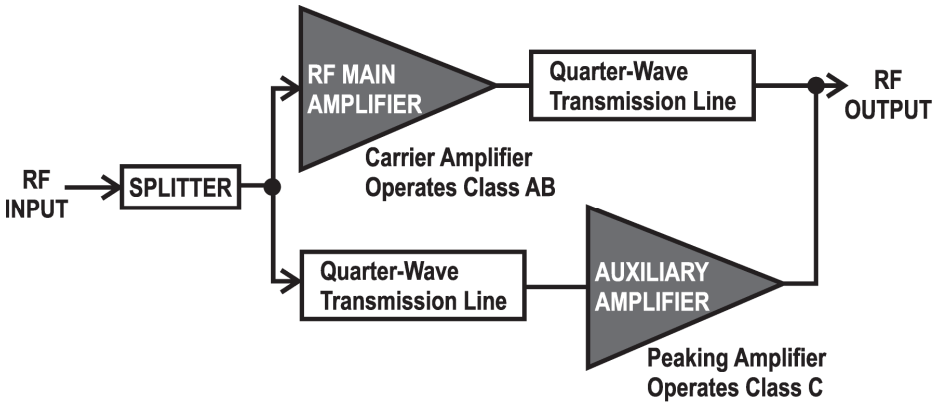

Figure 2.7: The Doherty amplifier configuration. (Figure is adapted from [48])

The basic configuration of Doherty amplifier is shown in Figure 2.7 and it consists of a main amplifier, a peaking amplifier, and quarter-wave transformers. The main idea of this technique is that, the combination of these two amplifiers results in the maximum system efficiency which is maintained from the maximum output power down to the 6dB backoff point [24]. The detail analysis of the Doherty amplifier can be found in [4, 24]. Research on

adapting the classical 'tube' Doherty to a modern 'transistor' Doherty amplifier is widely pursued [25], [26] due to its attractiveness in efficiency improvement. The Doherty amplifier has also found widespread commercial deployment in high power base station RFPAs. This is due in part to the fact that the Doherty amplifier's efficiency enhancement process is performed entirely at the radio frequency, and there is no fundamental requirement for baseband signal processing. There is however one element in the RF processing chain of this Doherty amplifier that introduces a fundamental bandwidth limitation; an impedance inverter [4].

2.3.2 The Chireix Outphasing Technique

The Chireix outphasing technique was first invented in 1935 by Chireix [27] and later in 1974 the idea of this technique was used in a new form of power amplification called linear amplification using nonlinear components (LINC) by Cox [28]. The basic configuration of the Chireix outphasing technique is shown in Figure 2.8.

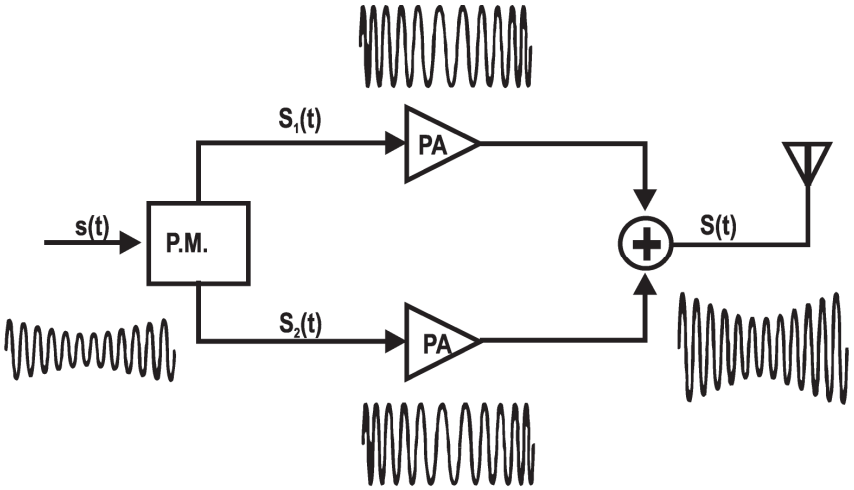

Figure 2.8: The Chireix outphasing basic configuration (Figure is adapted from [29])

In this configuration, the two amplifiers can be nonlinear, a major distinction from the Doherty technique. These two nonlinear amplifiers are operating with constant-envelope input signals with a phase shift controlled by a phase modulator (P.M.). The combination of these two amplified and out-phased signals results in the desired amplified AM modulated signal. The key

contribution of this technique in terms of the efficiency enhancement lies in the load modulation variable between the two amplifiers at the power combiner. This impedance inverter is the element that introduces a bandwidth limitation to the system. There are many other issues with this technique that come from the phase-mismatch problem at the input conditioner and the impedance matching at the output combiner [4], [29]. This phase and impedance mismatch reduction is discussed further in [29]. A recent application of this technique in a high power RFPA system for WCDMA applications can be found in [30] and [31].

2.3.3 The Kahn Envelope Elimination and Restoration

The third classic efficiency enhancement technique is the EER system that was introduced in by Kahn in 1952 [32]. In an EER system, a highly efficient, non linear RFPA and a highly efficient envelope amplifier (EA) are required.

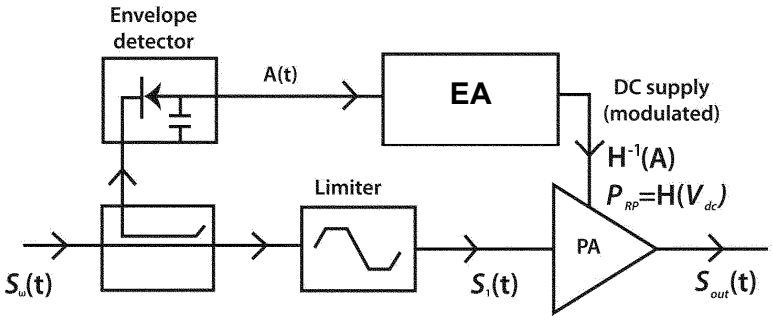

Figure 2.9: The EER system configuration (Figure is adapted from [4])

The EER system configuration is shown in Figure 2.9. The EER system separates the amplitude modulation and phase modulation into two paths. A limiter is used to produce the phase modulated signal that is later amplified by the RFPA. The construction of the original signal at the output of the RFPA is generated by voltage supply modulation. This modulating signal is produced by the envelope detector and is later amplified to the appropriate level by the EA [4]. Although the RFPA is highly efficient, in practice, this baseband signal processing requires high power amplification by the EA, which degrades the efficiency enhancement of the whole system [4]. In modern EER system designs, the fundamental EER operation of inputting the

phase modulated signal to the RFPA is modified. The RFPA is presented with the RF modulated signal and this system is usually called a 'hybrid' EER system [33] [34]. EER designers also concentrate on improving the performance of the EA by using different approaches such as hysteretic current feedback control [33] or employing multi-level converter in series with a linear regulator [35].

2.4 The Envelope Tracking System

A fourth technique of efficiency enhancement has emerged since 1980s, and this technique is referred to as 'Envelope Tracking' (ET) system [36] [37]. It has attracted increased attention recently, due to its potential for efficiency improvement in broader bandwidth applications. ET systems emerged from the EER system discussed earlier where both systems adopt the dynamic signal biasing to the RFPA, and the ET system looks more like the modern 'hybrid' EER system. There are two main distinctions between these two techniques; firstly, the ET RFPA needs to work in a linear mode while the EER RFPA is not required to be linear but needs to be highly efficient. Secondly, the ET RFPA amplifies both amplitude and phase while the EER RFPA will only reconstruct the phase.

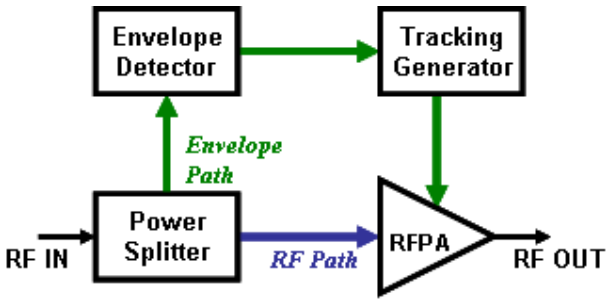

Figure 2.10: The basic configuration of ET system

The ET system's basic configuration is shown in Figure 2.10, where the input RF signal is split into two paths; the envelope path and the RF path. On the RF path, the input RF signal is input into a linear RFPA. On the envelope path, the envelope of the input signal is detected and the detected envelope

signal is amplified by the voltage converter, or also referred to as the tracking generator. The output of the tracking generator provides the voltage supply modulation that tracks the signal envelope of the input RF signal. This accurate tracking is the heart of the efficiency enhancement mechanism in the ET system. The efficiency improvement comes from the reduction of power dissipation compared to the fixed drain bias and this is illustrated in Figure 2.11. Note that, in this figure, the signal representation is the envelope of a two-carrier signal.

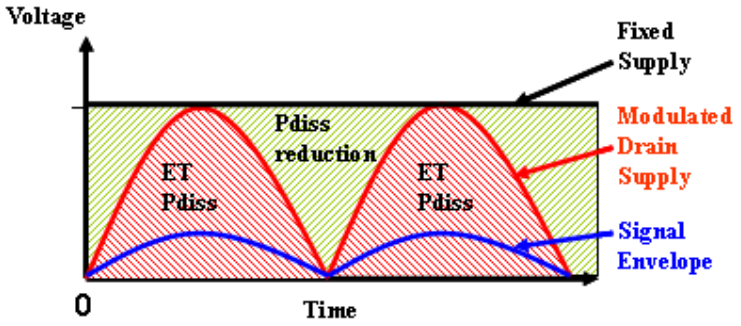

Figure 2.11: The representation of power dissipation reduction

Unlike the Doherty and Chireix outphasing techniques, the ET system does not require an impedance inverter. Hence, this system has a major advantage inasmuch as it is inherently broadband. But ET has the same requirement as EER in the need for a tracking power converter, which consumes additional power. The ET system however has a critical advantage in that the precision of the tracking only affects the efficiency improvement, but does not in principle affect the signal itself, so long as the RFPA gain is invariant with the supply voltage. In the EER transmitter, it is the tracking voltage which actually creates the required amplitude modulation, and as such must be generated with great precision. An ET tracking generator only needs to track the general trend of the signal envelope in order to give some degree of efficiency improvement. In particular, the ET generator can present a significantly band limited version of the signal envelope and still give close to the optimum efficiency enhancement performance [38],[39],[40].

The dynamic supply voltage variation does however usually re-modulate the signal in an unfavourable manner, and there is a fundamental conflict whereby at higher levels of efficiency enhancement the degradation in spectral purity escalates [41], [42]. In almost all published work on ET, the distortion problem is effectively removed by the use of digital signal processing (DSP), usually in the form of digital predistortion (DPD) at the signal input [38], [40], [43].

2.5 The Introduction of Auxiliary Envelope Tracking (AET) System

In this subchapter, we will introduce a derivative of the ET system we called the 'Auxiliary Envelope Tracking' (AET) system. In this AET system, both linearity and efficiency improvements to the RFPA can be achieved. We consider AET to be a novel technique with great potential in the field of RFPA design.

2.5.1 AET for Efficiency

As mentioned earlier, the AET system is a derivative of the ET system that is well known as an efficiency enhancement technique. The AET system shares the same basic system configuration as the ET system. The fundamental difference between conventional ET and AET is the mechanism of generating the drain modulated signal bias, which we call the AET signal to the drain port of the RFPA. In this mechanism, the generation of the DC and AC components of the AET signal is initially separated. These separately generated DC and AC signals are then combined in a specially designed combiner before this AET signal is applied to the RFPA. In comparison, for the ET system, the amplification of both DC and AC components of the bias signal are handled by an EA.

The idea of separating the DC and AC components of the AET signal has been widely used in the vacuum tube era. The technique is not widely recognized in the wireless communication industry. A decade ago, a similar idea was presented as split-band modulator in an EER system [44] and a

system for a radio satellite application [45] where the signal was split into two frequency bands.

In the AET system, unlike the split-band modulator in [44], the envelope signal is directly input into the EA, as shown in Figure 2.12, where some amplification is done at a buffer stage. The output of the EA is the source of the AC component of the AET signal and this signal is later inserted into the 'combiner'. The DC component of the AET signal comes directly from a DC voltage supply. The combination of both AC and DC components at the 'combiner' results in the AET signal that biases the drain port of the RFPA.

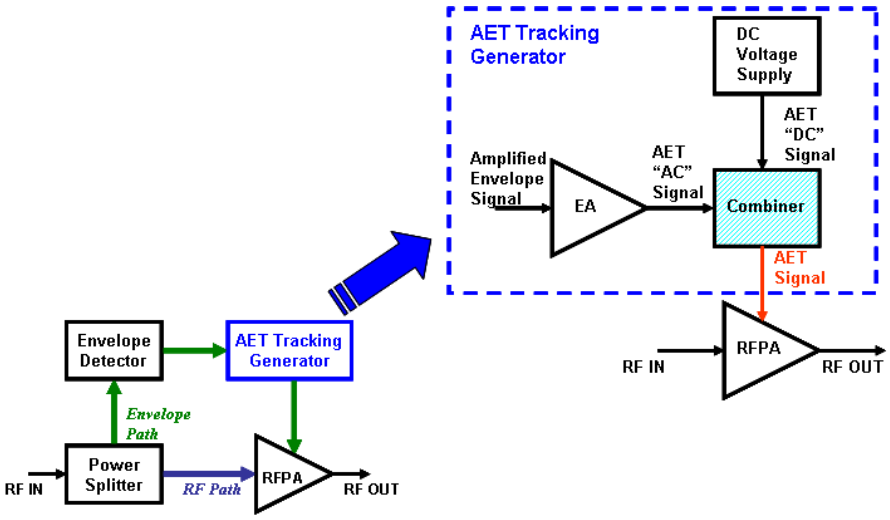

Figure 2.12: The AET signal generation concept illustration

The output of the EA contains the AC component of the AET signal with a DC offset. The DC offset contained in the output of the EA will be suppressed by a passive network in the 'combiner'. For the two-carrier signal measurement, the 'combiner' is a diplexer and the DC blocking capacitor in the diplexer design is used to remove the offset. Meanwhile, for the WCDMA measurement, the 'combiner' is an RF broadband transformer and the offset is handled by the DC isolation behaviour of the transformer.

The generation of separate DC and AC components of the AET signal has allowed us to design and implement a very simple, low cost AET tracking

voltage generator as compared to the split-band modulator and other EA designs in the literature such as the boost converter [41] and buck converter [40], [46]. In this AET system, the EA is designed using a simple source-follower configuration, while the diplexer and RF transformer design is also very straightforward. In addition, the principle of operation of the EA, diplexer and RF transformer is easy to understand and the implementation is cost effective.

The AET system also aims to provide a low amplitude tracking supply by generating a small amplitude AC component of the AET signal. In the mathematical analysis that is shown in Chapter 4, a useful improvement in overall efficiency can be achieved and the improvement can be better than the conventional ET system.

2.5.2 AET for Linearity

In AET system configuration, there is no additional building block dedicated to improving the linearity of the RFPA, unlike the other linearity enhancement techniques discussed earlier i.e. feedback, feedforward and predistortion. The linearity mechanism lies in same dynamic signal biasing to the drain port of the RFPA that provides efficiency improvements. This has been achieved, to some extent, by harnessing a useful performance characteristic in GaN transistors that is also described in Chapter 4. Hence, in this AET system, a GaN RFPA that exhibits gain variation behaviour is required. The low amplitude AET drain signal bias then, not only can improve the efficiency, but can also, simultaneously, improve the linearity performance.

2.5.3 Comparison between the ET and the AET system

The main differences between the ET and AET systems are summarized in Table 2.1 and the detailed mathematical analysis of the AET system in terms of efficiency and linearity improvements can be found in Chapter 4.

	ET SYSTEM	AET SYSTEM
Efficiency Improvement: 1. Voltage Supply Modulation 2. Envelope Amplifier and Supply Modulation Mechanism	1. Larger Tracking Amplitude 2. Highly efficient; Boost Converter, Buck Converter	1. Lower Tracking Amplitude 2. Source Follower Amplifier and 'Combiner', Separation between AC and DC Component
Linearity Improvement: 1. RFPA 2. DPD	1. Highly linear RFPA 2. Incorporated DPD	1. GaN RFPA (Gain variation behavior) 2.No DPD included
System Design:	Complex, Costly due to DPD inclusion	Simple, Low Cost

Table 2.1: The ET and AET system comparisons

2.6 Chapter Summary

In summary, the various linearity enhancement techniques that have been described extensively in the section 2.2 all have individual limitations. These can be summarised as follows:

- Feedback: essentially impractical for the wide signal bandwidths used in wireless communications systems.
- Feedforward: has fallen into disuse due to the requirement for an additional RFPA ('error' amplifier) which consumes as much power as the RFPA and hence greatly reduces efficiency.
- DPD: has become the default technique for recent generation base station transmitters. But the 'DSP overhead' in terms of cost and

complexity, make it much less attractive for the microcell infrastructure.

Efficiency enhancement techniques that were described in section 2.3 also have individual limitations:

- Doherty amplifier: fundamentally limited to RF bandwidths of less than 10% and usually requires remedial external linearisation.
- Chireix outphasing technique: not really a PA at all, more accurately described (as by its inventor in the original paper) as a high level modulator, it has similar RF bandwidth limitations to the Doherty amplifier due to the use of impedance inverters, and requires complex DSP in order to generate the input phase-modulated signals.
- Kahn EER: has fallen out of favour in wireless communication applications due to the stringent precision requirements on the envelope tracking power supply.
- ET: generically related to the AET technique proposed in this thesis, but usually considered primarily as an efficiency enhancement technique that will likely require substantial remedial linearisation. Although the envelope tracking modulator has less stringent requirements in ET, it will be shown in chapter 4 that unless the efficiency of this element is greater than 70%, the efficiency benefits are minimal.

The ET system that inherits the EER architecture of separating the input signal into two paths appears to be an attractive efficiency enhancement. This ET system is then adapted into a new approach called the AET system that is developed in this research project. AET can provide a low cost, simplistic method for obtaining useful improvements in linearity and efficiency with minimal RF bandwidth limitations. None of the standard techniques can provide this combination, which will become more important in micro-cell deployment.

2.7 References

[1] Kenington. P.N., "High-Linearity RF Amplifier Design", Norwood, MA: Artech House, 2000.

[2] Raab, F.H. et al., "RF and Microwave Power Amplifier and Transmitter Technologies - Part 4", High Frequency Electronics, November 2003. [Online] Available: http://www.highfrequencyelectronics.com/Archives/Nov03/HFE1103_RaabPart4.pdf

[3] Mitchell, A.F., "A 125MHz feedback amplifier," IEE Colloquium Broadband High Frequency Amplifiers: Practice and Theory, London, England, November 1979, pp2/1-6.

[4] Cripps, S., "Advanced Techniques in RF Power Amplifier Design", Norwood, MA: Artech House, 2002.

[5] Pedro, J.C., Perez, J., "An MMIC linearized amplifier using active feedback," 1993 IEEE MTT-S International Microwave Symposium Digest, pp.95-98 vol.1, 1993.

[6] Faulkner, M., "Amplifier linearization using RF feedback and feedforward techniques," IEEE Transactions on Vehicular Technology, vol.47, no.1, pp.209-215, Feb 1998.

[7] Arthanayake, T., Wood, H.B., "Linear amplification using envelope feedback," Electronics Letters, vol.7, no.7, pp.145-146, April 8 1971.

[8] Petrovic, V., Gosling, W., "A high efficiency, low-cost VHF/AM transmitter using V-MOS technology," Communication 78, IEE Conference on Communication Equipment and Systems, Birmingham, England, 4-7 April 1978, pp.281-285.

[9] Petrovic, V., Gosling, W., "Polar-loop transmitter," Electronics Letters, vol.15, no.10, pp.286-288, May 10 1979.

[10] Akamine, Y., Tanaka, S., Kawabe, M., Okazaki, T., Shima, Y., Masahiko, Y., Yamamoto, M., Takano, R., Kimura, Y., "A Polar Loop Transmitter with Digital Interface including a Loop-Bandwidth Calibration System," 2007 IEEE International Solid-State Circuits Conference (ISSCC 2007) Digest of Technical Papers, pp.348-608, 11-15 Feb 2007.

[11] Yang, H., Chen, J., Chen, Y., "A Polar Transmitter Using Interleaving Pulse Modulation for Multimode Handsets," IEEE Transactions on Microwave Theory and Techniques, vol.59, no.8, pp.2083-2090, Aug. 2011.

[12] Petrovic, V., "VHF SSB Transmitter Employing Cartesian Feedback", IEE Conference on Telecommunications, Radio and Information Technology, 1984.

[13] Wilson, C.N., Gibbins. J.M., "A new generation Cartesian loop transmitter for flexible radio solutions", EngineerIT, September 2006 [Online] Avalaible: http://www.eepublishers.co.za/images/upload/Cartesian%20loop.pdf

[14] Black, H.S., "Translating System", U.S. Patent 1,686,792, Issued 9 October 1928.

[15] "Adaptive Feedforward Linearization for RF Power Amplifiers", [Online] Available: http://cp.literature.agilent.com/litweb/pdf/5989-9100EN.pdf

[16] Honarvar, M.A., Moghaddasi, M.N., Eskandari, A.R., "Power amplifier linearization using feedforward technique for wide band communication system," 2009 IEEE International Symposium on Radio-Frequency Integration Technology, RFIT 2009, pp.72-75, 2009.

[17] Eun, C., Powers, E. J., "A predistorter design for a memory-less nonlinearity preceded by a dynamic linear system," Proc. IEEE Global Telecommun. Conf., vol. 1, pp. 152–156, Nov. 1995.

[18] Graboski, J., Davis, R. C., "An experimental M-QAM modem using amplifier linearization and baseband equalization techniques," in Proc. IEEE Nat. Telecommun.Conf., pp. E3.2.1–E3.2.6, Nov. 1982.

[19] Eun, C., Powers, E. J., "A new Volterra predistorter based on the indirect learning architecture," IEEE Trans. Signal Processing, vol. 45, pp. 223–227, Jan. 1997.

[20] Eskinat, E., Johnson, S. H., Luyben, W. L., "Use of Hammerstein models in identification of nonlinear systems," AIChE J., vol. 37, pp. 255–267, Feb. 1991.

[21] Lin, B., Wang, Y., Feuvrie, B., Dai, Q., "A Novel Power Amplifier Linearization Technique based on Pre-distortion Principle and Wiener model" International Journal of Advanced Science and Technology, Vol. 22, pp.59- 70, Sept 2010.

[22] Yi, J., Yang, Y., Park, M., Kang, W., Kim, B., "Analog predistortion linearizer for high-power RF amplifiers," IEEE Transactions on Microwave Theory and Techniques, vol.48, no.12, pp.2709-2713, Dec 2000.

[23] Doherty, W.H., "A new high efficiency power amplifier for modulated waves," Proceedings of the IRE, vol.24, no.9, pp. 1163-1182, September 1936.

[24] Cripps, S., "RF Power Amplifier for Wireless Communications", Norwood, MA: Artech House, Apr. 1999.

[25] Kim, J., Fehri, B., Boumaiza, S., Wood, J., "Power Efficiency and Linearity Enhancement Using Optimized Asymmetrical Doherty Power Amplifiers," IEEE Transactions on Microwave Theory and Techniques, vol.59, no.2, pp.425-434, Feb. 2011.

[26] Moon, J., Kim, J., Kim, J., Kim, I., Kim, B., "Efficiency Enhancement of Doherty Amplifier Through Mitigation of the Knee Voltage Effect," IEEE Transactions on Microwave Theory and Techniques, vol.59, no.1, pp.143-152, Jan. 2011.

[27] Chireix. H., "High power outphasing modulation", Proceedings of the IRE, vol. 23, no.11, pp.1370-1392, November 1935.

[28] Cox, D., "Linear Amplification with Nonlinear Components," IEEE Transactions on Communications, vol.22, no.12, pp. 1942- 1945, Dec 1974.

[29] Zhang, X., Larson, L.E., Asbeck, P.M., "Design of Linear RF Outphasing Power Amplifiers", Norwood, MA: Artech House, 2003.

[30] Qureshi, J.H., Pelk, M.J., Marchetti, M., Neo, W.C.E., Gajadharsing, J.R., van der Heijden, M.P., de Vreede, L.C.N., "A 90-W Peak Power GaN Outphasing Amplifier With Optimum Input Signal Conditioning," IEEE Transactions on Microwave Theory and Techniques, vol.57, no.8, pp.1925-1935, Aug. 2009.

[31] Huttunen, A., Kaunisto, R., "A 20-W Chireix Outphasing Transmitter for WCDMA Base Stations," IEEE Transactions on Microwave Theory and Techniques., vol.55, no.12, pp.2709-2718, Dec. 2007.

[32] Kahn, L.R., "Single sideband transmission by envelope elimination and restoration," Proceedings of the IRE, vol.40, no.7, pp.803-806, July 1952.

[33] Wang, F., Kimball, D.F., Popp, J.D., Yang, A.H., Lie, D.Y., Asbeck, P.M., Larson, L.E., "An Improved Power-Added Efficiency 19-dBm Hybrid Envelope Elimination and Restoration Power Amplifier for 802.11g WLAN Applications," IEEE Transactions on Microwave Theory and Techniques., vol.54, no.12, pp.4086-4099, Dec. 2006.

[34] Kim, I., Woo, Y., Kim, J., Moon, J., Kim, J., Kim, B., "High-Efficiency Hybrid EER Transmitter Using Optimized Power Amplifier," IEEE Transactions on Microwave Theory and Techniques, vol.56, no.11, pp.2582-2593, Nov. 2008.

[35] Vasic, M., Garcia, O., Oliver, J.A., Alou, P., Diaz, D., Cobos, J.A., "Switching capacities based envelope amplifier for high efficiency RF amplifiers," Applied Power Electronics Conference and Exposition (APEC), 2010 Twenty-Fifth Annual IEEE , vol., no., pp.723-728, 21-25 Feb. 2010.

[36] Saleh, A.A.M., Cox, D.C., "Improving the Power-Added Efficiency of FET Amplifiers Operating with Varying-Envelope Signals," IEEE Transactions on Microwave Theory and Techniques, , vol.31, no.1, pp.51-56, Jan. 1983.

[37] Geller, B.D., Assal, F.T., Gupta, R.K. and Cline, P.K., “A technique for maintenance of FET power amplifier efficiency under backoff,” IEEE 1989 MTT- Digest, Long Beach, California, pp. 949-952, June 1989.

[38] Jeong, J., Kimball, D.F., Kwak, M. C., Hsia, Draxler, P., Asbeck, P.M., "Wideband Envelope Tracking Power Amplifiers with Reduced Bandwidth Power Supply Waveforms and Adaptive Digital Predistortion Techniques," IEEE Transactions on Microwave Theory and Techniques, vol.57, no.12, pp.3307-3314, Dec. 2009.

[39] Draxler, P., Lanfranco, S., Kimball, D., Hsia, C., Jeong, J., van de Sluis, J., Asbeck, P.M., "High Efficiency Envelope Tracking LDMOS Power Amplifier for W-CDMA," IEEE MTT-S Int. Microwave Symposium Digest, 2006, pp.1534-1537, 11-16 June 2006.

[40] Kimball, D.F., Jeong, J., Hsia, C., Draxler, P., Lanfranco, S., Nagy, W., Linthicum, K., Larson, L.E., Asbeck, P.M., "High-Efficiency Envelope-Tracking W-CDMA Base-Station Amplifier Using GaN HFETs IEEE Transactions on Microwave Theory and Techniques, vol.54, no.11, pp.3848-3856, Nov. 2006.

[41] Hanington, G., Chen, P., Asbeck, P.M., Larson, L.E., "High Efficiency Power Amplifier using Dynamic Power-Supply Voltage for CDMA Applications IEEE Transactions on Microwave Theory and Techniques, vol. 47, no.8, pp. 1471-1476, Aug. 1999.

[42] Hyerby, M.C.W. and Andersen, M.A.E., "Optimized Envelope Tracking Power Supply for Tetra2 Base Station RF Power Amplifer", IEEE Appl. Power Electron Conference, pp. 777-783, Feb 2008.

[43] Kim, J. H., Jo, G. D., Oh, J. H., Kim, Y. H., Lee, K. C., Jung, J. H., Park, C. S., "High-Efficiency Envelope-Tracking Transmitter With Optimized Class-F-1 Amplifier and 2-bit Envelope Amplifier for 3G LTE Base Station," IEEE Transactions on Microwave Theory and Techniques, vol.59, no.6, pp.1610-1621, June 2011.

[44] F.H. Raab, "Split-band modulator for Kahn-technique transmitters," 2004 IEEE MTT-S International Microwave Symposium Digest, vol.2, pp.887-890, 6-11 June 2004.

[45] Meinzer, K., "A linear transponder for amateur radio satellites," VHF Communications, vol. I, pp. 42 - 57, Jan. 1975.

[46] Wang, N., Yousefzadeh, V., Maksimovic, D., Pajic, S., Popovic, Z.B., "60% efficient 10-GHz power amplifier with dynamic drain bias control," IEEE Transactions on Microwave Theory and Techniques, vol.52, no.3, pp. 1077-1081, March 2004.

CHAPTER 3

THE BENEFIT OF GALLIUM NITRIDE IN POWER AMPLIFIER SYSTEM – THE INITIAL MEASUREMENTS

3.1 Introduction

With the growth of cellular communication services, there are a variety of RF power transistors available on the market such as the laterally diffused metal oxide semiconductor (LDMOS) field effect transistor (FET), the gallium arsenide (GaAs) metal semiconductor FET (MESFET), the silicon germanium (SiGe) heterojunction bipolar transistor (HBT) and the gallium nitride (GaN) high electron mobility transistor (HEMT) [1], [2]. In this chapter, the transistor technology of choice is GaN HEMT and this transistor technology is compared to the LDMOS transistor. Although GaN HEMT technology is not as mature as LDMOS, its competitive advantages for future high power and high frequency base station power amplifiers are the reason this RF power transistor was chosen for this research [3], [4]. LDMOS transistors account for about 90% of the RFPA world market today [5], however, with ongoing research and development of GaN HEMTs [6-8], this technology has the potential to be the solution to many existing RFPA design problems that require higher efficiency and linearity. Hence, in this chapter, the benefit of the GaN-based RFPA is further explored and compared to a well known LDMOS RFPA.

3.2 GaN and LDMOS Brief Description

As mentioned earlier, RFPAs based on LDMOS technology have been widely used in the communication industry. The LDMOS transistor's structure has a short channel length that provides a high current handling capability and low

doping on the drain side of the FET that contributes to a high blocking voltage [9], [10]. These two properties are desirable for high power RFPAs. LDMOS is a popular technology choice due to its cost advantage.

However, GaN technology represents the future for microwave power amplifiers due to its benefits in output power, efficiency and linearity. As compared to LDMOS technology, GaN is a wide bandgap material, thus it offers high breakdown voltage that enables GaN devices to operate for high voltage applications [11]. The high power density property of GaN contributes to reduced parasitic capacitance thus offering wider bandwidth in RFPA broadband matching design as compared to LDMOS. GaN's high carrier mobility also enables GaN devices to operate at higher operating frequencies [11]. All of GaN's advantages in high power broadband RFPA design have therefore attracted a large amount of recent attention, both in research and industry.

A further detailed discussion on the comparison between LDMOS and GaN transistors' structure and performance can be found in [11] and [12]. In the next section, a characteristic of GaN RFPAs is presented that has been observed by CW measurement and it is found to be absent in LDMOS RFPAs. The GaN RFPA characteristic in question is the expansive gain characteristic as we increase the drain bias supply voltage. As well as the gain characteristic measurement, the performance in terms of drain efficiency is also measured. This gain characteristic of GaN, when properly exploited, can help improve the RFPA system linearity. The analysis on linearity improvement will be discussed in Chapter 4.

3.3 The Gain Characteristic of Gallium Nitride RFPA

3.3.1 The 10W GaN Class J RFPA

The first GaN RFPA measured was the 10W GaN Class J RFPA that was designed and reported in [7]. The discrete 10W GaN HEMT device was supplied by Cree [15] and this RFPA was biased in deep Class AB region. In the CW measurement at 2 GHz, the RF power was swept at different drain

bias voltage from 16V to 28V. The output power was measured and the gain in dBs versus output power was plotted. The measurement of the GaN RFPA showed that the gain varied significantly from 8dB to 12dB as shown in Figure 3.1 [13].

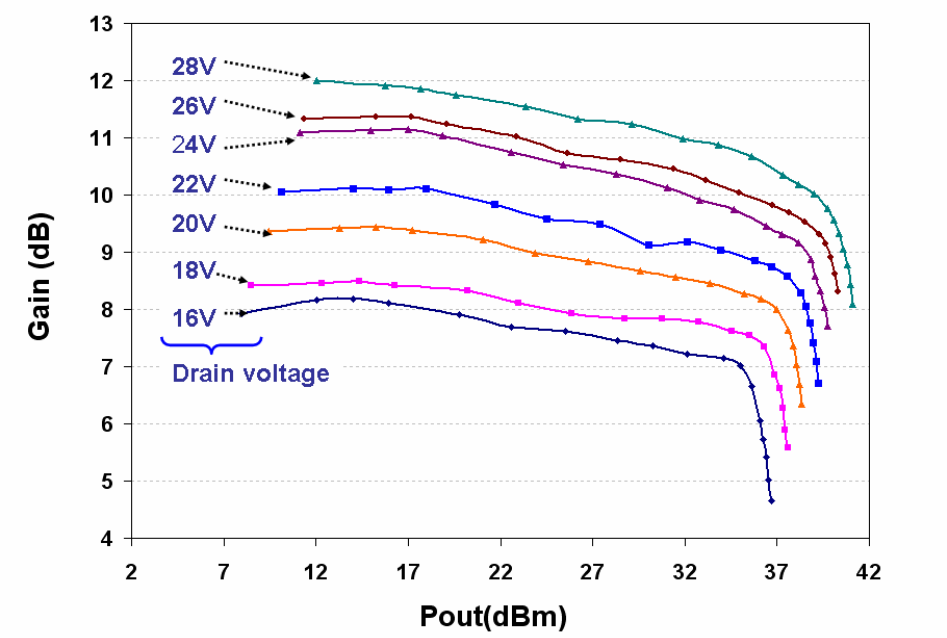

Figure 3.1: The 10W GaN Class J RFPA gain characteristic

At a drain voltage of 16V, the gain measured in linear region was around 8dB but compresses as the peak output level was reached. The gain behaviour at different drain bias voltages was similar but as the drain bias voltage was increased, the gain increased by about 0.5dB per 1V of drain bias [13].

In order to show the gain variation clearly, the gain was then plotted at a constant level of output power, 30dBm. The logarithmic gain was observed to change approximately linear with the drain bias voltage as shown in Figure 3.2. As observed in Figure 3.2, the rate of change is about 0.5dB per Volt

[13].

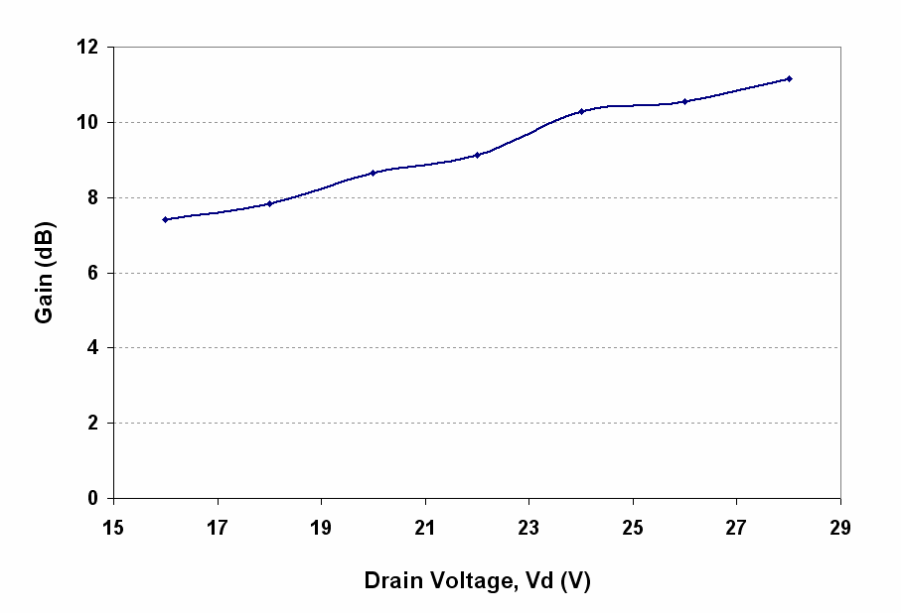

Figure 3.2: 10W GaN Class J RFPA gain characteristic at 30dBm output power

As we increase the drain voltage bias, we can also see that the drain efficiency remains high at different output powers as shown in Figure 3.3.

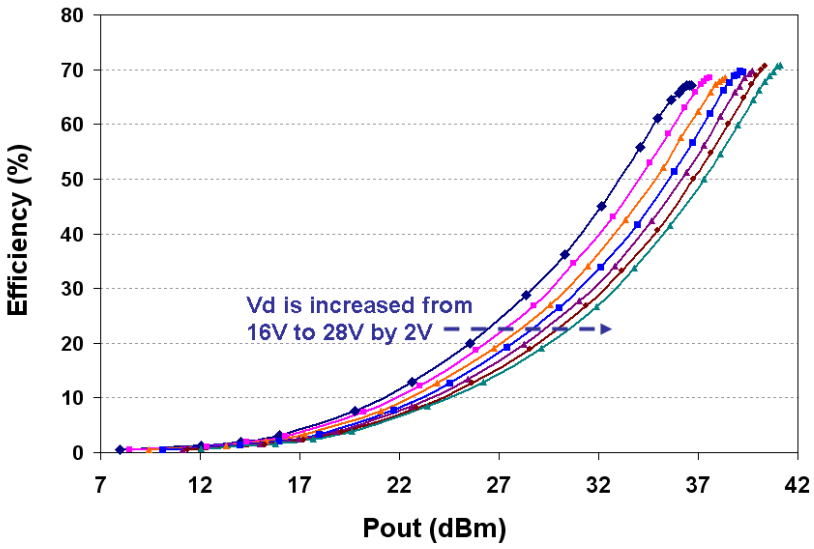

Figure 3.3: The 10W GaN Class J RFPA drain efficiency plot

3.3.2 The 10W GaN Inverse Class F RFPA

Another RFPA design employing the 10W GaN HEMT device is designed and reported in [14]. In this design, the gate bias voltage was swept with necessary fundamental and harmonic termination using load-pull system to find an optimum bias point. From the optimum gate bias, the predicted load impedances were optimized to obtain the best possible inverse Class F design.

For the CW measurements of the inverse Class F RFPA at 2 GHz, the RF power was swept at different drain bias voltage from 16V to 32V. The measurement of this GaN RFPA showed that the gain varied significantly from 11dB to 17dB, as shown in Figure 3.4.

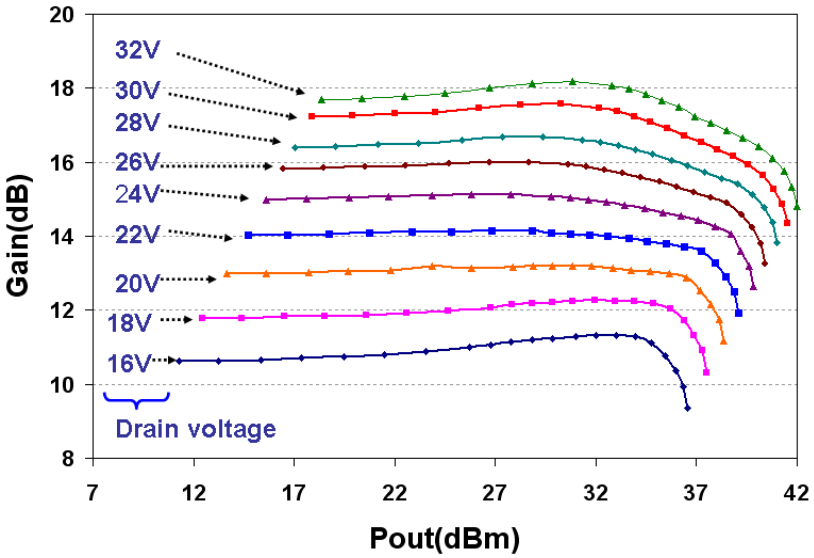

Figure 3.4: The 10W GaN Inverse Class F RFPA gain characteristic

For two different PA modes, similar gain expansion behaviour was observed for the same 10W GaN HEMT device. The drain efficiency performance for this inverse class F RFPA was also measured and the drain efficiency remained high for different output powers as shown in Figure 3.5.

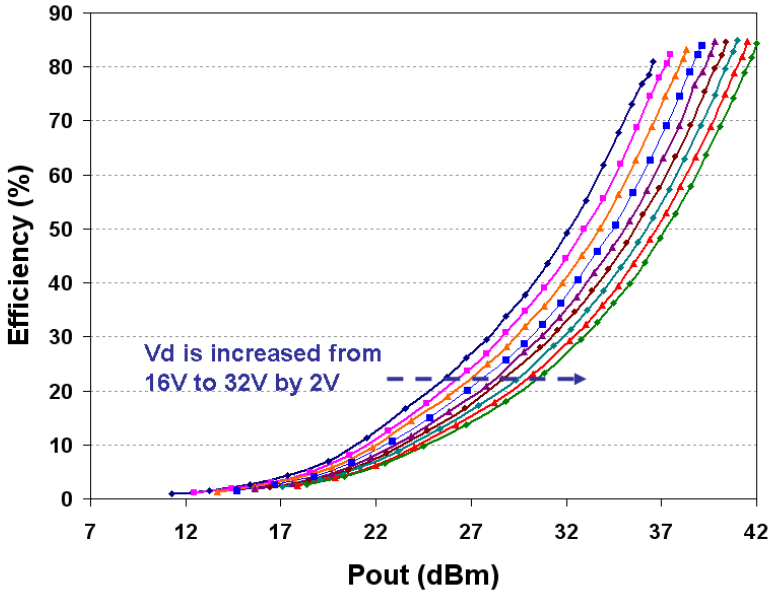

Figure 3.5: The 10W GaN Inverse Class F RFPA drain efficiency performance

3.3.3 The 25W GaN Class AB RFPA

From the observations made on both Class J and inverse Class F GaN RFPAs, the gain expansion with drain voltage increase can be of potential benefit to linearity improvement in an 'Auxiliary Envelope Tracking' (AET) system. This behaviour has led to another GaN RFPA being designed, employing a 25W GaN HEMT device from Cree [16]. The new 25W GaN RFPA has been specifically designed for the AET system operating in Class AB, and is reported in [6].

For the CW measurements made on the 25W GaN Class AB RFPA at 1.98 GHz, the RF power was swept at different drain bias voltages from 16V to 30V. The measurement of GaN RFPA showed that the gain varied significantly from 14dB to 17.5dB, as shown in Figure 3.6. For this 25W GaN HEMT RFPA, the gain expansion behaviour was consistent with the previous measurements on the 10W GaN HEMT RFPAs.

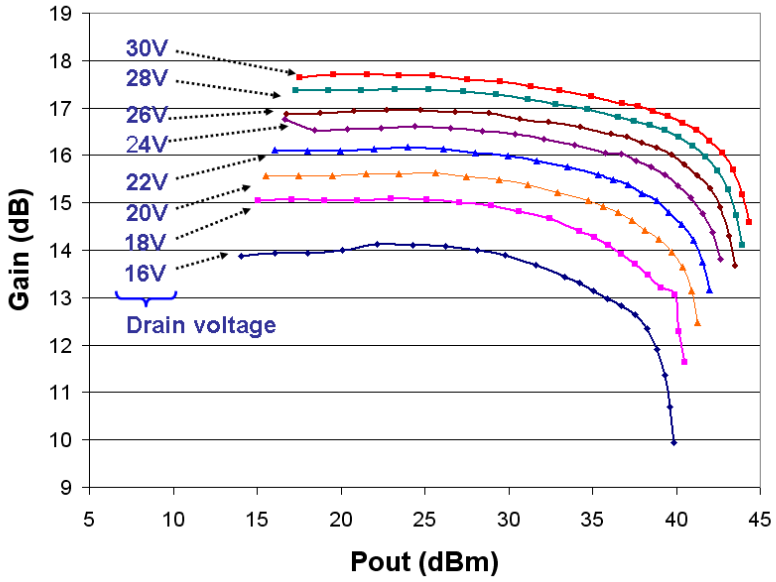

Figure 3.6: The 25W GaN Class AB gain characteristic

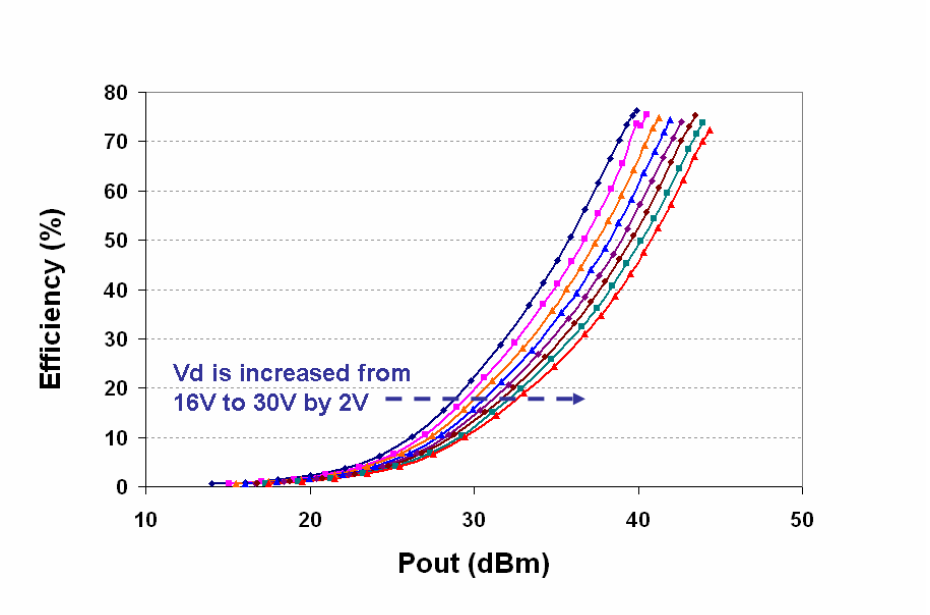

Figure 3.7: The 25W GaN Class AB RFPA drain efficiency performance

The drain efficiency performance for this 25W GaN Class AB RFPA was also measured and it can be seen in Figure 3.7 that the efficiency remains high for different output power.

3.4 The Gain Characteristic of LDMOS RFPA

3.4.1 The 20W LDMOS Class AB RF Power Amplifier

A 20W LDMOS Class AB RFPA was used for the gain characteristic comparison. The transistor has internal input matching and the RFPA was then designed for Class AB operation with external output matching network. The realised 20W LDMOS Class AB RFPA is shown in Figure 3.8.

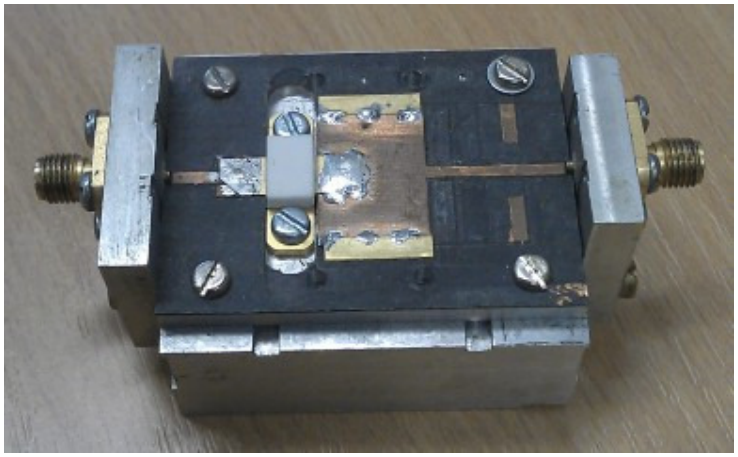

Figure 3.8: The 20W LDMOS Class AB RFPA used for the measurement

For the CW measurements at 2GHz that were made on the 20W LDMOS Class AB RFPA, the input RF power was swept at drain bias voltages from 16V to 28V. The gain measurement results are presented in Figure 3.9. The figure shows that the gain was linear but compressed towards peak output level. The gain behaviour of LDMOS RFPA was similar for all drain bias voltages. However, it was observed that the gain varied far less significantly with drain bias voltage in comparison to the GaN measurements. In order to see clearly the minimal rate of change in the gain versus drain bias voltage, the LDMOS gain was plotted at a constant level of output power, 30dBm. As shown in Figure 3.10, the gain was almost constant with the drain bias voltage [13].

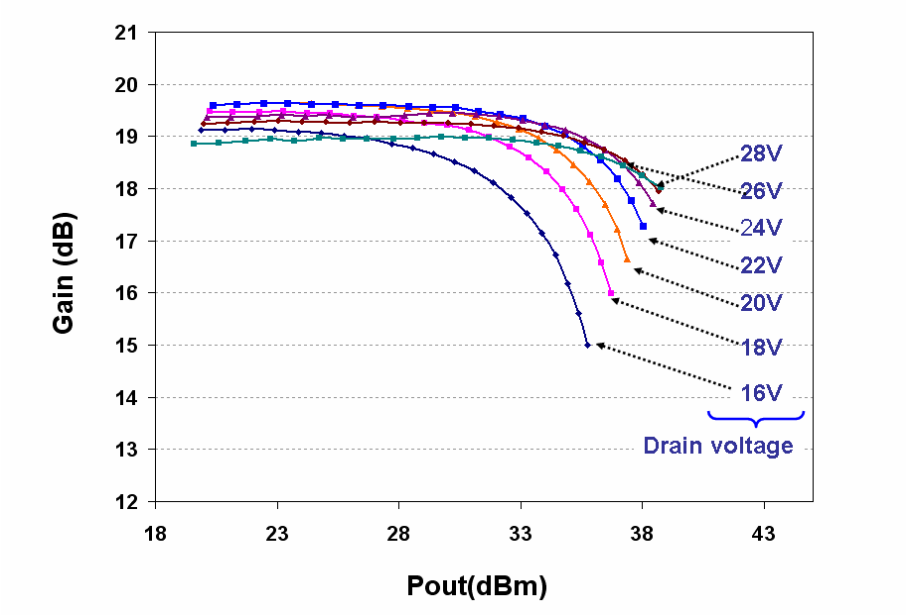

Figure 3.9: 20W LDMOS Class AB RFPA gain characteristic

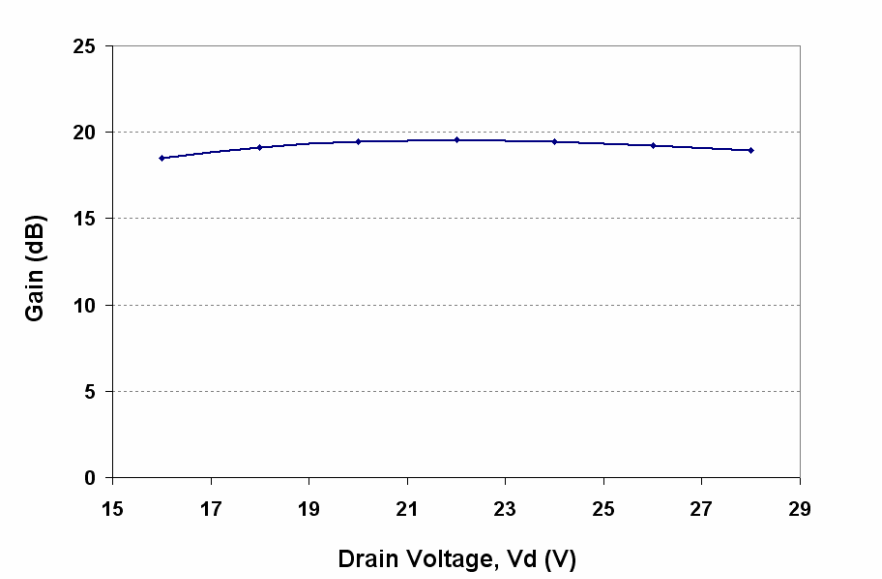

Figure 3.10: 20W LDMOS RFPA gain characteristic at 30dBm output power

The drain efficiency performance for this 20W LDMOS Class AB RFPA was also measured. From the drain efficiency performance plot, it can be observed that the drain efficiency was also increased at higher drain voltage bias and higher output powers, as shown in Figure 3.11. Note that this RFPA does not represent the latest LDMOS technology. The important trait to observe is that

the LDMOS gain characteristic does not vary significantly with drain voltage. The effect of this gain characteristic will be analysed in Chapter 4 and the measured linearity performance in terms of third-order intermodulation (IM3) distortion will be presented in Chapter 6.

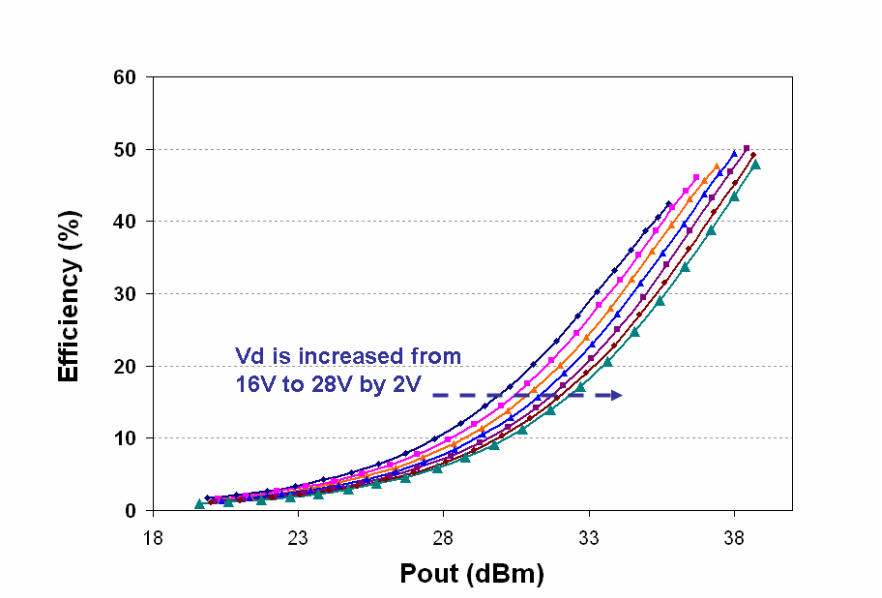

Figure 3.11: The 20W LDMOS Class AB RFPA drain efficiency performance

3.5 The GaN Device Transconductance Model

From the GaN RFPA measurements, we have seen that the gain increases as the drain voltage increases. This is an important GaN trait and has potential benefits for the RFPA design. Hence, we study the transconductance model provided by Cree for the 25W GaN device [16]. From basic electronics theory, we recognise that the gain of a transistor is a function of its transconductance. Hence, this 25W GaN HEMT model is simulated using Agilent's Advanced Design System (ADS) software to investigate if the variation of gain is the result of variation in transconductance value for a constant input signal. From the AC simulation results, we found that the transconductance value increases as the drain voltage increases. The simulation is done at 2GHz and the quiescent drain current is at 10% of the saturation drain current. These bias settings are chosen to be consistent with the previous GaN RFPA measurement settings. The transconductance simulation plot is shown in Figure 3.12. From this plot we can see that the

transconductance value is increased from 2.32 at a drain bias voltage of 16V to 5.15 at a drain bias voltage of 28V. This is a significant increase and this variation in the transconductance affects the gain of the designed RFPA.

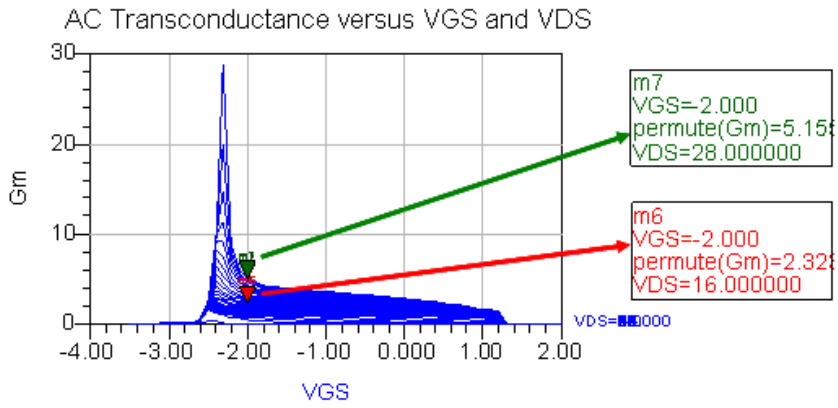

Figure 3.12: The AC transconductance of the 25W GaN RFPA device

3.6 Chapter Summary

In this chapter, RFPAs from two device technologies were measured and compared. From the CW measurement of three GaN RFPAs; 10W Class J RFPA, 10W Inverse Class F RFPA and 25W Class AB RFPA, the RFPAs have shown a substantial gain variation with the drain voltage has been shown. Another set of CW measurements was made on LDMOS RFPA, and there was no significant gain variation observed as the drain voltage was varied. A set of simulations was also performed using a model of the GaN transistor, and it was observed that the transconductance increased as the drain voltage increased. All of these initial measurements and simulations on the GaN RFPAs showed an important characteristic of the GaN transistor that, as later chapters will show, can lead to linearity improvements.

3.7 Reference

[1] F Raab et al, “RF and Microwave Power Amplifier and Transmitter Technologies – Part 1, ” High Frequency Electronics, pp. 34 – 48, 2003.

[2] Mishra, U.K., Parikh, P., Wu, Y.F., "AlGaN/GaN HEMTs: An overview of device operation and applications" [Online]. Available: http://my.ece.ucsb.edu/mishra/classfiles/overview.pdf

[3] "GaN Essentials: Application Notes", [Online]. Available: http://www.nitronex.com/ganessentials.html

[4] Vassilakis, B., Storniolo, J., Monroe, J., "High Efficiency Base Station Amplifier Architectures Utilizing LDMOS and GaN High Power Transistors", CS MANTECH Conference, May 18th-21st, 2009, Tampa, Florida, USA

[5] "GaN RF Market Analysis" [Online]. Available: http://www.i-micronews.com/upload/Rapports/GaN%20RF%20flyer%20nv%20prix.pdf

[6] Yusoff, Z., Lees, J., Benedikt, J., Tasker, P.J., Cripps, S.C., "Linearity improvement in RF power amplifier system using integrated Auxiliary Envelope Tracking system," IEEE MTT-S International Microwave Symposium Digest, 2011, vol., no., pp.1-4, 5-10 June 2011

[7] Wright, P., Lees, J., Tasker, P.J., Benedikt, J., Cripps, S.C., "An Efficient, Linear, Broadband Class-J-Mode PA Realised Using RF Waveform Engineering", IEEE/MTT-S International Microwave Symposium Digest, 7-12 June 2009, pp. 653-656.

[8] Akmal, M., Lees, J., Bensmida, S., Woodington, S., Carrubba, V., Cripps, S., Benedikt, J., Morris, K., Beach, M., McGeehan, J., Tasker, P., "The Effect of Baseband Impedance Termination on the Linearity of GaN HEMTs," 40th European Microwave Conference, 2010.

[9] Zeghbroeck, B.V., "Principles of Semiconductor Devices", [Online]. Available: http://ecee.colorado.edu/~bart/book/book/chapter7/ch7_8.htm#7_8_1

[10] "LDMOS", Microwave 101 Website, [Online]. Available: http://www.microwaves101.com/encyclopedia/LDMOS.cfm

[11] Nuttinck, S.; Gebara, E.; Laskar, J.; Rorsman, N.; Olsson, J.; Zirath, H.; Eklund, K.; Harris, M.; , "Comparison between Si-LDMOS and GaN-based microwave power transistors," *High Performance Devices, 2002. Proceedings. IEEE Lester Eastman Conference on* , vol., no., pp. 149- 154, 6-8 Aug. 2002

[12] Vassilakis, B., Cova, A, "Comparative analysis of GaAs/LDMOS/GaN high power transistors in a digital predistortion amplifier system," Microwave Conference Proceedings, 2005. APMC 2005. Asia-Pacific Conference Proceedings , vol.2, no., pp. 4 pp., 4-7 Dec. 2005

[13] Yusoff, Z., Akmal, M., Carrubba, V., Lees, J., Benedikt, J., Tasker, P.J., Cripps, S.C., "The benefit of GaN characteristics over LDMOS for linearity improvement using drain modulation in power amplifier system," 2011 Workshop on Integrated Nonlinear Microwave and Millimetre-Wave Circuits (INMMIC), vol., no., pp.1-4, 18-19 April 2011.

[14] Wright, P., Sheikh, A., Roff, C., Tasker, P.J., Benedikt, J., "Highly efficient operation modes in GaN power transistors delivering upwards of 81% efficiency and 12W output power," 2008 IEEE MTT-S International Microwave Symposium Digest, 15-20 June 2008, pp.1147-1150.

[15] "CGH 40010, 10W, RF Power GaN HEMT Datasheet" [Online]. Available: http://www.cree.com/products/pdf/CGH40010.pdf

[16] "CGH 40025, 25W, RF Power GaN HEMT Datasheet" [Online]. Available: http://www.cree.com/products/pdf/CGH40025.pdf

CHAPTER 4

THE CONCEPT OF AUXILARY ENVELOPE TRACKING

4.1 Introduction

The concept of 'Auxiliary Envelope Tracking' (AET) in a power amplifier system is derived from an efficiency enhancement technique called 'Envelope Tracking' (ET). The ET technique has been outlined and its distinction to the AET system is also summarised in Chapter 2. In this chapter, the mathematical analysis of the efficiency and linearity enhancement of the AET system is presented.

4.2 The AET Concept for Linearity

The concept of using AET to improve linearity was motivated by observing the gain characteristic of a GaN HEMT power device [1]. In this section, the 25W GaN HEMT Class AB RFPA gain performance data that has been presented in Chapter 3 is used in the analysis. The three-dimensional presentation of the RFPA's gain versus output powers and drain voltages is shown in Figure 4.1

As shown in the previous chapter (Figure 3.2), at a constant output power, the logarithmic gain was observed to change approximately linearly with the drain bias voltage. This positive gradient of gain is the basic property that is used here to improve the third-order intermodulation (IM3) distortion. It can be quantified by fitting the measured gain variation to a logarithmic function. After extrapolation and equation fitting, the gain, g_1 relationship is represented by equation (4.1) and this equation corresponds to Figure 4.2.

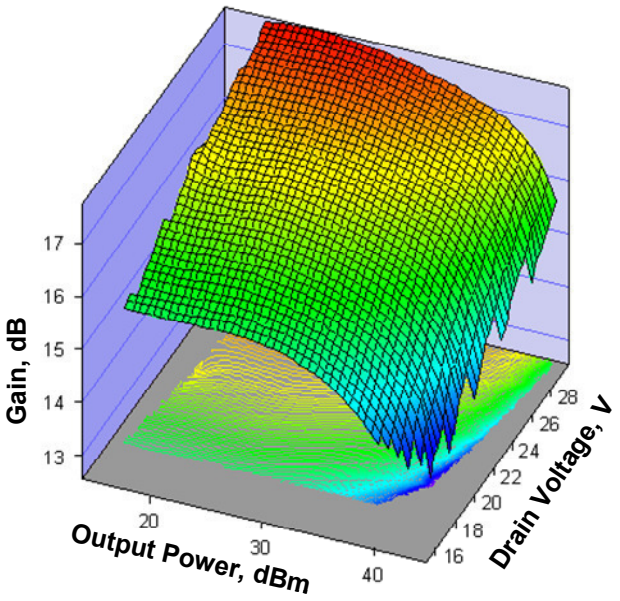

Figure 4.1: Gain performance over varying drain voltages

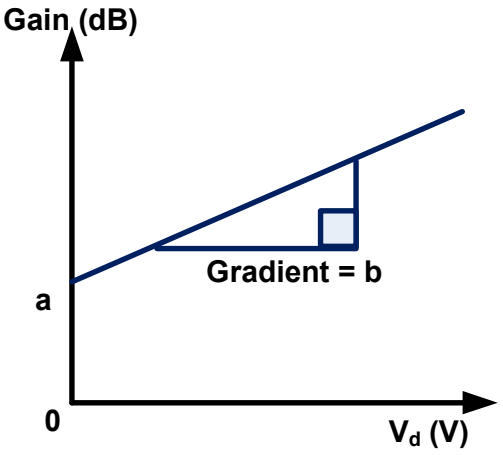

Figure 4.2: Gain variation in decibel scale at a constant output power

$$g_1 = a + bV_d \quad \text{(dB)}. \tag{4.1}$$

On a linear scale, the gain, g_1 will have an exponential variation with drain voltage, *Vd*, as in the expression (4.2) below, where where α and β are the constants extracted from the decibel scale measurements a and b.

$$g_1 = \alpha \exp\left(\beta V_d\right). \tag{4.2}$$

We assume that the GaN HEMT device has a non-linear transfer characteristic of (4.3) and that the drain voltage, V_d is tracking the envelope of input signal, v_{in} (4).

$$i_o = g_1 v_{in} + g_2 v_{in}^2 + g_3 v_{in}^3 + \ldots \tag{4.3}$$

$$V_d = \delta v_{in}. \tag{4.4}$$

Next, we substitute equation (4.4) into (4.2) and replace g_1 in (4.3) with the resulting equation. We expand the equation using an exponential series and truncate it at the third order terms. The output current, i_o, will be [1];

$$i_o = \alpha\left(1 + \beta\delta v_{in} + \frac{\left(\beta\delta v_{in}\right)^2}{2!} + \frac{\left(\beta\delta v_{in}\right)^3}{3!}\right) v_{in} + g_2 v_{in}^2 + g_3 v_{in}^3. \tag{4.5}$$

$$i_{o3} = \left(\frac{\alpha\beta^2\delta^2}{2} + g_3\right) v_{in}^3. \tag{4.6}$$

Since the source of IM3 distortion is caused primarily by the third order component (equation (4.6)), the tracking voltage characteristic opens up the possibility for cancelling the IM3 product. This can be done by choosing an appropriate value of δ given that g_3, the third-degree constant from the non-linear equation is usually negative [2]. The values of α and β are derived from the gain variation behaviour of the GaN device. Note that also, since the GaN device showed an expansive gain variation, the value of α is always positive and for any value of β its square is always positive.

More simply stated, the inherent device compression characteristic can be cancelled by the expansive gain that is provided by the increasing drain

voltage. This offers a linearising approach that requires an increasing supply voltage at higher drive levels and a decreasing supply voltage at lower drive levels. In the AET system, the modulated signal used for drain bias has the potential to linearise the RFPA with little or no overall efficiency degradation.

4.3 The AET Concept for Efficiency

In a conventional ET or EER system, the envelope amplifier (EA) or tracking generator's power dissipation is very critical. The overall drain efficiency of the ET system is the product of the envelope amplifier drain efficiency and the RFPA drain efficiency as shown in equation (4.7)[3].

$$\eta_{OVERALL} = \eta_{envelope.amplifier} \times \eta_{RF.power.amplifier} \tag{4.7}$$

In the AET technique however, the EA design requirement is eased by separating the AC component of the envelope tracking signal from the DC component. The separately generated AC component of the tracking voltage is thus superimposed on a fixed DC bias to form the AET tracking signal, which is supplied to the drain of the RFPA.

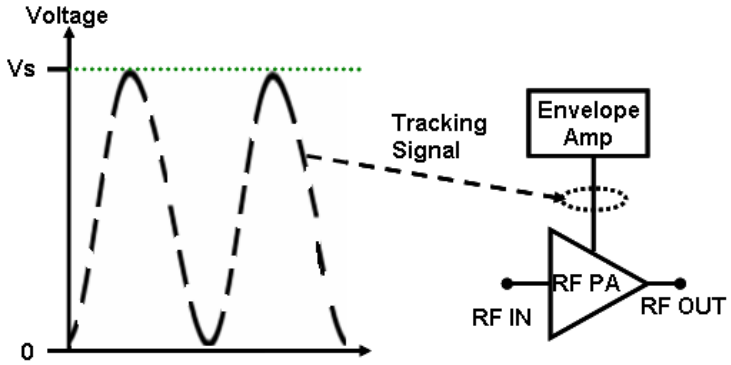

Figure 4.3: The 2-carrier signal envelope tracking

Since the AC component of the tracking voltage is very much smaller than the DC, the overall power consumption will be quite small. As an example, a 2-carrier signal envelope tracking system is shown in Figure 4.3. The tracking

signal is an ideal sinusoidal signal from 0V to V_S. Assuming the RFPA presents as a resistive load, R_L, then the DC component of the tracking signal has the voltage of $\frac{V_S}{2}$, and its power is $\frac{V_S^2}{4R_L}$. For the AC component of the tracking signal, the peak-to-peak amplitude of the sinusoidal is V_S, therefore, its power is $\frac{V_S^2}{8R_L}$. The total power is $\frac{3V_S^2}{8R_L}$. Therefore, the AC component of the tracking signal power consumption is only $\frac{1}{3}$ of the total power.

This calculation can be repeated for a more complex, representative, signal envelope as shown in Figure 4.4, which is a burst of WCDMA signal with 9.17dB PAR.

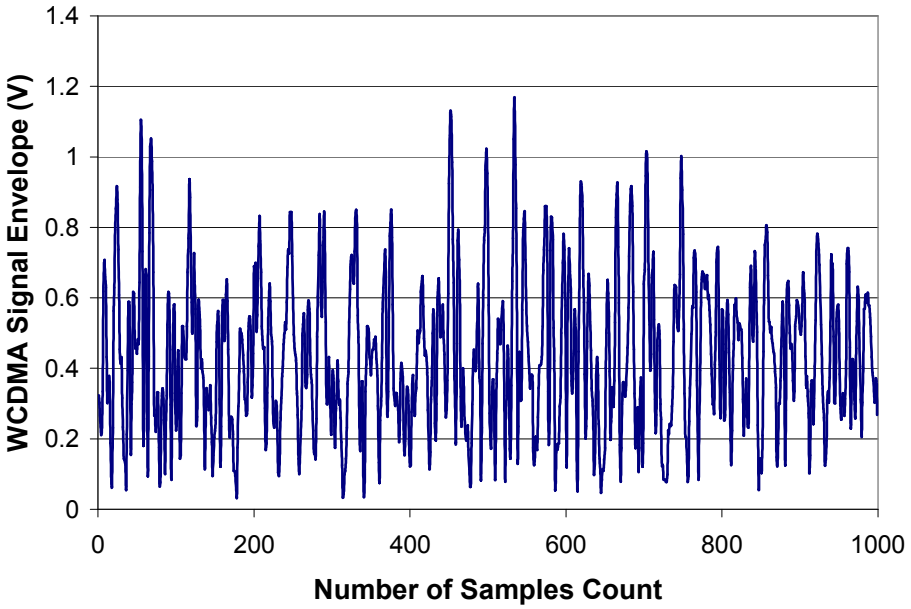

Figure 4.4: The WCDMA signal envelope with 9.17dB PAR.

If we assume that the RFPA supply tracks this envelope perfectly, and that the RFPA is operating in Class B mode, the supply current will also track the envelope amplitude function. If the envelope function is defined to be *env(nτ)*, where *n* is the sample count and *τ* is the sample interval, then the 'DC' component of the supplied voltage , V_{dc} and the supplied current, I_{dc}, are given by

$$I_{dc} = V_{dc} = \frac{1}{N}\sum\nolimits_{N} env(n\tau). \tag{4.8}$$

The total power, P_{total}, supplied is given by

$$P_{total} = \frac{1}{N}\sum\nolimits_{N} \{env(n\tau)\}^2 \tag{4.9}$$

In the case of the WCDMA burst shown in Figure 4.4, this can be calculated to have the following values;

$$P_{dc}=0.146,\ P_{total}=0.183,$$

so that the ratio of the AC component to the total power supplied is about 1 to 5, or 20%. This calculation also assumes that the tracking voltage will extend over the whole envelope range, and for AET, this will usually not be the case; reducing the range over which the envelope is tracked will further increase this ratio. This is a highly significant result, and means that if the tracking voltage supply is split into its constituent DC and AC components, only the AC component requires a 'converter'. The impact of the efficiency of this converter will be correspondingly reduced as compared to conventional ET systems, which generate the entire tracking signal as a single entity.

This can be illustrated quantitatively by considering the total power supplied to the RFPA in the cases of ET and AET. In the ET case, the total supplied power is;

$$P_{ET} = \frac{P_{total}}{\eta_{converter}}\ . \tag{4.10}$$

Whereas in the AET case, the total power supplied is;

$$P_{AET} = P_{dc} + \frac{\left(P_{total} - P_{dc}\right)}{\eta_{converter}} \quad . \tag{4.11}$$

The overall efficiency for ET system can therefore be expressed in the form;

$$\eta_{ET} = \frac{P_{total}}{P_{ET}} \eta_{peak} = \eta_{converter} \times \eta_{peak} \text{ (as (4.7))}.$$

Whereas in the AET case, the overall efficiency is;

$$\eta_{AET} = \frac{P_{total}}{P_{AET}} \eta_{peak} \, , \tag{4.12}$$

where P_{AET} is given in equation (4.11), and η_{peak} is the peak efficiency of the RFPA.

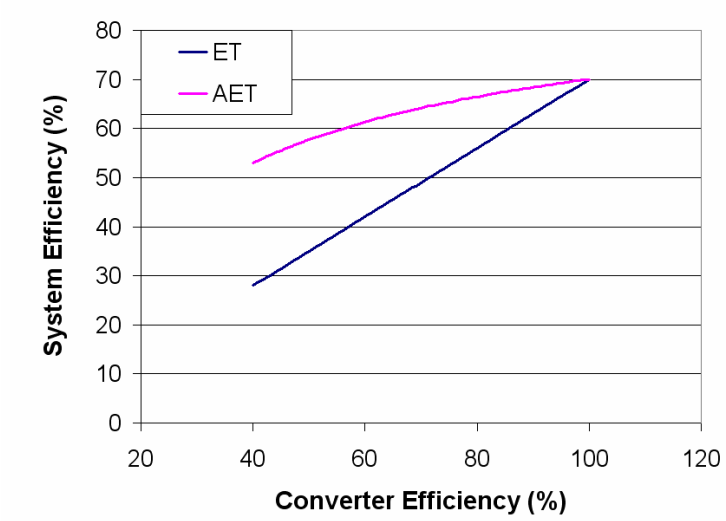

Figure 4.5: System efficiency of AET and ET

Figure 4.5 shows how the proposed AET system has a lower dependency on the efficiency of the tracking generator as compared to the ET system; so much so that in principle a simple linear baseband amplifier can be used to generate the AC component.

4.4 Envelope Simulations on AET Efficiency

4.4.1 Introduction

From the analysis on the AET efficiency above, we further investigate the impact of the converter or the tracking generator on the system efficiency by running WCDMA signal simulation on the CW measured data of the 25W GaN Class AB RFPA. From the RFPA CW measurement at 1.98GHz, the output power, the drain current and the drain voltage were measured. From this measured data, the correlation between the drain current and the input power was derived. This correlation is required to simulate the required drain current for a modulated WCDMA signal that has 6.06dB peak-to-average ratio (PAR). The correlation between the input and output power is also derived from this measured data in order to simulate the RF output power from the WCDMA input signal data.

4.4.2 CW Measurement of the 25W GaN Class AB RFPA

The CW measurements were performed at two different gate biases. The first gate bias voltage was -2.97V giving a quiescent drain current, I_{DQ} of 300mA. This quiescent current is 5% of the saturation drain current. The second gate bias was -2.56V giving a quiescent drain current, I_{DQ} of 750mA. This quiescent current is 12.5% of the saturation drain current. The drain bias voltage was 28V. In this measurement, the output power and drain current were measured. The drain efficiency performance of this RFPA is shown in Figure 4.6. The peak efficiency when I_{DQ} was 300mA was 72% while the peak efficiency for an I_{DQ} of 750mA was 66%.

From the drain current versus input power plot of Figure 4.7, the trend line derivation of the curves was performed using Microsoft Excel. The equation for drain current versus input power at I_{DQ} of 300mA is as follows:

$$I_d = -2\times10^{-7}P_{in}^{\ 5} + 1\times10^{-5}P_{in}^{\ 4} - 1\times10^{-4}P_{in}^{\ 3} + 7\times10^{-4}P_{in}^{\ 2} - 3\times10^{-3}P_{in} + 0.2877 \quad (4.13)$$

The equation for drain current versus input power at I_{DQ} of 750mA is as follows:

$$I_d = -2\times10^{-6}P_{in}^{\ 4} + 2\times10^{-4}P_{in}^{\ 3} - 4\times10^{-3}P_{in}^{\ 2} + 1.77\times10^{-2}P_{in} + 0.7374 \quad (4.14)$$

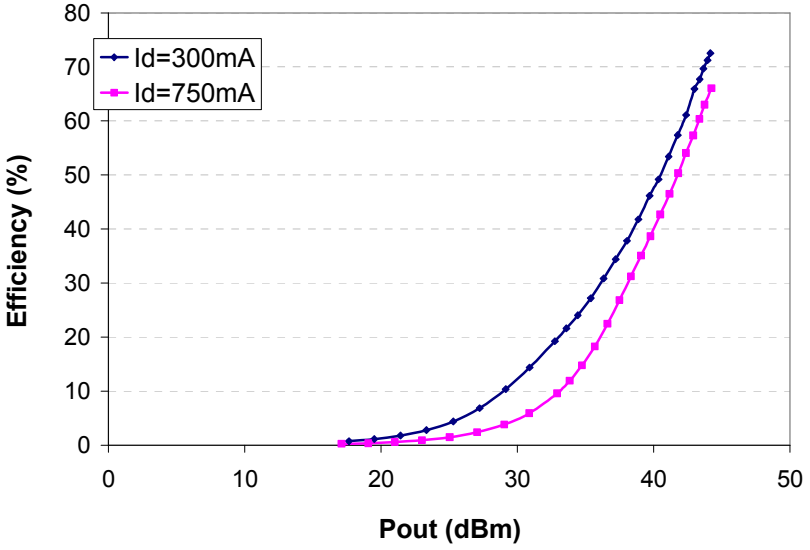

Figure 4.6: The drain efficiency performance for two gate biases

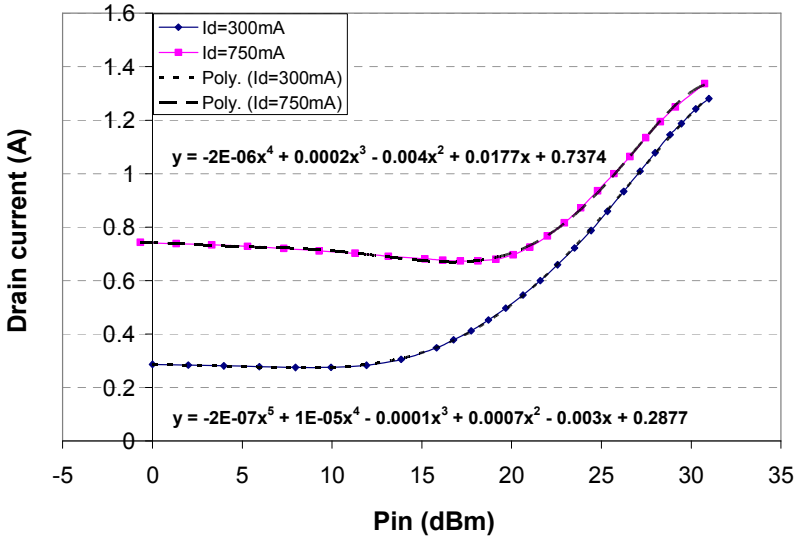

Figure 4.7: The correlation between the drain current and the input power of the RFPA.

The measured output power versus input power relationship of the RFPA is plotted in Figure 4.8. The trend line of the curves on this relationship between input and output is also derived.

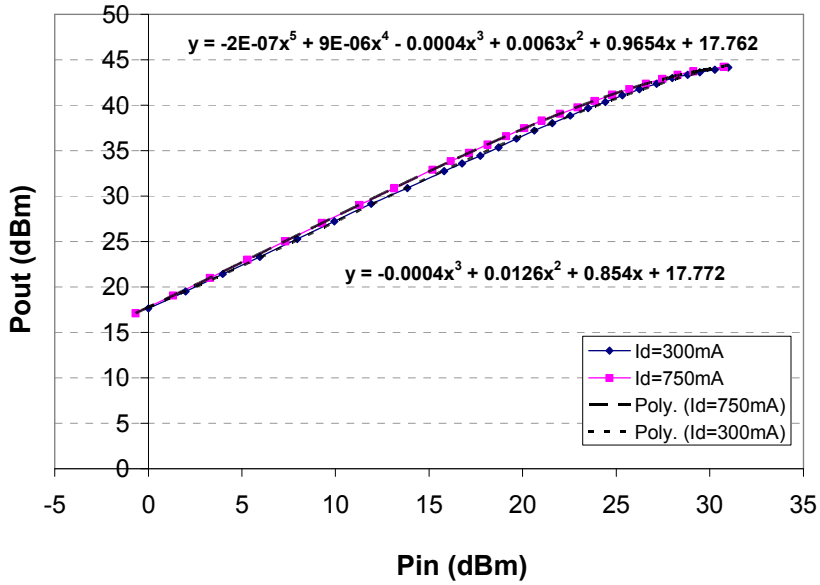

Figure 4.8: The output power versus input power performance of the RFPA

For I_{DQ} of 300mA, the equation is;

$$P_{out} = -4\times10^{-4}P_{in}^{\ 3} + 1.26\times10^{-2}P_{in}^{\ 2} + 0.854P_{in} + 17.772, \qquad (4.15)$$

and for I_{DQ} of 750mA, the equation is;

$$P_{out} = -2\times10^{-7}P_{in}^{\ 5} + 9\times10^{-6}P_{in}^{\ 4} - 4\times10^{-4}P_{in}^{\ 3} + 6.3\times10^{-3}P_{in}^{\ 2} + 0.9654P_{in} + 17.762 \qquad (4.16)$$

4.4.3 WCDMA Envelope Simulation

The WCDMA envelope signal is calculated from in-phase (I) and quadrature (Q) signals using equation (4.17) as follows;

$$env = sqrt(I^2 + Q^2). \qquad (4.17)$$

Then, by assuming the impedance is normalized to 1, the RF input power is equal to equation (4.18),

$$P_{in} = env_{in}^2 . \quad (4.18)$$

By using equation (4.13) and (4.14), the drain current for the corresponding input power is derived. For RF output power derivation for corresponding input power, equation (4.15) and (4.16) are used. The drain current for both gate biases for this WCDMA signal are plotted in Figure 4.9. Note that the total sample count for this measurement is 5123 and the plots in the figure only show 2000 samples for viewing purposes.

From Figure 4.9, the drain current swing for I_{DQ} of 300mA is observed to be slightly larger than the drain current swing for I_{DQ} of 750mA. This is because 300mA quiescent point is closer to Class B mode as compared to drain quiescent current of 750mA, and therefore the gate voltage swing is higher to maintain peak current [4].

At this point; RF input power, RF output power and drain current have been simulated. For ET and AET operation, the drain bias voltage of the RFPA is the tracking voltage that is derived from the WCDMA envelope signal. Therefore the drain bias voltage has the same wave shape as the envelope of the WCDMA signal. The plot of the drain bias voltage for ET/AET operation is shown in Figure 4.10. In this particular example, the tracking drain bias voltage is amplified to give a tracking amplitude of 12.7V where the maximum tracking drain bias voltage is 28V. This is the same voltage as the fixed drain bias voltage used for the CW measurement of the RFPA presented in section 4.4.1. The 28V drain bias voltage is also used for simulating the RFPA performance using WCDMA signal at fixed drain bias.

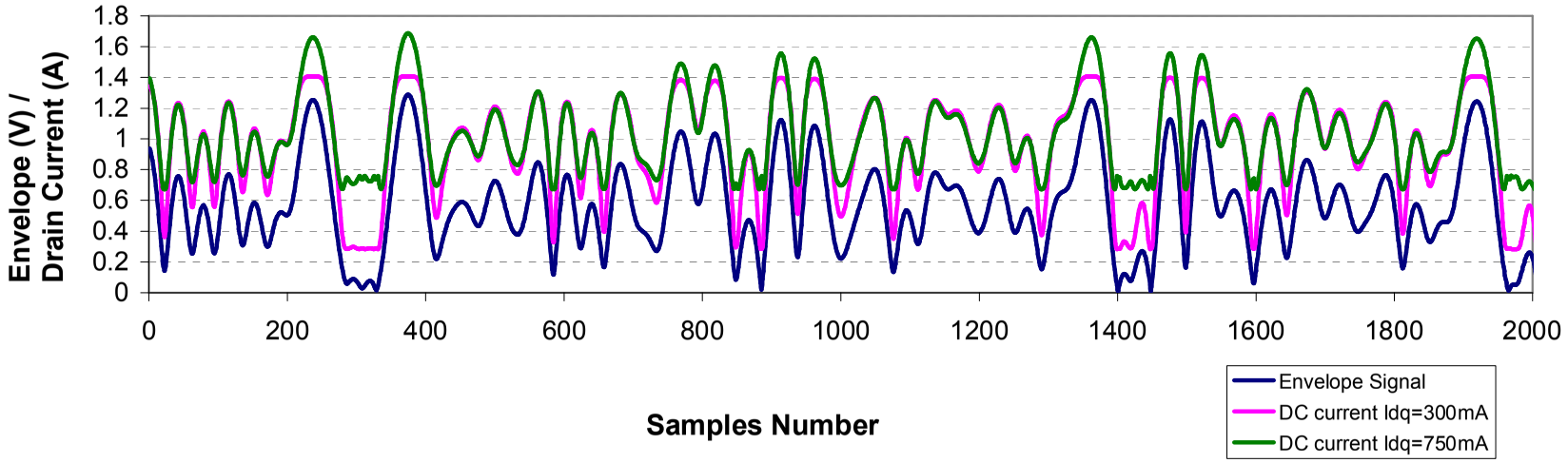

Figure 4.9: The drain current, I_d and WCDMA envelope signal

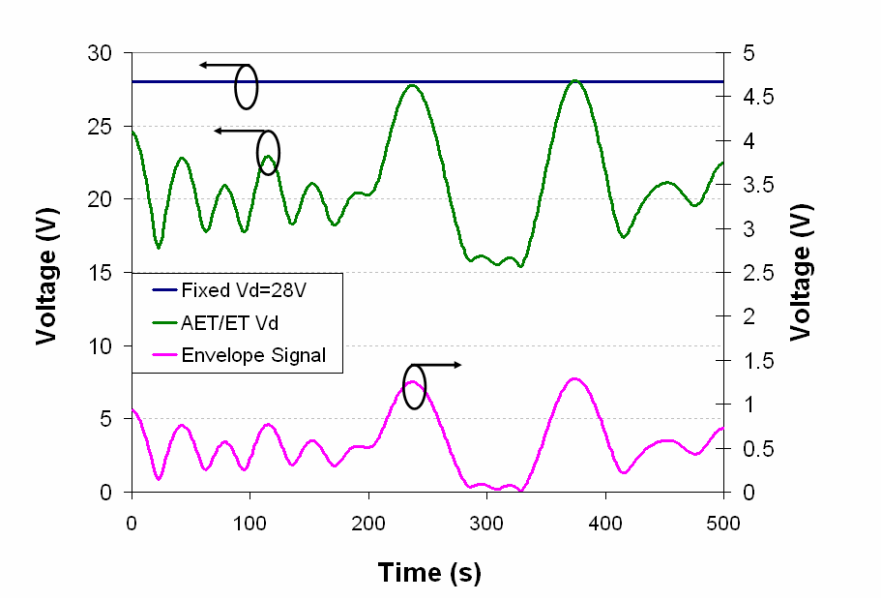

Figure 4.10: The drain bias voltage and the envelope signal

Using the equations analysed in the section 4.3, the simulated performance results for the RFPA biased at I_{DQ} of 300mA and 750mA are summarised in Table 4.1, Table 4.2 and Table 4.3.

I_{DQ} (mA)	Average Output Power (W)	Average DC Power (W)	Max Output Power (W/dBm)	Average Efficiency (%)
300mA	12.57	27.54	31.47/44.97	45.62
750mA	13.37	29.32	30.03/44.78	45.59

Table 4.1: The WCDMA average efficiency performance for fixed drain bias at 28V.

In Table 4.1, the average efficiency of the RFPA with a WCDMA signal for fixed drain bias is simulated. The average efficiency is calculated using the equation (4.19) as follows;

$$\eta_{avg} = \frac{P_{RFavg}}{P_{DCavg}} . \quad (4.19)$$

The average RF power, P_{RFavg} is calculated using equations (4.15) and (4.16). The average DC power is calculated using equation (4.20), where the drain current is calculated from equation (4.13) and (4.14) for I_{DQ} of 300mA and 750mA respectively.

$$P_{DCavg} = \frac{\sum_{0}^{N} (V_d \times I_d)}{N} . \quad (4.20)$$

In (4.20), N is the number of samples for the WCDMA signal and V_d is the fixed drain bias voltage of 28V.

From Table 4.1, the average efficiency simulated for I_{DQ} of 300mA is 45.62% while for I_{DQ} of 750mA is 45.59%. The results for both bias are encouraging, as the change in the gate bias results in only a slight change to the average efficiency. However, in this simulation, we are assuming that the RFPA neglects any memory effect caused by the characteristic of a modulated WCDMA signal with high PAR and wide signal bandwidth.

I_{DQ} (mA)	**P_{total} (W)**	**Converter Efficiency (%)**	**P_{ET} (W)**	**RFPA Peak Efficiency (%)**	**Overall ET System Efficiency (%)**
300mA	21.49	50	42.98	72	36.0
750mA	22.69	50	45.38	66	33.0
300mA	21.49	70	30.70	72	50.4
750mA	22.69	70	32.42	66	46.2

Table 4.2: The simulation of drain efficiency in ET system

In Table 4.2, the drain efficiency for the ET system is calculated using equation (4.7) while the total supplied power, P_{total}, and ET supplied power, P_{ET}, are calculated from equations (4.9) and (4.10). In this simulation, the

converter drain efficiency is considered for two cases. The first is when the converter drain efficiency is 50% and the second is when the converter drain efficiency is 70%. The RFPA peak efficiency values are taken from the CW measurements. From Table 4.2, it can be seen that the ET system efficiency with higher quiescent current is lower than the ET system efficiency with lower quiescent current. However, for the same gate bias, as we increase the converter efficiency, the ET system efficiency is improved.

I_{DQ} (mA)	P_{total} (W)	Pdc (W)	Pac (W)	Converter Efficiency (%)	P_{AET} (W)	RFPA Peak Efficiency (%)	AET System Efficiency (%)
300mA	21.49	20.68	0.82	50	22.31	72	69.4
750mA	22.69	22.00	0.69	50	23.38	66	64.1
300mA	21.49	20.68	0.82	70	21.84	72	70.8
750mA	22.69	22.00	0.69	70	22.99	66	65.2

Table 4.3: The simulation of drain efficiency for AET system

As explained in section 4.3, the concept of AET is to separate the generation of the DC and AC parts of the drain bias voltage, therefore, the simulation to find the DC and AC components of supplied power was performed. In this simulation, the total power supplied, P_{total} and AET supplied power, P_{AET} are calculated using equation (4.9), and (4.11). The DC component of power supplied, P_{dc} and AC component of power supplied, P_{ac} are calculated using equation (4.21) and (4.22) where V_{dc} and I_{dc} are initially calculated from equation (4.8). Finally, the AET system efficiency is calculated using equation (4.12).

$$P_{dc} = V_{dc} \times I_{dc} \tag{4.21}$$

$$P_{ac} = P_{total} - P_{dc} \tag{4.22}$$

The results from this simulation that are shown in Table 4.3 demonstrate that the AET system efficiency is lower when the drain quiescent current, I_{DQ} is increased and that for the same gate bias, the AET system has higher efficiency when converter efficiency is higher. This is consistent with the ET system however, the AET system is much better than the ET system in terms of its system efficiency.

4.5 Chapter Summary

In this chapter, the concept of AET is explored in detail. The contribution of GaN gain characteristics to RFPA linearity improvement was explained analytically. The key concept of separating the DC and AC component of supplied power to the RFPA leads to the efficiency improvement of the AET system. This efficiency improvement has been demonstrated mathematically by using the example of a two-carrier signal. The AET system efficiency analysis is further explored through WCDMA signal simulations. The simulations compare the RFPA when operated at a fixed voltage supply, with the ET system and also with the AET system. The simulated system efficiencies show that the AET system has potential to be the preferred method in efficiency enhancement.

4.6 Reference

[1] Yusoff, Z., Lees, J., Benedikt, J., Tasker, P.J., Cripps, S.C., "Linearity improvement in RF power amplifier system using integrated Auxiliary Envelope Tracking system," IEEE MTT-S International Microwave Symposium Digest, 2011, vol., no., pp.1-4, 5-10 June 2011.

[2] Cripps, S., “RF Power Amplifier for Wireless Communications”, Norwood, MA: Artech House, Apr. 1999.

[3] Wang, F., Kimball, D., Popp, J., Yang, A., Lie, D.Y.C, Asbeck, P., Larson, L., “Wideband envelope elimination and restoration power amplifier with high efficiency wideband envelope amplifier for WLAN 802.11g applications," IEEE MTT-S Int. Microwave Symposium Digest, 2005, vol., no., pp. 4 pp., 12-17 June 2005

[4] R. Gilmore and L. Besser, “Practical RF Circuit Design for Modern Wireless Systems Volume II - Active Circuits and Systems: Active Circuits and Systems”, Norwood, MA: Artech House, 2003.

CHAPTER 5

DESIGN OF THE 25W GALLIUM NITRIDE CLASS AB RF POWER AMPLIFIER

5.1 Introduction

The initial measurements of a 10W GaN Class J RFPA [1] have shown that the gain of the GaN RFPA varies with drain voltage. The gain variation behaviour of this GaN RFPA has been discussed in Chapter 3 and it can be exploited to improve the linearity of the RFPA using the AET technique. The concept of the AET technique, that can improve both linearity and efficiency has been presented analytically in Chapter 4. Experimental measurements using two-carrier and WCDMA signals were carried out to validate the AET analysis. A specially designed RFPA for the AET application has been realized to be used for the AET measurements, and the design and fabrication of this RFPA is presented in this chapter.

5.2 RFPA Design Consideration

When designing the power amplifier, some initial design considerations have to be taken into account before doing any simulation or fabrication. The first step is to choose the device to be used, in which the power rating, operating frequency and the transistor technology are determined. The second step is to choose the RFPA mode of operation and the operating bias condition. The third step is to check the device stability at the operating frequency of interest. All these steps are necessary in any RFPA design.

5.2.1 The 25W GaN High Electron Mobility Transistor (HEMT)

For the RFPA design, the 25W GaN HEMT (CGH40025) from Cree is chosen. As mentioned in the datasheet of Appendix B, this 25W GaN HEMT offers a typical operating voltage of 28V and maximum drain voltage of 84V.

This makes it suitable for AET, where the drain of the HEMT is supplied with modulated signal i.e. varying drain voltage. This HEMT also offers good performance in terms of efficiency, gain and bandwidth. The nonlinear device model that is provided by Cree was used in the non-linear simulator ADS, the computer-aided design (CAD) tool from Agilent. The DC-IV characteristics of this HEMT were simulated and are shown in Figure 5.1.

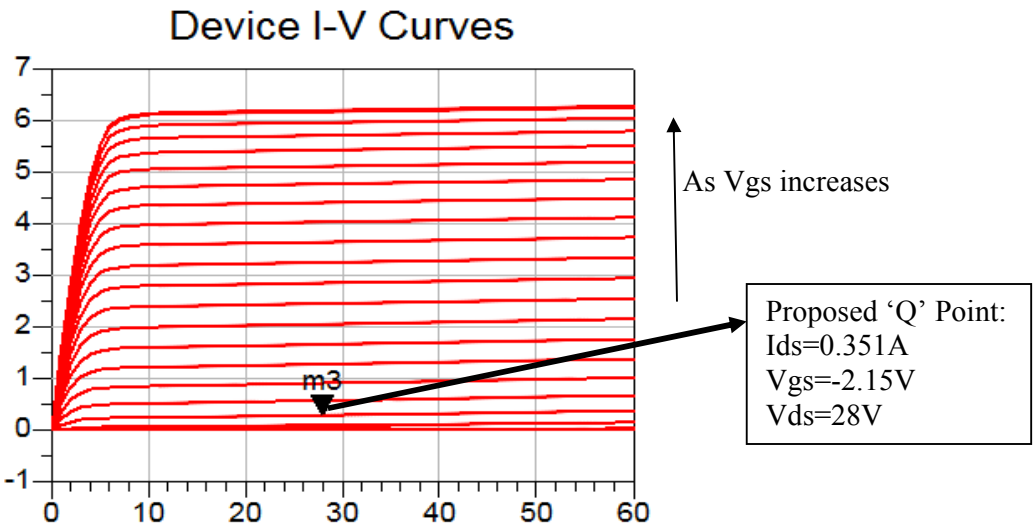

Figure 5.1: The DC-IV characteristic curve of the 25W GaN HEMT (CGH40025)

5.2.2 Class AB Power Amplifier for AET System

As explained in Chapter 4, both linearity and efficiency improvements can be achieved using the AET system. Therefore, in order to show any improvement in the RFPA performance, it was decided to operate the RFPA in the Class AB region; a compromise choice between the classical linear Class A mode and the classical efficient Class B mode [3]. The gate bias voltage was chosen so that the quiescent drain current, I_{DQ}, was around 5% of the maximum drain saturation current, $I_{d,max}$. The maximum drain saturation current, $I_{d,max}$ for this device is about 6A. Using Figure 5.2, the approximate quiescent drain current was 350mA corresponding to quiescent gate voltage of -2.15V.

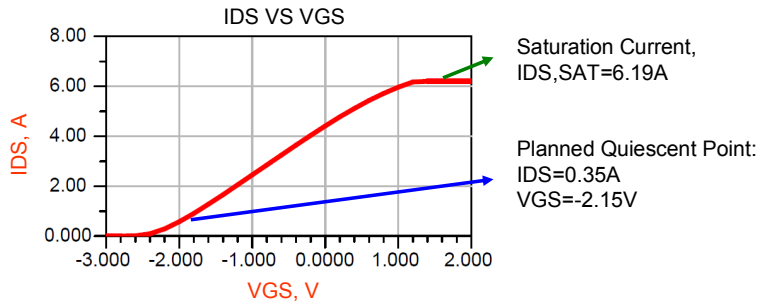

Figure 5.2: The approximation of the quiescent drain current and gate voltage.

5.2.3 Device Stability Simulation

The device stability analysis is an important step in RFPA design to avoid any oscillation from occurring. In this case, a device stability simulation is carried out using ADS at a frequency of about 2 GHz, as the application of this RFPA is for WCDMA systems. The device stability simulation used a standard ADS schematic template that can be found in the software.

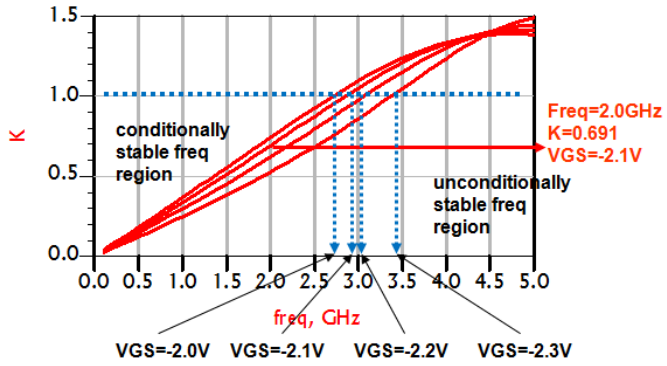

Figure 5.3: The stability factor simulation result for VGS value between -2.0V and -2.3V

The result of the device stability simulation in terms of stability factor 'K' is shown in Figure 5.3. The stability factor 'K' is a stability measure that is discussed in [4], and it is defined that a device is unconditionally stable if the 'K' factor is greater than 1 (K>1). As shown in Figure 5.3, the device stability factor is 0.691 at a frequency of 2GHz and a gate bias of -2.1V. This device is in the conditionally stable region (k<1) at the frequency range of interest,

of around 2.0 GHz, while the device is unconditionally stable at 2.6 GHz and above.

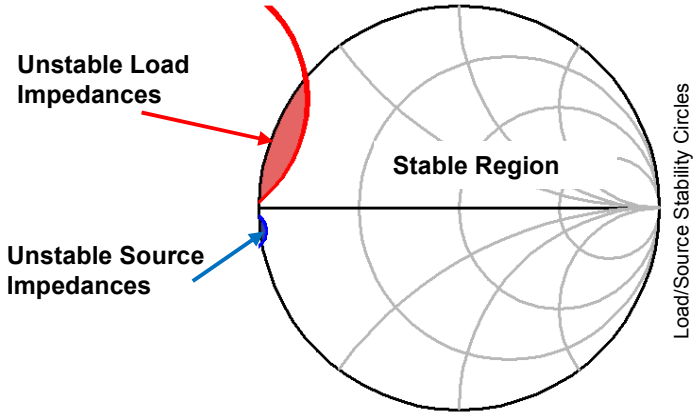

Figure 5.4: The load and source stability circles for the 25W GaN HEMT for (CGH40025) at 2GHz for the proposed bias point.

The load and source stability circles are also presented in Figure 5.4 which shows the stable and unstable region for the device. The device matching impedance therefore needs to be designed to be inside the stable region in the Smith Chart for both input and output network. We can also stabilise the device by using a resistor at the input port of the device.

Note that the device model used in these simulations includes the package parasitic impedance. The impedance consideration during this stability simulation is taken at the package plane as the reference plane. Therefore, the package parasitic elements need to be considered when designing the impedance matching network in a conditionally stable frequency region.

5.3 RFPA Design Simulation

When designing RFPAs, the impedance matching network is required to maximize the power transfer for specific gain and output power. The matching network is also needed to minimize any reflection coming from the load or source so that the device can operate with best performance. There are two impedance matching networks in RFPA design, namely the input matching network (IMN) and output matching network (OMN). IMN is the network to match the source impedance and the device input impedance

while OMN is the network to match the device output impedance and the load impedance. Both source and load impedance environment is the standard 50Ω. There is a series of ADS simulation performed in the process of designing the final IMN and OMN. In each simulation step the elements in the matching network and the bias network are tuned for performance and stability.

5.3.1 Output Parasitic Network of the 25W GaN HEMT Device Package.

The 25W GaN HEMT (CGH40025) device used in this RFPA design is provided by Cree in a flange type package. The nonlinear model of this device includes the package parasitic reactances. The package parasitic network consists of passive elements that include the output capacitance, bond wire inductance and the tab of the package. The circuit model of this parasitic network is shown in Figure 5.5. Port 1 of this output package parasitic network represents the current-generator plane of the device and port 2 represents the package plane of the device. The current-generator plane is the reference plane at which the actual current and voltage waveforms of the RFPA mode of operation are observed; in this case, Class AB mode. During the design simulation process, the negative counterpart of this network is presented as a de-embedding network in order to observe the current and voltage waveforms of the device at the current-generator plane.

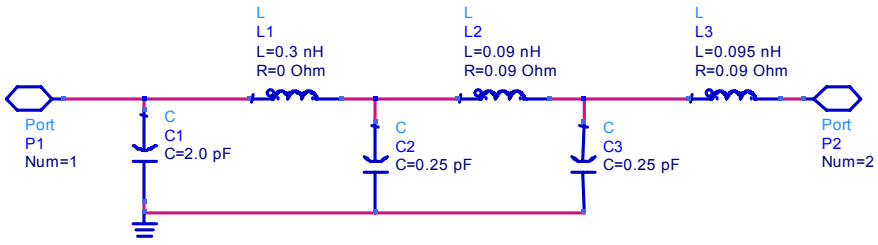

Figure 5.5: The 25W GaN HEMT device package parasitic network

5.3.2 Load pull Simulation

After the device has been chosen and the mode of operation has been decided, the device is now simulated to find its optimum impedance. The first

simulation step is to perform a single frequency load pull simulation. The load pull is defined as an analysis by using a set of contours on a Smith chart where load impedances on the contours are analyzed on the achievable optimum output power on the contours, and the concept is further explained in [3]. Using the template for the load pull simulation that is provided by ADS, the optimum matching impedance is found by calculating the optimum output power, the power-added-efficiency (PAE) and the drain efficiency at a specified coverage radius. The schematic for this load pull simulation is shown in Figure 5.6.

The fundamental load coverage is tuned by adjusting the coverage radius, the centre point of the coverage circle and number of points to be calculated for the load impedance. For source impedance tuning, the variable for source impedance is adjusted. For this device, the optimum fundamental source impedance was found to be 1.1 –j1.9 Ω and the fundamental load impedance was found to be 18.2+j3.5Ω. The simulation result is shown in Figure 5.7. Please note that this matching impedance is specified at the package plane, where the parasitic reactances of the device package are included.

5.3.3 Power Sweep Simulation with Load Tuner

Power sweep simulations were carried out after the load pull simulation and the schematic can be found in Figure 5.8. In the load pull simulation, the performance of the device in terms of efficiency and output power is simulated by matching the load at the package plane. In the power sweep simulation however, we are able to view the current and voltage behaviour at the current generator plane by introducing the parasitic de-embedding network. This is important to ensure that the RFPA operates in the desired mode of operation.

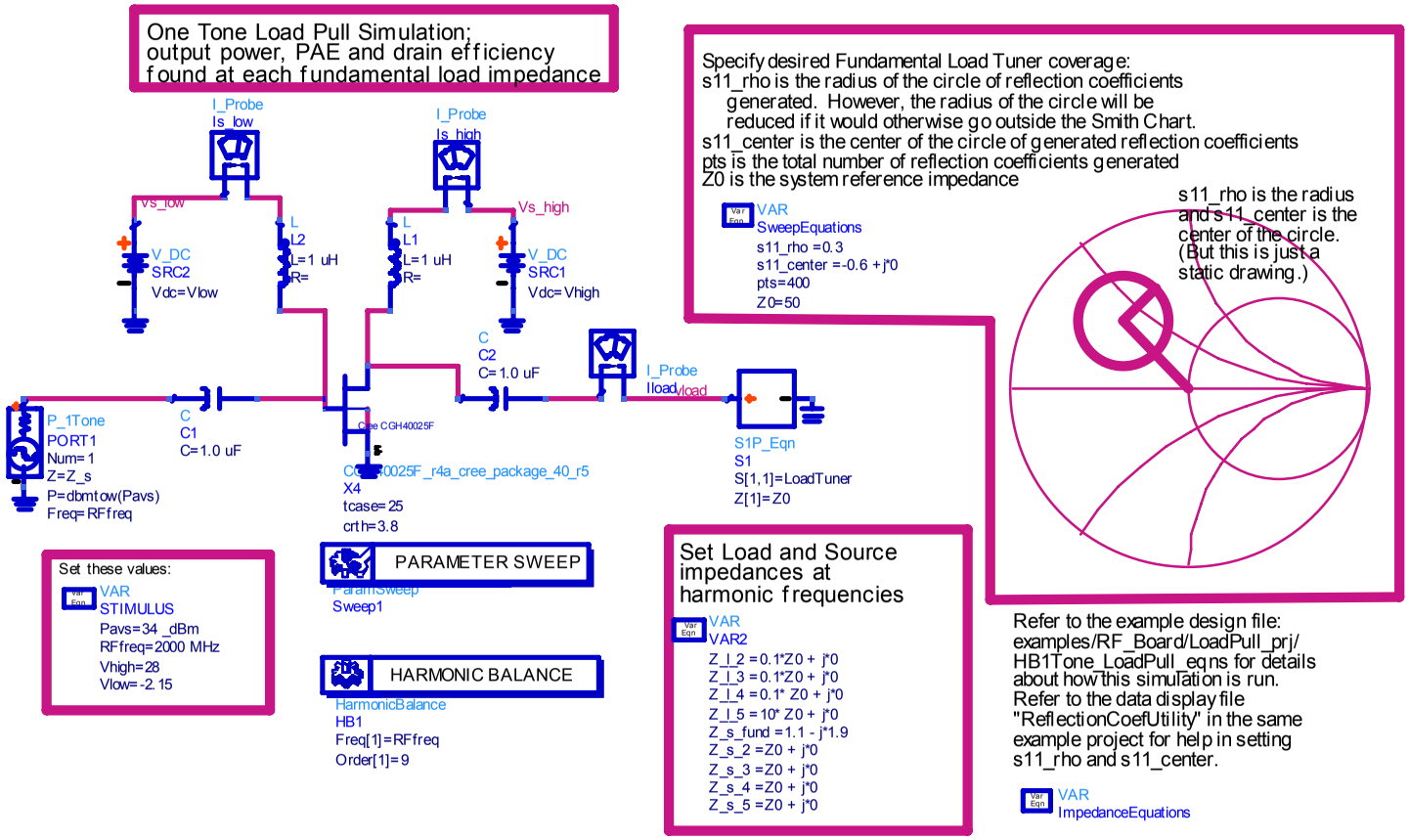

Figure 5.6: The load pull simulation schematic for the 25W GaN HEMT device.

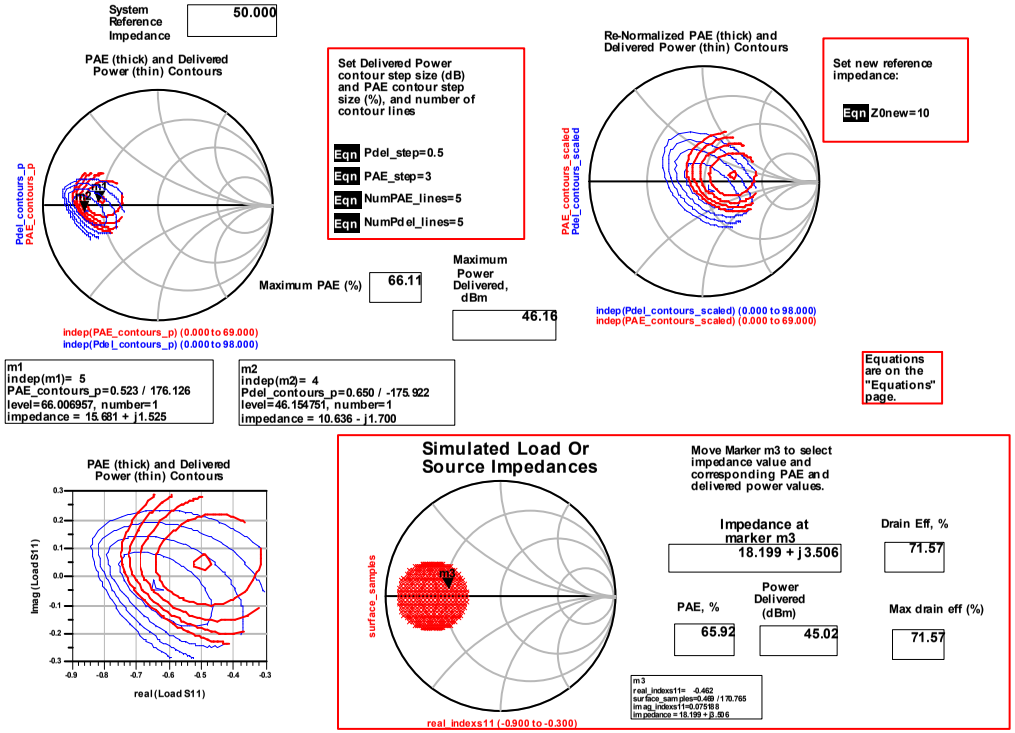

Figure 5.7: The load pull simulation result of the 25W GaN HEMT device.

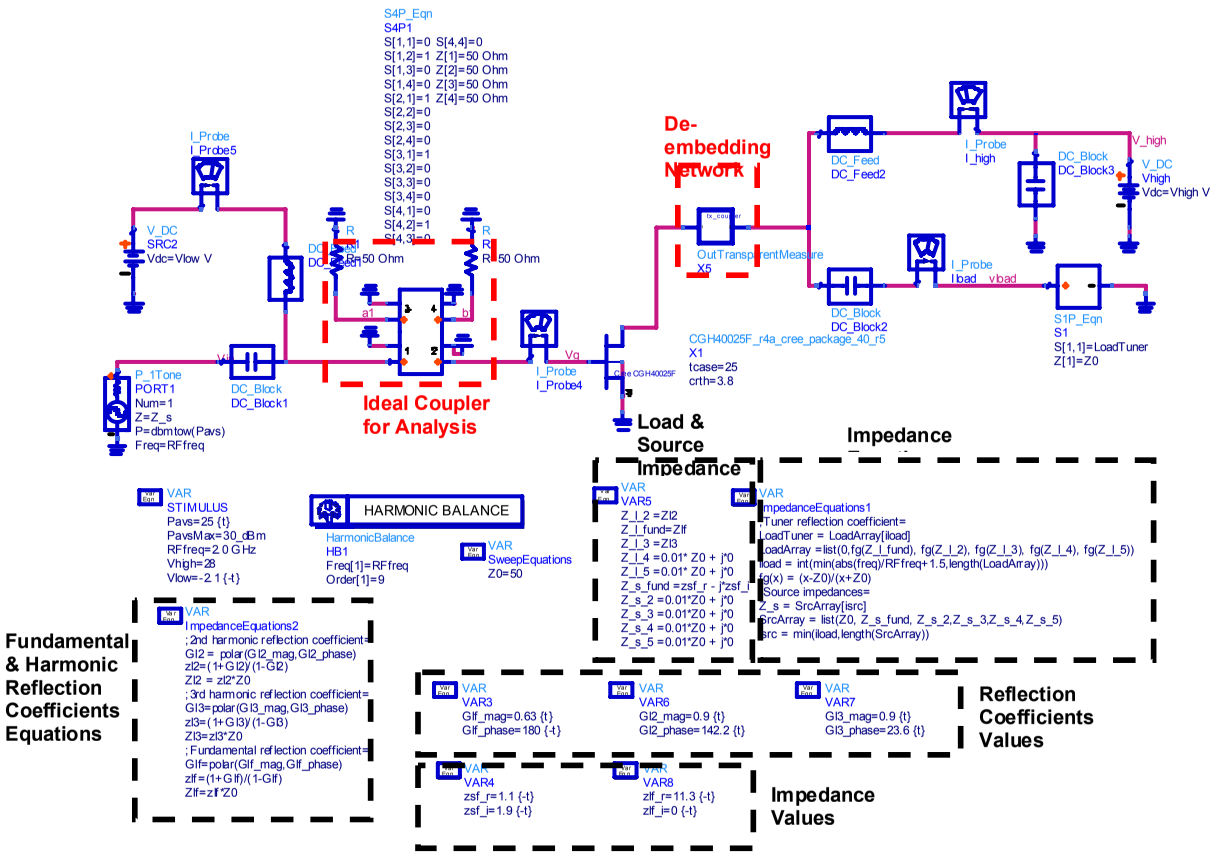

Figure 5.8: The schematic for Power Sweep Simulation where the de-embedding network is included

The parasitic de-embedding network consists of parasitic 'minus' network and parasitic 'plus' network. The parasitic 'plus' network is the device package parasitic network shown in Figure 5.5, while the parasitic 'minus' network is a negative counterpart of the device package parasitic network. This parasitic de-embedding network is included in the main schematic as shown in Figure 5.9 as the OutTransparentMeasure block. At this point, in order to give the correct Class AB current and voltage waveforms, the fundamental and harmonics loads are tuned. In the schematic, the waveforms are optimized by tuning the load and source complex impedance.

The de-embedding network in the OutTransparentMeasure block is expanded and shown in Figure 5.9. Using the ideal coupler block, the waveforms are plotted and shown in Figure 5.10, where the current and voltage waveforms at both current-generator plane and package plane are presented.

As shown in Figure 5.10, at the current-generator plane, the output current waveform of the device with the tuned impedances exhibits the Class AB current waveform. At the package plane however, this is not the case as it can be seen that there is some current flowing below zero voltage. This non-zero current is called displacement current [5] and is due to the charge stored in the drain source and package parasitic capacitor. The voltage waveform at the current-generator plane showed a Class J waveform instead of Class AB and this may be caused by excessive tuning for best RFPA performance during the impedance adjustment.

After tuning the impedance, the fundamental output matching impedance at package plane is 11.35 Ω while at current-generator plane is 13.69 Ω. As for fundamental input matching impedance, the value remained at 1.1 –j1.9 Ω. The performance in terms of gain and drain efficiency is shown in Figure 5.11 and the value of the simulated gain is 21dB, while the drain efficiency is 57% at an output power of 44dBm. The drain efficiency is quite low for Class AB mode and the improvement of this drain efficiency is addressed in the next simulation step.

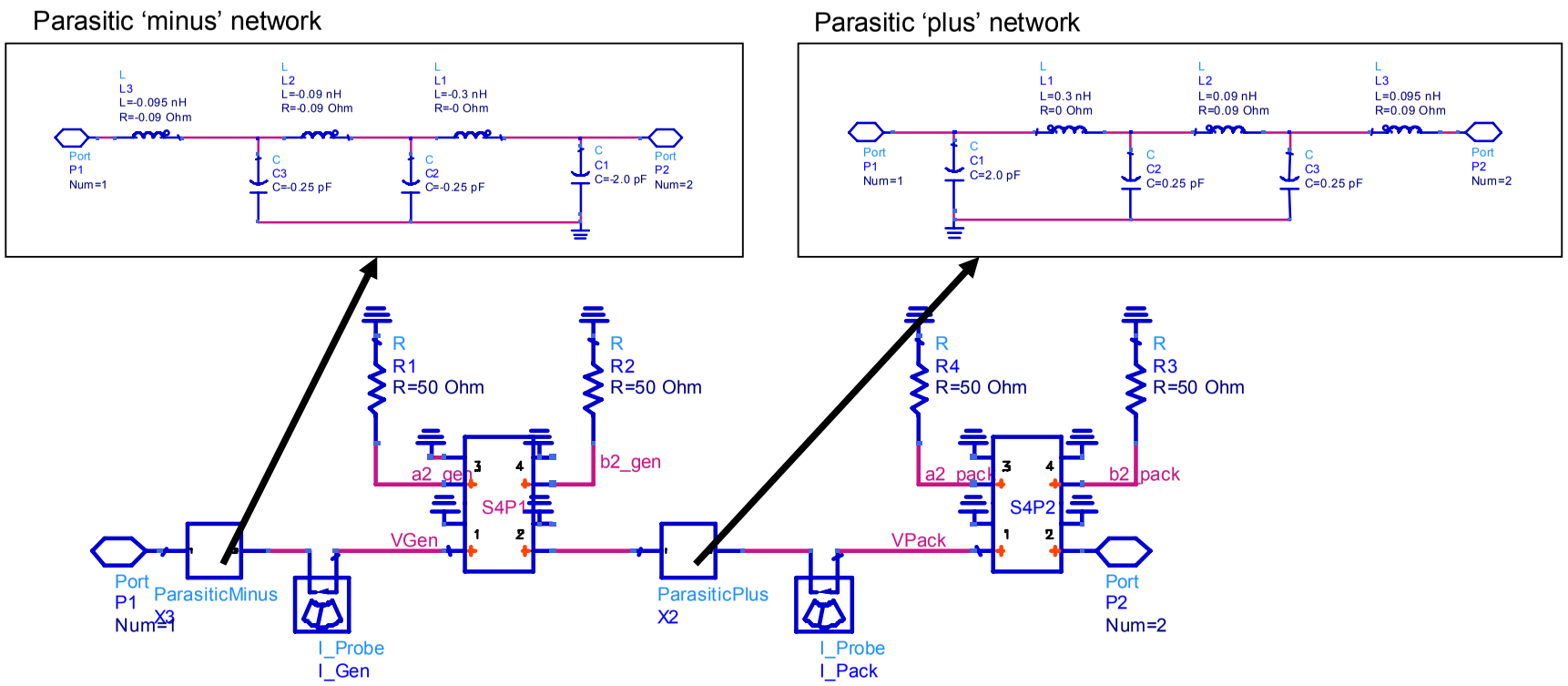

Figure 5.9: The expansion of the 'OutTransparentMeasure' block that consists of the parasitic de-embedding network.

5.3.4 Transmission Line ADS Simulation

The IMN complex impedance and OMN real impedance are now transformed into ideal transmission line. The Smith Chart utility tool in ADS is used and the ideal transmission lines for the input and output matching network are shown in Figure 5.12. The input matching impedance of 1.1 –j1.9 Ω is transformed to an open circuit stub in series with a transmission feed line, and the output matching impedance of 11.35 Ω is transformed into a quarter-wave transformer using an ideal transmission line. The ideal transmission line network is then simulated using the power sweep simulation setup shown in the schematic of Figure 5.12.

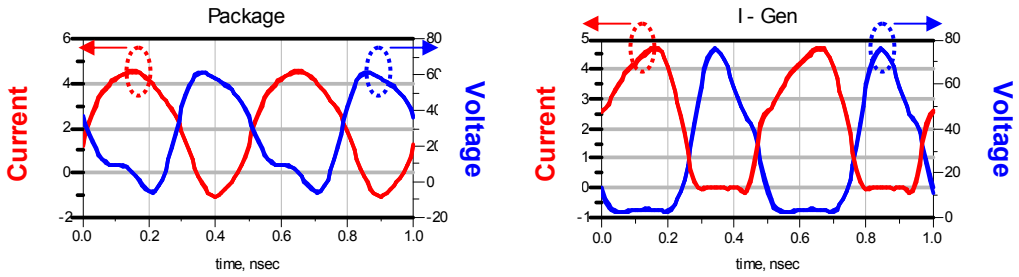

Figure 5.10: The current and voltage waveforms of the device (Load Tuner)

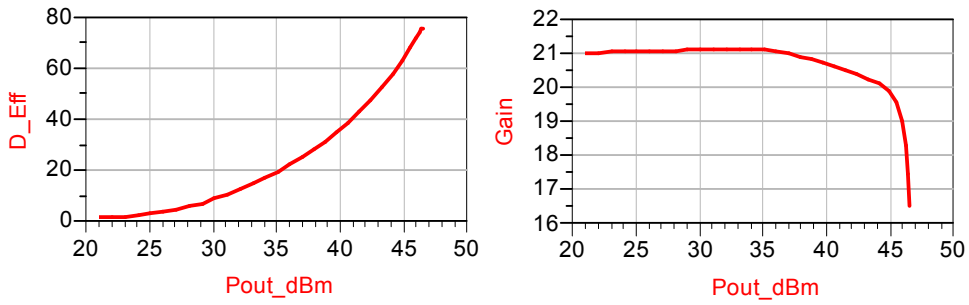

Figure 5.11: The drain efficiency and gain performance for the Power Sweep Simulation with Load Tuner.

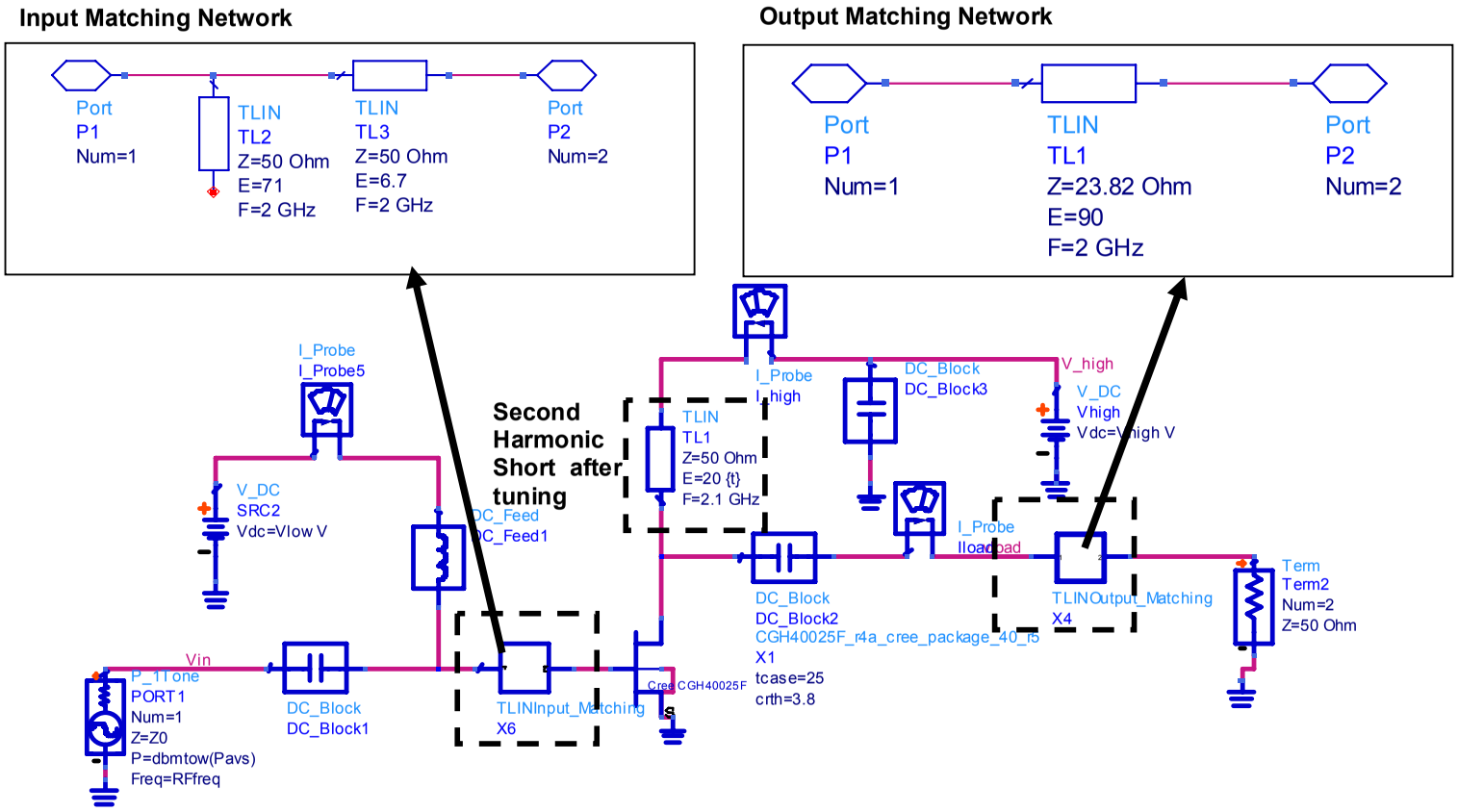

Figure 5.12: The ideal transmission line Power Sweep Simulation schematic and the input and the output matching network

In this schematic, the ideal DC feed inductor at the drain bias port was also replaced with an ideal quarter-wave transmission line. This quarter-wave transmission line provides a short circuit at DC and an open circuit at RF. Using this quarter-wave transmission line, the second harmonic impedance of the matching network is also shorted to improve the linearity of the RFPA. Due to parasitic elements between the current-generator plane and the matching transmission line, the quarter-wave transmission line is tuned so that the length of the line is no longer 90º but 20º as shown in Figure 5.12.

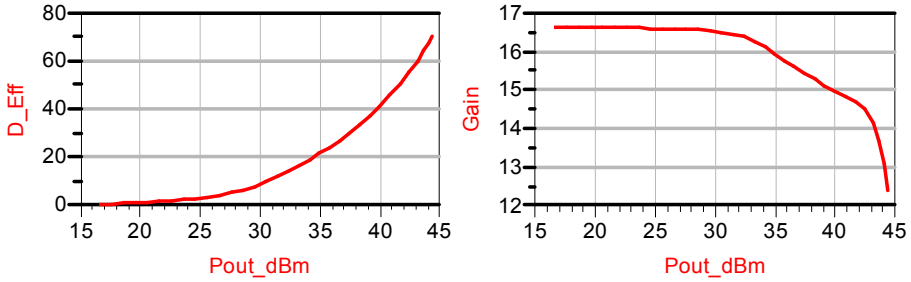

Figure 5.13: The drain efficiency and gain performance for the ideal transmission line simulation.

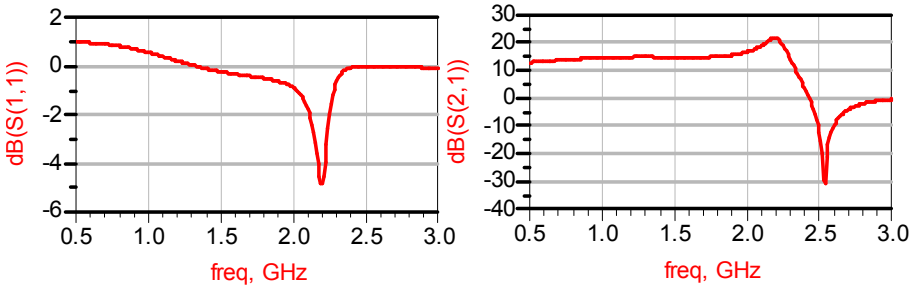

Figure 5.14: The linear simulation result in terms of S11 and S21 parameter.

From the quarter-wave transmission line tuning, the drain efficiency has improved as shown as in Figure 5.13, however the trade-off is that the gain

has dropped to 16.5dB from 21dB. The fundamental output matching impedance at the package plane has shifted to 7.92 Ω as a result of the tuning.

At this point, a linear simulation from the same schematic is also conducted, and the small signal input reflection coefficient, S_{11}, and small signal transmission gain, S_{21}, are shown in Figure 5.14. From this figure, the plot of S_{11} shows that the amplifier is not stable at lower frequencies. In order to remove this instability, a resistor is added to the input of the device, which will be explained in the next section.

5.3.5 Microstrip Line ADS Simulation with Bias Network

At this point, the ideal transmission lines are replaced with real microstrip lines. The microstrip line used in the RFPA design is a high frequency laminate RT/Duroid® 5880 from Rogers Corporation [6]. The properties of this laminate (Table 5.1) are included in the simulation.

Description	**Values**
Substrate Thickness, H	0.508mm
Relative Dielectric Constant, ϵ_r	2.20
Conductor Thickness, T	17.5μm
Relative permeability, M_{ur}	1
Conductor Conductivity, cond	$5.961 \times 10^7 Sm^{-1}$
Dielectric Loss Tangent, TanD	0.0009

Table 5.1: The RT/Duroid® 5880 high frequency laminate properties

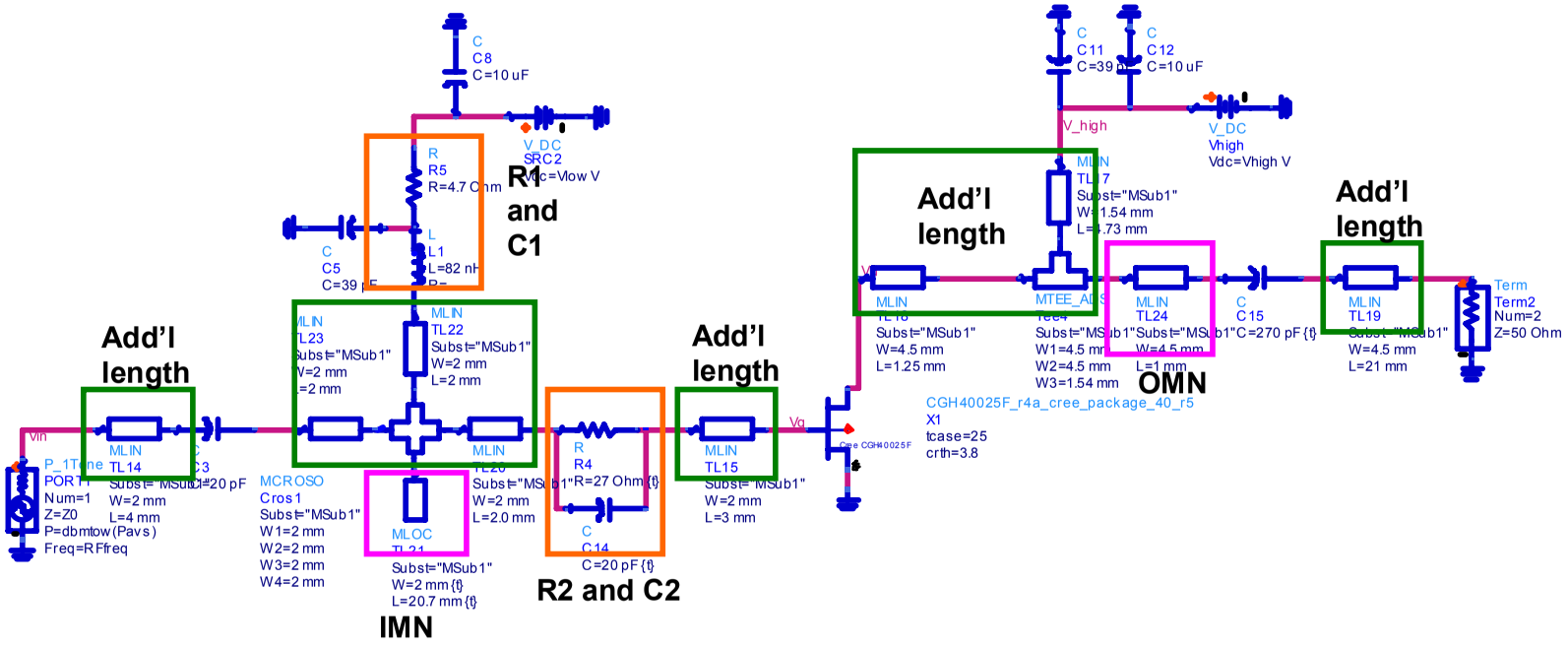

Figure 5.15: The Microstrip Line Simulation with Stability Measure

The ideal transmission lines and the quarter-wave DC feed from the previous simulation schematic are replaced with this RT/Duroid® 5880 microstrip line. Other than the matching network and the DC feed, the connections that link the passive components, device tabs and input and output connectors are also taken into consideration by adding necessary lengths of microstrip line. The additional lengths of microstrip line are shown in the schematic of Figure 5.15.

The ideal DC feed at the gate bias port of the device is now replaced with a real inductor. Actual blocking capacitor values for the input and output ports are also included in this schematic.

As noted for the previous linear simulation, the results showed that the device encountered some instability at lower frequencies. In order to improve the stability, a resistor, R1 (as shown in Figure 5.15), is inserted between the gate bias supply and the decoupling capacitor, C1. The resistor is used to remove the negative resistance that causes the oscillation at lower frequencies [3]. Another stability measure taken at the input of the device was adding a resistor, R2, in parallel with a capacitor, C2. A resistor can stable the device at all frequencies including those outside the operating frequency of interest. The resistor however, degrades the device transmission gain. Therefore, a capacitor in parallel is presented so that the resistor loss will only occur at low frequencies. At higher frequencies, the capacitor bypasses the resistor, and hence the gain is unaffected [7].

The linear simulation result (Figure 5.16) shows that the input reflection coefficient is negative for all frequencies between 500MHz and 3GHz. This is achieved whilst maintaining the small signal transmission gain, S_{21}. The performance in terms of drain efficiency and gain is shown in Figure 5.17. The gain from the microstrip line simulation is improved compared to the ideal transmission line simulation, whilst the drain efficiency is maintained. The fundamental output matching impedance at the package plane has changed to 11.11Ω after including the stability network and real values for

the blocking capacitors. Note that this output matching impedance value is closer to the one in the power sweep simulation with load tuning.

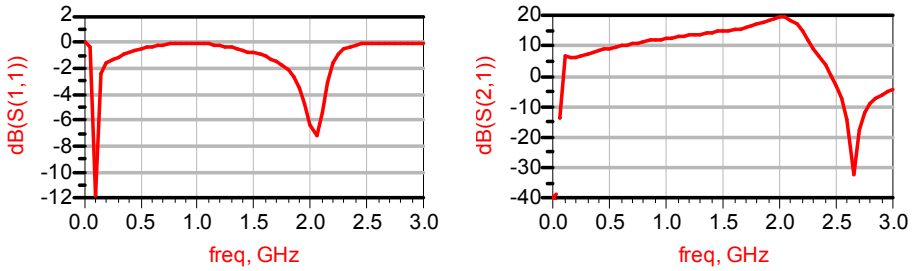

Figure 5.16: The linear simulation result

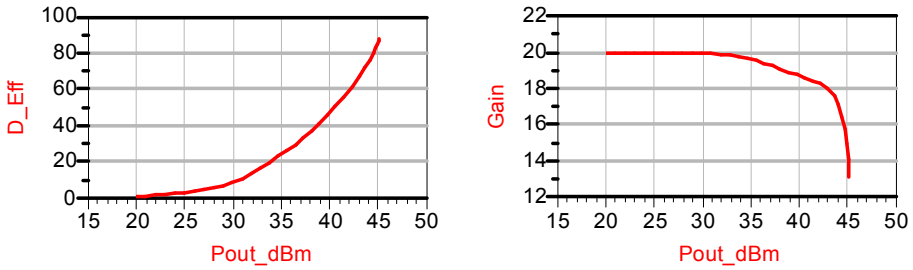

Figure 5.17: The RFPA performance in terms of drain efficiency and gain

5.3.6 Layout Simulation using Momentum

After the microstrip line simulations, specific lengths have been determined for the matching network transmission tines. The next step is to use the ADS Momentum simulator to simulate the electromagnetic (EM) effects of the microstrip line including coupling and parasitic capacitances [8]. These EM effects are taken into consideration to improve the RFPA performance. This step is necessary so that the realised RFPA meets the specification and gives the same measured performance as is predicted by simulation.

In this EM simulation, the layout of the microstrip line was drawn using the Schematic-to-Layout translation. Next, using ADS Momentum, the layout is simulated based on the microstrip line properties that are imported from the schematic window. Momentum simulates the layout and gives the output data in terms of S-parameters. The data from this simulation is then returned to the schematic and re-simulated using the power sweep simulation. The simulation result in terms of the S_{11} and S_{21} parameters are shown in Figure 5.18. The S_{11} result shows that stability is achieved for frequencies of interest. The S_{21} result shows a small change to the small signal gain at lower frequencies compared to the previous simulation. The gain and drain efficiency are compared to the measured result and is shown in Figure 5.21 and Figure 5.22 respectively.

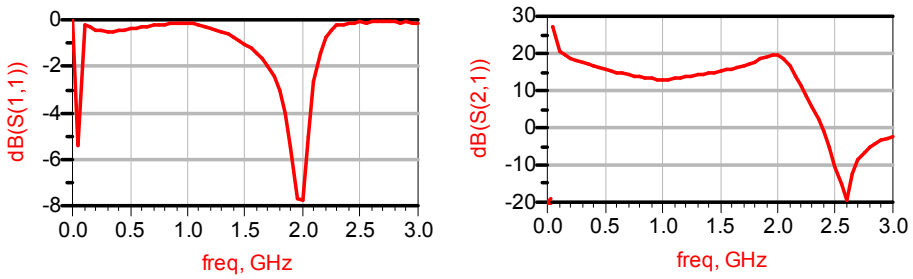

Figure 5.18: The linear simulation result using the s-parameter values extracted from the ADS Momentum simulation.

The final drawn layout as shown as in Figure 5.19, consists of all the microstrip lines, the position of vias, some space consideration for passive components and the transistor itself. The outline of the size of the board was also drawn for fabrication purposes. After the fabrication, the 25W GaN HEMT device and all passive components were connected to the board that contained proper tin-plated pin grounding. The realized 25W GaN RFPA is shown in Figure 5.20.

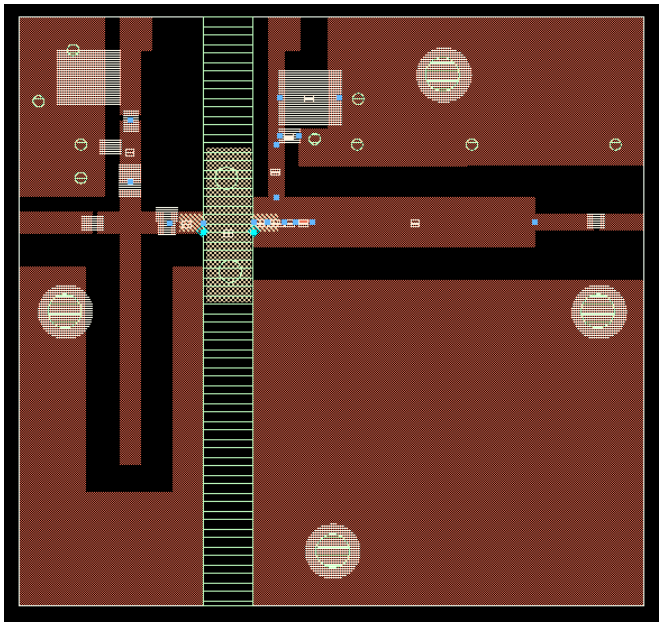

Figure 5.19: The final layout of the RFPA design

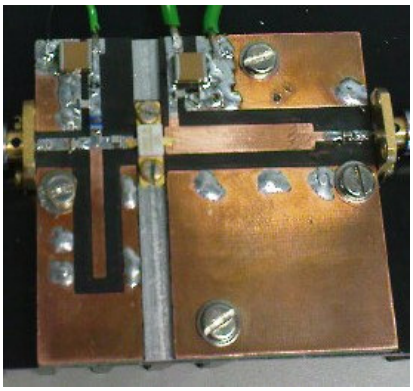

Figure 5.20: The complete and realized 25W GaN Class AB RFPA.

5.4 RFPA Performance Measurement

5.4.1 S21 Measurement Result

After the RFPA was fabricated, the final step was to measure the RFPA. First, the RFPA is checked for its stability and it was found that the RFPA was free from any oscillation. Then, the RFPA was measured for small signal gain, S_{21}, using a VNA between frequency of 30 kHz and 3GHz. The

measured result is compared to the power sweep simulation with EM-simulated microstrip lines. The results are shown in Figure 5.21. The design of this RFPA was simulated and optimised for a design frequency of 2.0GHz. The measured result however, shows that the optimum performance has shifted to a frequency lower than the initial intended operating frequency. For further measurement of using two-carrier and WCDMA signals, the operating frequency was chosen to be 1.98GHz, a frequency that is not far from the original operating frequency and one that gives good gain performance. The measurements also showed a resonance effect around 700MHz, and this was due to an inaccurate capacitor model at low frequency. Since the RFPA operating frequency for the AET system was chosen to be 1.98GHz, at this point we do not to address the resonance problem that occurred at a much lower frequency.

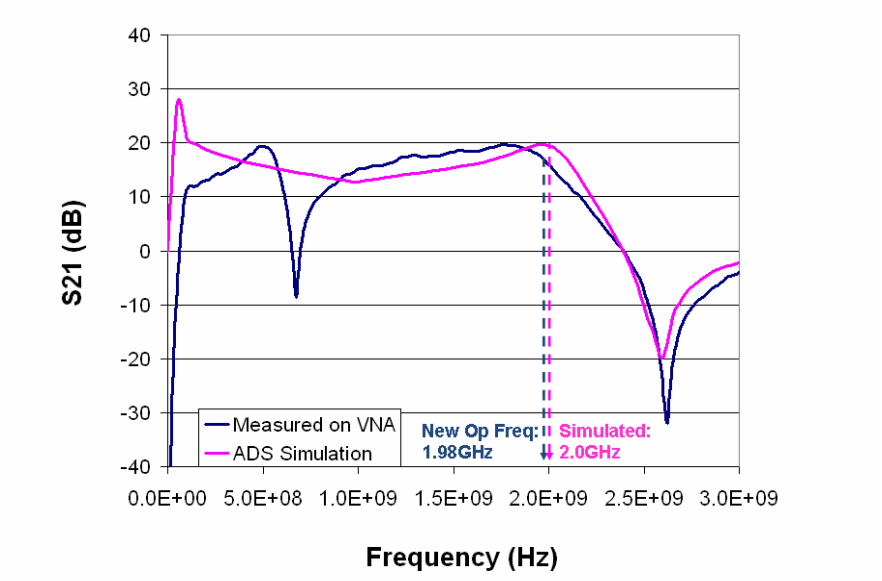

Figure 5.21: The measured and simulated S21 performance of the RFPA

5.4.2 Drain Efficiency and Gain Performance

The performance of this RFPA in terms of drain efficiency and gain is measured using a typical CW measurement setup. The frequency of this measurement was 1.98GHz and bias drain voltage was 28V. The quiescent drain current was chosen to be around 300mA. The measured drain efficiency of this 25W GaN RFPA is shown in Figure 5.22 and the gain is shown in Figure 5.23. The measured drain efficiency at an output power of 44dBm is

about 74%, and this is higher than the simulated result, which predicted a drain efficiency of about 68%. The trade-off from the improvement in drain efficiency is that the measured gain is 17.5dB, slightly lower than the simulated gain of 19dB. In general however, the RFPA still gives a good Class AB performance.

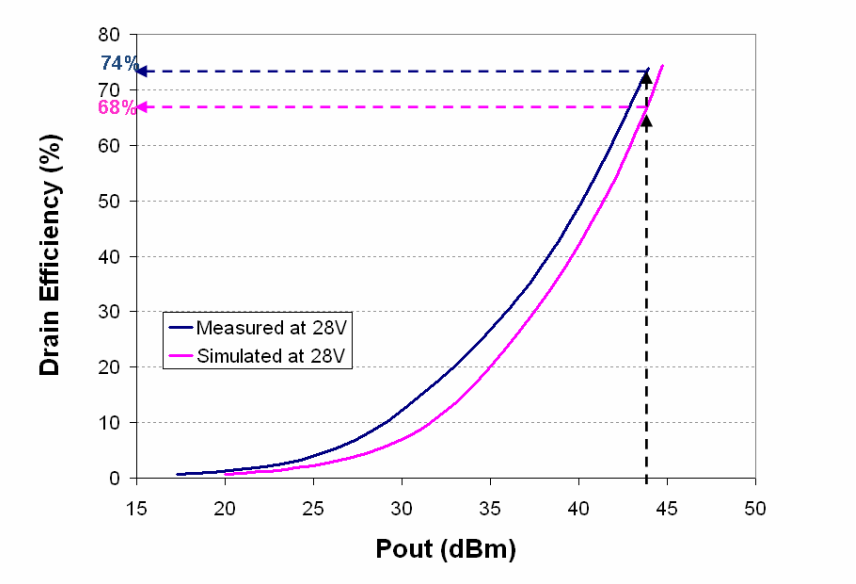

Figure 5.22: The drain efficiency performance of the RFPA

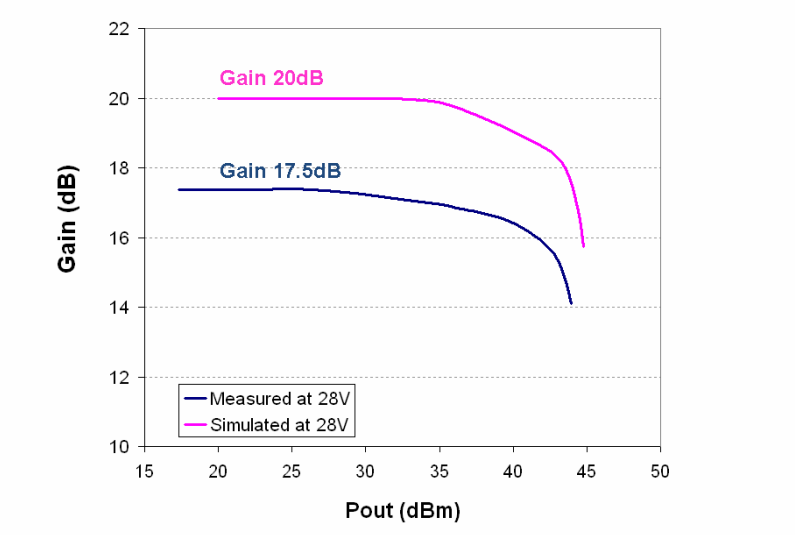

Figure 5.23: The gain performance of the RFPA

5.4.3 RFPA Performance at Varying Drain Voltages

As mentioned in section 5.1, this RFPA is designed specially for the AET system where the drain voltage of the device is varied. The RFPA was therefore measured at different drain voltages. A series of CW measurements were carried out for drain voltages between 16V and 30V. The gain performance of this RFPA is shown in Figure 5.24. From this figure, it can be observed that the gain increases as the drain voltage is increased. The gain behaviour of this RFPA is in agreement with the previous 10W Class J GaN RFPA measurements reported in Chapter 3, and this gain behaviour is a useful trait for linearity improvement using AET, as described in Chapter 4. The drain efficiency of the RFPA is also measured, as shown in Figure 5.25, and it is observed that the efficiency remains high for all drain voltages. The AM-PM distortion measurement shows that the phase varies with input power at a maximum of about 6º for a fixed drain voltage of 30V, as shown in Figure 5.26.

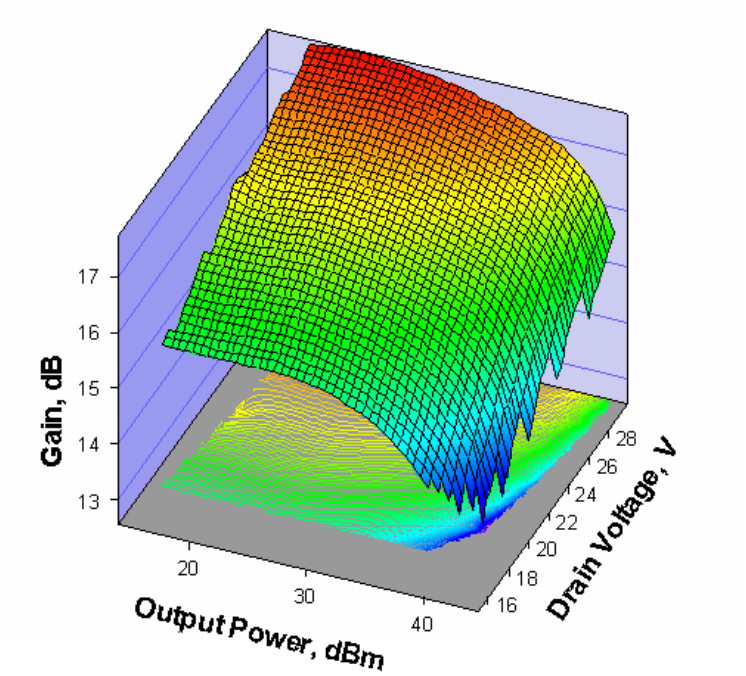

Figure 5.24: The RFPA gain performance at different drain voltages

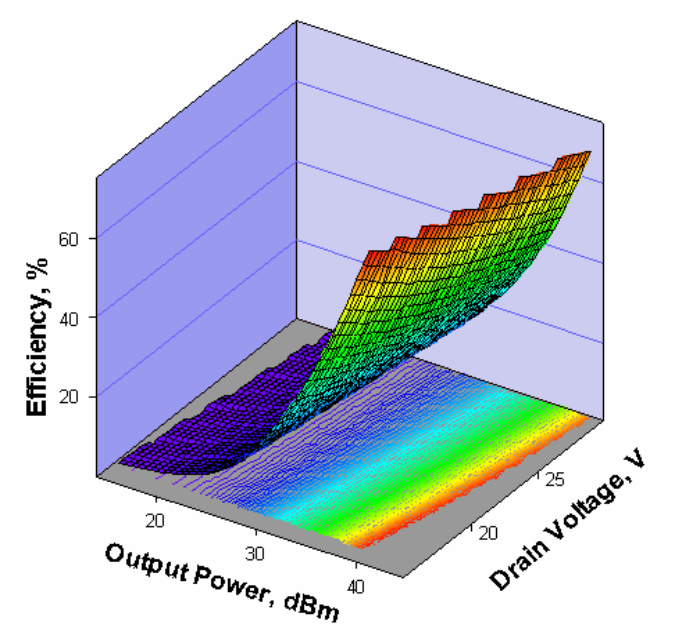

Figure 5.25: The RFPA drain efficiency performance at different drain voltages

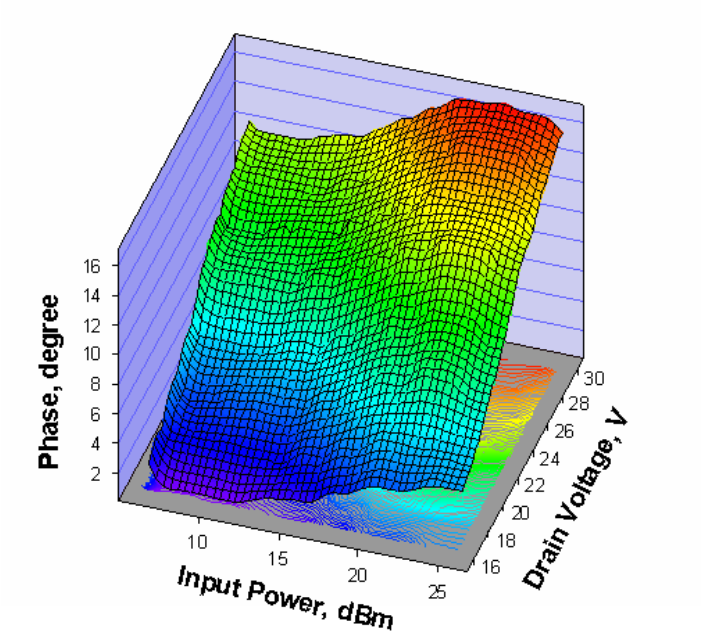

Figure 5.26: The RFPA AM-PM performance at different drain voltages.

5.5 Chapter Summary

In this chapter, the 25W GaN Class AB RFPA design is presented. A detailed description of the RFPA design from the load pull simulation to power sweeps simulation using load-pull tuner, ideal transmission lines and real

microstrip lines, is presented The layout is then drawn and, using ADS Momentum, is simulated for its EM effects. The RFPA layout design is then fabricated. The completed RFPA is measured and its performance is presented, including measurements at various drain voltages, which are required for AET analysis.

5.6 Reference

[1] Yusoff, Z., Woodington, S., Lees, J., Benedikt, J., Tasker, P.J., Cripps, S.C., "High Linearity Auxiliary Envelope Tracking (AET) System using GaN Class-J Power Amplifier" IEEE Power Amplifier Symposium, Arizona, USA, 13th -14th September 2010.

[2] Cree 25W GaN HEMT Datasheet [Online] Available: http://www.cree.com/products/pdf/CGH40025.pdf (Appendix B)

[3] Cripps, S., "RF Power Amplifier for Wireless Communications", Norwood, MA: Artech House, Apr. 1999.

[4] Pozar, D.M. Microwave Engineering. Hoboken, NJ: J. Wiley, 2005.

[5] Displacement Current Wikipedia Page [Online] Available: http://en.wikipedia.org/wiki/Displacement_current

[6] RT/Duroid® 5880 High Frequency Laminate Datasheet [Online] Available: http://www.rogerscorp.com/acm/products/10/RT-duroid-5870-5880-5880LZ-High-Frequency-Laminates.aspx

[7] Gilmore R., Besser L., "Practical RF circuit design for modern wireless systems Vol. II", Norwood, MA: Artech House, 2003.

[8] Agilent Momentum 3D Planar EM Simulator [Online] Available: http://www.home.agilent.com/agilent/product.jspx?cc=GB&lc=eng&ckey=18871
16&nid=-33748.0.00&id=1887116&cmpid=zzfindeesof-momentum

CHAPTER 6

TWO-CARRIER SIGNAL MEASUREMENTS ON THE AET SYSTEM

6.1 Introduction

The concept of AET as explained in Chapter 4, opens the possibility of improving both the linearity and efficiency of an RFPA. The efficiency improvement can be investigated using CW measurements. However, to investigate the linearity performance of an RFPA, an initial linearity measurement should be performed using the classical two-carrier signal measurement. More advanced linearity measurements using complex modulated signals i.e. WCDMA signals will be discussed in Chapter 8.

6.2 The Preliminary Two-Carrier Signal Measurement Using the 10W GaN Class J RFPA and the 20W LDMOS Class AB RFPA

From the CW measurements performed on the 10W Class J GaN RFPA and the 20W Class AB LDMOS RFPA, the results showed that the gain of the GaN RFPA varied substantially with the drain bias voltage while for the LDMOS RFPA, the gain did not show significant variation as the drain bias voltage was varied. This observation was analyzed in Chapter 4, and the analysis of the gain variation has shown that the third-order intermodulation (IM3) distortion can be improved by applying a modulated signal to the drain bias port of the RFPA. In this chapter, an experimental setup was developed to make 2-carrier signal measurements on the AET system, and the measurement results are presented.

6.2.1 Preliminary AET Experimental Setup

The 10W Class J GaN RFPA and the 20W Class AB LDMOS RFPA were tested on the preliminary AET setup developed for the two-carrier signal measurement shown in Figure 6.1. The concept of AET, as explained in earlier chapters, is adapted from the regular ET system where the drain bias signal is envelope tracked from the input RF signal. In this experimental measurement however, the drain bias signal is emulated using a third signal generator. The drain bias signal emulation is adequate at this stage of the investigation to evaluate the concept of AET as an efficiency and linearity enhancement technique. A complete AET system, including the envelope detection, will be discussed in Chapter 8.

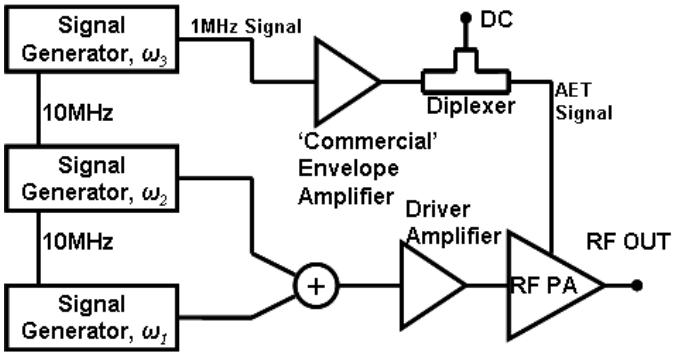

Figure 6.1: The preliminary AET experimental setup.

The operating frequency for the two-carrier signal measurement was chosen to be at 2GHz with 1MHz spacing. The measurement setup is divided into two paths; the RF path and the envelope path. On the RF path, the two-carrier signal is generated by two signal generators that are phase-locked and these two continuous wave (CW) signals are combined to produce the modulated signal. The two-carrier signal, as the input RF signal, is amplified by a driver power amplifier and referred to feed to the input of the RFPA.

On the envelope path, the amplitude and phase of the envelope signal is emulated using the third signal generator that is also phase-locked to the other generators. The envelope signal is a simple sinusoidal, which represents a

band-limited version of the full-wave rectified signal that is the envelope of an ideal two-carrier signal. In other words, the simple sinusoidal signal is a rectified signal where the harmonics are eliminated. The purpose of emulating the envelope signal with sinusoidal signal is to consider the impact of relaxing bandwidth requirement on the envelope detector.

The emulated envelope signal is amplified by a commercial off-the-shelf amplifier that is referred as the envelope amplifier (EA) in this AET system. This amplified envelope signal is then combined with the DC component using a bias tee. The combination of the amplified envelope signal and the DC component from the power supply is called the AET signal. The AET signal biases the RFPA, which of course has to have all bias decoupling components removed.

6.2.2 Preliminary Measurement Results

The AET measurements on both the 10W GaN RFPA and the 20W LDMOS RFPA using the two-carrier signal are compared to the measurements using a fixed drain supply. In the 2-carrier signal measurement for the 10W GaN RFPA, RF power was swept and the third-order intermodulation (IM3) products and average output power were measured. The GaN RFPA was measured at fixed drain bias of 37V. For the AET measurements, the peak drain bias voltage, the sum of the fixed and sinusoidal components was 37V. The values were chosen to make a fair comparison between the fixed drain supply and the drain modulated bias results measured. For the LDMOS RFPA, the fixed drain bias voltage was 28V and the peak voltage of AET signal was also 28V.

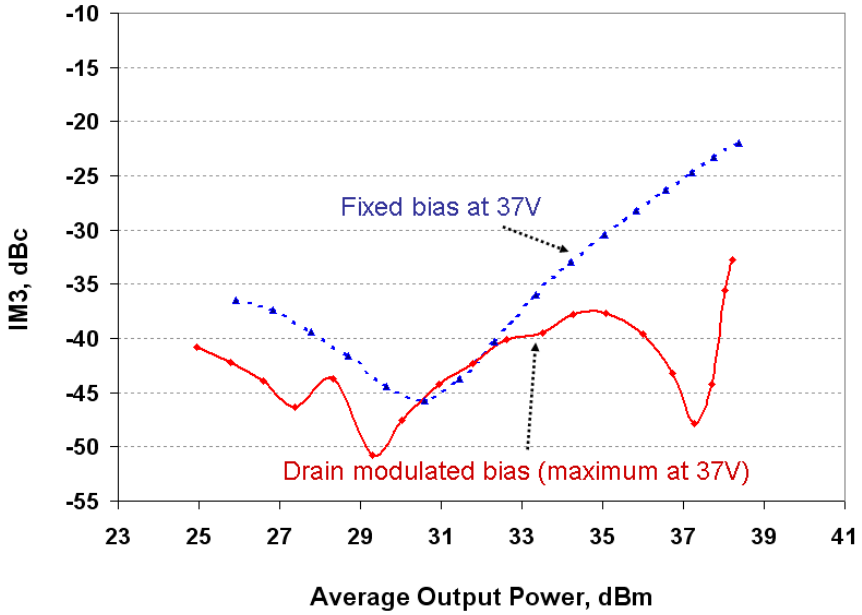

Figure 6.2: The IM3 performance of the 10W GaN Class J RFPA

For both fixed and modulated drain bias measurements, the IM3 performance was plotted. In Figure 6.2, the IM3 performance of the GaN RFPA when biased with fixed drain supply showed an IM3 value of less than -30dBc for average output powers lower than 35dBm. A 'null' effect was observed around average output power of 31dBm but at greater than 36dBm average output power, the IM3 level increased. The IM3 performance of the GaN RFPA with a modulated drain supply showed that the IM3 level was below -30dBc even at its maximum average output power.

At the maximum measured output power level, the IM3 performance with modulated drain supply was improved from -22dBc to -33dBc compared to the fixed drain supply case. An IM3 improvement between 10dB and just over 20dB was observed over a 3dB power back off (PBO) range, and significant improvements are still evident when the power is considerably backed off. This is a promising result for WCDMA and LTE applications, which require high linearity.

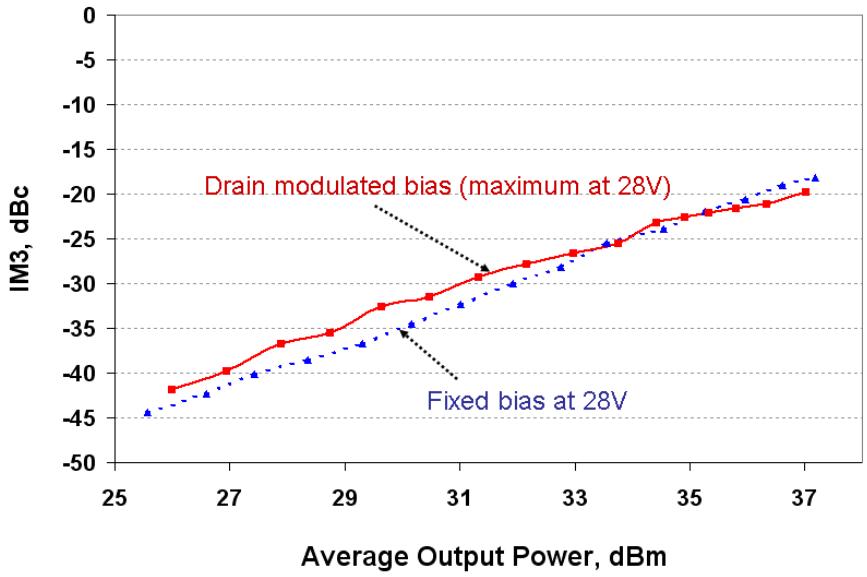

Figure 6.3: The IM3 performance for the 20W LDMOS Class AB RFPA

In Figure 6.3, IM3 performance of the LDMOS RFPA is presented and it can be observed that, as expected from the gain measurements, there was no substantial IM3 improvement. The IM3 performance of the LDMOS RFPA for fixed drain supply was less than -30dBc for average output powers below 33dBm. The IM3 products of this LDMOS RFPA under modulated drain supply showed a slight increase for average output powers lower than 33dBm but showed a slight improvement for average output powers greater than 33dBm.

The measurement results show that the drain modulation bias (the AET signal) has an impact on the linearity performance of the RFPA. In these preliminary measurements, the efficiency of the RFPA in the AET system was not able to be measured due to the use of the 'commercial' EA. This EA is a high voltage and low efficiency amplifier that consumes a large amount of power, which could be replaced by a high efficiency amplifier. Therefore, in the next section, an Integrated AET Block is designed and implemented to investigate the drain modulation effect on both linearity and efficiency.

6.3 The Two-Carrier Signal Measurements for the AET System using the Integrated AET Block

In most regular ET systems, the challenge is to design an efficient EA in order to improve the overall ET system efficiency. Many EA design approaches in the literature [1-3] for ET systems are quite complex and in conjunction with the pre-distorter, to improve linearity, can contribute a substantial cost to the overall system design.

In AET system described in Chapter 2 and Chapter 4, the concept of the system is to separate the generation of the AC and DC components of the AET signal. This idea has led us to a simple and low cost approach in designing the EA and the 'combiner'. In these two-carrier signal measurements, the 'combiner' is a simple passive diplexer. The combination of the EA, the diplexer and the RFPA is called the Integrated AET block. The design of the RFPA has been discussed in Chapter 5. Hence, in this chapter, the design of the EA and the diplexer are discussed.

6.3.1 Diplexer Design

A diplexer is a three-port network where two different frequency signals can be combined or separated. In the AET system, the diplexer is designed to combine the DC and AC components of the AET signal that is used to bias the drain port of the RFPA. The schematic design for this diplexer consists of capacitors and inductors, as shown in Figure 6.4. There are two different filters around Port 1 and Port 2, where the ends of these two filters are paralleled to form the output port of Port 3 [4]. The capacitor and inductor values are shown in Figure 6.4 and the implemented diplexer is shown in Figure 6.5.

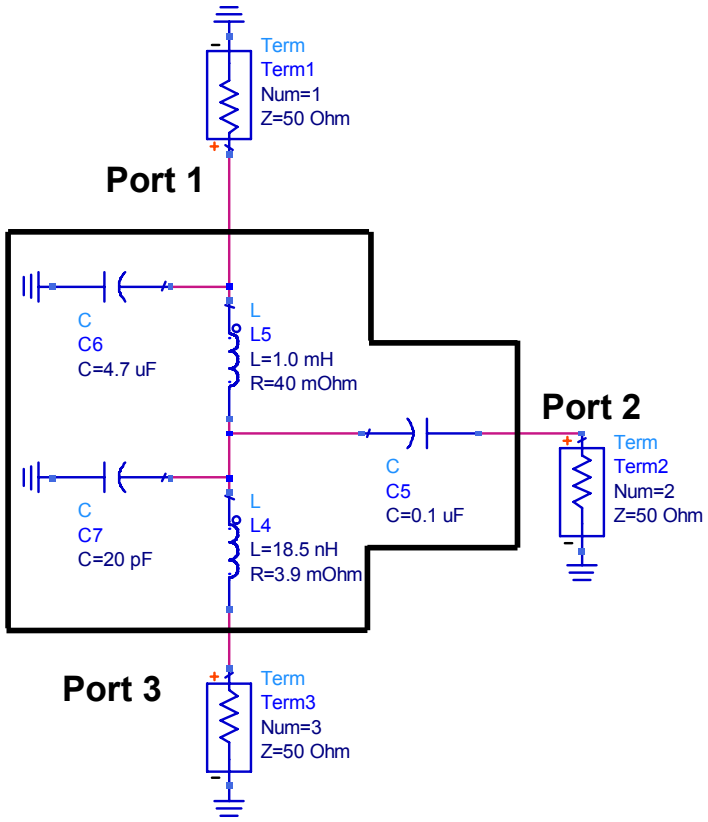

Figure 6.4: The schematic of the diplexer

The diplexer is designed as a high-pass filter to allow a signal frequency of 100 kHz and above to pass from Port 2 to Port 3, and as a low-pass filter to pass DC from Port 1 to Port 3.

The diplexer is designed on high frequency laminate RT/Duroid® 5880 from Rogers Corporation [5]. This is the same high frequency laminate that is used for the RFPA. Although this diplexer is operating at baseband frequencies, the reason for using this high frequency laminate is to integrate this diplexer with the RFPA into one AET block. The implemented diplexer is measured and the diplexer characterization in terms of its transmission loss is shown in Figure 6.6. The cross-over frequency for this diplexer is around 20 kHz and hence this diplexer is highly suitable for the two-carrier signal measurement inasmuch as the AC component of AET signal has a frequency of 1 MHz, which is much greater than the cross-over frequency.

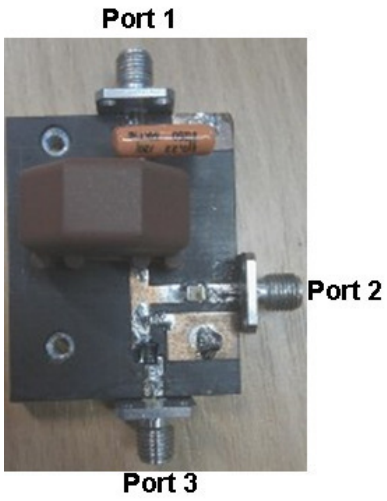

Figure 6.5: The implemented diplexer

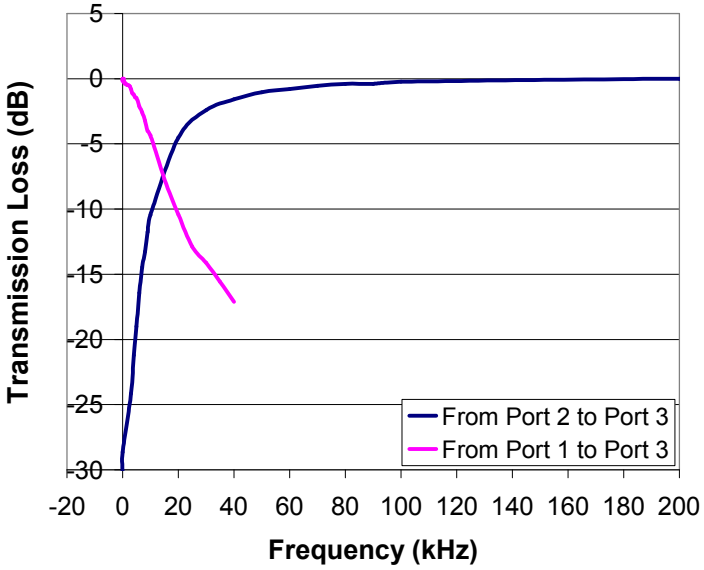

Figure 6.6: The diplexer characterization in terms of S21.

6.3.2 The Envelope Amplifier (EA) Design

The EA, part of the integrated AET block, is designed using a simple source follower amplifier configuration. This type of configuration is often used as a buffer amplifier due to its low output impedance [6]. The transistor used for the EA is the IRF510 transistor, an off-the-shelf n-channel power MOSFET from International Rectifier [7]. The IRF510 transistor was chosen for this EA design due to its fast switching capability to handle the high frequency AET signal. This transistor also has a low on-resistance that can keep the

minimum power dissipation low. The combination of the transistor's low-on resistance and the EA source follower configuration, contributes to a low output impedance thus the changes in the load resistance will not affect the voltage supplied. Another important reason this transistor was chosen is the transistor's cost; contributing to a low cost EA design for the AET system.

The EA source follower schematic is shown in Figure 6.7. A large inductor of 10uH is directly connected to the source of the n-channel FET, and a small value resistor of 5Ω is connected between the inductor and the ground. The combination of these two passive components maintains the minimum required DC current flowing through the transistor. The lowest possible DC current is required to maintain high efficiency for the RFPA in the AET system.

The envelope amplifier is implemented on the same high frequency laminate RT/Duroid® 5880 [5] for the same reason this laminate is used to implement the diplexer. The resistor R1 of 5Ω in the schematic is implemented in practice with a 4.7Ω resistor on the EA board, the closest value found with high current capability. The implemented EA design that is shown in Figure 6.8 is then measured for its small signal gain, S_{21}, performance and the result is shown in Figure 6.9. The S_{21} result has been normalized from the impedance mismatching between the VNA ports and the input and output ports of the EA. The performance of the EA in terms of S_{21} is promising between the frequency range of 100kHz and 10MHz. Note that both the two-carrier bandwidth of 1MHz and about 5MHz for the WCDMA baseband signal bandwidth lies within the frequency range measured and this makes the EA is suitable for both two-carrier signal and WCDMA measurements.

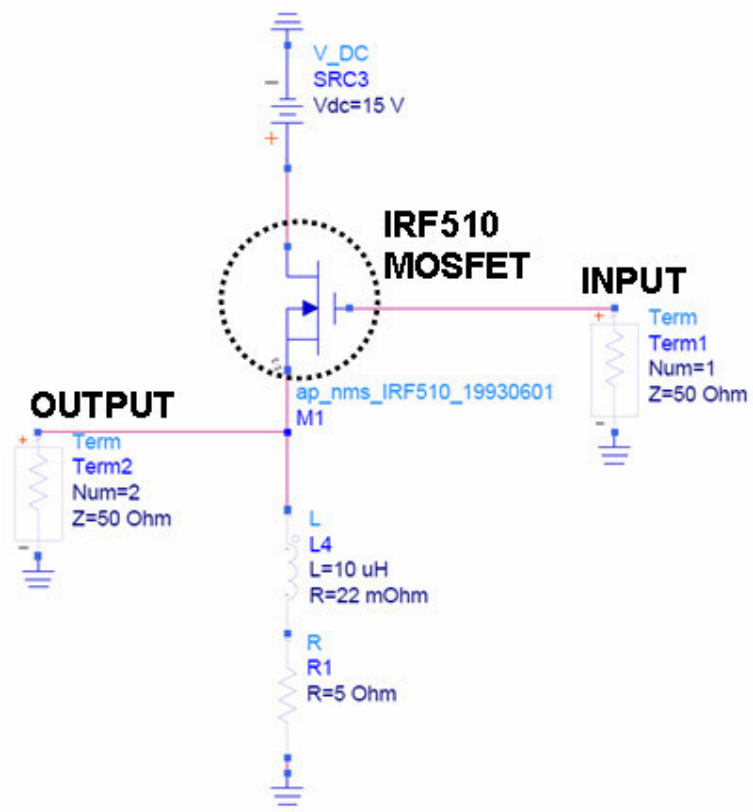

Figure 6.7: The Envelope Amplifier employing the source follower configuration

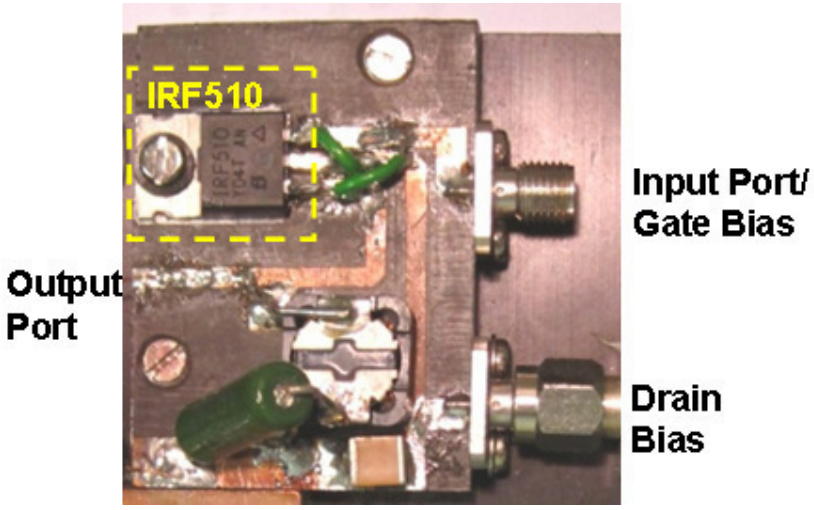

Figure 6.8.: The implemented Envelope Amplifier

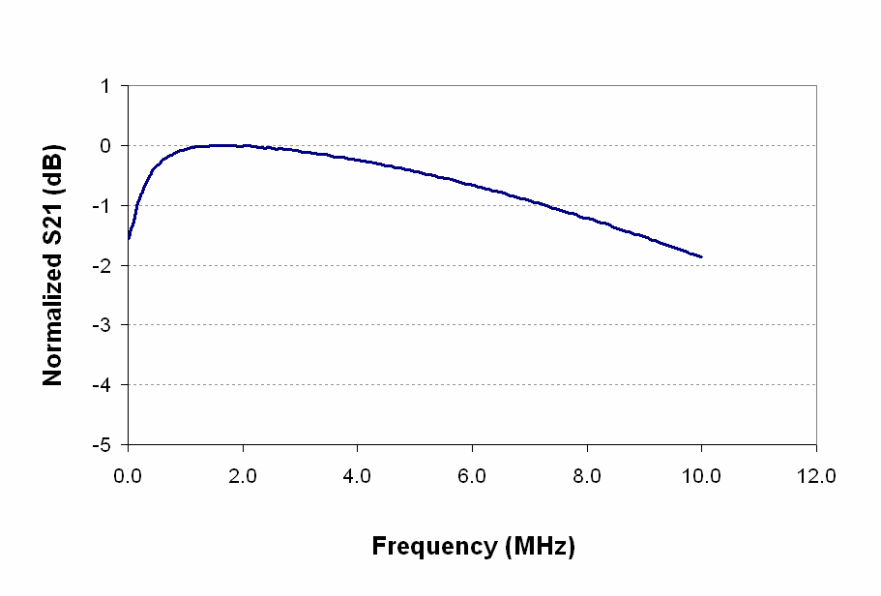

Figure 6.9: The EA normalized S21 measurement result

6.3.3 The Implemented Integrated AET Block

The RFPA, the diplexer and the EA blocks are connected to become one integrated AET block for the 2-carrier signal measurements. The integrated AET block is attached to a heat sink and some microstrip line connections are established between the EA and the diplexer and also between the diplexer and the RFPA. The implemented integrated AET block is shown in Figure 6.10.

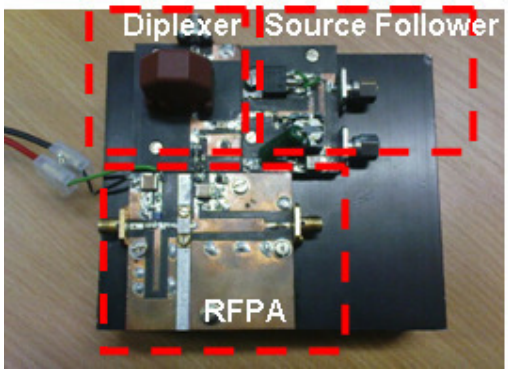

Figure 6.10: The implemented integrated AET block

6.4 The Two-Carrier Signal Measurement Result and Discussion

The new AET experimental setup was developed as shown in Figure 6.11, and the difference between the preliminary AET experimental setup and this new setup is the Integrated AET block. The principle of operation is similar to the preliminary AET setup. The operating frequency for the 25W GaN Class AB RFPA measurements was chosen to be 1.98GHz with 1MHz spacing. On the envelope path, the emulated envelope signal is input to one port of the bias tee. A DC signal is input to the other port of the bias tee to turn on the n-channel FET of the EA. This DC signal biases the transistor into saturation in order for this transistor to perform as a voltage source. The output of this EA is then combined with a DC component through a diplexer. The resulting AET signal biases the drain port of the RFPA.

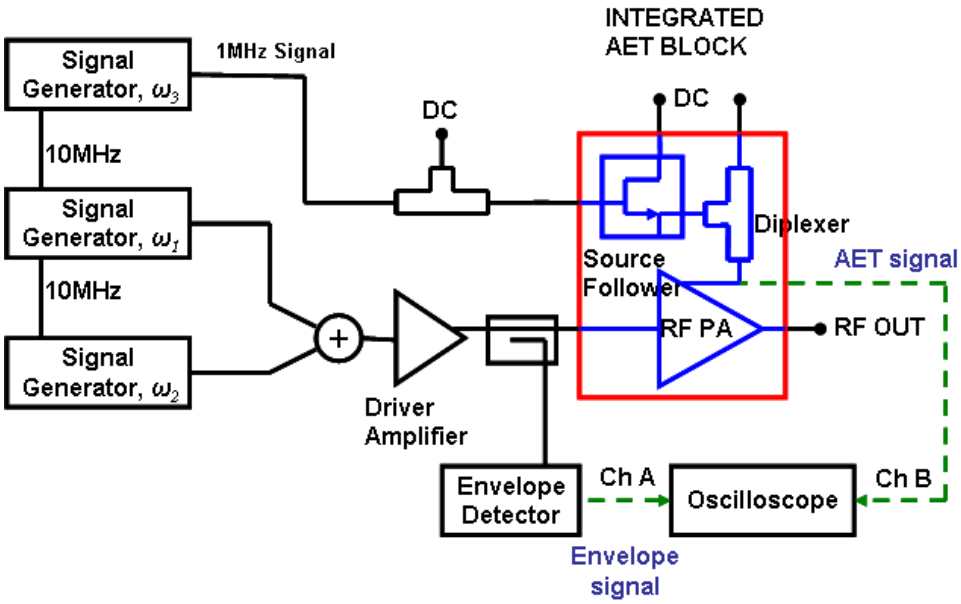

Figure 6.11: The AET Experimental setup with the Integrated AET Block

6.4.1 The AET Signal

The AET signal is an important part of the AET system. It is a tracking signal that biases the drain port of the RFPA and it consists of DC and AC components. The AC component of the AET signal is ideally an exact copy of the RF input signal envelope. Unlike the full tracking signal of the

Envelope, Elimination and Restoration (EER) system [8-9], in the AET system, the AET tracking signal will not track the input signal from the 0V DC. The AET signal will only track part of the full tracking signal. For example, if the full tracking EER signal is from 0V to 28V, then, the AET signal will only track from 18V to 28V, which means a 10V peak-to-peak tracking range. Note that, during the measurement, the AET signal's tracking voltage is varied and optimized at each power level. Furthermore, another advantage of the AET technique is that, the AET signal bandwidth does not have to track the whole envelope signal bandwidth in order to improve the performance of the RFPA.

During the AET system measurement for the two-carrier input signal, all of the three components of the integrated AET block were connected on the setup as shown in Figure 6.11. The AET signal at the drain port of the RFPA (Channel B) and the envelope signal detected at the input of the RFPA (Channel A) were observed on an oscilloscope as shown in Figure 6.12. The AET signal phase is adjusted so that the AET signal is aligned with the envelope signal. This alignment is necessary to achieve symmetry between the upper side and the lower side of the third-order intermodulation, IM3 products and between the upper side and lower side of the fifth-order intermodulation, IM5 products [10-11].

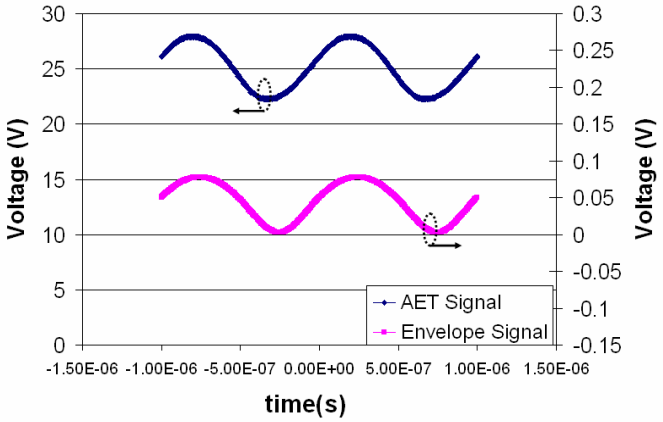

Figure 6.12: The sinusoidal AET signal and the envelope of the RF input signal

6.4.2 Linearity Performance

In this section, the linearity performance of AET system was assessed by measuring the IM3 and the IM5 performance of the RFPA. These measurements were compared to the RFPA biased at fixed drain voltage of 28V for a regular 2-carrier signal measurement. It should also be noted that the heat dissipation will be much lower in the AET case because of the rare occurrence of the peak AET signal, which depends on the peak-to-average ratio (PAR) of the envelope signal. This raises the possibility of using much higher peak AET voltages than would be allowable with a fixed supply.

From Figure 6.13, the IM3 performance from the AET system shows an improvement compared to the IM3 performance at fixed drain voltage for most measured powers. It should be noted that a small improvement is observed from an average output power of about 32dBm and a large improvement at higher power level i.e. about 12-18 dB improvement over a 3dB PBO range. The IM3 performance at the average output power less than 32dBm is not recorded as most RFPAs operate at high power levels to achieve higher efficiency and maximum output power.

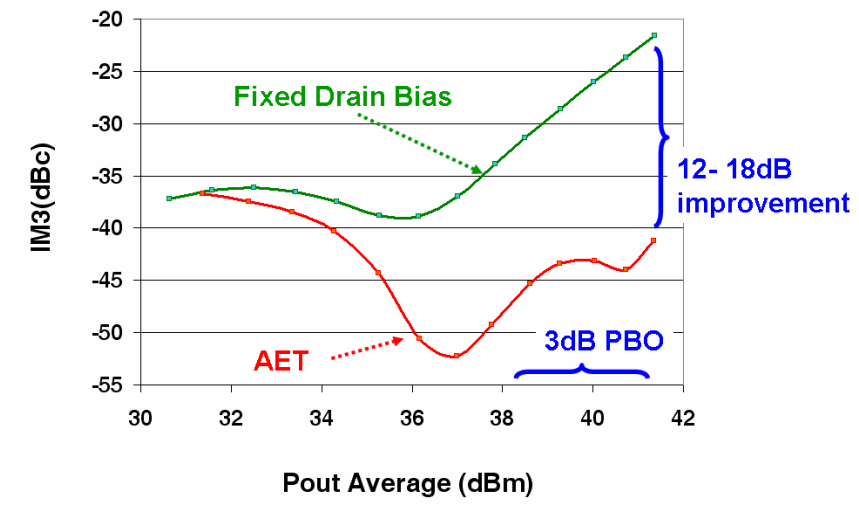

Figure 6.13: The comparison of IM3 performance between AET and fixed bias.

The IM3 performance result that is shown in Figure 6.13 validates the theoretical explanation in Chapter 4 of the varying drain voltage effect on linearity. This result also confirms the linearity improvement from measurements that have been performed separately [12] at a device level by emulating baseband impedances at the drain termination.

The IM5 performance was also measured and the result is shown in Figure 6.14. As shown in this figure, the IM5 performance of the AET system shows substantial improvement over the IM5 performance at a fixed drain voltage between average output powers of 35dBm to 39dBm. Although the IM5 performance does not show any improvement at average output powers higher than 39dBm and lower than 35dBm, the overall performance shows that the IM5 products of the RFPA operating in the AET system remain low compared to the RFPA operating at fixed bias. Since the IM5 products are relatively small, any effects on the RFPA can be removed easily using a filter, due to the fact that the IM5 frequencies are a reasonable distance from the operating frequency.

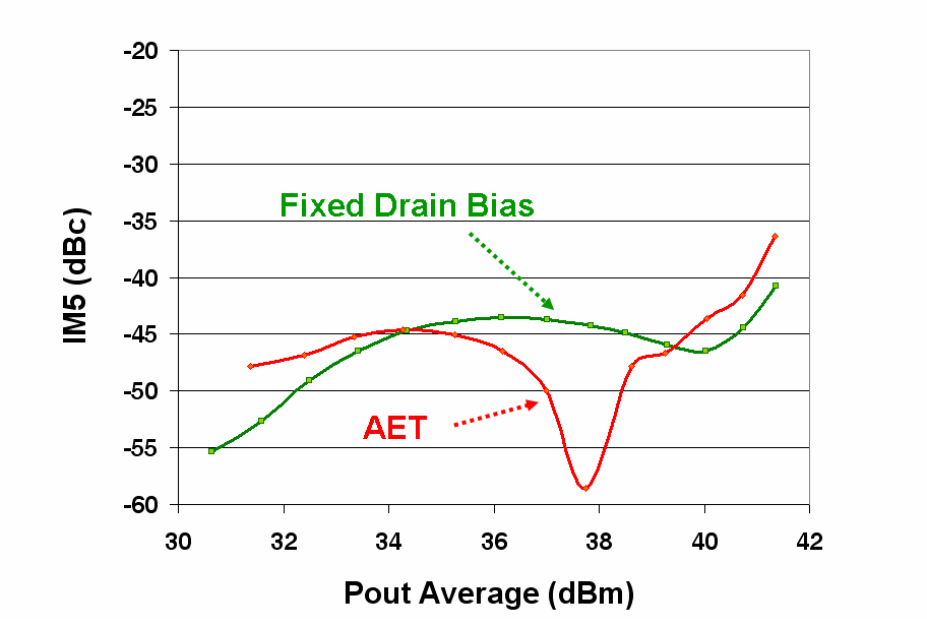

Figure 6.14: The comparison of IM5 performance between AET and fixed bias.

6.4.3 Efficiency Performance

The drain efficiency performance of the RFPA using the AET system is compared to the drain efficiency performance of the RFPA at fixed drain bias. The comparison is done at the same bias conditions as the linearity measurements. The drain efficiency results from the AET system and the fixed drain bias are shown in Figure 6.15.

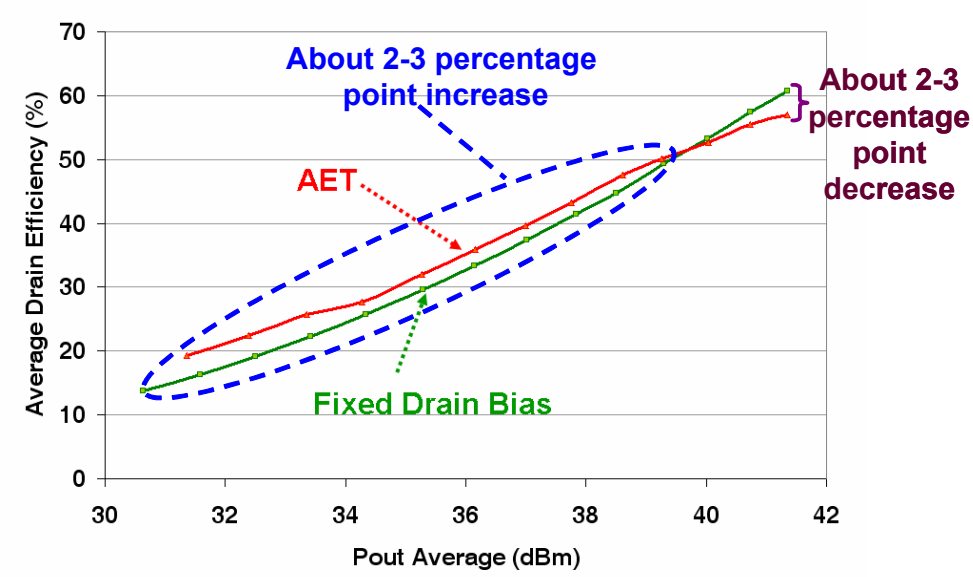

Figure 6.15: The comparison of drain efficiency performance between AET and fixed bias.

From this figure, it can be observed that the drain efficiency of the AET system shows a small improvement (an increase of 2-3 percentage points) compared to the drain efficiency of the fixed drain bias over most of the measured power range. The drain efficiency of the AET system is lower, however, at the maximum average power of about 41dBm. This decrease in efficiency is suspected to be due to the increase of the EA power consumption at higher power levels. Since the EA has a source follower configuration that operates in Class A mode, it consumes higher power compared to a Class B amplifier. Therefore, as will be discussed in Chapter 9, a higher efficiency EA design could improve the AET system efficiency in the future.

Note that, for the AET system drain efficiency calculation, the power consumption for both RFPA and the EA is fully taken into account. For the drain efficiency calculation at a fixed drain bias, only the RFPA power consumption is taken into account.

6.5 Chapter Summary

In this chapter, the two-carrier signal measurements using the AET system are presented. The diplexer and EA design are described. The AET signal that biases the RFPA for this AET system is defined and the RFPA linearity and efficiency performance on AET system is measured. The AET measurement is compared to fixed drain supply operation. The IM3 distortion improvement of between 10dB and 18dB has been observed over a 10dB power range, with an 18dB improvement at the highest power level. The drain efficiency measured shows a 7.5% increase at 3dB power back-off, and generally a small improvement over most of the measured power range. The substantial linearity improvement has been obtained with minimal impact on the overall efficiency of the system, even when the power consumption of the EA is fully taken into account. In fact, over most of the power range, both linearity and efficiency are improved.

6.6 Reference

[1] Wang, F., Kimball, D.F., Popp, J.D., Yang, A.H., Lie, D.Y., Asbeck, P.M., Larson, L.E., "An Improved Power-Added Efficiency 19-dBm Hybrid Envelope Elimination and Restoration Power Amplifier for 802.11g WLAN Applications," IEEE Transactions on Microwave Theory and Techniques., vol.54, no.12, pp.4086-4099, Dec. 2006.

[2] Kim, D., Kang, D., Choi, J., Kim, J., Cho, Y., Kim, B., "Optimization for Envelope Shaped Operation of Envelope Tracking Power Amplifier," IEEE Transactions on Microwave Theory and Techniques, vol.59, no.7, pp.1787-1795, July 2011.

[3] Jeong, J., Kimball, D.F., Kwak, M., Hsia, C., Draxler, P., Asbeck, P.M., "Wideband Envelope Tracking Power Amplifiers With Reduced Bandwidth Power Supply Waveforms and Adaptive Digital Predistortion Techniques,"

IEEE Transactions on Microwave Theory and Techniques, vol.57, no.12, pp.3307-3314, Dec. 2009

[4] "Diplexers Topics" [Online] Available: http://www.qrp.pops.net/dip2.asp

[5] RT/Duroid® 5880 High Frequency Laminate Datasheet [Online] Available: http://www.rogerscorp.com/acm/products/10/RT-duroid-5870-5880-5880LZ-High-Frequency-Laminates.aspx

[6] Sedra, A.S., Smith, K.C., "Microelectronic Circuits", Oxford: Oxford University Press, 2008.

[7] IRF510 N-Channel Power MOSFET Datasheet [Online] Available: http://www.datasheetcatalog.org/datasheet/irf/irf510.pdf

[8] Kahn, L.R., "Single sideband transmission by envelope elimination and restoration," Proc. IRE, vol.40, no.7, pp.803-806, July 1952.

[9] Raab, F.H., "Drive Modulation in Kahn-technique transmitters", Int. Microwave Symp. Digest, vol.2, pp.811-814, Anaheim, CA, June 1999.

[10] Cripps, S., "Advanced Techniques in RF Power Amplifier Design", Norwood, MA: Artech House, 2002

[11] Kenington, P.," High Linearity RF power Amplifier", Norwood, MA: Artech House, 2000.

[12] Akmal, M., Lees, J., Bensmida, S., Woodington, S., Carrubba, V., Cripps, S., Benedikt, J., Morris, K., Beach, M., McGeehan, J., Tasker, P., "The Effect of Baseband Impedance Termination on the Linearity of GaN HEMTs," 40th European Microwave Conference, 2010.

CHAPTER 7

RF BROADBAND TRANSFORMER DESIGN FOR THE AET SYSTEM

7.1 Transformer Modulation for the AET Tracking Generator

7.1.1 Motivation and Overview

Modulated communication signals such as WCDMA and OFDM have high peak-to-average ratio (PAR) and wide bandwidths. These signal properties present a big challenge to the conventional ET system due to the need to design a wideband and high speed tracking generator. Some tracking generator designs for ET system in the literature [1], [2], [3] involved switching, sensing and feedback approaches. These approaches, however, increase the effect of switching transients and the design of the switching and sensing circuitry becomes more complex. In addition, the cost of a broadband and high speed switching generator can be costly, which means its implementation is not cost-effective.

With the AET system, we offer a simplistic tracking generator design and cost-effective implementation whilst providing wide bandwidths and an improvement in the overall system efficiency. For the two-carrier signal measurement in Chapter 6, the AET tracking generator consists of a diplexer and an envelope amplifier (EA). The AET tracking generator in this two-carrier signal measurement used a choke modulation approach. In the WCDMA measurement setup, however, the AET tracking generator design involves a transformer modulation method that uses an RF broadband transformer. The diplexer design in the two-carrier measurement can no longer fulfil the bandwidth requirement of the WCDMA envelope signal. The

RF broadband transformer design in the new setup is capable of tracking a wide bandwidth WCDMA signal in order to provide the AET tracking signal for the RFPA.

7.1.2 Choke Modulation Technique

As previously described in Chapter 4, the concept of AET is to separate the AC component from the DC component in order to improve the overall efficiency of the system. Therefore, in our first AET test setup, using two-carrier signal measurements, we designed the AET tracking generator using a choke modulation approach. As shown in Figure 7.1, the AET generator consists of a diplexer and an EA. The RF choke inductor is part of the diplexer and its function is to present a high impedance in order to prevent any RF or IF signal from passing through to the DC supply. The DC blocking capacitor that is present between the RF choke and the EA stops the DC signal from passing through to the EA. The AC part of the tracking signal is provided by the EA, which will later combine with the DC part of the tracking signal from DC supply at point X. The combination of these two signals is called the AET signal, and biases the drain port of the RFPA.

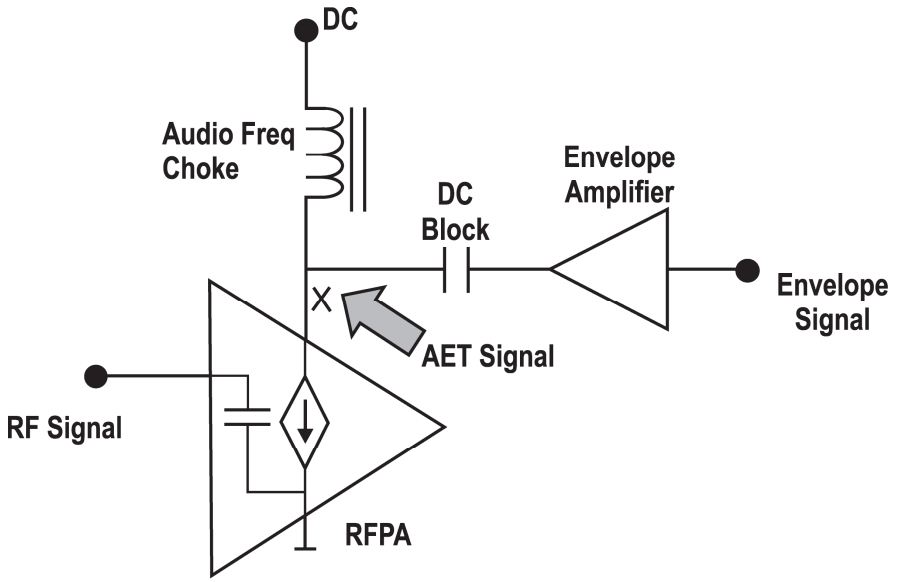

Figure 7.1: The AET tracking generator using choke modulation

Even though a high fidelity tracking signal is obtained using this approach for two-carrier measurements, two issues arise when implementing the same approach for a WCDMA application. The first issue is the bandwidth and PAR of the signal. For the two-carrier measurements discussed in Chapter 6, the bandwidth of the signal is 1MHz and the PAR is 3dB. However, the bandwidth and PAR of a WCDMA signal are more demanding compared to a two-carrier signal. The signal bandwidth of WCDMA is about 5MHz and the PAR can be as high as 10dB. Therefore, the diplexer design can be more challenging inasmuch as a higher inductance choke is required. A new 'in-house' inductor design is necessary to fulfil the bandwidth requirement.

The second issue is the efficiency of the EA that needs to be included in the overall RFPA drain efficiency calculation. The EA was designed using a source follower configuration that has been discussed in Chapter 6. For the EA to provide at least 10V tracking voltage, it can consume substantial amounts of DC power. Therefore, since our approach is to have a simplistic and cost-efficient envelope amplifier design, instead of redesigning the envelope amplifier, we developed the transformer modulation technique to be incorporated into the AET tracking generator design. This addressed the two issues that were identified for WCDMA test measurements.

7.1.3 Transformer Modulation Technique

In the transformer modulation approach, an RF broadband transformer is designed to replace the diplexer. A transformer is a very simple and versatile device with many benefits. Apart from the main ability to convert between different levels of voltage and current in AC circuits, the transformer also has electrical isolation between the primary and secondary winding circuits. This electrical isolation is important in AET system to ensure that the EA circuitry is not affected by any changes in baseband impedance viewed from the RFPA.

As shown in Figure 7.2, the AC part of the AET tracking signal is provided by the same EA used for the 2-carrier measurement and it is combined with the DC part of the tracking signal at point X. The AC signal from the EA is

transferred from the primary winding of the transformer to the secondary winding by the mutual electromagnetic induction. It is also designed to have a voltage transformation ratio of 1:2. In this case if a 10V tracking signal is required at point X, then the EA only needs to generate a 5V WCDMA envelope signal. Therefore the tracking signal requirement of the EA is relaxed through the use of this transformer voltage transformation. This voltage transformation is achieved whilst both primary and secondary windings are electrically isolated.

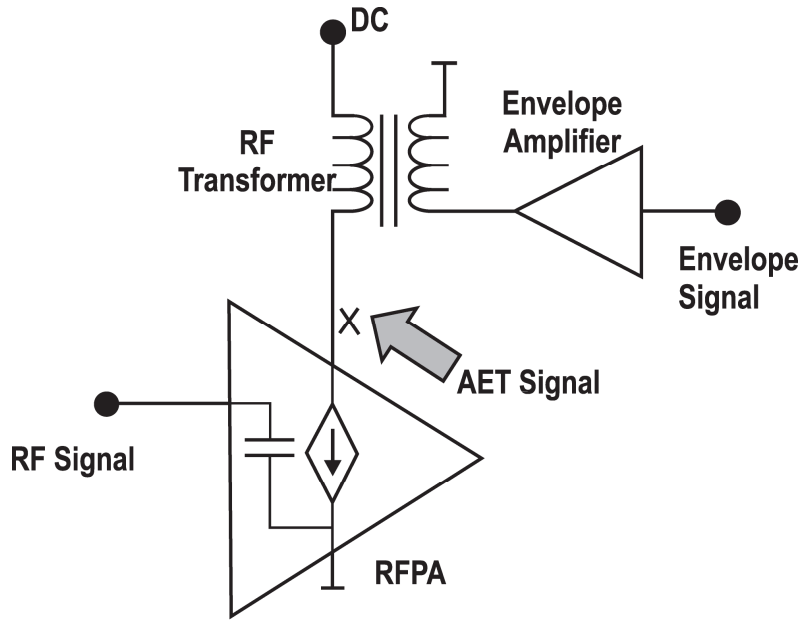

Figure 7.2: The AET tracking generator using the transformer modulation

7.2 Transformer Design for AET Operation

This research work is partly motivated from the lack of data capacity in mobile communication network. Although the communication industry is increasing the data capacity of their network, there is another issue regarding the signals propagation on macro-cell networks. As the operating frequency of the signal increases, the wavelength decreases and therefore, the signal attenuation increases in the macro-cell network. In order to solve this problem, the communications industry is now looking at smaller base stations in a micro or nano cell network as a solution. For a small base station, all the building blocks such as the RFPA are also required to be small in size and

low power consumption. Therefore, RF broadband transformer in an AET system must also be small in size, whilst being usable at RF frequencies and having a wide bandwidth. To fulfil these requirements, a small toroidal core is chosen. In order to accommodate wider bandwidth of the WCDMA communication signal, a ferrite-core material is selected.

7.2.1 Toroidal Core

There are a few types of transformer core, namely laminated steel cores, solid cores, toroidal cores and air cores. For this RF broadband transformer for the WCDMA application, we chose the toroidal core. A toroidal core is a ring-shaped core which usually has a square or a rectangular cross section. Examples of toroidal core transformers are shown in Figure 7.3.

The first advantage of using this toroidal core for the RF broadband transformer is its efficiency compared to transformers using other types of cores [4],[5],[6]. Windings on the toroidal core are usually wrapped evenly and tightly with no air-gap so that the magnetic flux occurs only within the windings. This winding orientation thus creates high flux density and reduces any flux leakage and so high electrical efficiency can be achieved. The overall efficiency of this toroidal transformer is usually about 90 to 95% [4].

Secondly, this toroidal transformer makes less noise and mechanical hum from magnetostriction during its operation because of the uniform distribution of its windings [4], [5], [6]. When this toroidal transformer is tightly wound, stray fields from the air gap can also be eliminated.

Another important benefit from using a toroidal core for this RF broadband transformer is its small size, which minimizes the required space in the overall system. This toroidal transformer can be mounted easily by using only one central screw, and therefore the production time is sped up and the number of parts required for mounting the hardware is lowered [4].

Figure 7.3: Example images of toroidal transformer

7.2.2 Trifilar Winding

In the RF broadband transformer, the toroidal core is wound with a trifilar winding. Trifilar winding consists of three closely spaced parallel wires that have three different colours, as shown in Figure 7.4. When the winding is arranged so that the current flows in the same parallel direction, the potential difference is magnified. On the other hand, when the winding is arranged so that the magnetic field created in one winding is in the opposite direction to the magnetic field created in the other winding, magnetic fields cancel [7].

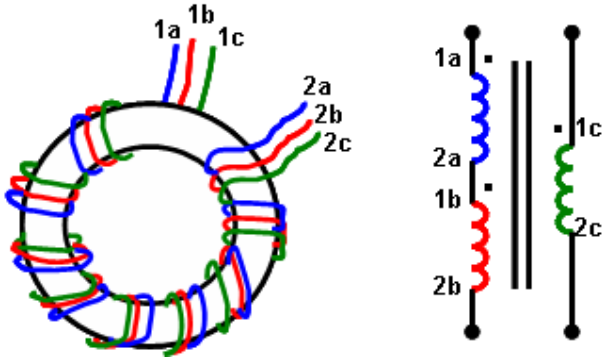

Figure 7.4: The trifilar wound transformer configuration

This toroidal transformer with trifilar winding can be used as a balanced signal splitter when the centre-tap (between point 2a and point 1b) is connected to ground. However, in our application, we connect point 2a and point 1b together, therefore; we will achieve a step-up or step down transformation depending on the connection of the transformer to the whole system.

7.2.3 Ferrite Core and its Effect on Bandwidth

The toroidal core can be made from materials such as iron or ferrite [5], [6]. Since ferrite has higher permeability, it is able to provide a wider bandwidth. Therefore, a ferrite toroidal core is chosen for the design of the RF broadband transformer for WCDMA applications.

Referring to Appendix A.3, the low cut-off frequency is determined by the load resistance, R_{LOAD}, the input resistance, R_{IN} and also the shunt inductance, L_E. This shunt inductance, L_E, is a representation of any non-linear effect resulting from magnetising current generating the flux in the primary winding. Therefore, this shunt inductance, L_E, is influenced by the permeability of the ferrite-core, the number of turns in the primary winding and the geometry of the ferrite-core [8]. The higher the permeability of the ferrite core and the number of turns in the primary winding, the greater the shunt inductance value. From equation (A.9) in Appendix A, it can be seen that shunt inductance, L_E is inversely proportional to the low cut-off frequency. Thus, the higher the core's permeability value, the lower the cut-off frequency of operation, which in turn increases the bandwidth of the transformer.

From equation (A.10) in Appendix A, the high cut-off frequency is determined by the leakage inductance, L_L and the distributed capacitance, C_D. As mentioned earlier, the leakage inductance is due to some loss in the flux at the primary winding and is not related to the secondary winding. Meanwhile, the distributed capacitance represents the stray capacitance of the coil that is created from any small distance that is unintentionally created between the core and the ground. These two elements are influenced by the number of

turns and the coil geometry, which can also be roughly estimated to be proportional to the coil volume. Hence, the higher the coil volume, the higher the two elements' values. The effect of this is to lower the high cut off frequency and reduce the bandwidth of the transformer [8].

7.3 Transformer Measurement, Results and Discussion

In order to investigate the best RF broadband transformer performance, ferrite core saturation, transmission return loss and transmission loss measurements were done. In this experimental investigation, three different types of ferrite core, three different numbers of turns on the core windings and two different core geometries were tested to find the most suitable design for the AET system.

7.3.1 Comparison of RF Broadband Transformer Performance in terms of Ferrite-Core Materials and Number of Turns on Core Windings

All toroidal ferrite cores used in these measurements were purchased from Fair-Rite [9]. Ferrite is a ceramic material that is created through a chemical reaction of metal oxide with some type of magnetic material [10]. The two types of ferrite core chosen for this testing were Material 78 and Material 43. Material 78 is made from a chemical composition of iron oxide (Fe_2O_3), manganese oxide (MnO) and zinc oxide (ZnO) that we called MnZn ferrite. Material 43 is made from a chemical composition of iron oxide (Fe_2O_3), nickel oxide (NiO) and zinc oxide (ZnO) that we called NiZn ferrite. Material 78 has an initial permeability of $2300Hm^{-1}$ while Material 43 has an initial permeability of $800Hm^{-1}$.

To test these materials for use in an RF broadband transformer, $7cm^3$ toroidal cores from these two materials are compared. These $7cm^3$ toroidal cores have 35.5mm outer diameter, 23mm inner diameter and 12.7mm thickness. These dimensions are clarified in Figure 7.5.

Each of these toroidal cores is wound with trifilar enamelled copper wire. Since we are also investigating the effect of the number of turns in each

winding on the performance of the RF transformer, different numbers of were tested. The numbers of turns wound on the primary winding were 8, 16 and 32. Therefore, to preserve the 1:2 transformation ratio, there were 16, 32 and 64 turns on the secondary winding respectively. All of these transformers are shown in Figure 7.7.

From the S_{21} measurement, the RF transformer performance in terms of the insertion loss can be plotted and the frequency bandwidth of the transformer can be measured. The S_{21} measurement setup is shown in Figure 7.6.

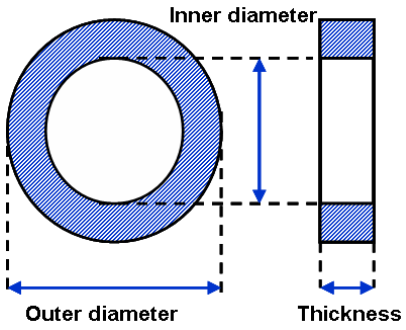

Figure 7.5: Configuration of the toroidal core

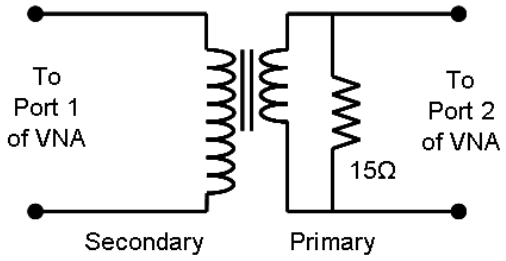

Figure 7.6: The S_{21} measurement setup

In the S_{21} measurement setup, the primary winding has a 15Ω shunt resistor between the transformer and Port 2 of the VNA. Ideally, for a 1:4 impedance ratio transformer, the impedance at primary winding is 12.5Ω and the impedance at the secondary winding is 50Ω. Since both ports of VNA are 50Ω terminated, 15Ω is the off-shelf resistor value chosen to give the resulting effective impedance which is closest to 12.5Ω. Note that the

effective impedance of 15Ω and 50Ω in parallel is about 11.5Ω which is closest to the experimental effective impedance of 12.5Ω. In this measurement, the operating frequency range was between 10 kHz and 20 MHz.

Figure 7.7: RF broadband transformers for two types of material with different number of turns on the core windings.

From the S_{21} measurement, the frequency response that shows the insertion loss of the transformer is plotted. The frequency response of the Material 43 and 78 transformers for 8, 16 and 32 winding turns are shown in Figure 7.8, 7.9 and 7.10 respectively. For 8 turns, the 3dB bandwidths for the two transformers were from about 40 kHz to 11.24 MHz for Material 43 and from below 10 kHz to 11.96 MHz for Material 78. Material 78 has a higher permeability, and hence a lower cut-off frequency. Note that the lowest measurement frequency of the VNA is 10 kHz.

From these plots we can observe that the 3dB bandwidth of the Material 78 transformer is slightly wider than the Material 43 bandwidth. We can also observe from these plots that the transformer with the least number of turns, in this case 8, has the widest bandwidth compared to other transformers.

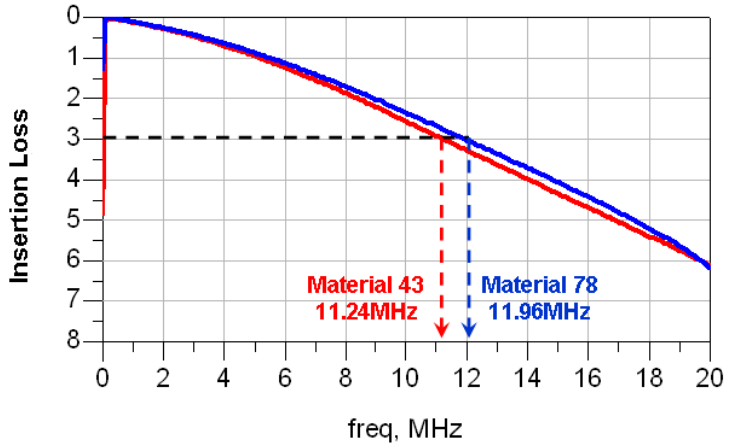

Figure 7.8: The frequency response for Material 43 and 78 transformers for 8 toroidal winding turns

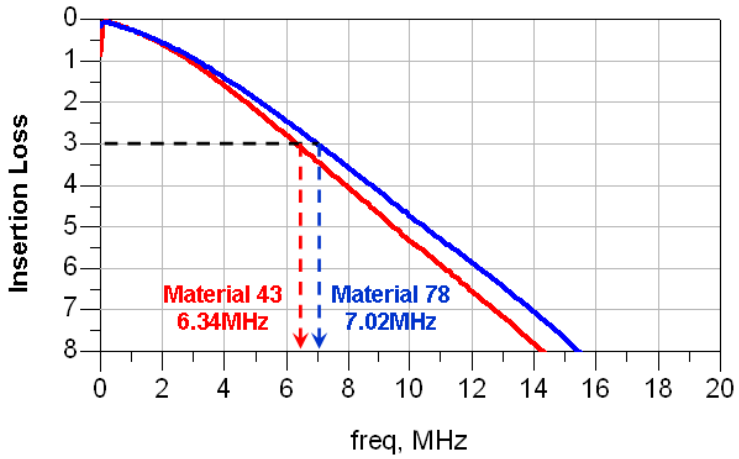

Figure 7.9: The frequency response for Material 43 and 78 transformers for 16 toroidal winding turns

The summary of the measurement results is shown in the Table 7.1 below.

PRIMARY TURNS NUMBER	8		16		32	
Core Material	f_L	f_H	f_L	f_H	f_L	f_H
Material 78	10kHz	11.96MHz	10kHz	7.02MHz	10kHz	4.30MHz
Material 43	40kHz	11.24MHz	10kHz	6.24MHz	10kHz	4.25MHz

Note: The VNA lowest measurement frequency is 10kHz.

Table 7.1: The summary of the 3dB bandwidth of the transformers for different core materials and different primary number of turns.

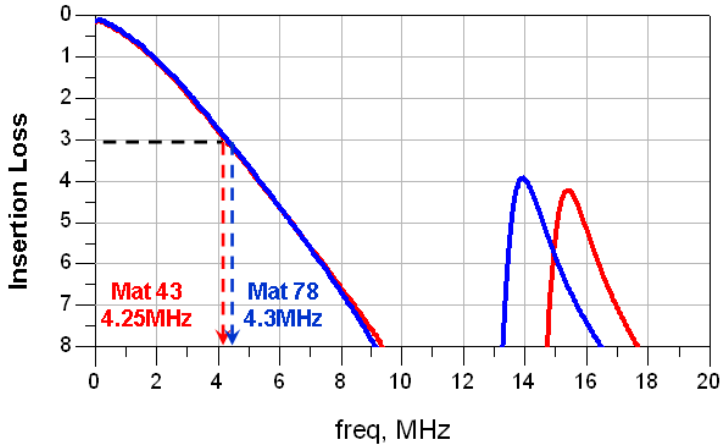

Figure 7.10: The frequency response for Material 43 and 78 transformers for 32 toroidal winding turns

7.3.2 Size Comparison for RF Broadband Transformer Performance

We have seen the effect of the permeability of the materials on the performance of the transformers. We have also seen the significant effect that the number of winding turns has on the performance of the transformer, in particular the bandwidth. In this section, we have considered two different core geometry sizes in order to assess the effect on the transformer. Both transformers have 8 winding turns and are made from Material 43. The first transformer core geometry has 7cm^3 effective core volume with 35.5mm outer diameter, 23mm inner diameter and 12.7mm thickness. The second

transformer core geometry has a 2.36cm^3 effective core volume with 21.0mm outer diameter, 13.2 inner diameter and 11.9mm thickness. The two transformers are shown in Figure 7.11.

From the frequency response shown in Figure 7.12, it can be observed that when the size of the transformer is decreased, the high cut-off frequency is slightly increased for the same material and number of turns. This is because as the size of the core decreases, the stray capacitance and leakage inductance, explained in section 7.2.3, is decreasing. The summary of the 3dB bandwidth of the transformers is shown in Table 7.2.

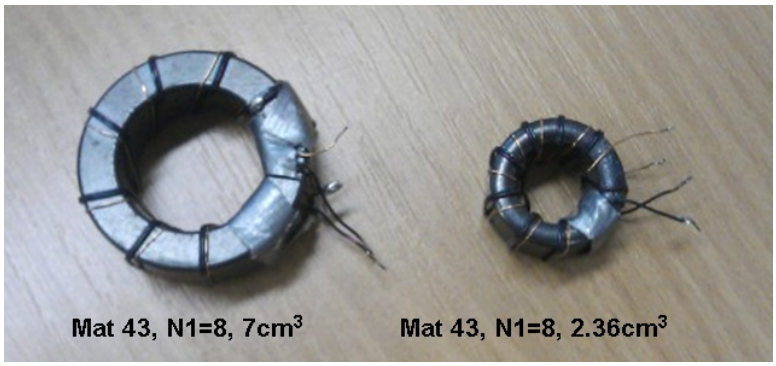

Figure 7.11: Two different size transformers used for the test

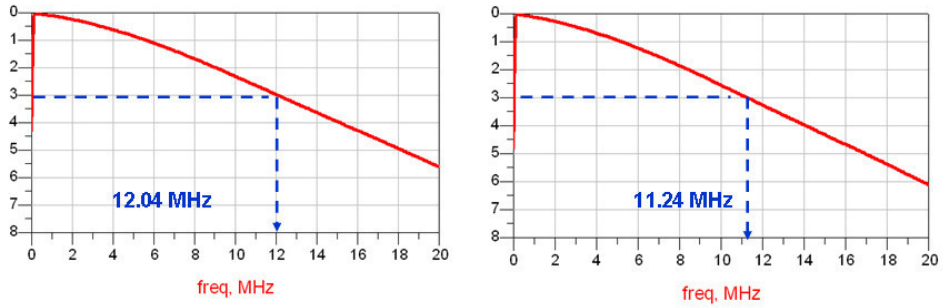

Material 43: N1=8
Outer diameter=29mm

Material 43: N1=8
Outer diameter=35.5mm

Figure 7.12: The frequency response of the two transformers

CORE VOLUME	$7CM^3$	$2.36CM^3$
f_L (kHz)	10	10
f_H (MHz)	11.24	12.04

Note: The VNA lowest measurement frequency is 10kHz.

Table 7.2: The summary of the 3dB bandwidth of the transformers for different size.

7.3.3 Ferrite Core Saturation Test

A ferrite core saturation test is carried out in order to ensure the saturation point of the ferrite core is not reached during the operation of the transformer in the AET system measurement. Since the magnetic core used for this transformer is a ferromagnetic material, there is a saturation limit to be observed. Precautionary steps should be taken to avoid saturation in the core when a signal is applied to the transformer. If the core saturation is reached, the induced voltage signal at the secondary winding will no longer be linear, but will be distorted [11]. This is undesirable as it will add nonlinearity to the AET signal. The temperature of the transformer can also increase when the core is saturated and consequently could cause the device or circuitry to become inoperative [12].

In order to understand the underlying reason behind the test, it is important to understand the magnetic limitations of the transformer core. Therefore, we have to understand the relationship between the current applied, I, the magnetic flux induced, B and the resulted magnetic field, H. The relationship will then determine the circuit parameters such as inductance and impedance.

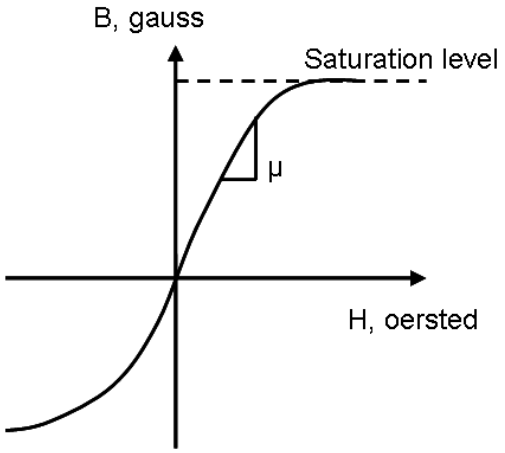

Figure 7.13: An example of a ferromagnetic material magnetisation curve

Inductance is defined as the instantaneous ratio of total magnetic flux linkage to the applied current [12]. This inductance is also proportional to the permeability, μ of the magnetic core. The relation of the inductance, permeability and magnetization can be illustrated by the magnetisation curve shown in Figure 7.13. This magnetisation curve shows the nonlinear relationship between the magnetic flux, B and the magnetic field, H. The gradient of this curve is defined as the permeability, μ of the core by the equation (7.1) below;

$$B = \mu H \,. \qquad (7.1)$$

At low frequency, equation (7.1) is scalar but at high frequency, the equation becomes complex [12]. From Figure 7.13, we can see that the gradient decreases when the magnetic field is increased. As mentioned earlier, the inductance, L, is proportional to the permeability, μ, therefore, the inductance of the transformer winding will decrease under large signal conditions. From the equivalent circuit shown in Figure A.2 (in Appendix A), the inductance that is affected by the core is represented by the shunt inductance, L_E. Referring to Figure A.2, let I_1 represent the current flowing in the primary winding, which has the relationship as in equation (7.2) below;

$$V = L_E \frac{\partial I_1}{\partial t}. \qquad (7.2)$$

When we integrate equation (7.2) and assume the applied voltage is a sinusoidal signal, the primary winding current, i_1 is then the integral form of equation (7.3);

$$i_1(t) = \frac{1}{L_E[i_1(t)]} \int_{-\infty}^{t} V \sin(2\pi ft) dt . \qquad (7.3)$$

Note that the inductance is also a function of instantaneous current. From equation (7.3) and Figure 7.13, it is shown that when the current in the primary winding becomes very large, the saturation level is reached. The slope of the magnetization curve becomes very small which means permeability drops to a very low value and so does the inductance of the primary winding L_1. This means that the impedance of the primary winding also decreases substantially [12].

As mentioned earlier, equation (7.1) becomes complex at higher frequencies. Therefore, core saturation is not only influenced by the signal applied to the transformer but also by the frequency of operation [12], [13]. Hence, in the core saturation test, we are observing whether there is any change in the return loss (S_{11}) over a specified frequency range. The core saturation test setup is shown in Figure 7.14.

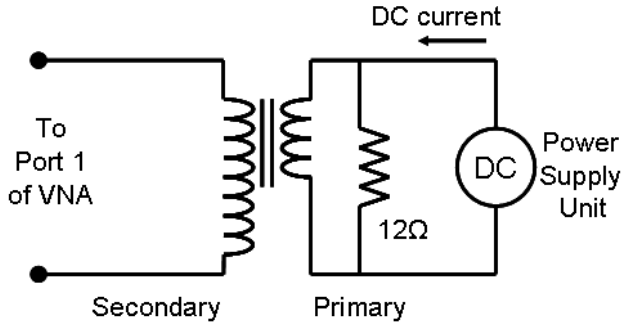

Figure 7.14: The core saturation test setup

For the AET tracking generator, the transformer will be connected to a Class AB RFPA. The maximum DC current required to bias the drain port of the RFPA is approximately 1A. Therefore, in this test, the DC current that is supplied to the primary winding is swept from 0 to 1A. Since the VNA present a 50Ω termination and the transformer has a 1:4 impedance transformation, a 12Ω shunt resistor needs to be placed between the primary winding and the DC power supply unit. The frequency range chosen for this measurement was between 10 kHz and 20 MHz.

As we increase the DC current from 0A to 1A, there are no changes observed in the S_{11} curves shown in Figure 7.15 and 7.16, measured on transformers of Material 43 and Material 78 respectively.

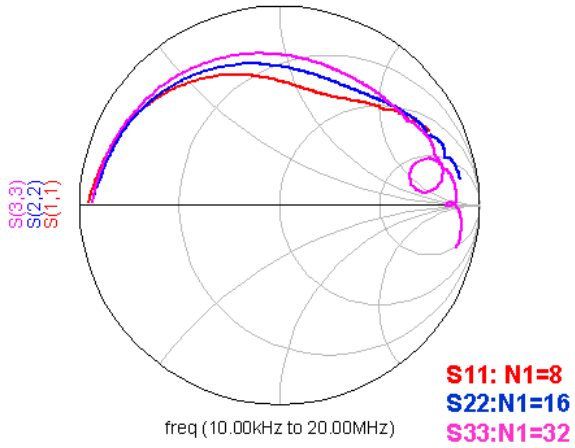

Figure 7.15: The saturation test measurements of Material 43 transformers

7.3.4 RF Broadband Transformer Performance Summary

As a result of the measurements on the transformers, the chosen transformer for the AET system was the transformer made from Material 43 with 8 winding turns and has a smaller effective cross-sectional area. Apart from the advantage of the transformer size on bandwidth, it saves space on the circuitry on the final AET system layout. Material 43, a NiZn ferrite material, is also recommended for high frequency broadband transformers due to its material properties [14].

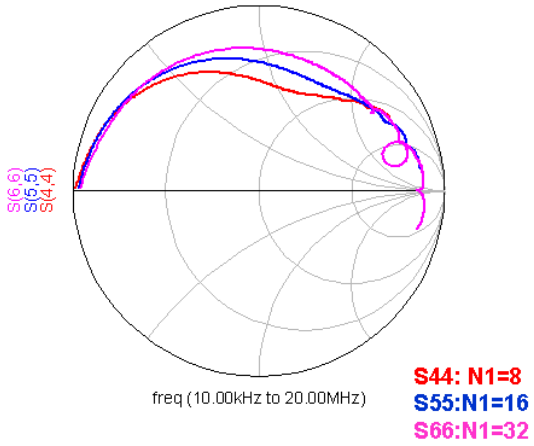

Figure 7.16: The saturation test measurements of Material 78 transformers

Note that, however, from the measurement results on the comparison between Material 43 and Material 78, Material 78 transformers have a slightly higher high-end cut-off frequency. It is recommended that the same smaller core size transformer made from Material 78 be measured in future in order to achieve higher bandwidth. Since the WCDMA signal bandwidth is about 5MHz, the small sized Material 43 transformer with 8 winding turns, which has a bandwidth from about 10kHz to 12MHz, is suitable for the AET system designed for WCDMA applications.

As explained in section 7.2.3, the high-end cut-off frequency of the transformer is influenced by the inductance leakage and stray capacitance. Therefore, the smaller the size of the core and the lower the number of turns, the lower the leakage inductance and stray capacitance, which leads to a higher high-end cut-off frequency. For the low cut-off frequency of the transformer, the effect of higher permeability can only be observed from the comparison between the transformer of 8 winding turns for Materials 43 and 78. The low cut-off frequencies of the transformers with 16 and 32 winding turns are too low to be measured on the VNA, which has a frequency range starting at 10 kHz.

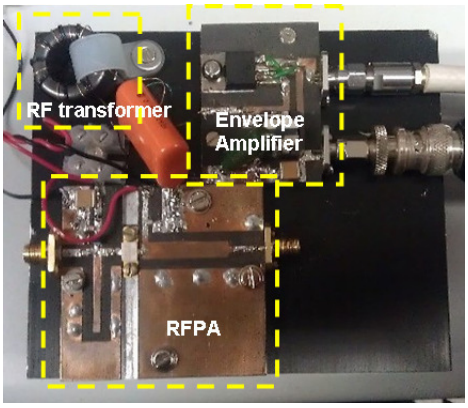

Figure 7.17: The implemented AET generator and the RFPA

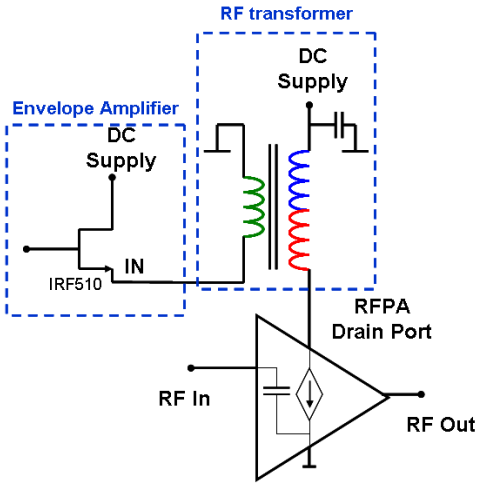

Figure 7.18: The schematic configuration of the AET generator and the RFPA

7.4 Integrated AET Tracking Block

The AET tracking generator for WCDMA applications, which utilises the transformer modulation technique that has been discussed in this chapter, consists of a RF broadband transformer and an envelope amplifier. The implemented AET generator is connected to the RFPA as shown in Figure 7.17. The configuration of the RF transformer, envelope amplifier and RFPA, which we term the Integrated AET Block, is shown in Figure 7.18.

7.5 Chapter Summary

The RF broadband transformer used in the AET tracking generator has been designed and discussed in this chapter. The chosen RF broadband transformer for the WCDMA application is made from Material 43 and the toroidal core used has an effective core volume of 2.36cm^3. The number of winding turns is 8. The choice of material, number of turns and size of the RF broadband transformer has been investigated in this chapter. The envelope amplifier in this integrated AET generator is the same envelope amplifier used for the two-carrier signal measurements; the design of which has been discussed in detail in Chapter 6. The combination of RF broadband transformer, envelope amplifier and RFPA is termed the Integrated AET block. The measurement of this AET block using WCDMA signals will be described and discussed in Chapter 8.

7.6 Reference

[1] Draxler, P., Lanfranco, S., Kimball, D., Hsia, C., Jeong, J., van de Sluis, J., Asbeck, P.M., "High Efficiency Envelope Tracking LDMOS Power Amplifier for W-CDMA," IEEE MTT-S Int. Microwave Symposium Digest, 2006, pp.1534-1537, 11-16 June 2006.

[2] Kimball, D.F., Jeong, J., Hsia, C., Draxler, P., Lanfranco, S., Nagy, W., Linthicum, K., Larson, L.E., Asbeck, P.M., "High-Efficiency Envelope-Tracking W-CDMA Base-Station Amplifier Using GaN HFETs IEEE Transactions on Microwave Theory and Techniques, vol.54, no.11, pp.3848-3856, Nov. 2006.

[3] Rahkonen, T., Jokitalo, O. P., "Design of a linearly assisted switcher for a supply modulated RF transmitter," 24th Norchip Conference, Proceedings, pp. 1-4, 2006.

[4] "Transformers Technical Notes", [Online] Available: http://www.avellindberg.com/transformers/tech_notes/tech_notes2.htm

[5] "Transformer", [Online] Available: http://en.wikipedia.org/wiki/Transformer

[6] "Toroidal Transformer Basics", [Online] Available: http://www.raftech.com/TECHNOLOGY/ElectromagneticBasics/ToroidalTransformerBasics/tabid/112/Default.aspx

[7] "Bifilar Coil", [Online] Available: http://en.wikipedia.org/wiki/Bifilar_coil

[8] W.M. Flanagan, "Handbook of Transformer Design & Applications", Boston, MA, McGraw-Hill, 1992.

[9] Fair-rite Product Corp. [Online] Available: http://fair-rite.com/newfair/index.htm

[10] Fair-rite Product Corp. Presentation [Online] Available: http://www.ieee.li/pdf/viewgraphs/ferrites.pdf

[11] "Transformers – Core Saturation" [Online] Available: http://www.opamp-electronics.com/tutorials/core_saturation_2_09_11.htm

[12] "Understanding Transformers: Characteristics and Limitations", [Online] Available: http://www.conformity.com/artman/publish/printer_47.shtml

[13] "RF Transformers", [Online] Available: http://www.minicircuits.com/app/TRAN14-2.pdf

[14] "Use of Ferrites in Broadband Transformers", [Online] Available: http://fair-rite.com/newfair/pdf/Broadband.pdf

CHAPTER 8

WCDMA SIGNAL MEASUREMENTS OF THE AET SYSTEM

8.1 Development of WCDMA Signal Measurements of the AET System.

8.1.1 Motivation and Overview

The developed AET technique has been tested using two-carrier signal measurement in [1], and the results in terms of efficiency and linearity are presented. It has been shown in [1] that, by applying the AET signal at the drain bias, the RFPA linearity performance improved in terms of IM3 when compared to fixed voltage drain bias operation. This is achieved whilst having a small improvement on the RFPA drain efficiency at most measured powers. It has been shown from this two-carrier measurement that the AET technique has the potential to improve both efficiency and linearity of the RFPA. With the existing technologies such as Wideband Code Division Multiple Access (WCDMA) and Enhanced Data for Global Evolution (EDGE), and emerging technology such as Long Term Evolution (LTE) in mobile communications system, it is useful to measure the AET technique using more complex modulated signals where practical linearity and efficiency performance will be investigated. In this work, a WCDMA signal was chosen as the modulated signal to test this AET technique.

8.1.2 Generation of WCDMA Signal

WCDMA is a third-generation (3G) wireless communication standard that uses frequency division duplexing (FDD). For WCDMA, the signal is spread

across a 5MHz bandwidth using quadrature-phase shift keying (QPSK) modulation. In this project, the WCDMA signal used is a standard-compliant 3GPP WCDMA test signal created using Agilent N700B Signal Studio. A single carrier WCDMA signal at 1.98GHz with a PAR of 9.17dB was downloaded to an Agilent PSG E8267D signal generator. The complementary cumulative distribution function (CCDF) of this signal is shown in Figure 8.1 and the signal spectrum is shown in Figure 8.2. From this WCDMA spectrum we can see that the bandwidth of the WCDMA signal is 5 MHz.

The maximum average output power that can be generated linearly by this PSG is 25dBm. The PAR of this WCDMA signal is 9.17dB, therefore, in order to maintain the linearity of the AET system, the maximum average output power to be generated was set to 15dBm so that the peak output signal of 24.17dBm can be generated. The PSG dynamic range was taken into account in order to avoid any additional distortion being included in the final RFPA linearity measurement.

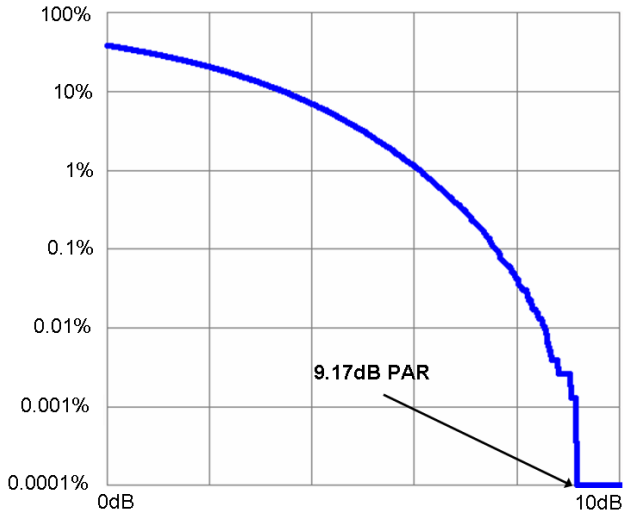

Figure 8.1: The CCDF of the WCDMA Signal with 9.17dB PAR.

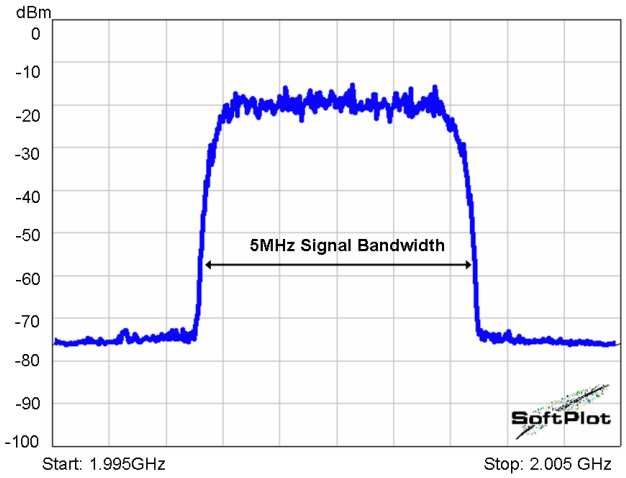

Figure 8.2: The WCDMA signal spectrum

For this WCDMA signal measurement, the signal baseband spectrum is also observed. It is important to measure in the baseband signal as the AET tracking signal is coming from the envelope of the RF signal. A suitable choice of envelope detector and the design of the tracking generator are dependent on the bandwidth of the baseband signal. From Figure 8.3 and 8.4, it is shown that the baseband signal of this WCDMA signal has a bandwidth of about 3 MHz and that most of this baseband signal lies between DC and 500 kHz.

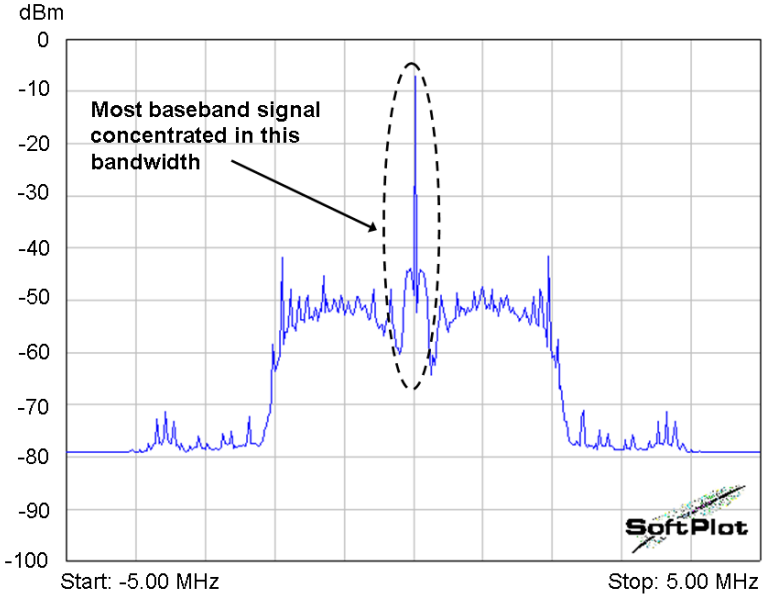

Figure 8.3: The WCDMA baseband signal

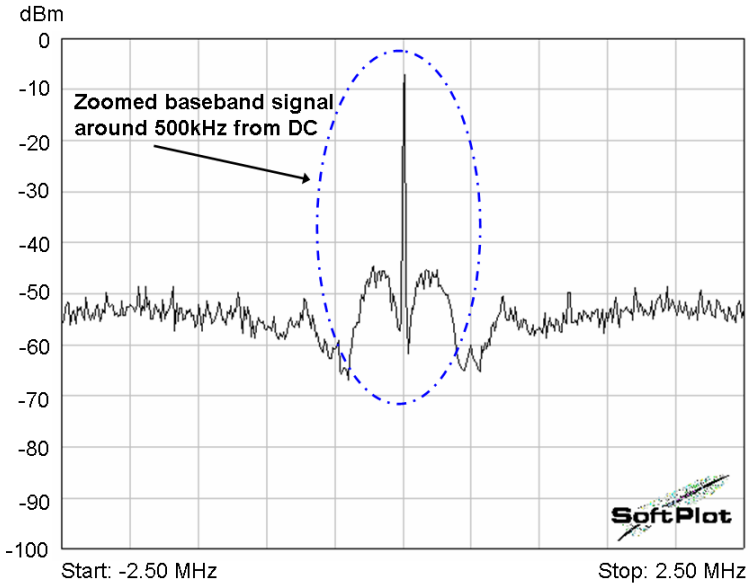

Figure 8.4: The WCDMA baseband signal zoomed in around 500kHz

8.1.3 WCDMA Signal Envelope Detection

One important concept in AET is that the RFPA should be biased with the modulated signal envelope at its drain port. In an EER system, the drain bias signal must track the whole bandwidth of the modulated signal envelope [2]. In AET however, the tracking signal has a relaxed requirement on the bandwidth that must be tracked. Since the WCDMA baseband signal bandwidth is between DC and 3 MHz, a suitable envelope detector needs to be selected. There are a number of detectors that were tested for this application, namely; AD8361 Tru Power Detector from Analog Devices, Marconi Detector, and also an HP Detector, as shown in Figure 8.5. The AD8361 detector is a mean-responding power detector which works up to 2.5GHz. The Marconi detector is a wide band detector that can detect signals from 50MHz to 12.4GHz while the HP detector is a negative detector that works from 2GHz to 18 GHz. All of these square law detectors were tested with the WCDMA signal generated using an Agilent PSG E8267D, and the waveforms were observed on an Agilent 54624A Oscilloscope. The test setup is shown in Figure 8.6.

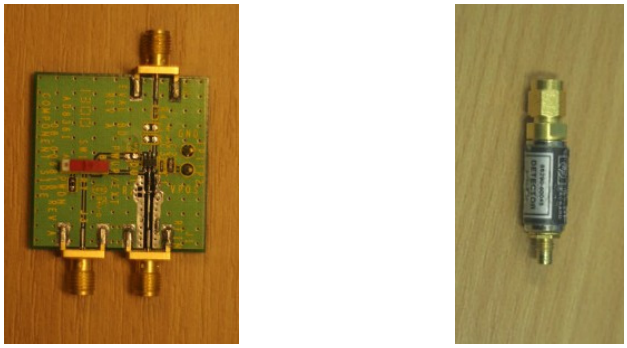

(a) (b)

(c)

Figure 8.5: (a) AD8361 detector (b) HP Detector (c) Marconi Detector

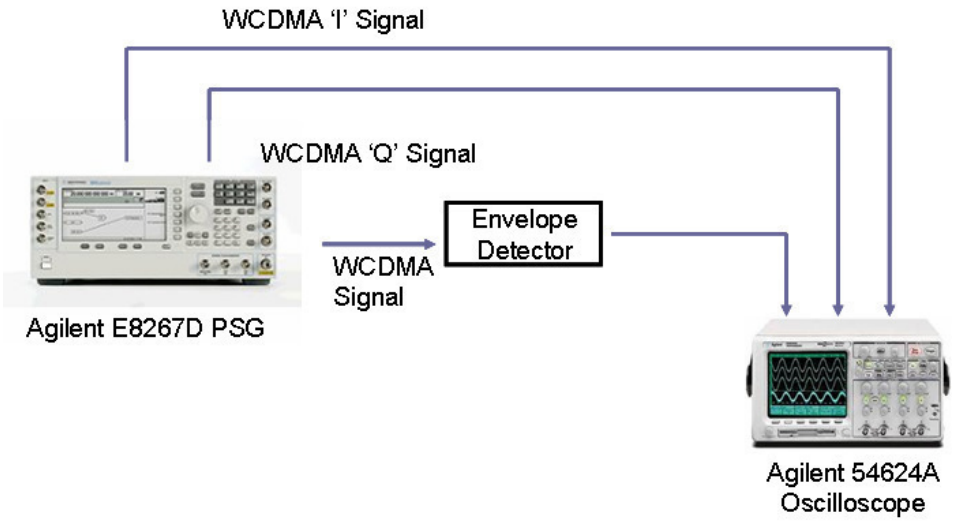

Figure 8.6: The envelope detection test setup

The WCDMA in-phase (I) and quadrature (Q) signals are simultaneously measured on the oscilloscope. The WCDMA I and Q signal is then calculated using equation (8.1) and compared to the output of the detector.

$$Envelope = sqrt(I^2 + Q^2) \tag{8.1}$$

The envelope detection measurements using signal with average output power of 10dBm were plotted. For AD8361, the envelope detection is shown in Figure 8.7, whilst for the Marconi and HP detectors, measured results are presented in Figures 8.8 and 8.9 respectively. Of these three detectors, the HP detector gives the best envelope detection and gives excellent performance at average output power below 10dBm. One important point to note is that linear envelope detection is required in the AET system to maintain the overall AET system linearity. Some possible distortion may be added to the AET system due to imperfect detection from the square law detector. Therefore, it is recommended in future work that envelope detection using a square law detector is replaced by envelope generation using I and Q signals.

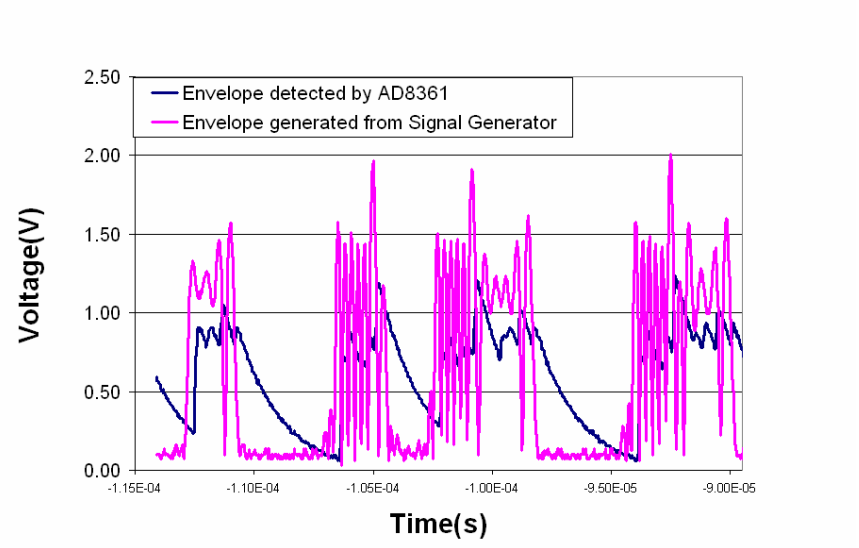

Figure 8.7: Envelope detection waveforms from the AD8361 detector

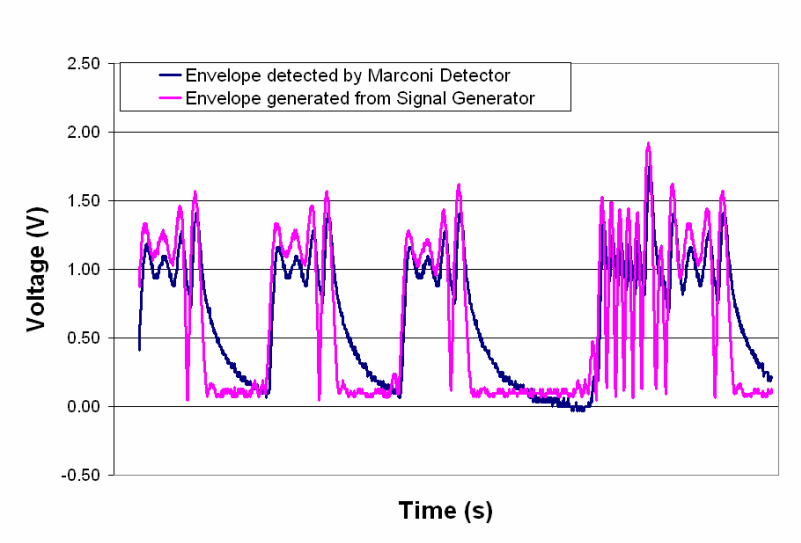

Figure 8.8: Envelope detection waveforms from the Marconi detector

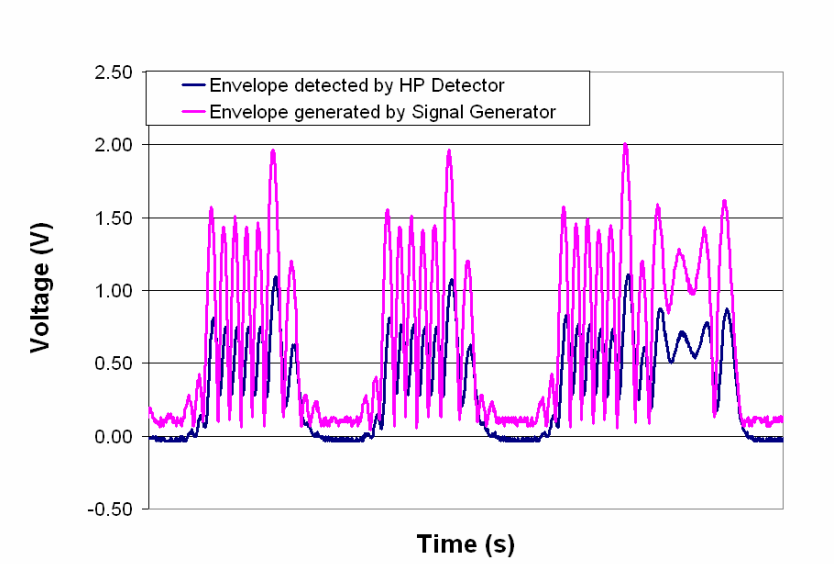

Figure 8.9: Envelope detection waveforms from the HP detector

8.1.4 Baseband Signal Amplification

Since the AET signal required at the drain port of the RFPA is large compared to the detected envelope, the signal requires amplification. In this AET setup for WCDMA measurements, a monolithic amplifier, ERA-5+ [3] from Mini Circuits is used and is shown in Figure 8.10. The ERA-5+ amplifier is a wideband amplifier that is capable of operation from DC to 4GHz. It uses only a single voltage supply and the amplifier is internally matched to 50Ω. The gain of this amplifier is about 20dB at an operating

frequency of 0.1GHz. The amplifier is then connected to an inverting amplifier that uses an AD811 op amp [4] from Analog Devices shown in Figure 8.11. AD811 is a high performance video op amp that has a wide bandwidth up to 120 MHz. This inverting amplifier is designed to have variable gain in order to control the amplitude of the AET signal inserted into the drain port of the RFPA. The closed-loop gain, G of this inverting amplifier defined in equation (8.2), is adjusted by varying the feedback resistor R_A. The schematic of this inverting amplifier is shown in Figure 8.12. The resistor R_B is added so that the inverting amplifier has a minimum linear gain of 2.

$$G = -\left\{\frac{1}{R_{IN}}\left(\frac{R_A R_B}{R_A + R_B}\right)\right\} \tag{8.2}$$

Since this inverting amplifier is the method used to control the AET voltage signal, it is designed to have a maximum linear gain of about 10. Even at this level of gain, the AD 811 op amp can amplify signal with a bandwidth up to 65MHz [4], which is much greater than the required bandwidth for this application.

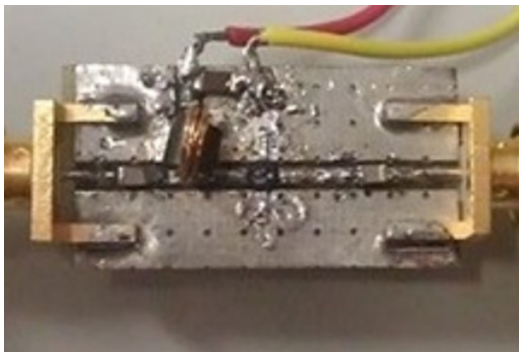

Figure 8.10: The ERA-5+ amplifier, part of the Envelope Buffer Amplifier

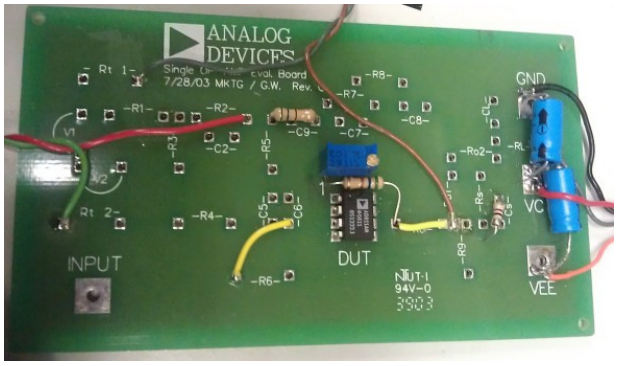

Figure 8.11: The inverting amplifier using an AD811 op amp.

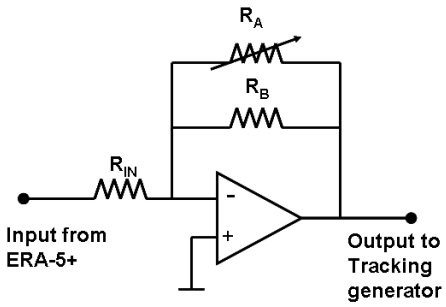

Figure 8.12: The inverting amplifier schematic

8.1.5 AET Tracking Generator

A key feature of the developed AET system is the separation of the DC and AC components of the tracking power supply. The analysis of the separation of AC and DC components has been discussed in Chapter 4, shows that a drain efficiency improvement can be achieved. The concept of separating the AC and DC components of the tracking signal is realised in the design and implementation of a very simple, low cost AET tracking voltage generator, described in detailed in Chapter 7.

8.1.6 Delay Line

On the RF path, the signal needs to be delayed in order to compensate for the delays in the AET generation circuitry on the envelope path. After observing the AET signal at the drain bias port of the RFPA and the envelope detected just before the input port of the RFPA, a cable length of about 9m is required in order to phase-align the two signals. This cable must be placed on the RF

path as any phase-offset between the signals can cause distortion and degrade to the power amplifier's linearity [5], [6].

The cable used for this delay line is a coaxial cable with 50Ω characteristic impedance and an attenuation value of 52.7dB per 100m at 1GHz [7]. The time delay was first measured by observing the AET signal at the drain port of the RFPA and the envelope signal at the input port of the RFPA. The measured delay was about 45ns, therefore by using equation (8.3), the length of cable needed for this time delay can be calculated. The specific length of cable is then cut and measured on the VNA. For this 9m cable length, the attenuation measured was 7.03dB.

$$Length = \left(\frac{2}{3}c \times t\right), \tag{8.3}$$

where c is the speed of light, 3.0×10^8m/s and t is the time delay.

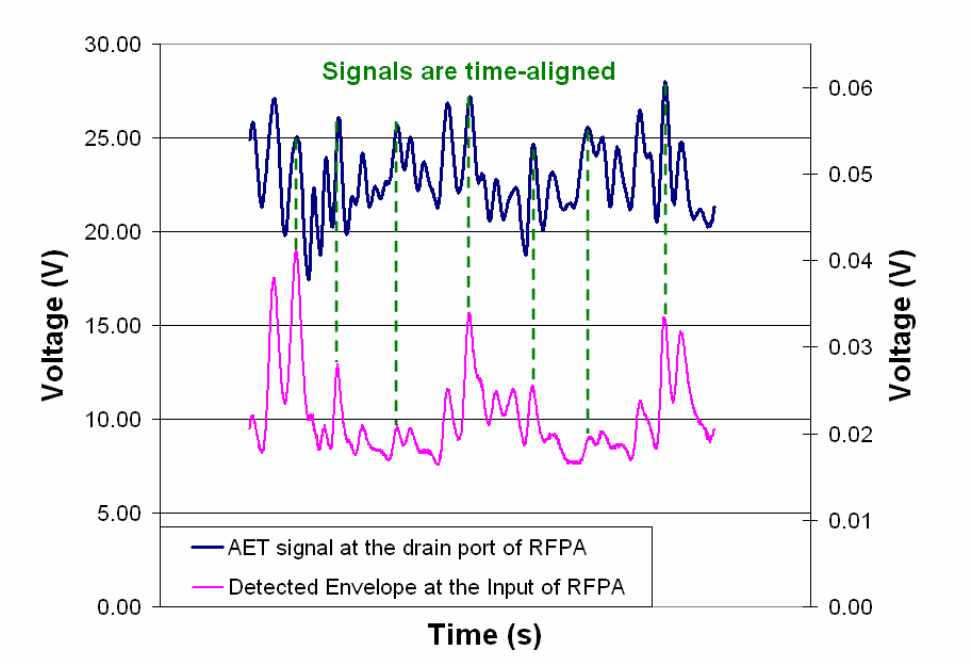

Figure 8.13: The measurement of time-alignment between the AET signal and detected envelope of input RF signal after the delay line is inserted into the AET system.

Obviously, in a full system implementation this delay would be performed using DSP, and the coaxial cable and associated losses, would not be taken into consideration. Figure 8.13 shows the time-aligned signals between the AET signal at the drain port of the RFPA and the envelope signal detected just prior to the input of the RFPA. Note that the signal at the input of RFPA is detected by a MI Sanders detector as shown in Figure 8.14, which has a low bandwidth. Therefore, the peaks of the signals are the reference for the time-alignment.

Figure 8.14: The MI Sanders Detector

8.1.8 RF Signal Amplification

As discussed in section 8.1.2, the maximum average power to be generated by the PSG for the WCDMA measurements was set to 15dBm. Therefore, in order to get the RFPA operating at its full peak output power rating of 44dBm or 25W, the RFPA is driven by another power amplifier. The driver power amplifier used for this measurement is the MW71C2240N from Freescale [8]. MW71C2240N is a RF LDMOS wideband integrated power amplifier that is capable of providing power gain of 30dB at 2GHz. This power amplifier is shown in Figure 8.15.

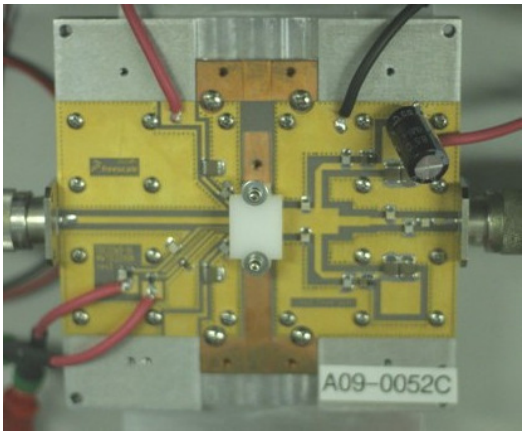

Figure 8.15: MW71C2240N, the driver power amplifier

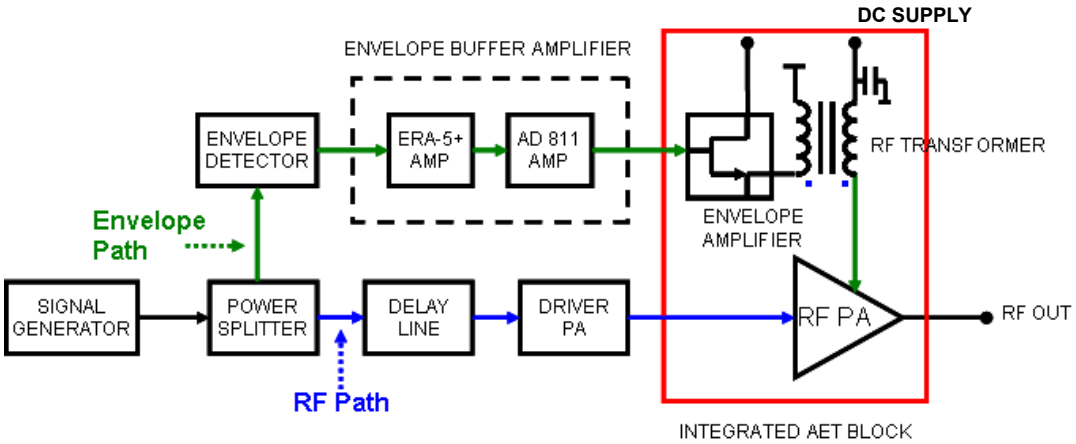

Figure 8.16: The AET experimental block diagram for WCDMA measurement

8.1.9 AET Principle of Operation for WCDMA Signal Measurements

For WCDMA signal measurements, the AET experimental setup is shown in Figure 8.16. The Agilent PSG generates the WCDMA single carrier signal at 1.98GHz. The WCDMA signal has a representative PAR of 9.17dB as described earlier. This WCDMA RF signal is then split into the envelope path and RF path by the power splitter. On the envelope path, the envelope of the WCDMA signal is detected. A buffer amplifier, which consists of the monolithic amplifier ERA-5+ and the inverting amplifier, is included to generate the necessary tracking voltage amplitude.

In between the detector and the monolithic amplifier, there is another RF broadband transformer, which has the same characteristics as the transformer used in the tracking generator. This broadband transformer is used for impedance matching between the HP detector, which requires a 470Ω termination and the monolithic amplifier, which requires 50Ω input impedance. The schematic diagram for this impedance transformer is shown in Figure 8.17(a) and the transformer itself is shown in Figure 8.17(b). Note that in a full system implementation of AET, the AET tracking signal would be generated directly by the DSP and as such the power consumption of the buffer amplifier is not included in efficiency calculations. Gain adjustment of the inverting amplifier also provides a convenient method of envelope amplitude control.

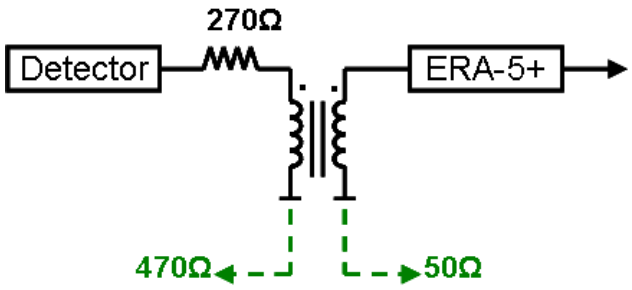

(a)

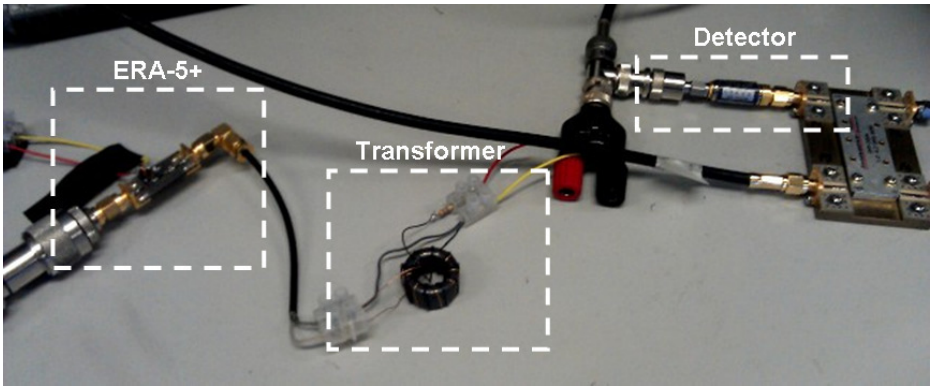

(b)

Figure 8.17: (a) The schematic and (b) implementation of the impedance transformer.

The envelope signal is then applied to the tracking generator, which consists of the envelope amplifier (EA) and the RF transformer. The envelope signal output from this EA is then connected to the primary side of the RF transformer that is designed to have a 1:2 voltage transformation. At the secondary winding, an AC-only signal from the amplified envelope signal can be detected at the same phase as the primary winding and becomes the AC component of the AET signal. The AC component of the AET signal is combined with its DC component at the secondary winding of the transformer. The DC component of AET signal is provided by a DC supply, which is connected to one end of the secondary winding of the transformer. The AET signal biases the RFPA by connecting the other end of the transformer to the drain port of the RFPA.

On the RF path, the WCDMA signal from the second path of the splitter is delayed by a length of cable and subsequently delivered to the input port of the driver power amplifier. The output of RFPA is connected to an Agilent Spectrum Analyzer 54624A to measure the average output power and also the linearity performance of this WCDMA signal in terms of its ACPR. The whole implementation of the AET setup for this WCDMA measurement is shown in Figure 8.18.

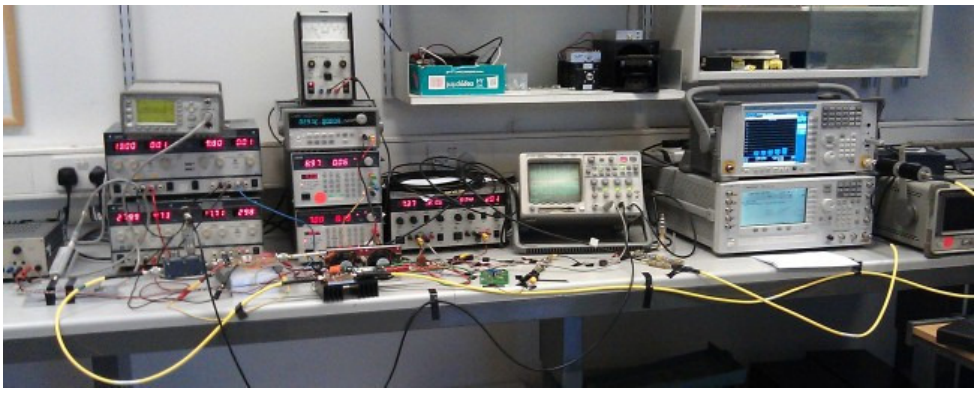

Figure 8.18: The AET experimental setup for WCDMA measurement

8.2 WCDMA Measured Performance and Discussion

8.2.1 Overview of the Measurement Settings.

For this WCDMA measurement, three gate bias settings were chosen; 5%, 8.3% and 12.5% of the GaN transistor's drain saturation current, corresponding to drain currents of 300mA, 500mA and 750mA respectively. All of the measurements for the RFPA in the AET setup are compared to the RFPA biased at a fixed voltage of 28V. The comparison is done with the RFPA biased at 28V, which is the same voltage as the peak voltage of the composite AET signal. The RFPA was measured across a 10dB dynamic range from an average output power of 23dBm to a maximum average output power of 33dBm. 33dBm is the maximum average output power for the 25W GaN device considering 9.17dB PAR of the WCDMA signal used in this measurement.

8.2.2 Derivation of AET Signal from the Detected Envelope Signal

As mentioned in section 8.1.9, the WCDMA signal is detected by a HP detector and the envelope is amplified by a buffer amplifier before the envelope signal is input to the tracking generator. The envelope path of this AET system is properly designed to cover the bandwidth of the WCDMA envelope signal.

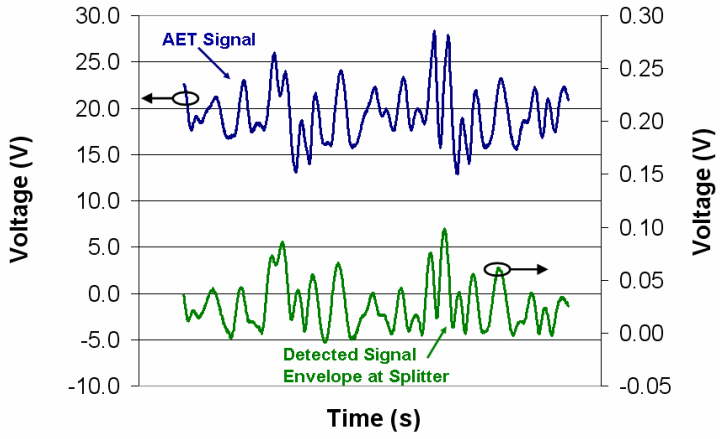

Figure 8.19: AET signal compared to the envelope signal at the power splitter

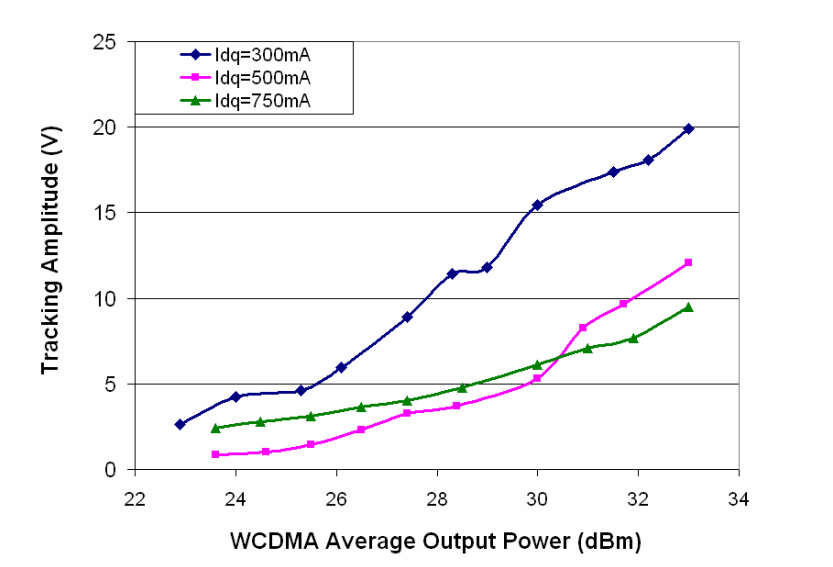

Figure 8.20: The AET tracking amplitude

In Figure 8.19, the detected AET signal at the drain port of RFPA and the WCDMA envelope signal at the power splitter measured on the oscilloscope are plotted. From this figure, it can be seen that the envelope shape is very well preserved at the drain supply point, despite the 25W RFPA being operated in deep Class AB mode. Note that this excellent tracking fidelity has been obtained without the use of a band-limiting feedback circuit [5], [9]. This preservation of WCDMA envelope signal shape can be observed for a range of output power measured, where the tracking amplitude can be as high as 20V for the case of a quiescent drain current of 300mA. The tracking amplitude measured for all the three bias settings is shown in Figure 8.20.

8.2.3 Drain Efficiency Results

In the WCDMA signal measurement, we observed the drain efficiency of the AET system. The drain efficiency of this AET system is calculated using equation 4.12 in Chapter 4, which also includes the tracking generator DC power consumption.

The result for the drain efficiency is very noteworthy. As shown in Figure 8.21, the drain efficiency of the AET system biased at I_{DQ}=300mA is 31% at an average power level of 33dBm, whereas the RFPA drain efficiency when

biased with fixed supply of 28V is 21%. Therefore, we can see that by applying the AET technique at this bias, we get a 47.6% improvement in drain efficiency as compared to the RFPA biased with a fixed supply, and this calculation includes the power consumed by the EA.

Figure 8.22 and Figure 8.23 show the result of changing the gate bias so the quiescent drain current becomes 500mA and 750mA respectively. From these figures, we observe that both AET drain efficiency and fixed supply drain efficiency decreased as we increased the gate bias settings. In Figure 8.21, the maximum AET drain efficiency is 19.5% and the maximum fixed voltage drain efficiency is 16.1%. In Figure 8.22, the maximum AET drain efficiency is 14.0% and the maximum fixed supply drain efficiency is 10.6%. In general, the drain efficiency decreases as we increase the gate bias. This is to be expected according to basic power amplifier theory, but it should be noted that the RFPA matching was designed at a specific gate bias for efficiency and power, in this case was an I_{DQ} of 300mA. As we change the gate bias, the performance of the RFPA is no longer optimum; however, although the drain efficiency decreases as the gate bias increases, we still observe useful improvements in drain efficiency when AET is applied.

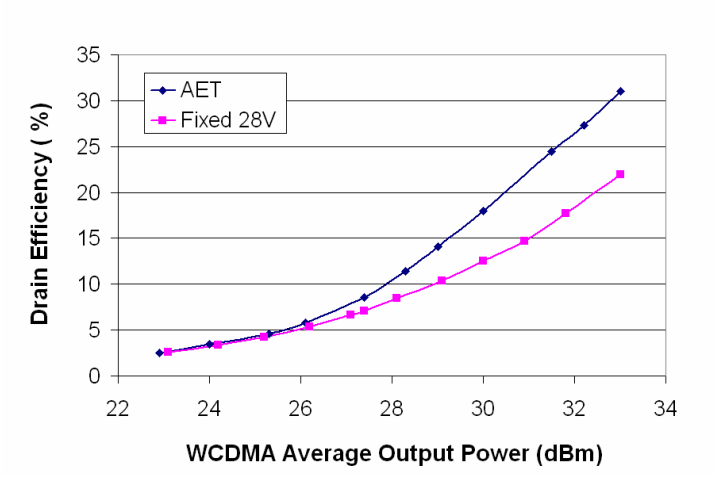

Figure 8.21: Drain efficiency at I_{DQ} of 300mA

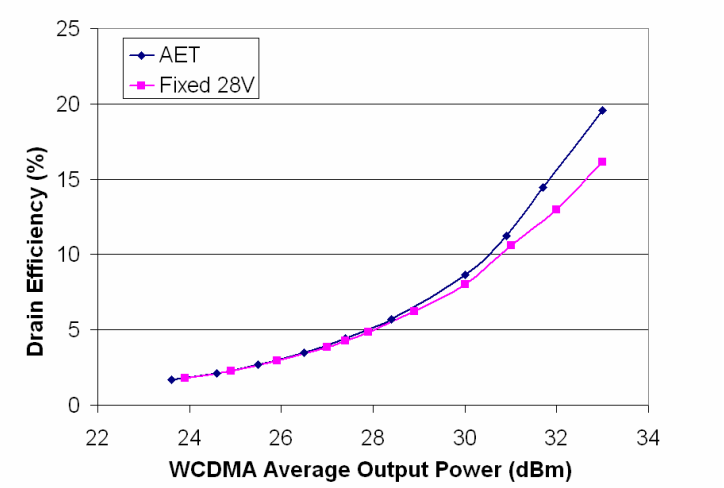

Figure 8.22: Drain efficiency at I_{DQ} of 500mA

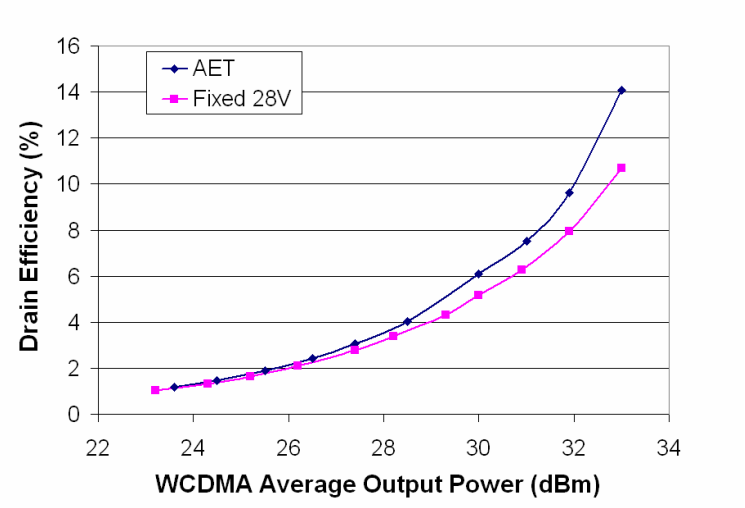

Figure 8.23: Drain efficiency at I_{DQ} of 750mA

8.2.4 ACPR Results

In this WCDMA signal measurement, the linearity performance in terms of ACPR was measured for three different gate biases. The performance is compared between the AET system and the fixed voltage supply. In Figure 8.24, the ACPR was plotted against average output power for an I_{DQ} of 300mA. In this figure, asymmetrical ACPR has been observed. We can see that the AET upper-side ACPR has variable ACPR improvement until an average output power of 31dBm and that the AET lower-side ACPR did not

show an improvement over most average output powers. As shown in Figure 8.25, at average output power of 30dBm, about 3dB PBO, we can see from the signal spectrum, the upper-side ACPR has some improvement while for lower-side ACPR, the fixed voltage supply has better linearity.

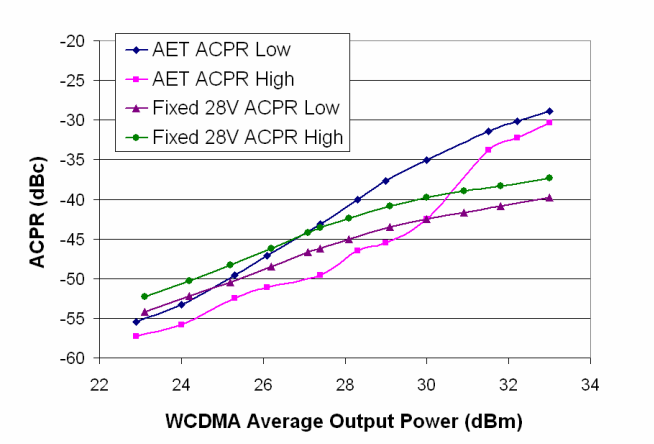

Figure 8.24: The ACPR performance at I_{DQ} of 300mA

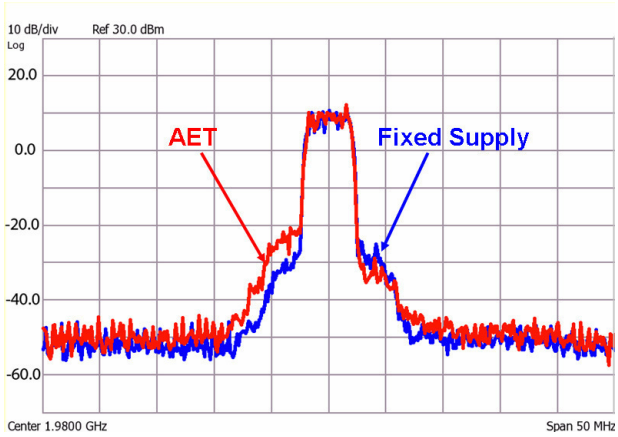

Figure 8.25: The WCDMA spectrum at average output power of 30dBm for I_{DQ} =300mA

For an I_{DQ} of 500mA, the ACPR for both AET and fixed voltage supply look symmetrical, as shown in Figure 8.26. The ACPR performance the AET system has similar performance to the fixed voltage supply at this bias. This can be also seen in the signal spectrum in Figure 8.27, at an average output power of 30dBm.

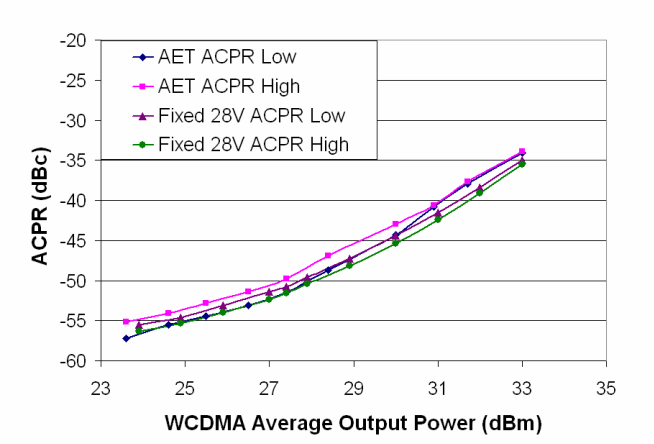

Figure 8.26: The ACPR performance at I_{DQ} of 500mA

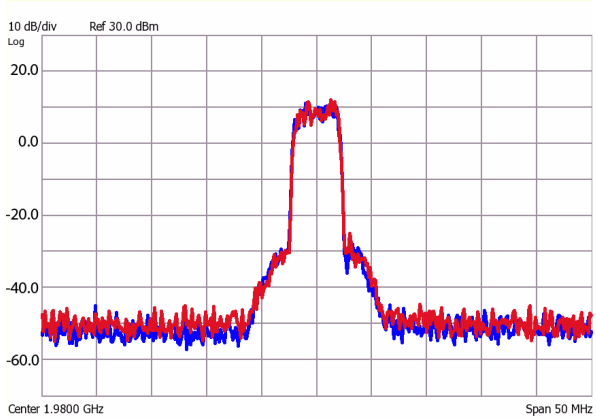

Figure 8.27: The WCDMA spectrum at average output power of 30dBm for I_{DQ} =500mA

For an I_{DQ} of 750mA, the ACPR performance of the RFPA in the AET setup has shown good improvement over most average output powers, and has the best linearity performance out of all three biases. At the peak average output power, 33dBm, the AET upper-side ACPR has shown about 5dBc improvement while the AET lower-side ACPR showed a similar performance at a low ACPR value of -43dBc, as shown in Figure 8.28. This ACPR improvement can also be seen in the signal spectrum at an average output power of 30dBm, as shown in Figure 8.29. The AET output spectrum in red shows significant improvement of about 11dBc on upper-side ACPR and 5.5dBc on lower-side ACPR as compared to the fixed voltage output spectrum in blue.

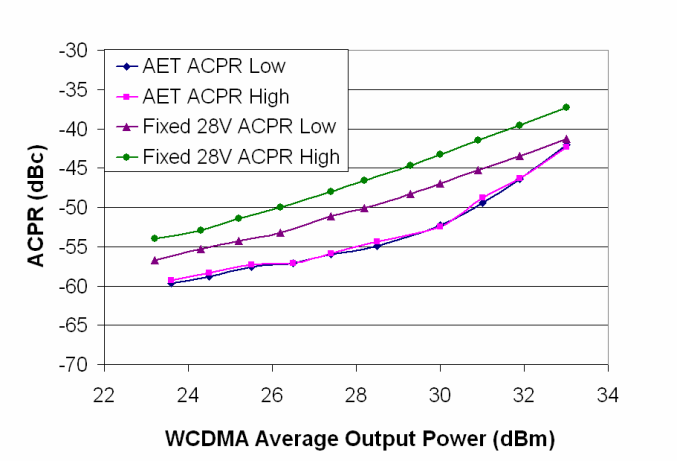

Figure 8.28: The ACPR performance at I_{DQ} of 750mA

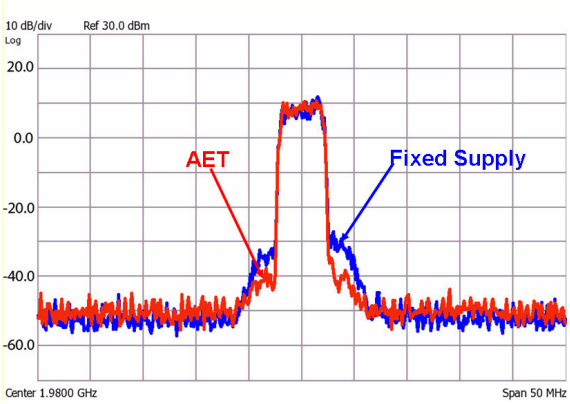

Figure 8.29: The WCDMA spectrum at average output power of 30dBm for I_{DQ} =750mA

From these ACPR measurements at three biases, we can see that the best linearity is achieved at the gate bias of I_{DQ} of 750mA, which is closest to the Class A bias point. This is due to gain compression behaviour that introduces more distortion in the Class B region as compared to the Class A region.

8.2.5 AC Power Consumption

As mentioned in Chapter 4, one important concept in AET is that the AC component of the AET signal is very small compared to the DC component

of the signal. Therefore, in this WCDMA AET setup, we measure both AC and DC components of the AET signal, which is included in the drain efficiency calculations presented earlier. The AC power component of the AET signal comes from the EA. The DC component of the AET signal is measured from the DC supply that is connected to the secondary winding of the transformer. Figure 8.30 shows the percentage of the AC power over the total AET power at all measured average output powers. As we can see from Figure 8.30, at a maximum WCDMA average output power of 33dBm, for an I_{DQ} of 750mA, the percentage of AC power was as small as 3%. For an I_{DQ} of 500mA and 300mA, the percentages are 7.5% and 20% respectively. These percentages are smaller than the ideal 2- carrier signal discussed in Chapter 4. This proves that the AET technique is very efficient as compared to the fixed voltage supply setup.

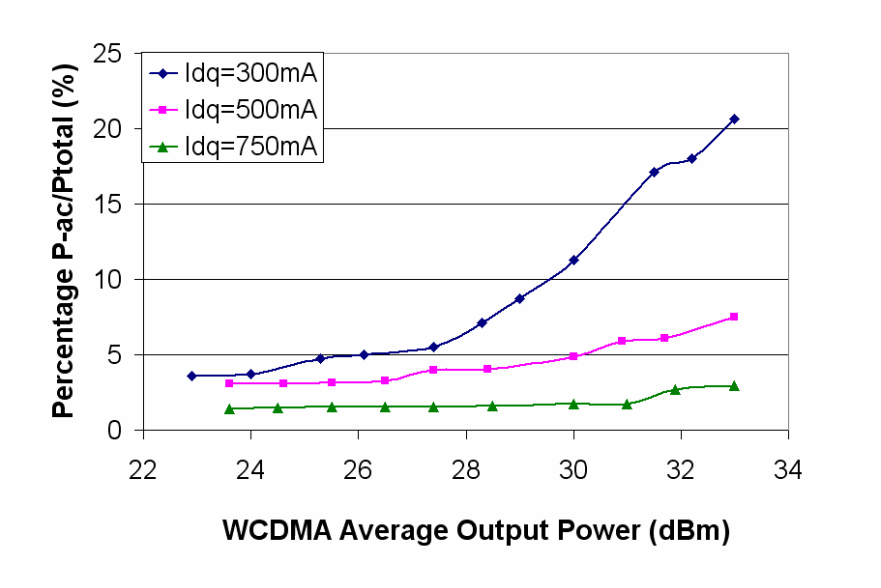

Figure 8.30: The percentage of AC power over total AET power

8.3 Chapter Summary

In this chapter, the WCDMA signal measurements of the AET system have been presented in detail. The full AET setup included envelope detection and a delay line that were absent in the two-carrier signal measurements. The RFPA drain efficiency results at the same bias points as the 2-carrier signal

measurements showed a substantial improvement in the AET system as compared to the fixed supply bias. The ACPR results however, did not show significant improvement in the AET system. This is due to the complexity of WCDMA signals, which have high bandwidth and high PAR. The WCDMA measurements were extended to other bias points for further investigation, and the measurements of the drain efficiency still showed a significant improvement for the AET system compared to the fixed bias supply. In these measurements, the ACPR also showed improvement compared to the fixed bias supply. The improvements in ACPR were achieved when the bias point was moved towards the Class A mode and used a very small percentage of AC power consumption. The ACPR improvement at this bias point has resulted in ideas for AET system enhancements to be investigated in future work.

8.4 References

[1] Yusoff, Z., Lees, J., Benedikt, J., Tasker, P.J., Cripps, S.C., "Linearity improvement in RF power amplifier system using integrated Auxiliary Envelope Tracking system," IEEE MTT-S International Microwave Symposium Digest, 2011, vol., no., pp.1-4, 5-10 June 2011

[2] Cripps, S., "RF Power Amplifier for Wireless Communications", Norwood, MA: Artech House, Apr. 1999

[3] Mini-Circuits Monolithic Amplifier ERA-5+ Datasheet [Online]. Available: http://www.minicircuits.com/pdfs/ERA-5+.pdf.

[4] Analog Device High Performance Op Amp Datasheet [Online]. Available: http://www.analog.com/static/imported-files/data_sheets/AD811.pdf

[5] Wang, F., Yang, A.H., Kimball, D.F., Larson, L.E., Asbeck, P.M., "Design of wide-bandwidth envelope-tracking power amplifiers for OFDM applications IEEE Transactions on Microwave Theory and Techniques, vol.53, no.4, pp. 1244- 1255, April 2005.

[6] Cripps, S., "Advanced Techniques in RF Power Amplifier Design", Norwood, MA: Artech House, 2002

[7] Cable Coax URM76 Datasheet [Online] Available: http://uk.rs-online.com/web/p/products/5218060/

[8] RF LDMOS Wideband Integrated Power Amplifiers Datasheet [Online] Available: http://cache.freescale.com/files/rf_if/doc/data_sheet/MW7IC2240N.pdf

[9] Rahkonen T., Jokitalo, O. P., "Design of a linearly assisted switcher for a supply modulated RF transmitter," Proceedings of the 24th Norchip Conference, pp. 1-4, 2006.

CHAPTER 9

CONCLUSIONS AND FUTURE WORK

9.1 Conclusions

The RFPA is the main device in the transmitter architecture. It is important to design a high performance RFPA that is efficient and linear. This is due to the requirements of the modern wireless communication system where the transmitted signal has a large bandwidth and a high peak-to-average ratio (PAR). In this project, the performance of the RFPA in terms of efficiency and linearity were investigated by using the 'Auxiliary Envelope Tracking' (AET) system. This AET system is adapted from the conventional 'Envelope Tracking' (ET) system that is well known as an efficiency enhancement technique, and operates by biasing the RFPA with an envelope tracking signal. The key variation of the AET system compared to the ET system is the method of the tracking signal generation. This novel method of tracking signal generation is achieved by separating the AC and DC components of the tracking signal, which results in a simple and cost-efficient hardware implementation.

In terms of system efficiency, conventional ET system designers tend to implement a high efficiency tracking generator that has a complex design in order to achieve high overall system efficiency. The AET system, on the other hand, generates a low amplitude tracking signal to bias the RFPA, which contributes to system efficiency enhancement. Mathematical analysis and signal simulation have been performed in Chapter 4 to show the performance improvement between the ET and the AET systems. While the conventional ET system improves the efficiency of the RFPA, the AET system can also improve the linearity of the RFPA by using a gallium nitride (GaN) RFPA without any extra circuitry dedicated to linearity improvement.

This is achieved by harnessing the GaN gain variation behaviour observed when the drain voltage of the RFPA is varied.

From the initial CW measurements, a substantial gain variation was observed in GaN RFPAs, and this behaviour was absent in the measured LDMOS RFPA. Three GaN RFPAs were measured to demonstrate this gain variation behaviour, as presented in Chapter 3. The GaN RFPA gain measurement result was fitted to a logarithmic function and this function was used to analyze the RFPA linearity performance in terms of third-order intermodulation (IM3). The gain variation and the drain tracking voltage bias equations were fitted to the non-linear transfer characteristic equation that was limited to the third order component for IM3 analysis. From the mathematical analysis, the final derivation showed that the IM3 distortion can be minimized by controlling the amplitude of the tracking signal.

The mathematical analysis of the GaN gain variation behaviour on the IM3 distortion was further quantified by the AET system measurement using two-carrier signals. In the initial two-carrier signal measurements performed on the 10W GaN Class J RFPA, a substantial reduction of IM3 distortion was observed as compared to the RFPA biased with a fixed supply. A 20W LDMOS RFPA was also measured using the same setup but there was no significant IM3 improvement observed. This IM3 distortion reduction observed motivated the development of a 25W GaN Class AB RFPA for further investigation of the AET system. The 25W GaN Class AB RFPA was designed using a series of ADS simulations, and was built and tested. The RFPA was then integrated with an envelope amplifier (EA) and a 'combiner' in a newly developed AET system. In this setup, the EA was designed using a simple source-follower configuration that used a cheap off-the-shelf transistor. Again, the IM3 performance of the 25W GaN Class AB RFPA was measured on this new AET system. The IM3 performance improved significantly compared to the fixed bias supply and the results were consistent with the initial measurement performed on the Class J RFPA. The drain efficiency performance of the 25W GaN RFPA was also measured and a

small improvement was observed compared to the fixed bias supply over most of the measured power range.

The two-carrier signal measurements on the AET system formed the basis for more measurements using complex signals. In this case, a WCDMA signal was chosen and the measurement setup was developed to investigate the RFPA performance enhancement. In the WCDMA measurement setup, the combiner used was an RF broadband transformer. This RF broadband transformer replaces the diplexer used in the two-carrier signal measurement. This was done to fulfil the bandwidth requirement of the WCDMA signal that has also a high peak-to-average (PAR) ratio. The RF broadband transformer ensures DC isolation is achieved between the primary and secondary windings. The RF broadband design methodology is presented in Chapter 7 where a number of transformers were designed and tested. The transformer that performed best is the transformer made from Material 43 with 8 winding turns and has a smaller effective cross-sectional area.

For the WCDMA signal measurement, a complete AET system was developed. A practical WCDMA signal with a challenging PAR (9.17dB) was generated to test the AET system. The tracking bias signal at the RFPA drain port was observed to track the envelope signal at the gate port of the RFPA. The performance of the RFPA was measured and presented in Chapter 8. The measurement at the same gate bias as the two-carrier signal measurement demonstrated a good efficiency improvement of about 47.6% compared to the fixed bias supply case. The AC power generated by the EA, resulting from a low tracking amplitude, was just a small percentage of the total power consumption. The low amount of AC power consumed is the reason that the AET setup was able to provide good efficiency compared to a fixed bias supply.

The AET linearity performance in terms of adjacent-channel-power ratio (ACPR) did show a small improvement at low output power but the ACPR performance showed some degradation at higher output powers compared to

the fixed bias supply. The reduced linearity performance of the RFPA at higher output powers is suspected to be caused by the nature of the complex WCDMA signal that has a high PAR, and will benefit from more in-depth investigation. Recent work using an active load pull test system [1] and a complex multi-carrier signal has indicated that there is still much potential for AET as a linearization technique, however this will require a more advanced AET voltage profile synthesis using digital techniques (see section 9.2 below). However, it should be noted that the substantial efficiency improvement is still of value, and the degraded ACPR may still meet the requirements of some applications. Thus, in future work, AET can be regarded as a stand-alone, low cost efficiency enhancement technique for some applications.

The investigation of the RFPA's performance was extended by exploring different gate bias conditions. In theory, the linearity performance of the Class A mode is better compared to the Class B mode due to the gain compression behaviour of the Class B mode that causes more distortion. The WCDMA measurements at different gate biases were consistent with the above theory. As the gate bias point moves closer to Class A mode, the ACPR performance of the RFPA improves. The RFPA however, showed a trade-off in terms of drain efficiency. As the gate bias moves towards Class A mode, the drain efficiency decreases. The measured results of AC power consumption, however, showed the impact of the AC power consumed by the tracking generator to the overall AET drain efficiency. As the gate bias moves closer to Class A mode, the AC power consumption is lower. From this result, the analysis can be further explored for future improvements in both efficiency and linearity. When the quiescent drain current of 750mA is chosen, the lower RFPA drain efficiency at this bias point can be improved by using a different EA design configuration that is more efficient, which leads to an improved overall AET system efficiency.

In conclusion, in this work a new technique called AET was developed, implemented and tested using a two-carrier signal and WCDMA signal. Both

the efficiency and linearity of the RFPA are improved using this technique. These improvements were shown in the two-carrier signal measurements. For WCDMA case, a substantial efficiency improvement was observed while for linearity performance, the RFPA showed some improvements at lower output powers and some degradation at higher output powers. The extended investigation at other gate biases showed that there was a trade-off between efficiency and linearity performances, which with a more efficient EA design can improve both performances at the same time. Although there is more investigation that can be done on the AET setup for WCDMA signal measurements, the concept of AET explained in Chapter 4 is still valid based on the outstanding performance on the two-carrier signal measurement. In addition, the implementation of the tracking generator that uses simple design and cost-effective component could have potential commercial applications. This in turn could be of direct benefit for micro-cell network products in mobile communications industry.

9.2 Future Work

The concept of the AET system has been defined in this work. The implementation of the AET system for a two-carrier signal measurement has led to a more challenging measurement using a WCDMA signal that has high bandwidth and high PAR. The RFPA performance results for the two-carrier measurement showed consistency with the mathematical analysis, however the WCDMA signal, which has higher bandwidth and higher PAR, has affected the performance of the AET system. There is further work therefore, that can be done to improve the performance of AET when applied to WCDMA signal.

9.2.1 Digital Approach for Tracking Signal Detection

In the AET system setup for WCDMA signal measurements presented in this work, the envelope detection was performed by a standalone envelope detector. This envelope detector is limited to a certain bandwidth, and introduces a fixed non-linear characteristic into the final composition of the tracking voltage. Although it has been highlighted that the AET tracking

signal does not need to have a great precision in replicating the envelope shape, it would be interesting to investigate whether the RFPA linearity and efficiency performance can be improved when a precise envelope is constructed using the I and Q signal elements of the WCDMA signal. Therefore, it is proposed that the AET tracking signal implementation is done using digital signal processing (DSP) as shown in Figure 9.1.

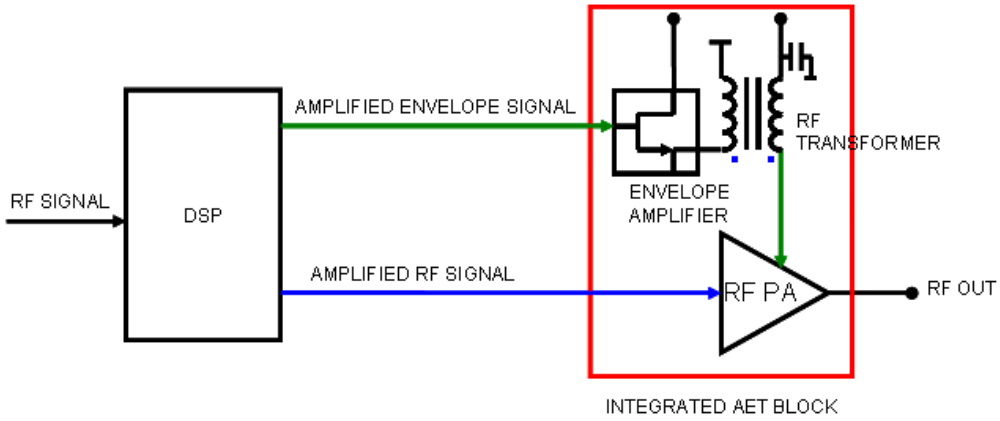

Figure 9.1: Proposed AET System with DSP

In addition, the necessary amplification of the envelope amplitude can be controlled easily without any extra power from the buffer amplifier. By omitting the buffer amplifier, the system is more compact, although this will add some complexity to the system design. The delay compensation can also be performed at this DSP stage and the baseband signal delay can easily be analysed.

9.2.2 Push-Pull Envelope Amplifier

In the discussion of AC power consumption mentioned in section 9.1, it is proposed that a new design of tracking generator can improve the overall AET system efficiency when the RFPA operates at a bias point closer to Class A mode. In Chapter 4, the WCDMA simulation results showed that when the tracking generator efficiency is higher, the overall system efficiency also improves. The current EA used in the AET system in this work is a Class A amplifier with a source-follower configuration. In theory, Class B amplifier efficiency is much higher than for the Class A amplifier. Therefore, it is

proposed that the new EA topology design uses the Class B push-pull configuration in order to achieve a better EA efficiency. The high efficiency EA will be able to relax the requirement on the RFPA efficiency, which means the RFPA could be biased at higher quiescent drain current towards Class A mode. By biasing the EA in Class B and the RFPA closer to Class A, the linearity of the RFPA could be improved without compromising on system efficiency.

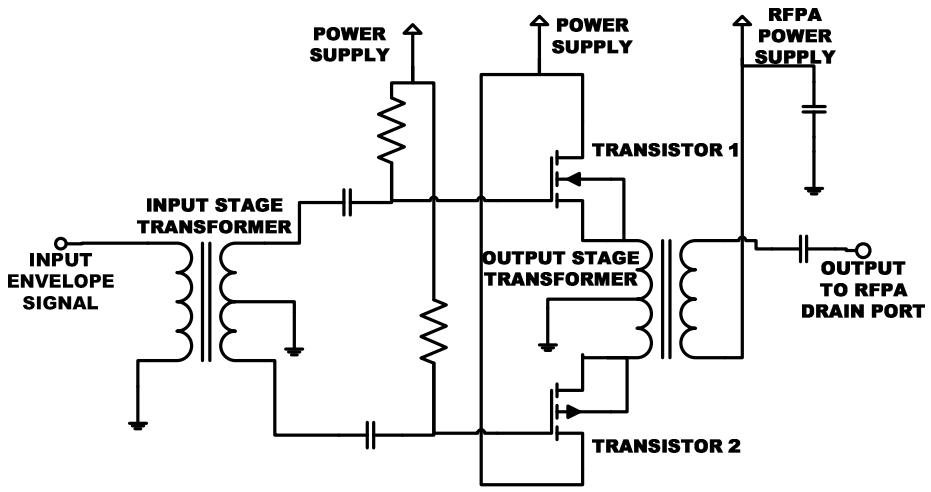

Figure 9.2: Proposed push-pull EA configuration

The proposed Class B push-pull configuration for the EA is shown in Figure 9.22 and it will be called push-pull source follower EA. In this configuration, two centre-tapped transformers are used. The transformer at the input stage changes the unbalanced envelope signal to a balanced signal. The RF broadband transformer developed in this research work, which consists of a trifilar winding on a toroidal core, could be used for this purpose. The second transformer is used at the output stage is to change the balanced signal back to an unbalanced signal. This second transformer can also function as a combiner for the AET system, where the DC component of the AET signal will be combined with the AC component of the AET signal. This can be implemented by connecting a DC power supply to the one end of the secondary winding of the transformer.

There are many advantages of using this proposed new EA configuration. First, the RF broadband transformer and the Class B push-pull configuration offer wide bandwidth signal operation, making this EA highly suitable for WCDMA envelope amplification. Secondly, the push-pull configuration of this amplifier can prevent the transformer from saturating when the DC bias currents from the two devices flow in the opposite directions and cancel out [2]. This can minimize any distortion that is coming from the magnetization of the transformer core [3]. Thirdly, the proposed Class B push-pull configuration benefits from the impedance conversion that is possible by using a transformer. By choosing appropriate 1:N number of turns ratio, a step-up impedance or voltage transformation of the RF transformer at the output stage can be achieved.

Finally, the improved AET tracking generator, employing the push-pull configuration, can enhance the overall efficiency of the AET system. The new tracking generator has also a direct commercial implementation especially in base station application of micro-cell network.

9.3 Reference

[1] Akmal, M., Carrubba, V., Lees, J., Bensmida, S., Benedikt, J., Morris, K., Beach, M., McGeehan, J., Tasker, P.J., "Linearity enhancement of GaN HEMTs under complex modulated excitation by optimizing the baseband impedance environment," 2011 IEEE MTT-S International Microwave Symposium Digest (MTT), vol., no., pp.1-4, 5-10 June 2011.

[2] 'What Do the Terms "Push-Pull" and "Single-Ended" Mean?' [Online] Available: http://www.aikenamps.com/SingleEnded.htm

[3] 'Electronics Tutorial about Class B Amplifiers' [Online] Available: http://www.electronics-tutorials.ws/amplifier/amp_6.html

APPENDIX A

RF BROADBAND TRANSFORMER FUNDAMENTALS

A.1 Basic Theory of Transformer

Transformer basically is a device which uses the phenomenon of mutual induction to change the values of alternating voltages and currents across a medium such as ferromagnetic core. The basic transformer principle of operation is explained as follows and is aided by Figure A.1. In this figure, the ferromagnetic core is shown; where at the left side of the core, there is a coil which we call the primary winding while at the right side of the core there is another coil that we call the secondary winding. In this example, the primary winding is connected to an AC source while the secondary winding is connected to a load. Hence, the transformer can also be viewed as a common core connection between two separate electrical systems.

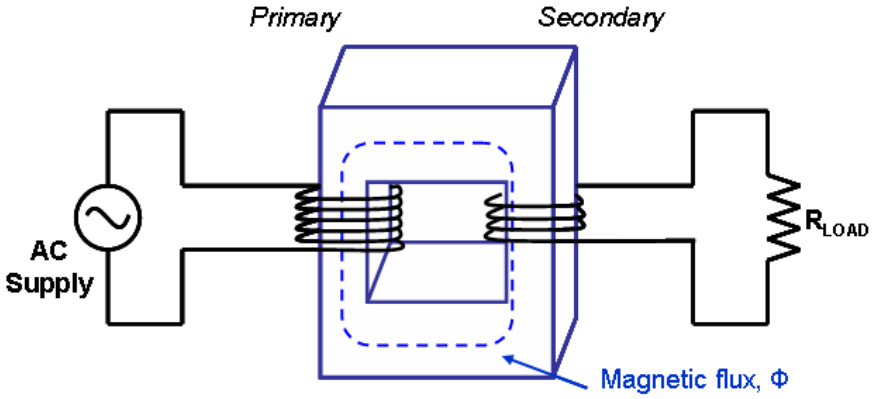

Figure A.1: The basic circuit configuration of transformer

When the AC signal is applied to the primary winding, a small current flows and magnetic flux is present at the ferromagnetic core. The AC signal generates alternating flux that links from the primary to the secondary winding and mutually induces the electromotive force (e.m.f) for both

windings as E_1 and E_2. The induced e.m.f, E is given by the Faraday Law equation (A.1) [1]:

$$E = N\frac{d\phi}{dt} volts, \qquad \text{(A.1)}$$

Where N is the number of turns of wire in the coil and $\frac{d\phi}{dt}$ is the rate of change of flux in Maxwells per second. For an ideal transformer, all flux generated by the primary winding is passed through to the secondary winding and therefore, by using equation (A.1), the ratio of induced e.m.f at the secondary winding, E_2 over the number of turns at the secondary winding, N_2 is proportional to the ratio of the induced e.m.f at the primary winding, E_1 over number of turns at the primary winding;

$$\frac{E_1}{N_1} = \frac{E_2}{N_2}, \qquad \text{(A.2)}$$

and assuming there is no losses, $E_1=V_1$ and $E_2=V_2$, then,

$$\frac{V_1}{N_1} = \frac{V_2}{N_2} \text{ or } \frac{V_1}{V_2} = \frac{N_1}{N_2}. \qquad \text{(A.3)}$$

From this equation (A.3), we can define the step-up or step down transformer by changing the number of turns of the coil. If we would like to design a step-up transformer, N_2 should have more turns than N_1 which therefore, V_2 has higher value than V_1 and if we would like to design a step-down transformer,N_2 should have less number of turns than N_1 which therefore, V_2 has lower value than V_1.

In Figure A.1, the secondary winding is connected to a load. Thus, there is a current I_2 flows to the load. Considering the transformer is ideal and losses are negligible, the input power from the primary winding is equal to the output power at the load of secondary winding. Then,

$$V_1 I_1 = V_2 I_2, \qquad \text{(A.4)}$$

and by equating the equation (A.3) and equation (A.4), we get the currents flowing at the coil and number of turns relationship as follows;

$$\frac{I_1}{I_2} = \frac{N_2}{N_1}. \qquad \text{(A.5)}$$

By dividing the equation (A.3) and equation (A.5), we get the impedances and number of turns relationship as follows;

$$\frac{Z_1}{Z_2} = \left(\frac{N_1}{N_2}\right)^2 \qquad \text{(A.6)}$$

From equation (A.6) relationship, when we design a step-up transformer with 1:2 voltage transformations, then the impedance transformation ratio will be 1:4.

A.2 Transformer Equivalent Circuit

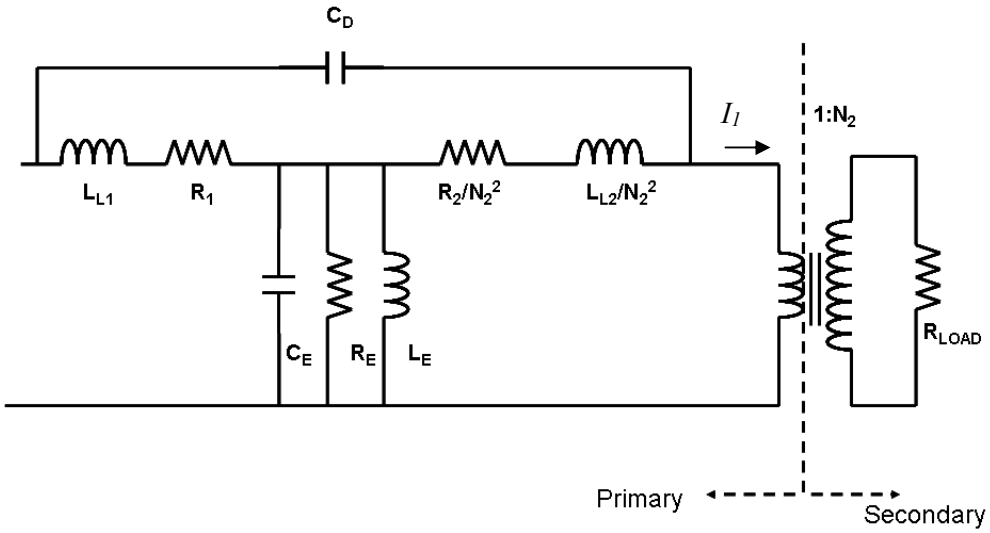

Figure A.2: The transformer equivalent circuit

The RF broadband transformer design for WCDMA applications mentioned earlier needs to be designed for wide bandwidth. In the analysis of designing this audio/RF transformer, an equivalent circuit that includes losses elements from the coil and core that used for constructing the transformer as shown in Figure A.2 [1]. The transformer equivalent circuit shown consists of the real

elements considered for both primary and secondary winding at the primary side of the transformer. The primary circuit is then cascaded with the secondary side of the transformer that is connected to a load. The number of turn's ratio between primary and secondary winding is $1:N_2$.

In this transformer equivalent circuit, the elements includes three parts; the losses due to the primary winding (L_{L1} and R_1), the losses due to the secondary winding (R_2/N_2^2 and L_{L2}/N_2^2) and the losses due to the ferromagnetic core of the transformer (R_E and L_E).

R_1 and R_2 are the lumped resistors representing the resistance associated with the primary and secondary windings that are made of conductors. From primary side of the transformer point of view, the secondary winding lumped resistor R_2, is transformed by equation (A.6) and becomes R_2/N_2^2.

In the ideal voltage transformation equation (A.3), it is assumed that all the flux links from the primary winding to the secondary winding. However, there is actually some flux leakage and not all the flux links to the secondary winding. This flux leakage is represented by the leakage lumped inductors L_{L1} and L_{L2}. And since L_{L2} is transformed to the primary side, then by equation (A.6) this secondary leakage inductor becomes L_{L2}/N_2^2.

The third type of losses in this equivalent circuit is the losses due to ferromagnetic material used for the core of this transformer. Since ferromagnetic material is a type of conductors, thus, there is a current called eddy current that is induced due to the changing of magnetic field with time. This current generates heat and it is a source of power loss. Due to this varying magnetic filed, there is another effect that is called hysteresis. Hysteresis is a phenomenon happens when the particles in the ferromagnetic core create a loop in the magnetization trace and this is another source of power loss. The combination of eddy current and hysteresis losses is called core loss and it is represented by the lumped resistor R_E.
Another type of loss associated with the ferromagnetic core is due to magnetizing current. This current is the current used to produce the flux in

the primary winding. Any nonlinear effect from this current generation can be represented by a lumped inductor, L_E.

There are two other capacitive elements needed to be taken into account; C_D and C_E. These two lumped capacitors represent the stray capacitance due to the insulation dielectric between conductors i.e. between the primary and secondary windings and also between the windings and the core or ground.

A.3 Circuit Performance of RF Broadband Transformer

The RF broadband transformer is used over the megahertz range. The key performance of this RF broadband transformer is the insertion loss. Insertion loss is defined as the loss of signal power resulting from the insertion of a device and usually expressed in decibels (dB) [2]. The insertion loss (*IL*) of a transformer can be represented by following equation;

$$IL(dB) = 10\log_{10}\frac{P_{load}}{P_{load} + P_{loss}} \qquad \text{(A.7)}$$

Where P_{load} is the power delivered to the load and P_{loss} is the loss in power due to the core losses and winding losses.

In a two-port measurement, *IL* can be defined as the magnitude of the reflected wave at port 2 over the incident wave at port 1, when port 1 is terminated in the system impedance. More simply stated, *IL* can be described as the forward voltage gain and expressed in dB. *IL* is represented by equation (A.8) and since *IL* is defined to have a positive value, then there is a minus sign in front of this equation;

$$IL(dB) = -20\log_{10}|S_{21}| \qquad \text{(A.8)}$$

In order to measure the bandwidth of the transformer, the low and high cut-off frequency is needed. By referring to the equivalent circuit in Figure A.2 and the details of the analysis can be found in [1], the low cut-off frequency, ω_L is defined as;

$$\omega_L = \frac{R_{LOAD} R_{IN}}{L_E \left(R_{LOAD} + R_{IN} \right)} \qquad \text{(A.9)}$$

$$\text{Where } R_{IN} = R_1 + \frac{R_2}{N_2^2} + \frac{R_{LOAD}}{N_2^2}$$

For high cut off frequency, ω_H, the equation is as follows;

$$\omega_H = \sqrt{\frac{1}{L_L C_D}} \qquad \text{(A.10)}$$

This equation (A.10) is derived by referring to a simplified equivalent circuit that can be found in [1]. In this simplified equivalent circuit, L_L is total loss due to the flux leakage.

A.4 Reference

[1] W.M. Flanagan, "Handbook of Transformer Design & Applications", Boston, MA, McGraw-Hill, 1992.

[2] "Insertion Loss", [Online] Available: http://en.wikipedia.org/wiki/Insertion_loss

APPENDIX B

CGH40025, 25W RF POWER HEMT DATASHEET

CGH40025

25 W, RF Power GaN HEMT

Cree's CGH40025 is an unmatched, gallium nitride (GaN) high electron mobility transistor (HEMT). The CGH40025, operating from a 28 volt rail, offers a general purpose, broadband solution to a variety of RF and microwave applications. GaN HEMTs offer high efficiency, high gain and wide bandwidth capabilities making the CGH40025 ideal for linear and compressed amplifier circuits. The transistor is available in a screw-down, flange package and solder-down, pill packages.

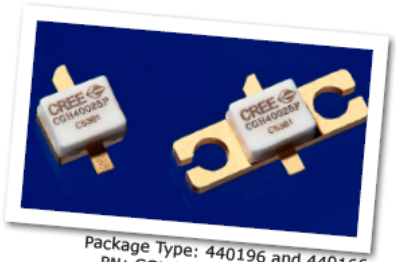

Package Type: 440196 and 440166
PN: CGH40025P and CGH40025F

FEATURES

- Up to 6 GHz Operation
- 15 dB Small Signal Gain at 2.0 GHz
- 13 dB Small Signal Gain at 4.0 GHz
- 30 W typical P_{SAT}
- 62 % Efficiency at P_{SAT}
- 28 V Operation

APPLICATIONS

- 2-Way Private Radio
- Broadband Amplifiers
- Cellular Infrastructure
- Test Instrumentation
- Class A, AB, Linear amplifiers suitable for OFDM, W-CDMA, EDGE, CDMA waveforms

RoHS COMPLIANT

Rev 3.2 – July 2011

Large Signal Models Available for SiC & GaN

Subject to change without notice.
www.cree.com/wireless

1

Absolute Maximum Ratings (not simultaneous) at 25°C Case Temperature

Parameter	Symbol	Rating	Units
Drain-Source Voltage	V_{DSS}	84	Volts
Gate-to-Source Voltage	V_{GS}	-10, +2	Volts
Storage Temperature	T_{STG}	-65, +150	°C
Operating Junction Temperature	T_J	225	°C
Maximum Forward Gate Current	I_{GMAX}	7.0	mA
Soldering Temperature[1]	T_S	245	°C
Screw Torque	τ	60	in-oz
Thermal Resistance, Junction to Case[2]	$R_{\theta JC}$	4.8	°C/W
Case Operating Temperature[2,3]	T_C	-40, +150	°C

Note:
[1] Refer to the Application Note on soldering at www.cree.com/products/wireless_appnotes.asp
[2] Measured for the CGH40025F at P_{DISS} = 28 W.
[3] See also, the Power Dissipation De-rating Curve on Page 6.

Electrical Characteristics (T_C = 25°C)

Characteristics	Symbol	Min.	Typ.	Max.	Units	Conditions
DC Characteristics[1]						
Gate Threshold Voltage	$V_{GS(th)}$	-3.8	-3.3	-2.3	V_{DC}	V_{DS} = 10 V, I_D = 7.2 mA
Gate Quiescent Voltage	$V_{GS(Q)}$	–	-3.0	–	V_{DC}	V_{DS} = 28 V, I_D = 250 mA
Saturated Drain Current	I_{DS}	5.8	7.0	–	A	V_{DS} = 6.0 V, V_{GS} = 2.0 V
Drain-Source Breakdown Voltage	V_{BR}	120	–	–	V_{DC}	V_{GS} = -8 V, I_D = 7.2 mA
RF Characteristics[2] (T_C = 25°C, F_0 = 3.7 GHz unless otherwise noted)						
Small Signal Gain	G_{SS}	12	13	–	dB	V_{DD} = 28 V, I_{DQ} = 250 mA
Power Output[3]	P_{SAT}	20	30	–	W	V_{DD} = 28 V, I_{DQ} = 250 mA
Drain Efficiency[4]	η	55	62	–	%	V_{DD} = 28 V, I_{DQ} = 250 mA, P_{SAT}
Output Mismatch Stress	VSWR	–	–	10 : 1	Ψ	No damage at all phase angles, V_{DD} = 28 V, I_{DQ} = 250 mA, P_{OUT} = 25 W CW
Dynamic Characteristics						
Input Capacitance	C_{GS}	–	9.0	–	pF	V_{DS} = 28 V, V_{gs} = -8 V, f = 1 MHz
Output Capacitance	C_{DS}	–	2.6	–	pF	V_{DS} = 28 V, V_{gs} = -8 V, f = 1 MHz
Feedback Capacitance	C_{GD}	–	0.4	–	pF	V_{DS} = 28 V, V_{gs} = -8 V, f = 1 MHz

Notes:
[1] Measured on wafer prior to packaging.
[2] Measured in CGH40025-TB.
[3] P_{SAT} is defined as I_G = 0.72 mA.
[4] Drain Efficiency = P_{OUT} / P_{DC}

Cree, Inc.
4600 Silicon Drive
Durham, NC 27703
USA Tel: +1.919.313.5300
Fax: +1.919.869.2733
www.cree.com/wireless

Typical Performance

Small Signal Gain and Return Loss vs Frequency of the CGH40025F in the CGH40025-TB

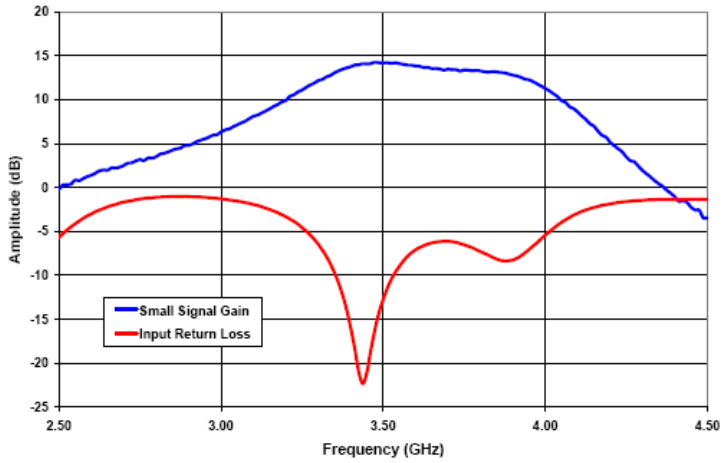

P_{SAT}, Gain, and Drain Efficiency vs Frequency of the CGH40025F in the CGH40025-TB
V_{DD} = 28 V, I_{DQ} = 250 mA

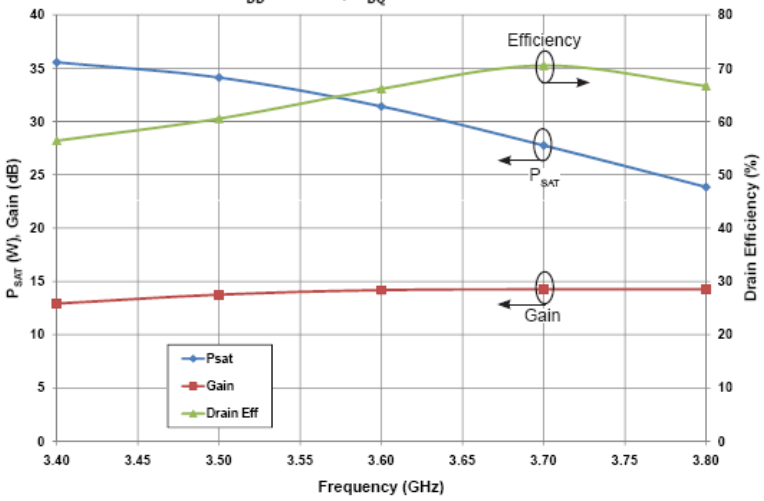

Cree, Inc.
4600 Silicon Drive
Durham, NC 27703
USA Tel: +1.919.313.5300
Fax: +1.919.869.2733
www.cree.com/wireless

Typical Performance

Swept CW Data of CGH40025 vs. Output Power with Source and Load Impedances Optimized for P_{SAT} Power in CGH40025-TB
V_{DD} = 28 V, I_{DQ} = 250 mA, Freq = 3.7 GHz

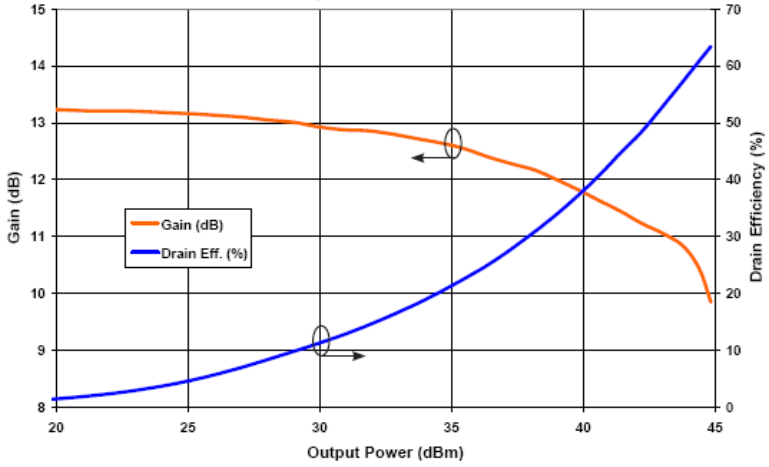

Maximum Available Gain and K Factor of the CGH40025
V_{DD} = 28 V, I_{DQ} = 250 mA

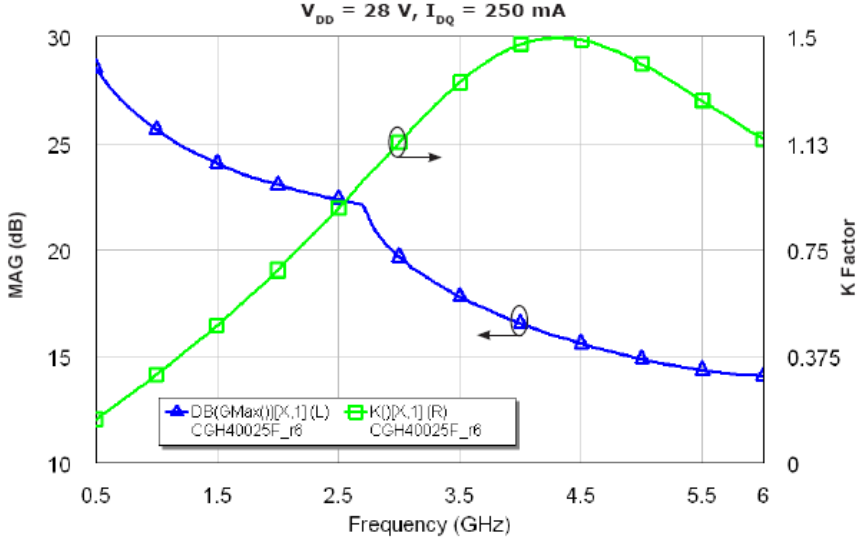

Cree, Inc.
4600 Silicon Drive
Durham, NC 27703
USA Tel: +1.919.313.5300
Fax: +1.919.869.2733
www.cree.com/wireless

Typical Noise Performance

Simulated Minimum Noise Figure and Noise Resistance vs Frequency of the CGH40025F
V_{DD} = 28 V, I_{DQ} = 250 mA

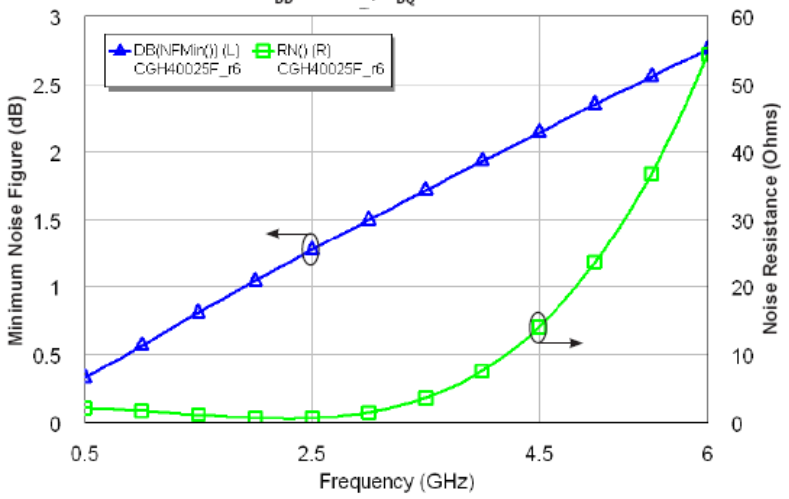

Electrostatic Discharge (ESD) Classifications

Parameter	Symbol	Class	Test Methodology
Human Body Model	HBM	1A > 250 V	JEDEC JESD22 A114-D
Charge Device Model	CDM	1 < 200 V	JEDEC JESD22 C101-C

Cree, Inc.
4600 Silicon Drive
Durham, NC 27703
USA Tel: +1.919.313.5300
Fax: +1.919.869.2733
www.cree.com/wireless

Source and Load Impedances

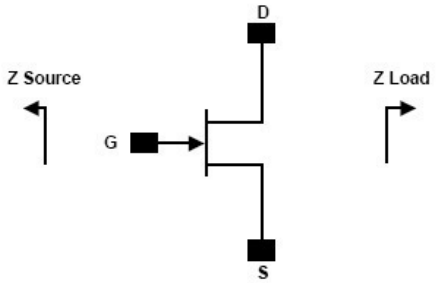

Frequency (MHz)	Z Source	Z Load
500	7.75 + j15.5	20 + j5.2
1000	3.11 + j5.72	17 + j6.66
1500	2.86 + j1.63	16.8 + j3.2
2500	2.4 - j3.52	8.02 + j4.32
3500	1.31 - j7.3	5.85 - j0.51

Note 1. V_{DD} = 28V, I_{DQ} = 250mA in the 440166 package.
Note 2. Optimized for power gain, P_{SAT} and PAE.
Note 3. When using this device at low frequency, series resistors should be used to maintain amplifier stability.

CGH40025 Power Dissipation De-rating Curve

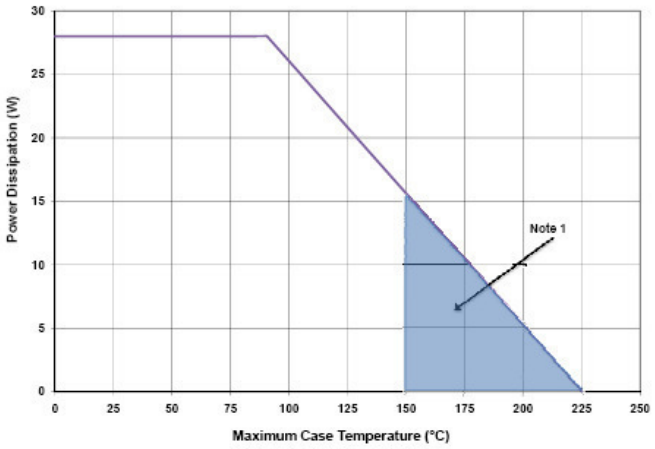

Note 1. Area exceeds Maximum Case Operating Temperature (See Page 2).

Cree, Inc.
4600 Silicon Drive
Durham, NC 27703
USA Tel: +1.919.313.5300
Fax: +1.919.869.2733
www.cree.com/wireless

CGH40025-TB Demonstration Amplifier Circuit Schematic

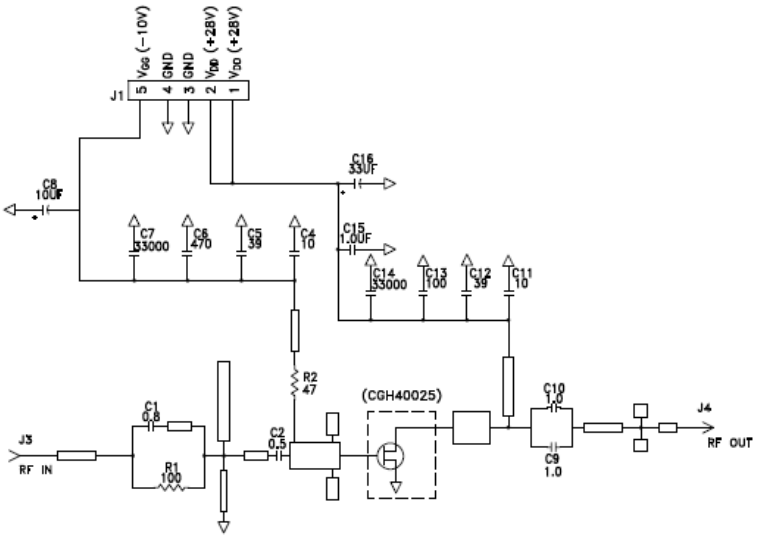

CGH40025-TB Demonstration Amplifier Circuit Outline

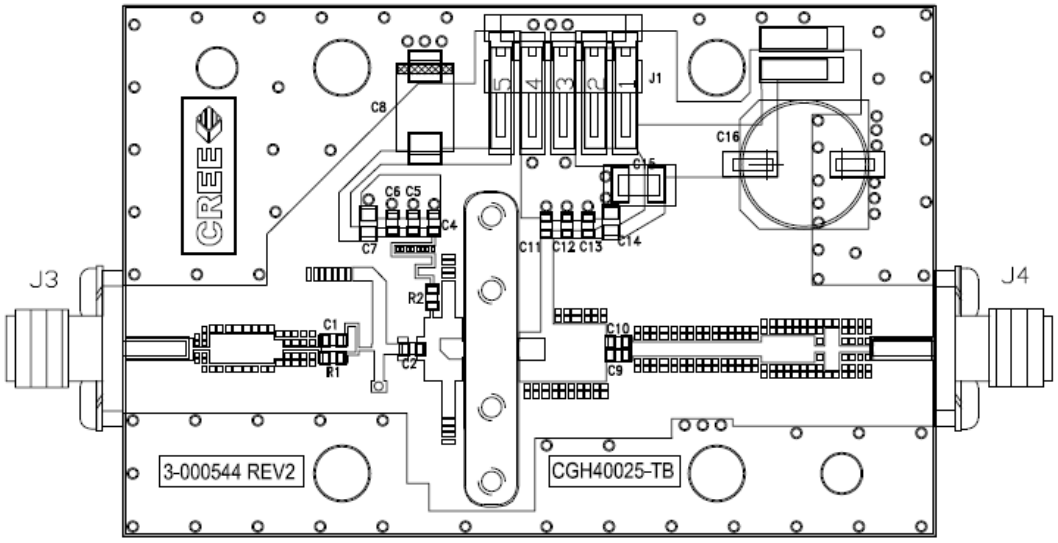

Cree, Inc.
4600 Silicon Drive
Durham, NC 27703
USA Tel: +1.919.313.5300
Fax: +1.919.869.2733
www.cree.com/wireless

CGH40025-TB Demonstration Amplifier Circuit Bill of Materials

Designator	Description	Qty
R2	RES,1/16W,0603,1%,47 OHMS	1
R1	RES,1/16W,0603,1%,100 OHMS	1
C6	CAP, 470PF, 5%,100V, 0603	1
C16	CAP, 33 UF, 20%, G CASE	1
C15	CAP, 1.0UF, 100V, 10%, X7R, 1210	1
C8	CAP 10UF 16V TANTALUM	1
C13	CAP, 100.0pF, +/-5%, 0603	1
C1	CAP, 0.8pF, +/-0.1pF, 0603	1
C2	CAP, 0.5pF, +/-0.05pF, 0603	1
C9,C10	CAP, 1.0pF, +/-0.1pF, 0603	2
C4,C11	CAP, 10.0pF,+/-5%, 0603	2
C5,C12	CAP, 39pF, +/-5%, 0603	2
C7,C14	CAP,33000PF, 0805,100V, X7R	2
J3,J4	CONN SMA STR PANEL JACK RECP	2
J1	HEADER RT>PLZ .1CEN LK 5POS	1
-	PCB, RO4350B, Er = 3.48, h = 20 mil	1
-	CGH40025F or CGH40025P	1

CGH40025-TB Demonstration Amplifier Circuit

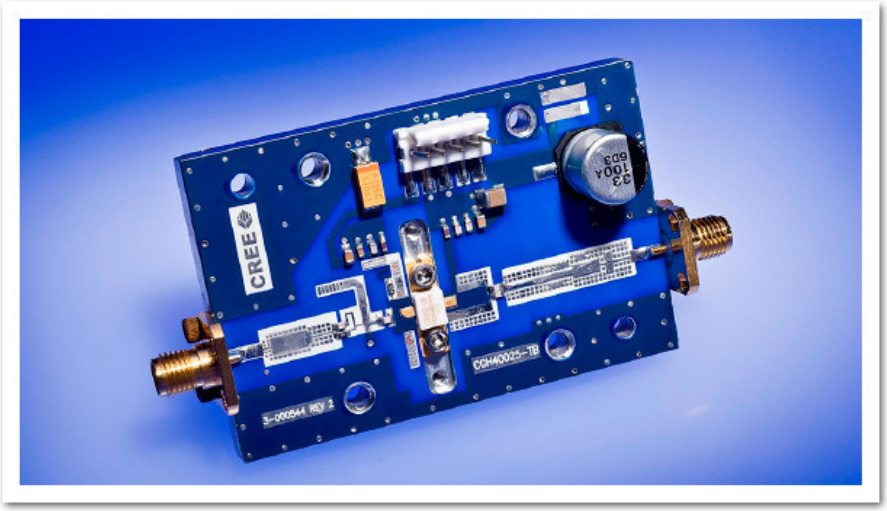

Cree, Inc.
4600 Silicon Drive
Durham, NC 27703
USA Tel: +1.919.313.5300
Fax: +1.919.869.2733
www.cree.com/wireless

CREE

Typical Package S-Parameters for CGH40025
(Small Signal, V_{DS} = 28 V, I_{DQ} = 100 mA, angle in degrees)

Frequency	Mag S11	Ang S11	Mag S21	Ang S21	Mag S12	Ang S12	Mag S22	Ang S22
500 MHz	0.902	-151.72	11.80	92.09	0.025	6.22	0.393	-140.34
600 MHz	0.901	-157.13	9.89	87.31	0.025	2.28	0.402	-143.54
700 MHz	0.900	-161.20	8.49	83.18	0.025	-0.99	0.412	-145.64
800 MHz	0.900	-164.41	7.42	79.49	0.025	-3.82	0.424	-147.11
900 MHz	0.901	-167.04	6.58	76.10	0.024	-6.33	0.436	-148.22
1.0 GHz	0.902	-169.26	5.89	72.93	0.024	-8.60	0.449	-149.12
1.1 GHz	0.903	-171.19	5.33	69.93	0.024	-10.69	0.462	-149.91
1.2 GHz	0.904	-172.89	4.86	67.07	0.023	-12.61	0.476	-150.65
1.3 GHz	0.905	-174.43	4.45	64.33	0.023	-14.39	0.489	-151.38
1.4 GHz	0.906	-175.84	4.10	61.68	0.022	-16.06	0.503	-152.12
1.5 GHz	0.907	-177.14	3.80	59.12	0.022	-17.61	0.517	-152.87
1.6 GHz	0.909	-178.36	3.54	56.64	0.022	-19.05	0.531	-153.65
1.7 GHz	0.910	-179.52	3.30	54.22	0.021	-20.38	0.545	-154.46
1.8 GHz	0.912	179.38	3.09	51.87	0.021	-21.62	0.558	-155.29
1.9 GHz	0.913	178.33	2.90	49.58	0.020	-22.75	0.571	-156.15
2.0 GHz	0.914	177.30	2.73	47.34	0.020	-23.78	0.584	-157.04
2.1 GHz	0.916	176.31	2.58	45.15	0.019	-24.70	0.596	-157.95
2.2 GHz	0.917	175.34	2.44	43.02	0.019	-25.52	0.608	-158.88
2.3 GHz	0.918	174.39	2.31	40.92	0.018	-26.22	0.620	-159.82
2.4 GHz	0.920	173.46	2.19	38.88	0.018	-26.82	0.631	-160.78
2.5 GHz	0.921	172.54	2.09	36.87	0.017	-27.29	0.642	-161.76
2.6 GHz	0.922	171.63	1.99	34.91	0.016	-27.64	0.652	-162.74
2.7 GHz	0.923	170.73	1.90	32.98	0.016	-27.85	0.662	-163.73
2.8 GHz	0.925	169.84	1.82	31.09	0.015	-27.92	0.672	-164.73
2.9 GHz	0.926	168.95	1.74	29.24	0.015	-27.85	0.681	-165.73
3.0 GHz	0.927	168.07	1.67	27.41	0.014	-27.61	0.690	-166.74
3.2 GHz	0.929	166.30	1.54	23.86	0.013	-26.63	0.706	-168.76
3.4 GHz	0.931	164.54	1.42	20.42	0.013	-24.89	0.721	-170.79
3.6 GHz	0.932	162.78	1.33	17.08	0.012	-22.30	0.735	-172.82
3.8 GHz	0.934	161.00	1.24	13.84	0.011	-18.80	0.748	-174.85
4.0 GHz	0.935	159.21	1.16	10.67	0.011	-14.40	0.759	-176.88
4.2 GHz	0.936	157.39	1.10	7.58	0.010	-9.18	0.769	-178.90
4.4 GHz	0.937	155.55	1.04	4.55	0.010	-3.38	0.778	179.07
4.6 GHz	0.938	153.67	0.98	1.57	0.010	2.65	0.787	177.04
4.8 GHz	0.939	151.77	0.94	-1.36	0.011	8.52	0.794	175.00
5.0 GHz	0.939	149.82	0.89	-4.25	0.011	13.87	0.801	172.96
5.2 GHz	0.939	147.82	0.86	-7.11	0.012	18.48	0.807	170.90
5.4 GHz	0.939	145.78	0.82	-9.95	0.013	22.25	0.812	168.83
5.6 GHz	0.940	143.68	0.79	-12.78	0.014	25.17	0.817	166.74
5.8 GHz	0.939	141.53	0.77	-15.59	0.016	27.32	0.821	164.62
6.0 GHz	0.939	139.31	0.74	-18.41	0.017	28.77	0.825	162.48

Download this s-parameter file in ".s2p" format at http://www.cree.com/products/wireless_s-parameters.asp

Cree, Inc.
4600 Silicon Drive
Durham, NC 27703
USA Tel: +1.919.313.5300
Fax: +1.919.869.2733
www.cree.com/wireless

Typical Package S-Parameters for CGH40025
(Small Signal, V_{DS} = 28 V, I_{DQ} = 250 mA, angle in degrees)

Frequency	Mag S11	Ang S11	Mag S21	Ang S21	Mag S12	Ang S12	Mag S22	Ang S22
500 MHz	0.917	-157.22	12.62	91.45	0.018	7.56	0.458	-158.97
600 MHz	0.916	-161.92	10.57	87.33	0.018	4.70	0.465	-160.93
700 MHz	0.916	-165.46	9.07	83.78	0.018	2.41	0.472	-162.19
800 MHz	0.916	-168.28	7.94	80.58	0.018	0.51	0.478	-163.04
900 MHz	0.916	-170.61	7.05	77.64	0.017	-1.12	0.485	-163.64
1.0 GHz	0.916	-172.60	6.33	74.88	0.017	-2.55	0.493	-164.09
1.1 GHz	0.917	-174.33	5.74	72.25	0.017	-3.82	0.500	-164.45
1.2 GHz	0.917	-175.88	5.24	69.73	0.017	-4.94	0.508	-164.77
1.3 GHz	0.918	-177.28	4.82	67.30	0.017	-5.95	0.516	-165.06
1.4 GHz	0.918	-178.57	4.46	64.94	0.017	-6.84	0.525	-165.36
1.5 GHz	0.919	-179.78	4.14	62.65	0.016	-7.63	0.533	-165.67
1.6 GHz	0.919	179.09	3.87	60.41	0.016	-8.31	0.542	-165.99
1.7 GHz	0.920	178.01	3.62	58.22	0.016	-8.90	0.550	-166.35
1.8 GHz	0.921	176.98	3.40	56.07	0.016	-9.39	0.559	-166.73
1.9 GHz	0.921	175.99	3.21	53.97	0.015	-9.77	0.568	-167.14
2.0 GHz	0.922	175.03	3.03	51.90	0.015	-10.06	0.577	-167.59
2.1 GHz	0.923	174.09	2.87	49.87	0.015	-10.24	0.585	-168.07
2.2 GHz	0.924	173.17	2.73	47.87	0.014	-10.31	0.594	-168.57
2.3 GHz	0.924	172.27	2.60	45.91	0.014	-10.27	0.602	-169.11
2.4 GHz	0.925	171.39	2.47	43.97	0.014	-10.12	0.610	-169.67
2.5 GHz	0.926	170.51	2.36	42.07	0.014	-9.85	0.619	-170.26
2.6 GHz	0.926	169.65	2.26	40.19	0.013	-9.46	0.626	-170.88
2.7 GHz	0.927	168.79	2.16	38.34	0.013	-8.95	0.634	-171.52
2.8 GHz	0.928	167.93	2.08	36.52	0.013	-8.31	0.642	-172.17
2.9 GHz	0.928	167.08	1.99	34.72	0.013	-7.54	0.649	-172.85
3.0 GHz	0.929	166.24	1.92	32.94	0.013	-6.65	0.656	-173.55
3.2 GHz	0.930	164.54	1.78	29.45	0.012	-4.49	0.670	-175.00
3.4 GHz	0.931	162.85	1.66	26.05	0.012	-1.85	0.683	-176.50
3.6 GHz	0.932	161.14	1.55	22.72	0.012	1.19	0.695	-178.06
3.8 GHz	0.933	159.42	1.46	19.46	0.012	4.55	0.706	-179.66
4.0 GHz	0.933	157.68	1.38	16.27	0.012	8.08	0.716	178.70
4.2 GHz	0.934	155.91	1.31	13.12	0.012	11.64	0.726	177.02
4.4 GHz	0.934	154.11	1.24	10.03	0.013	15.08	0.735	175.30
4.6 GHz	0.935	152.28	1.18	6.97	0.013	18.26	0.743	173.56
4.8 GHz	0.935	150.41	1.13	3.95	0.014	21.09	0.750	171.78
5.0 GHz	0.935	148.49	1.08	0.96	0.015	23.50	0.756	169.97
5.2 GHz	0.935	146.53	1.04	-2.00	0.016	25.48	0.762	168.12
5.4 GHz	0.935	144.52	1.00	-4.96	0.017	27.02	0.768	166.24
5.6 GHz	0.935	142.45	0.97	-7.90	0.018	28.12	0.773	164.32
5.8 GHz	0.934	140.31	0.94	-10.84	0.020	28.83	0.777	162.36
6.0 GHz	0.934	138.12	0.91	-13.79	0.021	29.18	0.781	160.36

Download this s-parameter file in ".s2p" format at http://www.cree.com/products/wireless_s-parameters.asp

Cree, Inc.
4600 Silicon Drive
Durham, NC 27703
USA Tel: +1.919.313.5300
Fax: +1.919.869.2733
www.cree.com/wireless

Typical Package S-Parameters for CGH40025
(Small Signal, V_{DS} = 28 V, I_{DQ} = 400 mA, angle in degrees)

Frequency	Mag S11	Ang S11	Mag S21	Ang S21	Mag S12	Ang S12	Mag S22	Ang S22
500 MHz	0.924	-159.12	12.64	91.13	0.015	8.27	0.485	-163.72
600 MHz	0.923	-163.56	10.58	87.23	0.015	5.84	0.491	-165.34
700 MHz	0.923	-166.92	9.08	83.86	0.015	3.96	0.497	-166.41
800 MHz	0.923	-169.60	7.95	80.83	0.015	2.43	0.502	-167.13
900 MHz	0.923	-171.82	7.06	78.03	0.015	1.16	0.508	-167.65
1.0 GHz	0.923	-173.72	6.34	75.40	0.015	0.08	0.514	-168.05
1.1 GHz	0.923	-175.39	5.75	72.89	0.015	-0.84	0.520	-168.36
1.2 GHz	0.924	-176.88	5.26	70.48	0.015	-1.62	0.526	-168.63
1.3 GHz	0.924	-178.24	4.84	68.15	0.015	-2.29	0.533	-168.88
1.4 GHz	0.924	-179.50	4.48	65.89	0.015	-2.85	0.539	-169.13
1.5 GHz	0.925	179.33	4.17	63.68	0.014	-3.31	0.546	-169.38
1.6 GHz	0.925	178.22	3.89	61.52	0.014	-3.67	0.553	-169.65
1.7 GHz	0.926	177.17	3.65	59.41	0.014	-3.93	0.560	-169.94
1.8 GHz	0.926	176.16	3.43	57.34	0.014	-4.09	0.568	-170.26
1.9 GHz	0.927	175.18	3.24	55.30	0.014	-4.16	0.575	-170.60
2.0 GHz	0.927	174.24	3.07	53.29	0.014	-4.13	0.582	-170.97
2.1 GHz	0.928	173.32	2.91	51.32	0.013	-4.00	0.589	-171.36
2.2 GHz	0.928	172.41	2.76	49.38	0.013	-3.76	0.597	-171.79
2.3 GHz	0.929	171.53	2.63	47.46	0.013	-3.43	0.604	-172.24
2.4 GHz	0.929	170.65	2.51	45.57	0.013	-2.99	0.611	-172.71
2.5 GHz	0.929	169.79	2.40	43.71	0.013	-2.44	0.618	-173.22
2.6 GHz	0.930	168.93	2.30	41.87	0.013	-1.79	0.625	-173.75
2.7 GHz	0.930	168.08	2.20	40.05	0.012	-1.04	0.632	-174.30
2.8 GHz	0.931	167.24	2.12	38.26	0.012	-0.18	0.638	-174.87
2.9 GHz	0.931	166.40	2.04	36.48	0.012	0.77	0.645	-175.47
3.0 GHz	0.932	165.56	1.96	34.73	0.012	1.82	0.651	-176.08
3.2 GHz	0.932	163.88	1.82	31.28	0.012	4.18	0.663	-177.37
3.4 GHz	0.933	162.20	1.70	27.91	0.012	6.83	0.675	-178.72
3.6 GHz	0.934	160.51	1.60	24.60	0.012	9.69	0.686	179.86
3.8 GHz	0.934	158.80	1.51	21.35	0.012	12.64	0.696	178.39
4.0 GHz	0.935	157.07	1.42	18.16	0.013	15.58	0.706	176.88
4.2 GHz	0.935	155.32	1.35	15.01	0.013	18.40	0.715	175.31
4.4 GHz	0.935	153.53	1.29	11.91	0.014	21.01	0.723	173.70
4.6 GHz	0.935	151.70	1.23	8.84	0.014	23.33	0.730	172.05
4.8 GHz	0.935	149.84	1.17	5.80	0.015	25.32	0.737	170.36
5.0 GHz	0.935	147.93	1.13	2.79	0.016	26.96	0.743	168.63
5.2 GHz	0.935	145.98	1.09	-0.20	0.017	28.24	0.749	166.86
5.4 GHz	0.935	143.97	1.05	-3.19	0.018	29.16	0.754	165.05
5.6 GHz	0.934	141.91	1.01	-6.16	0.020	29.75	0.759	163.20
5.8 GHz	0.934	139.78	0.98	-9.14	0.021	30.02	0.763	161.30
6.0 GHz	0.933	137.58	0.96	-12.12	0.023	29.99	0.767	159.35

Download this s-parameter file in ".s2p" format at http://www.cree.com/products/wireless_s-parameters.asp

Cree, Inc.
4600 Silicon Drive
Durham, NC 27703
USA Tel: +1.919.313.5300
Fax: +1.919.869.2733
www.cree.com/wireless

Product Dimensions CGH40025F (Package Type — 440166)

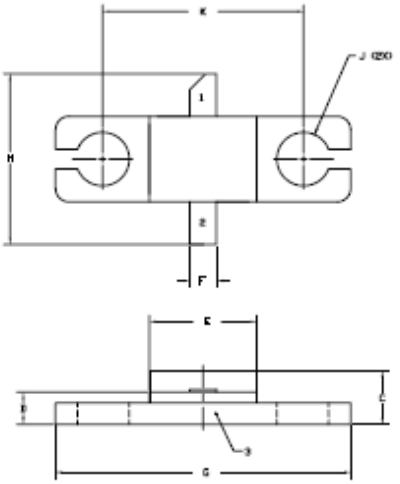

DIM	INCHES		MILLIMETERS	
	MIN	MAX	MIN	MAX
A	0.155	0.165	3.94	4.19
B	0.004	0.006	0.10	0.15
C	0.115	0.135	2.92	3.43
D	0.057	0.067	1.45	1.70
E	0.195	0.205	4.95	5.21
F	0.045	0.055	1.14	1.40
G	0.545	0.555	13.84	14.09
H	0.280	0.380	7.87	8.38
J	ø .100		2.54	
K	0.375		9.53	

PIN 1. GATE
PIN 2. DRAIN
PIN 3. SOURCE

Product Dimensions CGH40025P (Package Type — 440196)

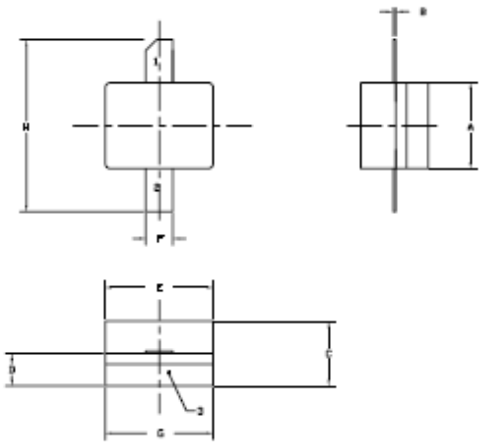

DIM	INCHES		MILLIMETERS	
	MIN	MAX	MIN	MAX
A	0.155	0.165	3.94	4.19
B	0.003	0.006	0.10	0.15
C	0.115	0.135	2.92	3.17
D	0.057	0.067	1.45	1.70
E	0.195	0.205	4.95	5.21
F	0.045	0.055	1.14	1.40
G	0.195	0.205	4.95	5.21
H	0.280	0.360	7.112	9.114

PIN 1. GATE
PIN 2. DRAIN
PIN 3. SOURCE

Cree, Inc.
4600 Silicon Drive
Durham, NC 27703
USA Tel: +1.919.313.5300
Fax: +1.919.869.2733
www.cree.com/wireless

Disclaimer

Specifications are subject to change without notice. Cree, Inc. believes the information contained within this data sheet to be accurate and reliable. However, no responsibility is assumed by Cree for any infringement of patents or other rights of third parties which may result from its use. No license is granted by implication or otherwise under any patent or patent rights of Cree. Cree makes no warranty, representation or guarantee regarding the suitability of its products for any particular purpose. "Typical" parameters are the average values expected by Cree in large quantities and are provided for information purposes only. These values can and do vary in different applications and actual performance can vary over time. All operating parameters should be validated by customer's technical experts for each application. Cree products are not designed, intended or authorized for use as components in applications intended for surgical implant into the body or to support or sustain life, in applications in which the failure of the Cree product could result in personal injury or death or in applications for planning, construction, maintenance or direct operation of a nuclear facility.

For more information, please contact:

Cree, Inc.
4600 Silicon Drive
Durham, North Carolina, USA 27703
www.cree.com/wireless

Ryan Baker
Marketing
Cree, RF Components
919.407.7816

Tom Dekker
Sales Director
Cree, RF Components
919.407.5639

Cree, Inc.
4600 Silicon Drive
Durham, NC 27703
USA Tel: +1.919.313.5300
Fax: +1.919.869.2733
www.cree.com/wireless

APPENDIX C

IRF 510, HEXFET POWER MOSFET DATASHEET

International
IOR Rectifier

PD-9.325Q

IRF510

HEXFET® Power MOSFET

- Dynamic dv/dt Rating
- Repetitive Avalanche Rated
- 175°C Operating Temperature
- Fast Switching
- Ease of Paralleling
- Simple Drive Requirements

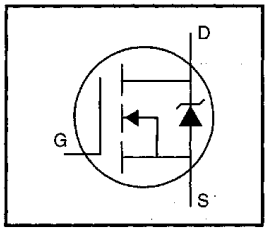

V_{DSS} = 100V

$R_{DS(on)}$ = 0.54Ω

I_D = 5.6A

Description

Third Generation HEXFETs from International Rectifier provide the designer with the best combination of fast switching, ruggedized device design, low on-resistance and cost-effectiveness.

The TO-220 package is universally preferred for all commercial-industrial applications at power dissipation levels to approximately 50 watts. The low thermal resistance and low package cost of the TO-220 contribute to its wide acceptance throughout the industry.

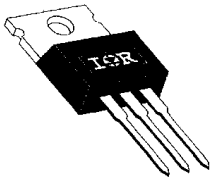

TO-220AB

Absolute Maximum Ratings

	Parameter	Max.	Units
I_D @ T_C = 25°C	Continuous Drain Current, V_{GS} @ 10 V	5.6	A
I_D @ T_C = 100°C	Continuous Drain Current, V_{GS} @ 10 V	4.0	
I_{DM}	Pulsed Drain Current ①	20	
P_D @ T_C = 25°C	Power Dissipation	43	W
	Linear Derating Factor	0.29	W/°C
V_{GS}	Gate-to-Source Voltage	±20	V
E_{AS}	Single Pulse Avalanche Energy ②	100	mJ
I_{AR}	Avalanche Current ①	5.6	A
E_{AR}	Repetitive Avalanche Energy ①	4.3	mJ
dv/dt	Peak Diode Recovery dv/dt ③	5.5	V/ns
T_J T_{STG}	Operating Junction and Storage Temperature Range	-55 to +175	°C
	Soldering Temperature, for 10 seconds	300 (1.6mm from case)	
	Mounting Torque, 6-32 or M3 screw	10 lbf•in (1.1 N•m)	

Thermal Resistance

	Parameter	Min.	Typ.	Max.	Units
$R_{\theta JC}$	Junction-to-Case	—	—	3.5	°C/W
$R_{\theta CS}$	Case-to-Sink, Flat, Greased Surface	—	0.50	—	
$R_{\theta JA}$	Junction-to-Ambient	—	—	62	

IRF510

IOR

Electrical Characteristics @ T_J = 25°C (unless otherwise specified)

	Parameter	Min.	Typ.	Max.	Units	Test Conditions
$V_{(BR)DSS}$	Drain-to-Source Breakdown Voltage	100	—	—	V	V_{GS}=0V, I_D= 250μA
$\Delta V_{(BR)DSS}/\Delta T_J$	Breakdown Voltage Temp. Coefficient	—	0.12	—	V/°C	Reference to 25°C, I_D= 1mA
$R_{DS(on)}$	Static Drain-to-Source On-Resistance	—	—	0.54	Ω	V_{GS}=10V, I_D=3.4A ④
$V_{GS(th)}$	Gate Threshold Voltage	2.0	—	4.0	V	V_{DS}=V_{GS}, I_D= 250μA
g_{fs}	Forward Transconductance	1.3	—	—	S	V_{DS}=50V, I_D=3.4A ④
I_{DSS}	Drain-to-Source Leakage Current	—	—	25	μA	V_{DS}=100V, V_{GS}=0V
		—	—	250		V_{DS}=80V, V_{GS}=0V, T_J=150°C
I_{GSS}	Gate-to-Source Forward Leakage	—	—	100	nA	V_{GS}=20V
	Gate-to-Source Reverse Leakage	—	—	-100		V_{GS}=-20V
Q_g	Total Gate Charge	—	—	8.3	nC	I_D=5.6A
Q_{gs}	Gate-to-Source Charge	—	—	2.3		V_{DS}=80V
Q_{gd}	Gate-to-Drain ("Miller") Charge	—	—	3.8		V_{GS}=10V See Fig. 6 and 13 ④
$t_{d(on)}$	Turn-On Delay Time	—	6.9	—	ns	V_{DD}=50V
t_r	Rise Time	—	16	—		I_D=5.6A
$t_{d(off)}$	Turn-Off Delay Time	—	15	—		R_G=24Ω
t_f	Fall Time	—	9.4	—		R_D=8.4Ω See Figure 10 ④
L_D	Internal Drain Inductance	—	4.5	—	nH	Between lead, 6 mm (0.25in.) from package and center of die contact
L_S	Internal Source Inductance	—	7.5	—		
C_{iss}	Input Capacitance	—	180	—	pF	V_{GS}=0V
C_{oss}	Output Capacitance	—	81	—		V_{DS}=25V
C_{rss}	Reverse Transfer Capacitance	—	15	—		f=1.0MHz See Figure 5

Source-Drain Ratings and Characteristics

	Parameter	Min.	Typ.	Max.	Units	Test Conditions
I_S	Continuous Source Current (Body Diode)	—	—	5.6	A	MOSFET symbol showing the integral reverse p-n junction diode.
I_{SM}	Pulsed Source Current (Body Diode) ①	—	—	20		
V_{SD}	Diode Forward Voltage	—	—	2.5	V	T_J=25°C, I_S=5.6A, V_{GS}=0V ④
t_{rr}	Reverse Recovery Time	—	100	200	ns	T_J=25°C, I_F=5.6A
Q_{rr}	Reverse Recovery Charge	—	0.44	0.88	μC	di/dt=100A/μs ④
t_{on}	Forward Turn-On Time	Intrinsic turn-on time is neglegible (turn-on is dominated by L_S+L_D)				

Notes:

① Repetitive rating; pulse width limited by max. junction temperature (See Figure 11)

② V_{DD}=25V, starting T_J=25°C, L=4.8mH R_G=25Ω, I_{AS}=5.6A (See Figure 12)

③ I_{SD}≤5.6A, di/dt≤75A/μs, V_{DD}≤$V_{(BR)DSS}$, T_J≤175°C

④ Pulse width ≤ 300 μs; duty cycle ≤2%.

APPENDIX D

RELEVANT PUBLICATIONS

High Linearity Auxiliary Envelope Tracking (AET) System using GaN Class-J Power Amplifier

Z.Yusoff, S.Woodington, J.Lees, J.Benedikt, P.J. Tasker, S.C.Cripps

Abstract— **A technique which we term Auxiliary Envelope Tracking (AET) is proposed, where a small amplitude tracking voltage is superimposed on the fixed DC bias to an RF power amplifier (RFPA). This represents a potentially useful alternative to a conventional ET system, and in particular significant linearity improvement can be obtained. Using a 2GHz two-carrier signal with 1MHz separation, an AET system has been developed using a 10W GaN Class J power amplifier which demonstrates large reduction in third order intermodulation products (10-25dB), and has less than -30dBc IM3 level at average drain efficiency of 40%. This linearity improvement is remarkable inasmuch as the AC power consumption of the injected AET signal can be lower than 10% of the DC supply.**

I. INTRODUCTION

Linearity has become a very important specification in designing RF power amplifiers (RFPAs). In particular it is crucial to maintain both high efficiency and meet the spectral requirements in modern wireless communication systems. One efficiency enhancement technique, Envelope Tracking (ET), as shown in Fig. 1 has been widely reported [1, 2, 3] as a method for improving the overall efficiency of an RFPA. ET does however present some problems, most notably the need for a highly efficient baseband tracking amplifier and a heavy dependency on digital predistortion (DPD) techniques. In this paper we propose an important variation on ET, Auxiliary Envelope Tracking (AET), which demonstrates useful efficiency enhancement and major linearity improvements through the use of an injected, low power tracking signal. The key point in AET is that the power content of the injected AET signal typically remains a very low percentage (<10%) of the DC supply to the RFPA.

II. AUXILIARY ENVELOPE TRACKING

The two-carrier signal is used in AET system and both efficiency and linearity are achieved. The AET system is shown in Fig. 2. The two-carrier signal is amplified by a driver amplifier before being applied to the 10W Class J RFPA. This 10W Class J PA was designed and realized using RF waveform engineering techniques developed in Cardiff University [4]. In the system described, the 1MHz AET signal is generated by a third signal generator. This signal is amplified by an external envelope amplifier (EA), and the DC component is inserted through a diplexer. The combined AET signal is then fed to the RFPA supply, which of course has to have all bias decoupling components disconnected. The resulting AET signal is no longer perfectly sinusoidal due to the voltage drop across the output impedance of the EA, as for example indicated in Fig. 3.

III. MEASUREMENT RESULTS AND DISCUSSIONS

In this reported experiment the AET signal modulates the 28V supply up to 37V at the maximum peak envelope power (PEP) level of 41dBm. Both high efficiency and linearity are achieved. The maximum average drain efficiency of the AET system is 40% while maintaining the third-order IM distortion (IM3) lower than -30dBc with respect to the power of each carrier (Fig.4). In comparison, the RFPA alone was measured at fixed drain supplies of 28V, 34V and 37V for both efficiency and linearity. The average drain efficiency of the RFPA at fixed supply is lower than the RFPA using the AET system, even for the case where the DC supply is raised to the same level as the peak AET voltage (37V) as shown in Fig. 4. Although these efficiency calculations do not include the power consumption of the EA, it is important to note that the injected AC component of the AET signal power is less than 10% of the DC supply (Fig.5). At maximum PEP of 41dBm, the DC power consumed is 15.5W but, remarkably, the measured AET AC component power is only 1W.

In the data presented in Fig. 4, the amplitude and the phase of the AET signal were optimized at each power level. The IM3 performance of the RFPA using the AET system is outstandingly improved by as much as 25dB. It is believed that the IM3 improvement is due to a significant functional dependency of gain with supply voltage, which thus appears to be a valuable asset of GaN devices in RFPA applications where linearity is of paramount importance.

IV. CONCLUSIONS

The AET system presented has been observed to demonstrate major linearity improvement as well as efficiency enhancement at a low injected AC power consumption.

REFERENCES

[1] Kimball, D.F. et al: 'High-Efficiency Envelope-Tracking W-CDMA Base-Station Amplifier Using GaN HFETs,' IEEE Transaction on Microwave Theory and Techniques, Vol. 54, No.11, November 2006, pp.3848-3856

[2] Kim, I. et al: 'High-Efficiency Hybrid EER Transmitter Using Optimized Power Amplifier,' IEEE Transaction on Microwave Theory and Techniques, Vol.56, No.11, November 2008, pp.2582-2593

[3] Harju, H. et al: 'Envelope Tracking Power Amplifier with Static Predistortion Linearization,' 2007 European Conference on Circuit Theory and Design, Vols 1-3, 2007. pp. 388-391.

[4] Wright, P.: 'An Efficient, Linear, Broadband Class-J-Mode PA Realised Using RF Waveform Engineering', IEEE/MTT-S International Microwave Symposium Digest, 7-12 June 2009, pp. 653-656S

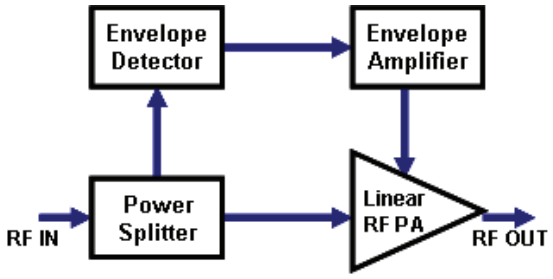

Fig.1: Basic Envelope Tracking System

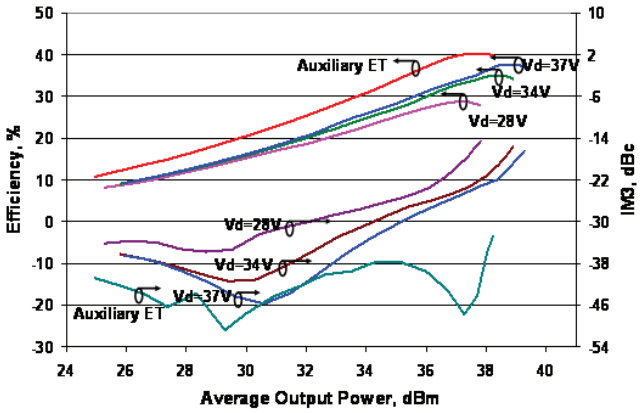

Fig.4: Drain efficiency and third-order intermodulation distortion (IM3) performances

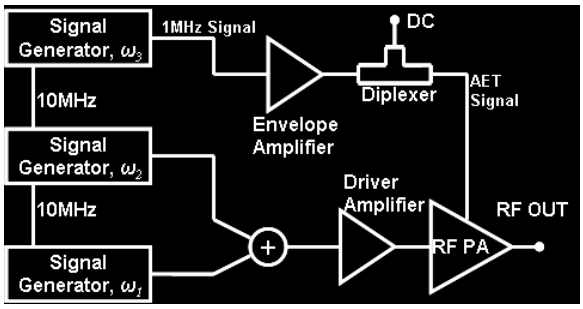

Fig.2: Auxiliary Envelope Tracking System Block Diagram

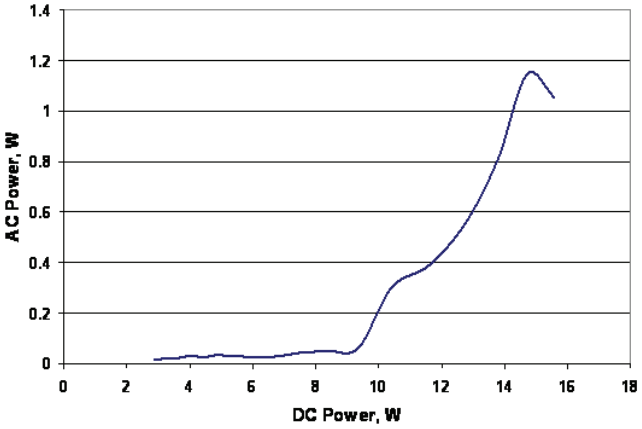

Fig.5: The AC power consumption of AET signal

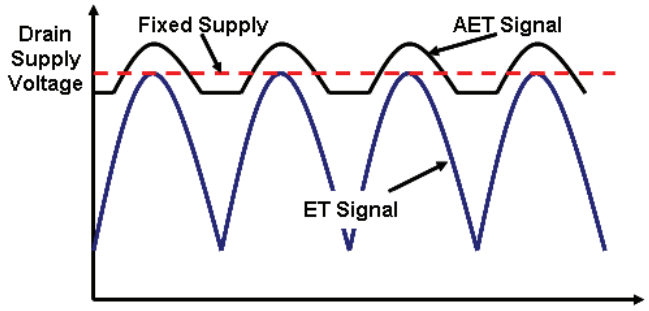

Fig.3: Example of AET, conventional ET and fixed supply signal

The Benefit of GaN Characteristics over LDMOS for Linearity Improvement using Drain Modulation in Power Amplifier System

Z. Yusoff, M. Akmal, V. Carrubba, J. Lees, J. Benedikt, P.J. Tasker and S.C. Cripps

School of Engineering, Cardiff University,
Cardiff, CF24 3AA, United Kingdom.

yusoffz@cardiff.ac.uk

Abstract — **This paper reports that significant linearity improvement can be obtained in gallium nitride (GaN) RF power amplifiers (RFPAs) in comparison to laterally diffused metal oxide semiconductor (LDMOS) RFPAs through the use of a modulated drain supply. It is shown that the gain characteristic of a GaN RFPA has significant variation with the drain bias voltage and this results in a 10-20dB reduction in intermodulation (IM) levels. The LDMOS RFPA was measured and the result showed that the gain of LDMOS did not change substantially with drain bias voltage. As a consequence, when the LDMOS RFPA is measured using modulated drain bias, the IM levels showed only a much smaller improvement. These results appear to indicate that GaN devices have an important advantage over LDMOS in linear RFPA applications.**

Keywords-component; Gallium nitride (GaN), Linearity, Power amplifiers, Intermodulation.

I. INTRODUCTION

In today's advanced wireless communication technology, such as WCDMA and Long Term Evolution (LTE), linearity performance has been an important aspect in designing the RF power amplifiers (RFPAs). Future applications such as mobile TV and multimedia streaming will also require high spectral efficiency and linear output power. Currently, the expected adjacent channel interference requirement for both standards is about -30dBc to assure that two adjacent frequency operators to operates without any interference [1-2]. There are three methods of power amplifier linearization mentioned in [3] which are categorized by the way the RFPA's input signal, output signal or bias signal is being modified. The most popular method is by modifying the input signal (e.g. pre-distortion), secondly by modifying the output signal (e.g. feed forward) and the least popular is by modifying the amplifier characteristics dynamically (e.g. adaptive bias). This paper explores the last method by investigating the gain characteristic of GaN HEMT and Si-LDMOS RFPAs at different drain bias voltages and measuring the linearity performances of the RFPAs by supplying modulated signal to the drain bias.

RFPAs based on LDMOS technology have been widely used in to the communication industry. The short channel length of the LDMOS structure provides a high current handling capability and low doping on drain side of this FET contributes to high blocking voltage [4]; this combination is a desired property for high power RFPAs. The low cost of LDMOS technology has resulted in it becoming the technology of choice for RFPA. However, as the LDMOS device operation reaches its limit, GaN technology represents the future for microwave power amplifiers. As compared to LDMOS technology, GaN is a wide band gap material thus it offers high breakdown voltage, higher carrier mobility and high temperature applications [5]. The high power density property of GaN contributes to reduced parasitic capacitance thus offering wider bandwidth in RFPA broadband matching design as compared to LDMOS. GaN also offers higher operating frequency because LDMOS performance degrades when operating frequency is greater than 3 GHz [6]. All of these advantages towards high power broadband RFPA design have therefore attracted a large amount of recent attention, both in research and industry.

In this paper, GaN RFPA linearity characteristics are compared to corresponding LDMOS RFPA performance. It is shown that the GaN RFPA gain characteristic has possibility for linearity improvement using a modulated drain supply voltage. An earlier investigation of linearity on the same 10W GaN device using an advanced active IF load pull measurement setup has been presented in [7] where IM3 and IM5 distortions were observed to improve significantly by emulating appropriate negative baseband impedance terminations. Such negative impedance terminations can be implemented in practice by using a suitably modulated supply voltage.

II. GAIN CHARACTERISTIC OF GAN AND LDMOS PA

A 10W GaN Class J RFPA that was reported in [8] and a 20W LDMOS Class AB RFPA were used in this measurement. GaN HEMT is a depletion mode device, therefore, the 10W GaN Class J PA is biased with negative voltage at the gate of the RFPA. Both RFPAs are however biased in deep Class AB region. In the CW measurement at 2 GHz, the RF power was swept at different drain bias voltage from 16V to 28V. The output power was measured and the gain in dBs versus output power was plotted. The measurement of GaN RFPA showed that the gain varied significantly from 8dB to 12dB as shown in Figure 1. At drain voltage of 16V, the gain measured was linearly around 8dB but compresses as the peak output level was reached. The behavior of gain at different drain bias voltage was

almost similar but at each higher drain bias voltage, the gain increased by about 0.5dB.

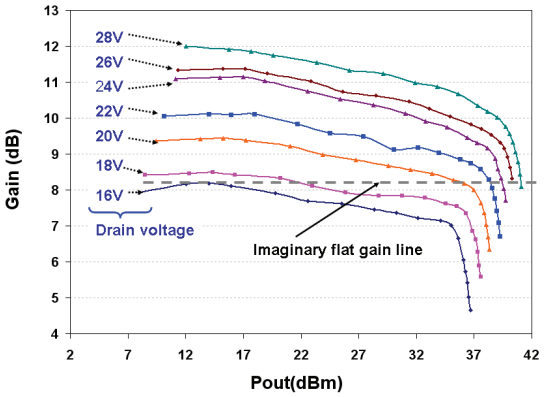

Figure 1. GaN PA gain characteristic as drain voltage was varied

In order to show the gain variation clearly, the gain in decibel scale was then plotted at a linear level of output power, 30dBm. The logarithmic gain was observed to change approximately linearly with the drain bias voltage as shown in Figure 2. As observed in Figure 1, the rate of change of this linear gain in decibel in Figure 2 is about 0.5dB per Volt.

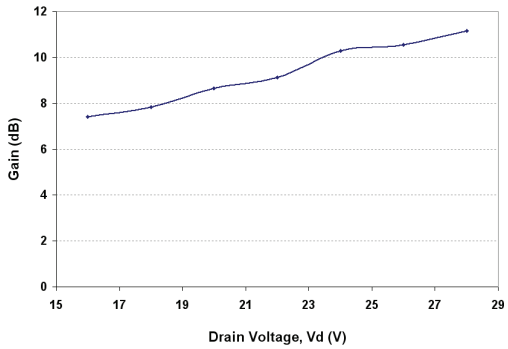

Figure 2. GaN PA gain characteristic at 30dBm output power

CW measurement was also done on the 20W LDMOS Class AB RFPA. The same RF power was swept at drain bias voltage from 16V to 28V. The output power was measured and the again the logarithmic gain was plotted against the output power. This measurement result is presented in Figure 3. The figure shows that the gain was linear but compressed towards peak output level. The gain behavior of LDMOS RFPA was almost similar for all drain bias voltages. However, it is observed that the gain varied much less significantly with drain bias voltage in comparison to the GaN measurements. In order to see clearly the insignificant rate of change in the logarithmic gain versus drain bias voltage, the LDMOS gain was plotted at a linear level of output power, 30dBm. As shown in Figure 4, the gain was seen to be almost constant with the drain bias voltage.

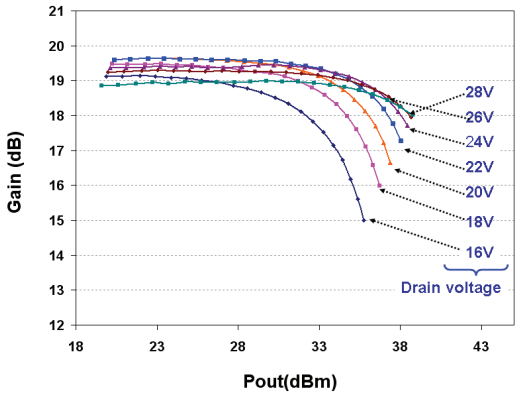

Figure 3. LDMOS gain characteristic as drain voltage was varied.

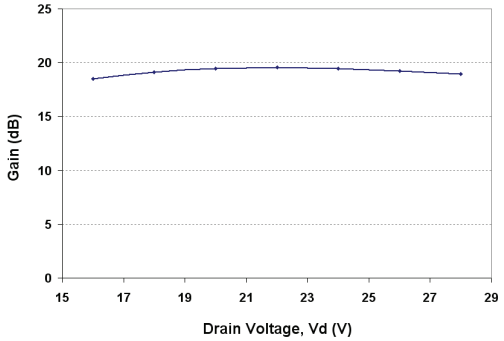

Figure 4. LDMOS PA gain characteristic at 30dBm output power

The measurement results above show that the GaN RFPA has an expansive gain characteristic with increasing drain voltage. Theoretically, when the device reaches the peak power level the device compressive behavior can be linearized by the expansive gain characteristic if the drain bias voltage is suitably increased. In order to visualize the linearizing effect, an imaginary linear line is drawn in Figure 1. From this figure, as we increase a suitable drain bias voltage in the compressive area at the peak power level, a flat gain can be achieved. As we improve a linear gain at its peak power level, the linearity of the RFPA will be observed as well. We have called such drain voltage adjustment "Auxiliary Envelope Tracking (AET)", inasmuch as the voltage tracking is primarily intended to linearize the PA, rather than improve its efficiency.

III. IMD MEASUREMENT FOR GAN AND LDMOS PA

For intermodulation distortion (IMD) investigation, the GaN RFPA and LDMOS were measured on two experimental setups. The first experimental setup was used to measure the IMD of the RFPA when the RFPAs were biased by a fixed drain supply as shown in Figure 5 (a). This IMD measurement using fixed drain supply is needed to make comparison to RFPA when biased with modulated signal. The second experimental setup was used to measure the IMD when the RFPAs were biased with a modulated drain supply

voltage as shown in Figure 5(b). In the first setup, the 2-carrier input signal at 2GHz with frequency separation of 1MHz was generated by two signal generators. The input signal is then amplified before the input signal was fed into the gate of RFPA. The drain of the RFPA was biased from a fixed supply.

In this second experimental setup, there were three signal generators used for this measurement. Two signal generators generated a 2-carrier input signal for the RFPA at 2 GHz with frequency separation of 1MHz. The input signal was amplified by a driver amplifier before inserted to the gate of RFPA. The drain bias of the RFPA was provided with the sinusoidal signal at the 2-carrier signal envelope frequency of 1MHz by the third signal generator. This 1MHz sinusoidal signal was then amplified by an amplifier that we termed Envelope Amplifier and the DC component is inserted through a diplexer. The combined signal that we called AET signal was then fed to the RFPA drain supply, which of course has to have all bias decoupling components disconnected.

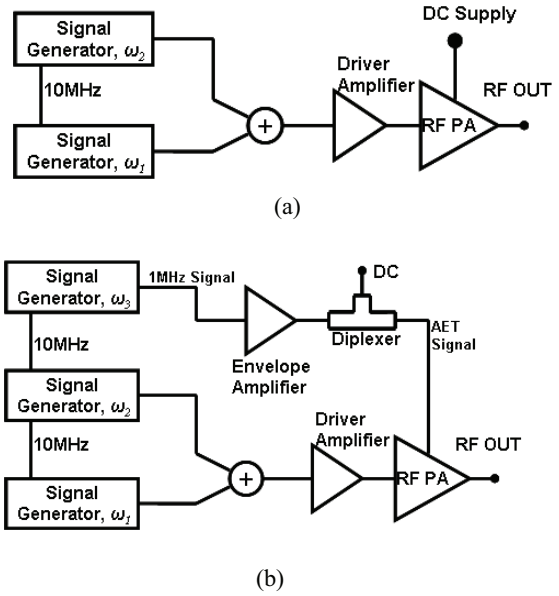

Figure 5. Experimental setup for intermodulation distortion measurement

(a) Fixed drain supply (b) Modulated drain supply

In the 2-carrier signal measurement for GaN RFPA, RF power was swept and the third-order intermodulation (IM3) and average output power were measured. For the GaN RFPA, on the first experimental setup for fixed drain bias measurement, the GaN RFPA was measured at fixed drain bias of 37V. On the second experimental setup; the peak voltage that was provided to the drain bias, (that is the sum of the fixed and sinusoidal components) was 37V. The values were chosen to make a very fair comparison between the fixed drain supply and the drain modulated bias results measured on the modulated drain supply setup. For the LDMOS RFPA, the fixed drain bias voltage on the first setup was 28V and the peak voltage of the combined fixed and sinusoidal signal that was provided to the drain bias on the second setup was 28V.

For both fixed and drain modulated bias measurements, the IM3 performance were plotted. In Figure 6, the IM3 performance of the GaN RFPA when biased with fixed drain supply showed that the IM3 value of lower than -30dBc for average output power lower than about 36dBm. A 'null' effect was observed around average output power of 31dBm but greater than 36dBm average output power, the IM3 level was worsening. The IM3 performance of GaN RFPA under modulated drain supply however showed that the IM3 level was below -30dBc even at its maximum average output signal. This is a promising performance for WCDMA and LTE technology that require high linearity. At the maximum measured output power level, the IM3 performance under modulated drain supply as compared to fixed drain supply was improved from -22dBc to -33dBc, and an IM3 improvement between 10dB and just over 20dB was observed over a 3dB power backoff (PBO) range, and significant

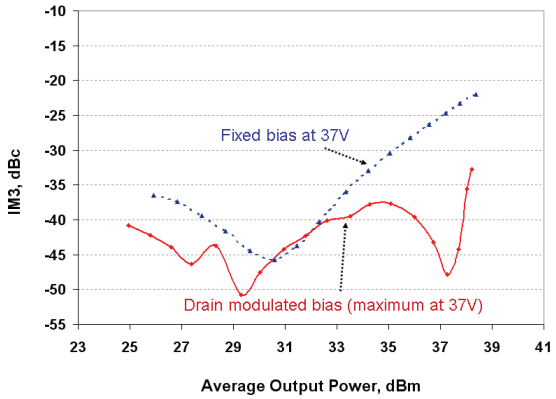

Figure 6. IM3 for GaN PA at fixed and drain modulated bias

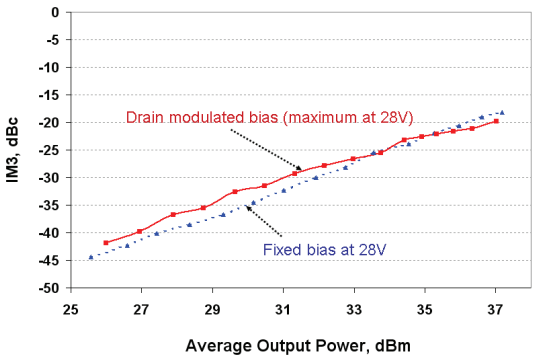

Figure 7. IM3 for LDMOS PA at fixed and drain modulated bias

In Figure 7, the LDMOS performance in IM3 is presented and it is observed that the LDMOS, as expected from the gain measurements, did not show substantial IM3 improvement. The IM3 performance of LDMOS RFPA for fixed drain supply was less than -30dBc for average output power greater than 33dBm. The IM3 performance of this LDMOS RFPA under modulated drain supply showed a slight decline for average output power lower than 33dBm but showed a slight but insignificant improvement for average output power greater than 33dBm.

CONCLUSIONS

It has been shown that the gain variation of GaN device has a potential to contribute substantial linearity improvement using drain modulation, an effect which is absent in an LDMOS device. The improvement in linearity using the AET system showed that the GaN RFPA can be useful for modern communication systems that require the RFPA to be optimized at highest power rating while maintaining the linearity and spectrum purity of the signal. Future work on this research program is to investigate the gain characteristic on higher power GaN devices and at different bias point, and also to explore the possibility of this drain modulation method to improve efficiency.

ACKNOWLEDGMENT

This work has been carried out as part of EPSRC grant EP/F033702/1. The authors would also like to thank CREE for supporting this activity and supplying the devices and Yayasan Telekom Malaysia, Kuala Lumpur for PhD student sponsorship.

REFERENCES

[1] H. Lilja, H. Mattila," WCDMA Power Amplifier Requirements and Efficiency Optimization Criteria", 1999 IEEE MTT-S International Microwave Symposium Digest, Anaheim, USA, vol.4, pages 1943-1846.

[2] Y. Li, R. Zhu, D. Prikhodko, Y. Tkachenko, " LTE Power Amplifier Module Design: Challenges and Trends", 2010 10th IEEE International Conference on Solid-State and Integrated Circuit Technology (ICSICT), Shanghai, China, pages 192-195.

[3] S. Cripps, "RF Power Amplifier for Wireless Communications", Norwood, MA: Artech House, Apr. 1999.

[4] Bart Van Zeghbroeck, " Principles of Semiconductor Devices", http://ece-www.colorado.edu/~bart/book/

[5] "LDMOS", Microwave 101 Website, http://www.microwaves101.com/encyclopedia/LDMOS.cfm

[6] "GaN Essentials- Application Notes", AN009 – AN 013, Nitronex Corporation, http:// www.nitronex.com/ganessentials .html

[7] M.Akmal,J. Lees, S. Bensmida, S. Woodington, V. Carrubba, S. Cripps, J. Benedikt, K. Morris, M. Beach, J. McGeehan, P.Tasker, "The Effect of Baseband Impedance Termination on the Linearity of GaN HEMTs," 40th European Microwave Conference, 2010.

[8] P. Wright, J. Lees, P.J. Tasker, J. Benedikt, S.C. Cripps, "An Efficient, Linear, Broadband Class-J-Mode PA Realised Using RF Waveform Engineering", IEEE/MTT-S International Microwave Symposium Digest, 7-12 June 2009, pp. 653-656

Linearity Improvement in RF Power Amplifier System using Integrated Auxiliary Envelope Tracking System

Z. Yusoff, J. Lees, J. Benedikt, P. J. Tasker, S.C. Cripps

Centre for High Frequency Engineering, Cardiff University, Cardiff, CF24 3AA, Wales, United Kingdom.

***Abstract* — A new technique called Auxiliary Envelope Tracking (AET) is proposed, which demonstrates substantial improvement in linearity of RF power amplifiers. A small amplitude envelope-tracking voltage is superimposed on the fixed DC bias of a specially designed 25W GaN HEMT Class AB RF power amplifier (RFPA). A large improvement in third-order intermodulation (IM3) distortion has been observed while maintaining low fifth-order intermodulation (IM5). The overall drain efficiency of the RFPA is also observed to improve, even when the power consumption of the envelope tracking generator is included. The AET concept uses a simple and easily integrated system that consists of an RFPA, a diplexer and an envelope amplifier.**

***Index Terms* — Linearization techniques, Power amplifiers, Intermodulation, Gallium nitride (GaN).**

I. Introduction

Advance digital communications systems place increasing demands on RFPA efficiency and linearity. There are a number of linearization techniques that have been extensively researched and well documented in the literature [1]-[3] namely, feed-forward, feedback and pre-distortion. All of these techniques however add significant complexity and cost to the system design.

Here, we propose a new linearization technique that we call Auxiliary Envelope Tracking (AET), which can be applied to any RFPA. The name of this technique is derived from the regular Envelope Tracking (ET) system that is a well-known efficiency enhancement technique for power amplifiers. However, here, the emphasis of the AET system is on linearity improvement. The basic operation has some similarities to regular ET. In AET, the RF input signal is split into RF and envelope paths. The RF signal on the envelope path is detected and amplified by a low frequency envelope amplifier before this signal is injected into the drain port of the RF PA via a diplexer. In this AET, the combined injected amplified envelope signal and dc component is called AET signal. In regular ET, the envelope tracking drain bias signal will improve the efficiency, but only if the tracking voltage generator is itself highly efficient (>80%). In the AET system however, the combination of the tracking drain bias signal with the characteristic of the GaN HEMT device gives a major improvement in the linearity of the power amplifier. This AET system also has the potential to present a simple and low cost solution to linear-efficient RFPA design. The additional circuitry involves a simple diplexer and a low cost envelope amplifier. In our ongoing work, we believe AET can be used not only for linearity improvement but also for significant efficiency enhancement.

II. Characteristic of GaN HEMT Device and Linearity Analysis

The concept of using AET to improve linearity was motivated by observing the gain characteristic of a Gallium nitride (GaN) high electron mobility transistor (HEMT) power device. A 25W GaN HEMT Class AB power amplifier was designed and the performance of this amplifier was measured. The gain of the amplifier was observed to change in an approximately linear fashion with the drain supply voltage on a decibel scale as shown in Fig. 1. This positive slope of gain is the basic property that is used here to improve the IM3. It can be further quantified by fitting the measured gain variation to a logarithmic function. The gain, g_1 will have an exponential variation with drain voltage, *Vd*, as in the expression (1) below.

$$g_1 = \alpha \exp(\beta V_d) \tag{1}$$

where α and β are the constants extracted from the decibel scale measurements.

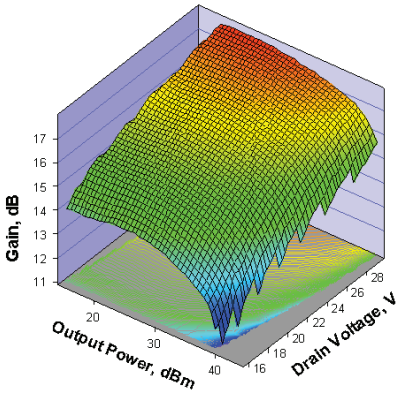

Fig. 1. Gain performance over varying drain voltages

Assume this GaN HEMT power amplifier device has non-linear transfer characteristic of (2) and the drain voltage, *Vd* is tracking the envelope of input signal, v_{in} (3).

$$i_o = g_1 v_{in} + g_2 v_{in}^2 + g_3 v_{in}^3 + \ldots \tag{2}$$

$$V_d = \delta v_{in} . \tag{3}$$

Substituting equation (3) to (1) and inserting back to (2), expanding the equation using an exponential series and limiting the interest up till the third degree, then, the output current, i_o will be simplified into the following equation (4).

$$i_o = \alpha\left(1+\beta\delta v_{in}+\frac{(\beta\delta v_{in})^2}{2!}+\frac{(\beta\delta v_{in})^3}{3!}\right)v_{in} + g_2 v_{in}^2 + g_3 v_{in}^3 \tag{4}$$

$$i_{o3} = \left(\frac{\alpha\beta\delta}{2}+g_3\right)v_{in}^3 . \tag{5}$$

Since the source of IM3 distortion is caused primarily by the third-degree component, equation (5), the tracking voltage characteristic open up a possibility, through the appropriate selection of values of α, β, and δ for cancellation of the IM3, given that g_3 is usually negative.

More simply stated, the inherent device compression characteristic can be cancelled by the expansive gain that is provided by the increasing drain voltage. This offers a linearizing approach that requires an increasing supply voltage at higher drive levels and a decreasing supply voltage at lower drive levels, much like regular ET. The difference here is that AET has the potential to linearize with little or no overall efficiency degradation.

Fig. 2. The implemented Integrated AET Block

III. Integrated AET Block

The AET integrated block consists of an RFPA, a diplexer and an envelope amplifier. The implemented integrated AET block is shown in Fig. 2.

In this AET system, the amplified tracking envelope voltage is superimposed on to fixed DC bias to produce the AET signal that will be the drain supply of the RFPA. The AET signal has a varying drain voltage and results in improved linearity of the power amplifier.

A. RFPA: 25W GaN HEMT Class AB Power Amplifier

The RFPA used in the Integrated AET block employs a 25W GaN HEMT transistor. The RFPA is then designed using microstrip elements to give input and output impedance matching. This transistor is biased in Class AB mode and has fundamental matching with the second harmonic shorted. The maximum measured forward gain, S21 is about 19dB at drain bias of 30V and this RFPA achieved more than 10dB gain across more than 1 GHz bandwidth as shown as in Fig. 3.

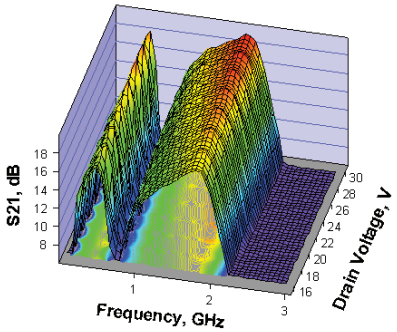

Fig. 3. The forward gain, S21 across the frequency for 25W GaN HEMT Class AB PA.

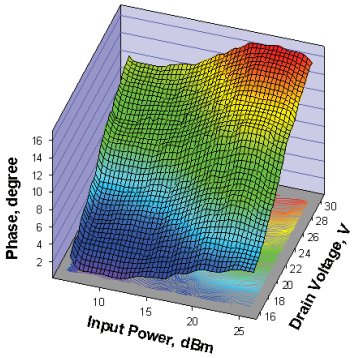

Fig. 4. AM-PM measurement for 25W GaN HEMT Class AB PA

The AM-PM measurement shows that the RFPA is well behaved as the phase changes across input power at maximum of about 6 degree at fixed drain voltage of 30V as shown in Fig. 4. The drain efficiency measured remains high at different value of drain voltages as shown in Fig. 5.

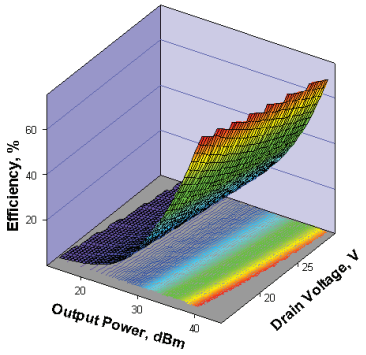

Fig. 5. The drain efficiency of the RFPA over varying drain voltages

B. Diplexer and Envelope Amplifier

The second element in the integrated AET block is the diplexer, and the schematic is shown in Fig. 6(a). The implemented diplexer consists of passive capacitors and inductors and has three ports.

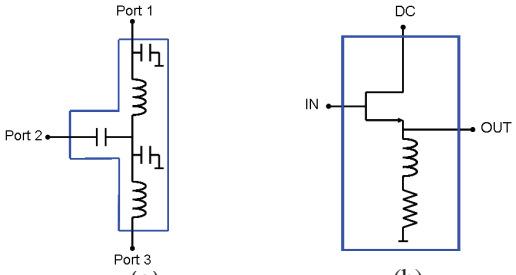

Fig. 6. (a) The diplexer and (b) the envelope amplifier schematics

The diplexer is designed to allow a signal of frequency 100 kHz and above to pass from Port 2 to Port 3, and to pass DC from Port 1 to Port 3.

The envelope amplifier is the final part of the integrated AET block, and is shown schematically in Fig.6 (b). This envelope amplifier is designed using a source follower amplifier configuration to achieve a low output impedance at baseband frequency. The low output impedance is required to achieve voltage source functionality. A large inductor is directly connected to the source of the n-channel FET and a small value resistor is connected between the inductor and the ground. The combination of these two passive components maintains the minimum required DC current flowing through the transistor. The lowest possible DC current is required to maintain high efficiency for the RFPA in AET system.

IV. AET EXPERIMENTAL SETUP

The AET experimental setup for 2-carrier signal measurement at 1.98GHz with 1MHz spacing is shown in Fig. 7. The 2-carrier signal is generated by two signal generators that are phase-locked and these two continuous wave (CW) signals are combined using a combiner to produce the modulated signal. The amplitude and phase of the envelope signal is emulated using the third signal generator that is also phase-locked with the other generators. The RF signal is amplified by a driver amplifier and then the signal is fed to the RF input of the RFPA. The emulated envelope signal is a sinusoidal signal and this signal is inserted to a bias tee. A dc component is combined with the emulated envelope signal through a bias tee. A DC component is needed to turn on the n-channel FET and bias this transistor into saturation to perform as a voltage source. This emulated envelope signal is inserted to an envelope amplifier and this signal is combined with a DC component through a diplexer. The resulted AET signal will bias the RFPA.

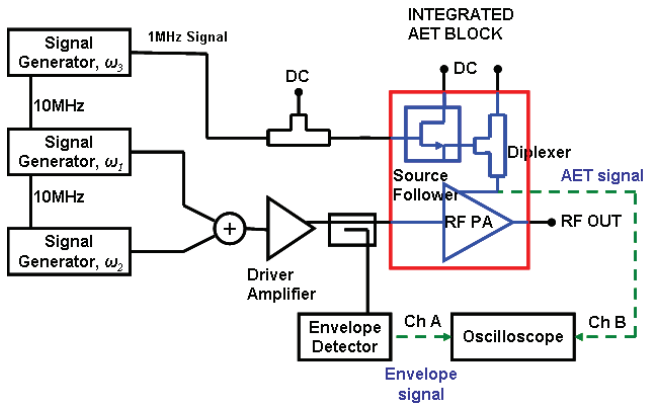

Fig. 7. The AET experimental setup

V. MEASUREMENT RESULT

During the measurement the AET signal and the envelope signal waveforms were observed on an oscilloscope, as shown in Fig. 7 and the waveforms are shown in Fig. 8 (note that the 2-carrier envelope is distorted by the square law detector).

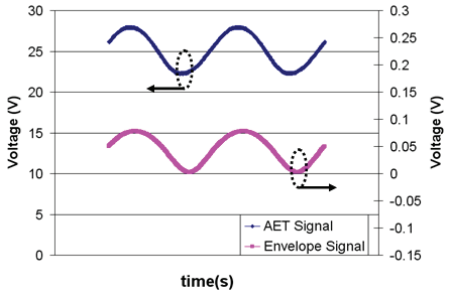

Fig. 8. AET tracking and envelope signal waveforms

The AET signal phase is adjusted so that the AET signal is aligned with the envelope signal so IM3 and IM5 will be symmetrical [2], [3]. The AET amplitude is also adjusted to give optimum IM3 and IM5 performance.

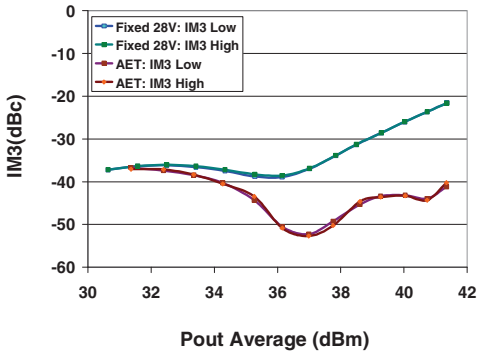

Fig. 9. IM3 performance for AET system and fixed drain bias

The optimum IM3 performance of the RFPA using AET shows a large improvement at higher power level i.e. 18 dB at an average output power of 41dBm. This measurement is

compared to the RFPA biased at fixed voltage of 28V as shown in Fig. 9. The comparison is done for the RFPA biased at 28V, which is the same as the peak level of the composite AET signal. But it should be noted that the heat dissipation will be much lower in the AET case, raising the possibility of using much higher peak AET voltages than would be allowable with a fixed supply.

The IM5 performance was also measured and the result is shown in Fig. 10. The IM5 of the RFPA operating in the AET system shows that the performance remains low as compared to the RFPA operating on fixed bias.

This AET system confirms the results from measurements that have been performed separately [4] at the device level by emulating baseband impedance at the drain termination.

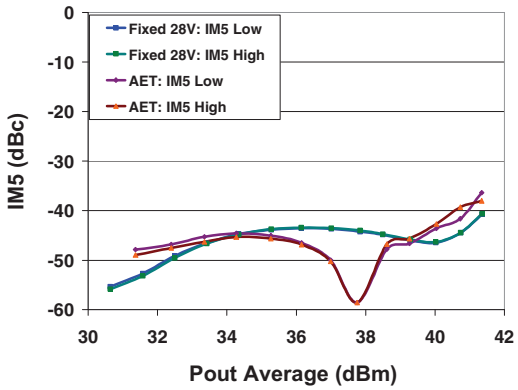

Fig. 10. IM5 performance for AET system and fixed drain bias

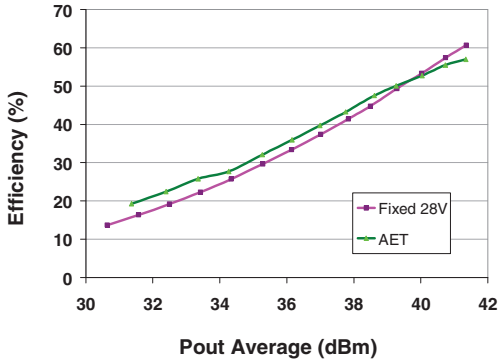

Fig. 11. Drain Efficiency performance for AET system and fixed drain bias

Although the focus of this paper is on the improved linearity, the drain efficiency was also measured and the result in Fig. 11 shows a small improvement in drain efficiency over most of the measured power range. This shows that the linearity improvement observed using AET is obtained with minimal overall reduction in efficiency, even when the power consumption of the linearizer is fully taken into account. We note in passing that published results on other linearization methods, e.g. digital pre-distortion, customarily do not account for the extra power consumption of the linearization.

VI. CONCLUSION

A novel linearization technique called AET has been described. A compact integrated system based on a 25W GaN RFPA device has been demonstrated. IM3 improvement between 10dB and 18dB has been observed over a 10dB power range, with an 18dB improvement at the highest power level. This linearity improvement has been obtained with negligible impact on the overall efficiency of the system. Future work will investigate more complex modulation systems, and possibilities for more substantial efficiency improvement in comparison to single supply operation.

ACKNOWLEDGEMENT

This work has been carried out as part of EPSRC grant EP/F033702/1. The authors would also like to thank CREE for supporting this activity and supplying the devices and Yayasan Telekom Malaysia, Kuala Lumpur for PhD student sponsorship.

REFERENCES

[1] S. Cripps, "*RF Power Amplifier for Wireless Communications*", Norwood, MA: Artech House, Apr. 1999.

[2] S. Cripps, "*Advanced Techniques in RF Power Amplifier Design*", Norwood, MA: Artech House, 2002

[3] Kenington, P.," High Linearity RF power Amplifier", Norwood, MA: Artech House, 2000.

[4] M. Akmal, J. Lees, S. Bensmida, S. Woodington, V. Carrubba, S. Cripps, J. Benedikt, K. Morris, M. Beach, J. McGeehan, P. Tasker, "The Effect of Baseband Impedance Termination on the Linearity of GaN HEMTs," 40th European Microwave Conference, 2010.